THESIS / THÈSE

DOCTOR OF SCIENCES

Drug-drug cocrystallization or salt formation as an alternative to combination drugs
A case study on clofazimine

BODART, Laurie

Award date:
2021

Awarding institution:
University of Namur

Link to publication

UNIVERSITÉ DE NAMUR

FACULTÉ DES SCIENCES

Drug-drug cocrystallization or salt formation as an alternative to combination drugs:
A case study on clofazimine

A thesis submitted by **Laurie Bodart**
for the fulfillment of the requirements
for the degree of Doctor in Sciences

Thesis committee:
Prof. Yoann Olivier (Université de Namur, president of the thesis committee)
Prof. Johan Wouters (Université de Namur, advisor)
Dr. Luc Aerts (UCB Pharma)
Prof. Tom Leyssens (Université Catholique de Louvain-la-Neuve)
Dr. Nikolay Tumanov (Université de Namur)
Prof. Carmela Aprile (Université de Namur)

September 2021

**La cocristallisation ou la salification de plusieurs médicaments comme alternative aux combinaisons médicamenteuses:
Une étude de cas sur la clofazimine**

par **Laurie Bodart**

Résumé

Le problème de résistance aux antibiotiques est un enjeu de santé publique à l'échelle mondiale qui s'est accompagné de la mise en place de multithérapies. Dans ce contexte, le nombre de médicaments administrés simultanément augmente, ce qui peut s'accompagner d'une mauvaise compliance, elle-même associée au développement de résistances. Des combinaisons médicamenteuses ont alors vu le jour afin de faciliter les traitements et d'améliorer la compliance des patients. Cependant, ces combinaisons sont parfois difficiles à développer à cause d'incompatibilités entre les médicaments à combiner. Une option viable est la cocristallisation ou la salification de plusieurs médicaments, qui consiste à les combiner au sein d'un même réseau cristallin (mélange des espèces au niveau moléculaire). Les techniques de cocristallisation et de salification permettent également une modulation de leurs propriétés physico-chimiques.

L'objectif de cette thèse est de préparer des sels ou des cocristaux combinant plusieurs médicaments, dont la clofazimine, une molécule connue pour ses propriétés antiléprotiques et antituberculeuses. Ces nouveaux solides sont préparés afin de caractériser leur tendance à cristalliser sous forme solvatées ou non-solvatées. Ils sont également caractérisés en termes de stabilité thermique, de solubilité aqueuse et d'hygroscopicité. Pour ce faire, l'aptitude de la clofazimine à cristalliser avec des solvants ou d'autres molécules (solvates, sels /cocristaux) a été étudiée. Sur la base de ces résultats, d'autres molécules médicamenteuses présentant des groupements susceptibles d'interagir avec la clofazimine, et qui pourraient présenter un avantage dans le cadre du traitement de la tuberculose, ont été sélectionnées. Les nouvelles phases cristallines ont été principalement préparées par mécanochimie et/ou par cristallisation en présence de solvant (évaporation lente). Les nouvelles phases cristallines obtenues ont été caractérisées par diffraction des rayons X sur échantillons de poudres et sur monocristaux, par analyse thermogravimétrique et par calorimétrie différentielle à balayage. La solubilité aqueuse des sels ou cocristaux non-solvatés a été caractérisée par des méthodes HPLC ou UV-visible. Ces résultats ont révélé en quoi la préparation de solides cristallins multi composant combinant plusieurs médicaments permet de moduler leurs propriétés physico-chimiques.

Université de Namur
FACULTÉ DES SCIENCES
Rue de Bruxelles 61, 5000 Namur, Belgique

Drug-drug cocrystallization or salt formation as an alternative to combination drugs:
A case study on clofazimine

by **Laurie Bodart**

Abstract

The problem of antibiotic resistance is a global public health issue that has been accompanied by the implementation of multi-therapies. In this context, the number of drugs simultaneously administered to patients is increasing. This may be associated to poor compliance and thus also to the development of new resistance. Drug combinations have emerged to facilitate treatment and improve patient compliance. However, parent drugs incompatibility (e.g., in terms of physico-chemical properties) can hamper their development. A viable option is the cocrystallization or salification of several drugs, which consists of combining them within the same crystal lattice (mixing of species at the molecular level). Cocrystallization/salt formation techniques further allow modulation of the physico-chemical properties of the drugs.

The objective of this thesis is to prepare salts or cocrystals combining several drugs, including clofazimine, a molecule known for its antileprotic and antituberculosis properties. These new solids are prepared in order to characterize their propensity to crystallize in solvated or non-solvated forms and their thermal stability, aqueous solubility and hygroscopicity. To this end, the ability of clofazimine to crystallize with solvents or other molecules (solvates, salt/cocrystals) has been studied. On the basis of these results, other drug molecules with functional groups potentially interacting with clofazimine, and which could be of benefit in the treatment of tuberculosis, were selected. The new crystalline phases were mainly prepared by mechanochemistry and/or by solvent crystallization. They were then characterized by X-ray diffraction on powder samples and on single-crystals, by thermogravimetric analysis and by differential scanning calorimetry. The aqueous solubility of the non-solvated salts or cocrystals was further characterized by HPLC or UV-visible methods. These results revealed how the preparation of multicomponent crystalline solids combining several drugs allows to modulate their physico-chemical properties.

PhD thesis in Chemistry
Namur, September 2021

iv

"La science doit s'accommoder à la nature, la nature ne peut s'accommoder à la science"

Ferdinant Brunot

Acknowledgements

First of all, I would like to thank Prof. Johan Wouters, my thesis advisor who was present throughout this work and who was always of good advice. I cannot thank him enough for having welcomed me in his laboratory since the beginning of my master thesis.

My gratitude also goes to Dr. Nikolay Tumanov, who trained me in the use of XRD diffractometers, who guided me in solving my first structures and who was always present to help me with more complex structures as well as in writing publications. I would also like to thank him for allowing me to discover the synchrotron and structure resolution by powder XRD.

My thanks also go to Dr. Luc Aerts for the fruitful discussions around this project, for his advice concerning the characterization of salts and for his welcome at UCB Pharma.

Many thanks to Prof. Tom Leyssens of the IMCN/MOST laboratory and to the members of his team and especially to Dr. Xavier Buol, for the fruitful discussions around this project, for the welcome in their laboratory, whether for thermal analysis or for DVS measurements. I would also like to thank them for their precious help in the interpretation of the thermal analysis data.

I would also like to thank Dr. Luca Fusaro for the solid-state NMR data collections and his assistance in their interpretation.

I would like to thank the members of my thesis committee and my thesis jury (Prof. Johan Wouters, Prof. Yoann Olivier, Prof. Carmela Aprile, Prof. Tom Leyssens, Dr. Luc Aerts and Dr. Nikolay Tumanov) for their careful reading of this work.

My gratitude also goes to my master thesis student Amélie Derlet and to Maria Prinzo, for their involvement and the fruitful collaboration.

I also thank the F.R.S-F.N.R.S. for the financial support they gave me.

To my colleagues from the CBS laboratory, Marie, Mégane, Kalina, Élise, Manon, Andrea, Sébastien, Thomas, Quentin, Dr. Laurence Leherte and all the others, thank you for the good times spent together, the laughter and, as I cannot mention the CBS team without talking about food, the good shared meals.

Finally, I thank with all my heart those without whom none of this would have been possible: my friends and my family, my parents, my sisters and my husband, Maxime, for all that they have brought me.

List of abbreviations

ADME absorption, distribution, metabolism and excretion

ADMET absorption, distribution, metabolism, excretion and toxicity

FDA Food and Drug Administration

EMA European Medicines Agency

FDC fixed drug combination

API active pharmaceutical ingredient

EAFUS everything added to food in the United-States

GRAS generally regarded as safe

CSD Cambridge structural database

SCXRD single-crystal X-ray diffraction

PXRD powder X-ray diffraction

LAG liquid-assisted grinding

NG neat grinding

PolAG polymer-assisted grinding

M. tb *Mycobacterium tuberculosis*

TB tuberculosis

RR-TB rifampicin resistant tuberculosis

MDR-TB multidrug resistant tuberculosis

XDR-TB extensively drug resistant tuberculosis

HIV human immunodeficiency virus

AIDS acquired immune deficiency syndrome

HDT host-directed therapy

WHO World Health Organization

CFZ clofazimine

NSAID non-steroidal anti-inflammatory drug

ROS reactive oxygen species

COX cyclo-oxygenase

PGH$_2$ prostaglandin H$_2$

DCF diclofenac

PAS 4-aminosalicylic acid

BCS biopharmaceutics Classification System

SMEDDS self-microemulsifying drug delivery systems

FA fumaric acid

SA succinic acid

SACC saccharin

DL-MAL DL-malic acid

L-ASP L-aspartic acid

CIT citric acid

2,4-DHBA 2,4-dihydroxybenzoic acid

TRPTA terephthalic acid

FIM full interaction map

DFT density functional theory

EtOH ethanol

MeOH methanol

EtOAc ethyl acetate

MeCN acetonitrile

PPP propiophenone

SAL salicylaldehyde

PEO polyethylene glycol

DMF *N, N'*-dimethylformamide

VT-PXRD variable-temperature powder X-ray diffraction

VH-PXRD variable-humidity powder X-ray diffraction

TGA thermogravimetric analysis

TG thermogravimetric / thermogravimetry

DSC differential scanning calorimetry

Et$_2$O diethyl ether

GI gastro-intestinal

FaSSIF fasted-state simulated intestinal fluid

FeSSIF fed-state simulated intestinal fluid

FaSSGF fasted-state simulated gastric fluid

HPLC high-performance liquid chromatography

DVS dynamic vapour sorption

IR infra-red

ss-NMR solid-state nuclear magnetic resonance

HSM hot-stage microscopy

SEM scanning electron microscopy

CP/MAS ss-NMR cross polarization/magic angle spinning solid-state nuclear magnetic resonance

NQS non quaternary suppression

Contents

Chapter 1

Introduction

1.1 Drug development process

1.1.1 A multidisciplinary, time consuming, costly and risky process

The process going from discovery to marketing of new drugs is long, costly and multidisciplinary. The overall process can be divided in two main phases: discovery and development. [1, 2] The discovery phase can further be divided in sub-steps (Figure 1.1):

Target identification and validation This step consists in finding a biological target that is relevant to the disease. This can be achieved by several techniques such as phenotypic screening. [3] In this technique, compounds are evaluated in cell-based assays or in animal models in order to identify the ones that result in phenotypic changes. Then the target of these compounds are identified by, among others, genetic, *in silico* or chemical approaches. Target validation consists in checking that the identified target has a real function in the disease of interest. This can be achieved by antisense technology (through the use of siRNA or knock-out/knock-in animals).

Hit generation and confirmation Several compounds are screened (most often by high-throughput methods) to identify those that generate the desired activity (e.g., inhibition or activation) on the therapeutic target. Identified hits are then re-evaluated by the same method to confirm their activity. Other tests can be performed to ensure that the results are not false positives. Dose-response curves are also performed in order to classify the hits according to their efficiency (based on IC_{50} values for example).

Lead generation and optimization At this stage, the identified hits are optimized and several series of compounds are chosen. Analogues are also synthetized in order to establish quantitative structure-activity relationships. Target selectivity, absorption, distribution, metabolism and excretion (ADME), pharmacokinetics and potential toxicity of the analogues are also studied *in vitro*. During lead optimization, the aim is to maintain the desired properties of the lead while reducing its potential deficiencies (e.g., target selectivity, absorption, distribution, metabolism, excretion and toxicity (ADMET)).
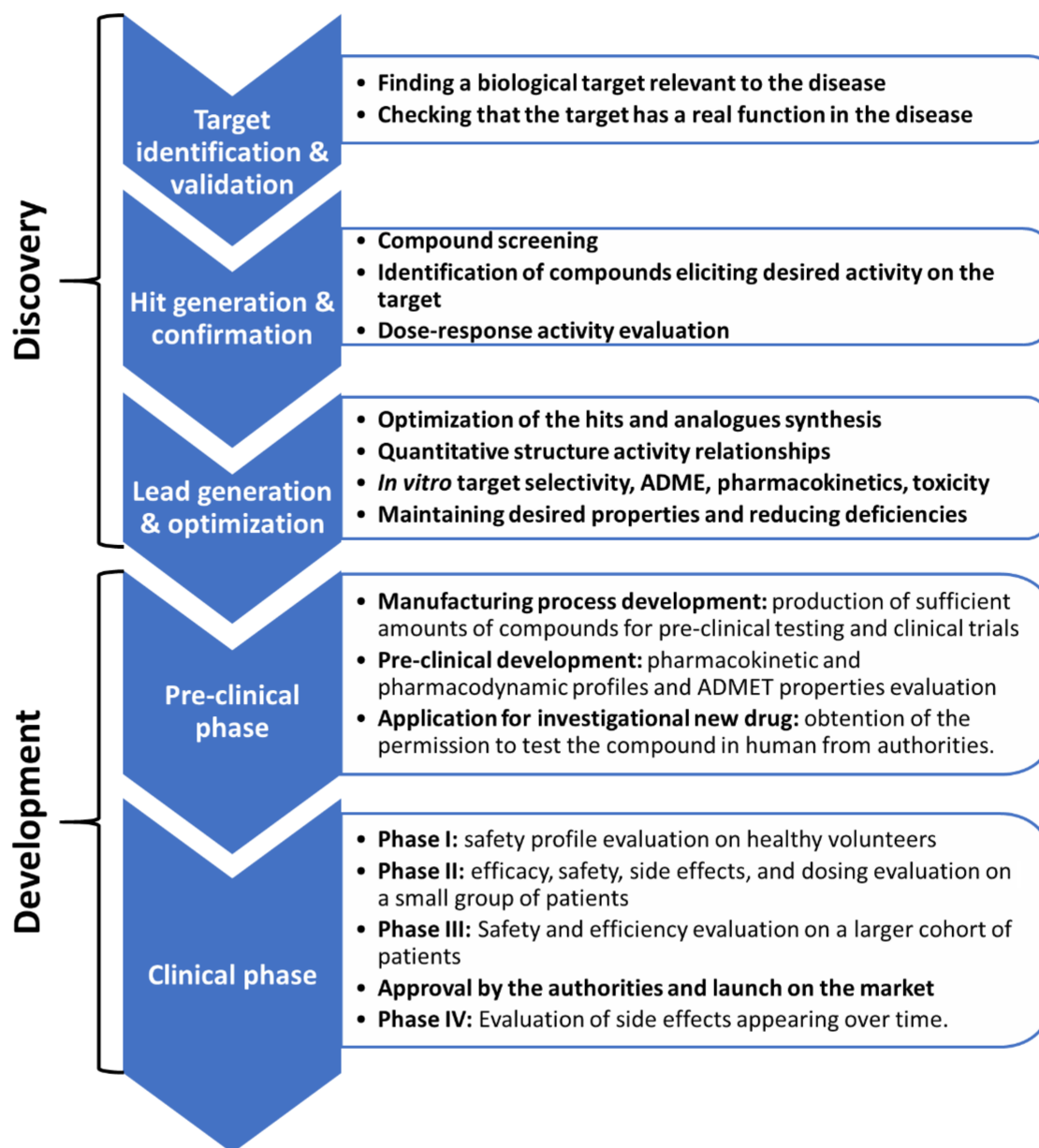
Figure 1.1: Drug discovery and development general workflow.

The development phase can also be subdivided in the pre-clinical and the clinical steps. [2] The pre-clinical phase, is itself divided in three key steps (Figure 1.1):

Development of the manufacturing process This is performed to allow the production of sufficient amounts of the compound for pre-clinical testing and clinical trials.

Pre-clinical development At this stage, the aim is to assess pharmacokinetic and pharmacodynamic profile of the selected candidate as well as its ADMET properties.

Application for investigational new drug This step consists in introducing an application to regulatory offices in order to obtain the permission to administer the candidate to human.

When the administration to human has been authorized, the clinical development which is divided in four phases (three before marketing of the drug) can begin (Figure 1.1). [1, 2]

Phase I The safety profile of the candidate is evaluated in human (on 10-100 healthy volunteers). ADME, safety and pharmacodynamics are monitored, the maximum tolerated dose is determined.

Phase II The drug is tested on 50-500 patients (suffering of the targeted disease) and its efficacy, safety and side effects are evaluated. The dosing regimen is also established (dose, frequency).

Phase III The safety and effectiveness of the drug is evaluated on a much larger group of patients. A control group receiving standard treatment or a placebo is involved in this phase in order to allow a comparison with the current best existing treatment for the target disease.

When the candidate is considered as safe and effective after the phase III trials, the drug has to be approved by the regulatory authorities (e.g., Food and Drug Administration (FDA) in the United States, European Medicines Agency (EMA) in European Union) before its launch on the market.

Phase IV Side effects that appear over time and that were not detected in earlier trials continue to be assessed after the drug has been launched on the market.

The estimated cost for the development of a new drug is around 2 billion dollars while the average time from drug discovery to release on the market is estimated to be between 10 to 15 years with an average of 13.5 years. [4, 5, 6] Currently, the number of new compounds on the market is declining, in particular due to a tightening of the regulations and analyses required for the marketing of new drugs and formulations. [7] It is estimated that only one out of around 5000 to 10000 new chemical entities will reach the market. [8, 9] To avoid unnecessary expenditures, potential problems of a compound should be detected as early as possible. Accordingly, pharmaceutical industry currently pays particular attention to the pre-clinical drug development step, in order to avoid as much as possible late-stage failure of clinical candidates.

1.1.2 Drug repurposing

In this context, finding new therapeutic targets for drugs already on the market (i.e., drug repurposing) may present several advantages in terms of time and cost since the pharmacokinetics, toxicity profile and pre-clinical data are already available for approved molecules. [10, 7, 6] The availability of these data also means that the repurposed compounds could directly enter phase II of clinical trials. [10, 11, 12, 13]

Drug repositioning has however also some limitations. Indeed, it often happens that the compound is not potent enough for the new identified therapeutic activity. The plasma concentration that can be achieved in the accepted dosages may be too low for the intended therapeutic application, which means that a higher dosage would be required. In such cases, a new optimal dosage and formulation are needed, and so new pre-clinical data and clinical trials are also required. If the new dosage goes along with toxicity, then a solution could be to identify synergistic compounds to be co-administered. [10, 11] Another disadvantage of drug repositioning arises from an intellectual property point of view. Indeed, to obtain a patent for an already known drug, the medical use has to be new and non-obvious, however, many repurposing uses are already reported in scientific literature. Furthermore, patents covering a new indication for an already existing compound may be difficult to obtain as it may be considered as simply presenting incremental advances. [13] Moreover, if generics are available, then they could also be used for the same purpose than the repositioned drug. These difficulties related to intellectual property, make drug repurposing less profitable for pharmaceutical companies. If drug repositioning is to be considered in terms of financial benefits, then it is necessary to establish a good intellectual property strategy, but this would also require greater investment. Indeed, if the repurposed drug presents a new patentable formulation, a combination of drugs, a new molecule associated to the drug, or a patentable delivery mechanism, then a 'composition of matter'patent could be applied for. [11]

1.2 Interests in preparing drug-drug combinations

Monotherapies are increasingly considered as ineffective, in part because of the emergence of drug-resistant pathogens. Not only are such strains difficult to treat with monotherapies, but, because they usually act on one therapeutic target at a time, monotherapies also promote the emergence of such drug-resistant pathogens. In this context, drug combinations present several advantages. [14, 7, 15, 10] First, the combination of drugs can help circumvent resistance problems (e.g., by combining a drug with a compound that inhibits the resistance mechanism by which the pathogen resists). Second, the combination of active pharmaceutical agents could allow coverage of a broader spectrum of pathogens (e.g., through the combination of antibiotics active on different bacterial strains). Then, emergence of drug-resistant pathogens is more limited when several drugs acting on different pathways are co-administered. This can be explained by two phenomena: the combination of drugs may allow the disease to be treated more rapidly, leaving less time

for the development of resistant strains, and moreover, the pathogen must simultaneously develop several resistance mechanisms (to counter-act the effect of the different drugs), which is less likely to happen. Finally, drug combinations can lead to synergistic effects. Two important difficulties however associated with drug combinations are the possibility of drug-drug interaction and the necessity to optimize drug ratio and/or dosage. [10, 11]

Combination of several drugs in the form of a single pill, fixed drug combination (FDC), has become more and more popular. A first advantage of FDCs is that they reduce the number of pills to be taken and, at the same time, they reduce the likelihood of the emergence of resistant pathogens. [14, 7, 15] For pharmaceutical companies and physicians, the marketing of FDCs also has the added advantage of reducing packaging costs as well as the number of drugs to be prescribed. However, there are also several disadvantages associated with the preparation of FDCs. Besides an obvious decrease in dosing flexibility, the drugs to be combined may be incompatible. For example, the respective solubility of both active pharmaceutical ingredients (APIs) to combine may be too different to allow proper preparation of efficient FDC and stability issues may also appear when the drugs are combined as physical mixtures. [14, 16, 15] Such kind of issues can potentially be circumvented by the preparation of multi-component solids (i.e., solids in which intermolecular interaction between both APIs are present), such as salts, cocrystals or co-amorphous systems instead of physical mixtures. [14, 17, 15]

1.3   Solid-state properties of drug products

Solid-state properties are of paramount importance during the development of all forms of a drug. This is obvious for solid-dosage forms of course, but also for other dosage forms (suspension, cream, solution, etc) because they are either prepared from solid drug or they require the use of solid excipients. Solid-form is closely related to physico-chemical properties of the compound such as stability and solubility. In consequence, investigating the various solid forms achievable for a drug allows the scientist to modulate these properties. For example, solid forms such as salts, cocrystals, metastable polymorphs can lead to improved solubility. Solid form screening is also required in order to find physical forms that are stable enough to stay unchanged during manufacturing process and storage and that present adequate mechanical properties (compressibility, hardness, etc). More particularly, the solid-state properties (and so the investigation of the various solid forms) start to play a major role at the stage of lead identification and optimization stage of drug development. Solubility and permeability are indeed evaluated for the first time at this step. [18]

1.3.1   Amorphous and crystalline solids

Solids can be divided in two subclasses: amorphous and crystalline. Amorphous solids do not present long-range order of their atomic, ionic or molecular constituents and can be single- or multi-component (hydrate/solvate, amorphized salts or amorphized cocrystals).

As opposed to amorphous solids, crystalline compounds are characterized by an ordered arrangement of their components. Like amorphous solids, crystalline compounds can be single- or multi-component. [18, 19]

Single-component crystals contain only the API (in case of a pharmaceutical crystal) while multi-component crystals consist of the API and either solvent, water, ions, molecules or a combination of these. According to the composition of the crystal, the terms solvate/hydrate, salt, cocrystal, cocrystal of salt, solvated/hydrated salt, solvated/hydrated cocrystal or solvated/hydrated cocrystal of salt are used (Figure 1.2). These terms can be defined as follows: [20]

- non-solvate or anhydrate: crystalline solid that does not contain a solvent molecule (i.e., neutral compound that is liquid under ambient conditions (at a temperature of 293.15K and a pressure of 10^5Pa)) or water molecule(s).

- solvate or hydrate: crystalline solid that contains at least a solvent or water molecule.

- (solvated/hydrated) salt: crystalline solid containing at least two ions (and at least one solvent/water molecule if solvated/hydrated).

- (solvated/hydrated) cocrystal: crystalline solid in which the arrangement in the crystal lattice is not based on ionic bonds and containing at least two different neutral or ionic components (and at least one solvent/water molecule if solvated/hydrated).

- (solvated/hydrated) cocrystal of salt: crystalline solid containing at least two ions and one neutral molecule (and at least one solvent/water molecule if solvated/hydrated).

Furthermore, solids of the same chemical composition which have different crystal structures are called polymorphs. It is to note that different solvated forms of an API are often referred as pseudo-polymorphs.
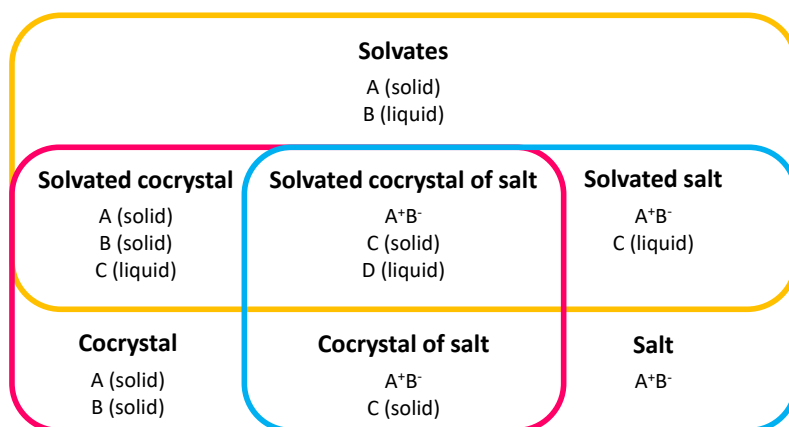
FIGURE 1.2: Classification of multicomponent crystalline solids.

When dealing with poorly soluble compounds, an amorphous solid dispersion (i.e., dispersion of an amorphous API in a polymer carrier) may be preferred as it can lead to improved dissolution and solubility in comparison with crystalline solids. Amorphous solid dispersions have to be thoroughly evaluated in terms of chemical and physical stability as amorphous compounds may tend to crystallize over time. Because of these potential stability problems, amorphous solid dispersions are not widespread. [18]

1.3.2 Crystalline solids: importance of polymorph screening and characterization

Even if hydrates are acceptable solid forms for pharmaceutical compounds, their physical stability under ambient condition can rise concerns. Such as for hydrates, stability concerns are present for solvates and furthermore, because of toxicity issues, only limited amount of certain solvents are allowed by the regulatory offices. In consequence anhydrates are often preferred over solvates or hydrates for further development. Their stability against humidity is however important to study as the selected solid form should not change during storage or manufacturing. [18]

Besides humidity and thermal stability studies, polymorph screening has also to be performed. Indeed, polymorphs may present very different physico-chemical properties (such as, for example solubility). It is furthermore estimated that more than 50% of pharmaceutical compounds exhibit polymorphism. [21, 22] Depending on the stage of drug development and on the desired formulation, the target properties of a solid material may vary. Selection of a particular polymorph will thus be determined by its associated physico-chemical properties. Usually, the thermodynamically stable polymorph will be selected over metastable ones. However, other parameters are also important for the solid form selection (such as solubility or mechanical properties) and in some case a metastable polymorph may be preferred.

Polymorph screening can be achieved by various crystallization methods that can be divided in two main categories: solid-state and solvent-mediated techniques. Solvent mediated methods include: cooling crystallization, evaporation, slurrying, antisolvent addition or diffusion. Solid-state techniques comprise, among others, cooling from the melt, exposure to solvent or humidity, and to controlled temperature cycles. Of course, cooling from the melt and exposure to humidity are two methods that can be applied in conjunction with the investigation of thermal and humidity stability. [18]

Solvents selected for polymorph screening experiments have to be as various as possible (and toxic solvents should not be eliminated at this step). Non-solvating solvents, so those ones that do not lead to crystallization of solvates, may be used in competitive slurry experiments aiming to determine the relative stability of the polymorphs. Another key aspect in polymorph screening is the temperature at which the experiments are performed. Indeed, the occurrence of some polymorphs is temperature dependent such as for

enantiotropically related polymorphs (one polymorph being more stable below the transition temperature and another one above this temperature). [18] Furthermore, desolvation of a solvated crystalline form may also lead to the discovery of new polymorphic forms.

1.4 Solubility issue of approved and under development drugs

The biopharmaceutics Classification System (BCS) has been created in order to classify drugs according to their solubility and permeability properties (determined under well-defined conditions). [23] According to this system, a highly soluble and permeable drug belongs to class I, a poorly soluble but highly permeable compound is classified in class II, substances belonging to class III have a high solubility but low permeability and finally class IV includes compounds with low solubility and low permeability (Figure 1.3). [24]
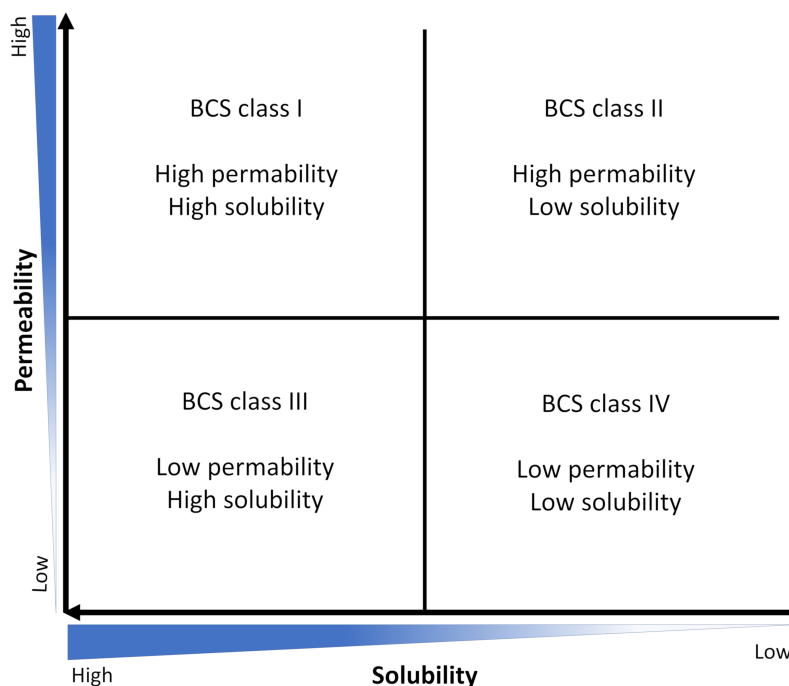
FIGURE 1.3: BCS classification system

In this particular context, a drug is considered as highly soluble if its highest therapeutic dose is soluble in 250 mL (or less) of water over a pH range of 1 to 6.8 and at 37±1 °C. Furthermore, high permeability is considered when at least 85% of the administered dose is absorbed in human. Permeability can be assessed based on a mass balance determination (with additional data proving that the compound is stable in the gastrointestinal tract) or in comparison with the dose that would be administered intravenously. [24]

It is estimated that 40% of the drugs already on the market have a low solubility and that between 70 and 90% of the compounds under development will present the same problem. [25, 7] Most of these candidates are BCS II (>50%) or IV (>25%). [26]

1.4.1 Techniques to improve drug solubility

Solubilization requires breaking solute-solute (and solvent-solvent) intermolecular interactions and replacing them with solute-solvent interactions. Usually, solubility enhancement techniques are classified in two categories: physical and chemical modifications. Many review articles are dedicated to solubility enhancement techniques and in this section, we will only briefly describe some methods that can improve drug solubility. [27, 28, 29, 30, 31, 32, 33, 34, 35]

1.4.1.1 Physical modifications

Particle size reduction   Particle size and size distribution are two key factors affecting solid physico-chemical properties such as dissolution rate, flowability, powder cohesion and sticking. Particle size reduction goes along with an increase of the surface area and of dissolution rate. [27, 28, 18] Particle size reduction does not however change equilibrium solubility of the compound. It is not so efficient on very poorly soluble drugs and sometimes polymorphic changes can occur during the particle size reduction process. [29, 32]

Nanosuspension   Nanocrystals and nanosuspensions are two common methods when dealing with poorly soluble solids. Nanosuspensions are biphasic systems consisting of nanosized drug particles stabilized by surfactants. On average, particle size distribution in nanosuspensions is in the 200-600 nm range. [29, 36]

Crystal habit modification (solvates/hydrates and polymorphs)   Controlling the crystallization conditions can yield powders with well-defined properties in terms of particle size and shape. Obtention of such specific powders may require solvate or hydrate formation. However, the amount of organic solvent that can be administered is limited because of toxicity concerns and solvates are often undesirable on a pharmaceutical point of view. Most organic compounds exhibit polymorphism. As polymorphs are different crystalline forms of a same drug, their physico-chemical properties are different from one polymorph to another and improved solubility can thus be achieved through the control of the crystallized polymorphic form. [29, 32]

Surfactant assisted solubilization   Several techniques based on surfactants have been developed, among which are found microemulsions and self-microemulsifying drug delivery systems (SMEDDS) as well as micellar solutions. Microemulsions consist of a mixture of oil, surfactant and hydrophilic solvent. SMEDDS are anhydrous microemulsion systems usually containing oil, surfactant and cosurfactant. [27] Upon contact with water and under gentle agitation, this system self-emulsifies to give a clear emulsion in which very small oil droplets, containing the sparingly water-soluble drug, are dispersed in water. The size of the droplets is usually between 20 and 200 nm. [27] These kinds of systems are generally administered as gelatine capsules. [27] Micellar solutions are formed when a surfactant is used at a concentration exceeding its critical micelle concentration. Such a concentration

allows formation of micelles in which a hydrophobic drug can be entrapped. Some commonly used surfactants are fatty-acid esters of low-molecular weight, polyethylene glycol and polysorbates. [27]

Preparation of inclusion complexes Drug complexation is often performed with cyclodextrins. Cyclodextrins are cyclic oligosaccharides forming truncated cone-shaped molecular cages. They possess a hydrophilic outer surface and a hydrophobic cavity. Most commonly used cyclodextrins are α-, β- and γ-cyclodextrins constituted respectively of 6, 7 and 8 dextrose units. Hydrophobic organic molecules can form non-covalent inclusion complexes with a cyclodextrin of appropriate size. [27, 28]

Solid dispersions The preparation of solid dispersions requires the dispersion of a poorly soluble compound (drug) in a highly soluble hydrophilic matrix. Two main types of dispersion can be obtained depending on whether the components are mixed at the molecular level (solid solutions) or not (eutectic solid dispersion). [27, 28]

1.4.1.2 Chemical modifications

Prodrugs Sometimes chemical modification of a drug can be useful in order to prepare a prodrug with improved solubility. [29] A prodrug is a compound that, under *in vivo* conditions (metabolization), releases the active component. Preparation of prodrugs can also sometimes improve selectivity of the drug for its target (e.g., reduction of the prodrug in the hypoxic environment of cancer cells).

Co-solvency To improve the solubility of a drug, one possibility is to use one (or a mixture of) water-miscible solvent(s) in which the drug is well soluble. Some acceptable solvents are polyethylene glycol, propylene glycol, dimethyl sulfoxide, glycerol or ethanol. The co-solvent method can be combined with other techniques such as pH-adjustment to further increase drug solubility. [27, 33] Depending on the amount of co-solvent added, toxicity and/or tolerability concerns should be considered. [27, 33]

Hydrotrophy This phenomenon occurs when solubility improves upon addition of a large amount of a second solute (ionic organic salt). This 'salting in'effect results from weak interactions between the hydrotropic agent and the solute. Mixing of different hydrotropic compounds can show synergistic effects on solubility improvement of the solute. [27, 33] Some examples of hydrotropic agents are sodium benzoate, sodium salicylate, 4-aminobenzoic acid hydrochloride, procaine hydrochloride, sodium alkanoate. [27, 33]

pH adjustment If the poorly soluble drug has basic or acidic groups, modulating the pH of the dissolution medium can result in an improved solubility. pH adjustment can be achieved through the use of alkalizing or acidifying excipients. This principle can be applied for oral or intravenous administration. However, the strong buffering capacity

of blood may cause the reprecipitation of the poorly soluble drug when administered intravenously. The buffer capacity of the medium and the pH tolerability are thus critical parameters to consider. Upon oral administration, the degree of solubility can also fluctuate because of gastrointestinal pH (1-2 in the stomach and 5-7.5 in the duodenum). [27, 35]

Salt formation and cocrystallization Salt formation is maybe the most common way to increase solubility and dissolution rate of acidic or basic drugs. Usually, it is considered that a pKa difference higher than 3 between the drug and the selected counter-ion will result in salt formation. The equivalent to salt formation for a non-ionizable drug is cocrystallization. Pharmaceutical salts/cocrystals usually contain one active pharmaceutical ingredient with a pharmaceutically acceptable compound (often selected from the list of generally regarded as safe (GRAS)). [31] The insertion of a second component (counter-ion or coformer) modifies the intermolecular interactions which in turn can lead to different solubility properties.

In this thesis, we will focus on approaches related to crystal engineering and more particularly on salt formation/cocrystallization (and on their related solvates and polymorphs). The following sections are therefore more specifically dedicated to salts and cocrystals, to their preparation methods and to the characterization techniques associated with these solid forms.

1.5 Cocrystallization and/or salt formation for the preparation of drug-drug combinations

Modulation of the intermolecular interactions allows the preparation of solids with tuned properties. [37] In this context, salt formation and cocrystallization are two techniques commonly used to modulate various physico-chemical properties (such as, among others, solubility, dissolution rate, stability and bioavailability) of the APIs. [14, 15, 38, 39] Depending on the compounds of interest, each approach has advantages and disadvantages. For example, APIs presenting an ionizable functionality may be implied in salification attempts whereas cocrystallization would be an alternative for APIs without any ionizable functional groups. Amorphization, and more particularly in the context of multidrug solids, co-amorphous systems are also known to improve drugs solubility. Such amorphous systems are however prone to crystallization over time. [7, 37] In consequence, these systems often need to be stabilized with crystallization inhibitors or through interaction with polymers. Because of this instability regarding crystallization, crystalline multi-component complex (salts/cocrystals) may be preferred over co-amorphous systems. [39, 40]

1.5.1 Definitions

Pharmaceutical cocrystals and salts have attracted interest of pharmaceutical scientists because their preparation does not alter the chemical structure of an API while allowing a diversification of its crystalline forms and so of its physico-chemical properties. Most pharmaceutical salts and cocrystals are made up of one API combined with a GRAS or everything added to food in the United-States (EAFUS) compound. [39] In contrast, drug-drug cocrystals/salts are formed through the combination of two (or more) APIs instead of an API with a GRAS/EAFUS compound. These multidrug crystalline materials could also lead to additive or synergistic effects. [15, 38]

The FDA considers cocrystals as drug product intermediates and, from a regulatory point of view, they are considered to be similar to polymorphs of a same API. FDA defines cocrystals as: [41]

> *'Cocrystals are crystalline materials composed of two or more different molecules, typically active pharmaceutical ingredient and cocrystal formers (co-formers), in the same crystal lattice.'*

The European Medicines Agency (EMA) considers that cocrystals are rather similar to salts of a same API (except that the arrangement in the crystal lattice is not based on ionic interactions). EMA cocrystal definition is: [42]

> *'Homogenous (single phase) crystalline structures made up of two or more components in a definite stoichiometric ratio where the arrangement in the crystal lattice is not based on ionic bonds (as with salts). The components of a cocrystal may nevertheless be neutral as well as ionized.'*

From a regulatory point of view, according to the EMA, cocrystals containing more than one API (so drug-drug cocrystals), fall within the regulation of fixed-dose combination.

Although the definition of cocrystal is still debatable, the scientific community often recognizes that cocrystals should be defined more broadly than the proposed definition of the FDA and that they should be rather classified like salts (as both can lead to similar effects on the physico-chemical properties of the solid form, in terms of, among others, solubility, bioavailability and stability modulation). [19] In the particular context of drug-drug combinations through salification or cocrystallization, the above definitions of cocrystals could be adapted. More particularly, Thipparaboina *et al.* have defined multidrug cocrystals as: [14]

> *'Dissociable crystalline supramolecular complexes comprising two or more effective components in a stoichiometric ratio within the same crystal lattice, wherein the components may predominantly interact via non-ionic interactions and rarely through hybrid interactions (a combination of ionic and non-ionic interactions involving partial proton transfer and hydrogen bonding) with or without the presence of solvate molecules'*

It is interesting to note that this definition encompasses solvates and what is sometimes called cocrystal of salt (a crystalline supramolecular complex containing, for example, a cation, an anion and a neutral molecule). By analogy, multidrug salts could be defined as:

> *'Crystalline supramolecular complexes in which at least two active pharmaceutical ingredients coexist in an ionic state and interact through ionic, hydrogen bond and non-covalent interactions.'*

Even if the distinction between salt and cocrystal is important in the context of intellectual property (mainly as they fall in distinct categories according to the FDA), in this work, both salts and cocrystals will be considered as similar entities which could be encompassed by the term 'multicomponent crystalline material'. This is because, on a structural point of view, they mainly differ by the position of a proton in the crystal lattice. The position of a proton across an hydrogen bond (and so the cocrystal or salt nature of the solid) can further be influenced by some parameters such as temperature. [43]
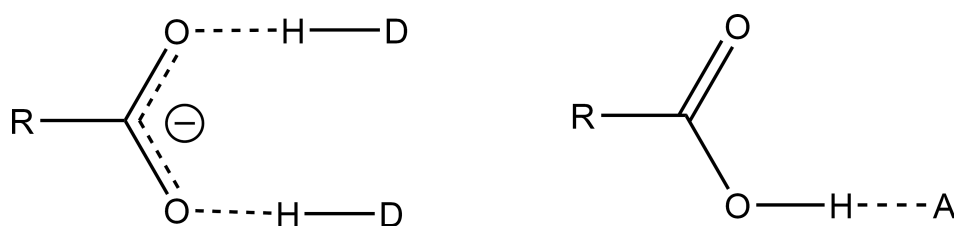
FIGURE 1.4: Carboxylate is a more demanding H-bond acceptor than carboxylic acid.

On other aspects, some differences are however interesting to notice between cocrystals and salts. First, salts implying a carboxylate moiety have a higher tendency to result in structures with unexpected stoichiometry than their cocrystal equivalents (i.e., a cocrystal with a molecule bearing a carboxylic acid group). This is most probably because the carboxylate moiety is more prone to interact with two H-bond donors than carboxylic acid which is a less demanding H-bond acceptor. In consequence, if a second H-bond donor is not available to interact with the carboxylate, a second molecule of the partner bearing the carboxylic acid (or a H-bond donating solvent) could be included in the structure, resulting in a cocrystal of salt (or a solvated salt) instead of a simple salt [44] (Figure 1.4). Then, intermolecular interactions between partners are expected to be stronger in a salt (because of the presence of charge-assisted H-bonds and electrostatic interactions), than in a cocrystal. Finally, salt stability is dependent on pH conditions. For example, in the solid state, the use of basic or acidic excipients can result in salt disproportionation because of the modification of the microenvironmental pH that they induce. Such dependence of stability with pH is not expected for non-ionizable compounds forming cocrystals. For salts, a solubility-pH dependence is also expected. This aspect will be further discussed at the end of this manuscript.

1.5.2   Salt/cocrystal screening in the drug development process

Search for salts and cocrystals is typically performed at different stages of the drug development process. In the early stage, the aim is to quickly find a solid form with suitable physico-chemical properties (crystallinity, hygroscopicity, solubility, *etc.*) to allow the compound to be used in further stages. [39]

In the late phase development, the objective is to find a form that will be further formulated, and which must therefore be stable when exposed to the formulation process (micronization, blending, *etc*). In consequence, the experiments are designed according to the conditions of the process to which the solid form will be subjected. These experiments further allow to anticipate the potential risks associated with this process such as, for example, the change of polymorphs or salt disproportionation. [39]

1.5.3   Salts and cocrystals: selecting ionic/molecular partners

Depending on the presence or absence of ionizable sites on the drug of interest, scientists can either prepare salts or cocrystals. In the context of the preparation of drug-drug salts/cocrystals, the counter ion or coformer is another API. It is often considered that a ΔpKa (pKa of base - pKa of acid) value superior or equal to 3 (4 according to Cruz-Cabeza) will result in salt formation while a ΔpKa inferior to zero (-1 according to Cruz-Cabeza) will result in a cocrystal. In the 0-3 (-1 - 4) ΔpKa range, either a salt or a cocrystal can form. [45, 46, 39] However, one has to remind that pKas are determined in solvent medium and more often in water and not in the solid-state. Therefore, the crystal packing can have a significant impact on the probability of proton transfer between two compounds in the solid-state. [40, 45] In pharmaceutical development, the properties of the solid form are more important than its nature (salt or cocrystal), although the nature of the solid matters in terms of compound filing. In consequence, many compounds tested as counter-ion in salt screening can also be included in cocrystal screening (such as weak carboxylic acids for example) to increase the chance of finding a solid with desired properties. [47] Usually, the design of cocrystals is based on the identification of supramolecular synthons. The latter can be considered as the connectors between molecules and are defined as follows: [48]

> *'Structural units within a supermolecule which can be formed and/or assembled by known or conceivable synthetic operations involving intermolecular interactions.'*

Several other methods and descriptors have been identified to assist in cocrystal prediction. For example, Fábián has shown that the majority of cocrystals deposited on the Cambridge structural database (CSD) are formed between molecules having similar polarity and shapes (i.e., flat molecules tend to cocrystallize with other flat molecules). [49, 50] Here we will focus on knowledge-based methods, and more particularly on these relying on hydrogen-bonds.

Hydrogen bonds are most commonly considered when selecting coformers, due to the relative strength and directionality of these intermolecular interactions. Etter was the first to propose rules to predict the most plausible H-bond interactions between different molecules in a crystal packing [51]. She established the following three rules:

- All good H-bond donors and acceptors are used to form H-bonds.

- When a 6-membered ring can be formed *via* intramolecular H-bonds, this intramolecular bonding is favoured over intermolecular H-bonds.

- The best H-bond donors and acceptors that are not already involved in intramolecular H-bonds, form intermolecular H-bonds with one another.

These rules require to identify the best H-bond donors and acceptors (and thus their relative strength). This can be done on the basis of the crystal structures already available on the CSD. Several knowledge-based methods relying on hydrogen-bonds have been proposed to predict cocrystal formation (such as hydrogen-bond coordination and hydrogen-bond propensity). [52]

The hydrogen-bond coordination method consists of determining the relative probability of observing a coordination number (i.e., the number of non-covalent interatomic contacts involving an H atom) for each of H-bond donor and acceptor. To determine if a cocrystal can form, the donor and the acceptor with the highest coordination number are combined. If best donor and acceptor pair belong to API and coformer then a cocrystal is considered as possible. On the contrary, if best donor and acceptor both belong to the API (or to the coformer) crystallization of individual parent compounds is expected. [53, 52, 50]

The hydrogen-bond propensity method relies on the previously determined structures that were deposited on the CSD to predict which donors and acceptors form H-bond with one another. Using the CSD as a data source, relevant crystal structures are searched based on their chemical similarity with the target molecules (for example, molecules A and B). These structures are used as a training set. In the target molecules (A and B), hydrogen bond donors and acceptors are identified. The data extracted from de training set are then used to calculate a probability (the propensity) of H-bond formation for each H-bond donor-acceptor pair. [54, 55, 56] To apply this method for cocrystal prediction, H-bond propensities (i.e., a score between 0 and 1) is calculated for all donor and acceptor pairs of the target molecules. To evaluate the probability of cocrystal formation a score is determined to compare the likelihood of hetero-interactions *vs.* homo-interactions. To this aim, only the best hetero-interaction (A-B H-bond with the highest propensity) and homo-interaction (A-A or B-B H-bond with the highest propensity) are considered (Table 1.1): [57, 58]

$$Score = Propensity_{best\ hetero-interaction} - Propensity_{best\ homo-interaction}$$

TABLE 1.1: Illustration of multi-component H-bond propensity calculation result.

Best A:A interaction	Best B:B interaction	Best A:B interaction	Score	Cocrystal?
0.25	0.10	0.32	0.07	yes
0.13	0.29	0.20	-0.09	no

A positive score indicates that cocrystallization is favourable, while a negative score means that homomeric interactions are more likely than heteromeric ones. [54, 55, 56, 57, 58]

Computational methods can also be useful when dealing with salts but are often considered as more challenging for salts than for cocrystals because of the presence of long-range ionic interactions and polarization effects. [39]

1.5.4 Salts and cocrystals preparation techniques

Several techniques (solvent-mediated or solid-state methods) are commonly used for salts and cocrystal screening and many parameters (often related to the nature of the solvents and of the API/coformer) can influence the obtained solid form. Usually, the screening technique to be selected is dependent on the APIs that are investigated, the objective of the screening and the development stage. For example, a solvent-mediated *in situ* salt screening, in which a basic solid API is dispersed in an acidic aqueous solution may be challenging if the API is highly soluble in water. Indeed, in such case, saturation of the salt may be difficult to achieve. Furthermore, if this screening technique aims at determining aqueous solubility of the salt directly from the screening medium, then only water is possible as solvent (as the addition of organic solvent would result in solubility data that do not reflect the real aqueous solubility). This would limit the screening to aqueous soluble acids as potential counter-ions. Furthermore, depending on the selected method, amorphous or metastable/kinetically stable salts or cocrystals may be favoured. This is the case, for example, with methods relying on rapid evaporation of organic solvent whereas solvent-mediated methods may facilitate the identification of thermodynamically stable forms (because the solid can be aged several days in the solvent). [59] Commonly used techniques for the preparation of salts and cocrystals can be classified as solution-based (i.e., the method necessitates a large excess of solvent) and solid-state (i.e., methods for which no or a little amount of solvent is required). [60] For each of these classes, some techniques are briefly described in the next sections.

1.5.4.1 Solution-based techniques

Several solution-based techniques exist and some of these are described hereafter.

Solvent evaporation This method consists in preparing a solution containing the target compounds (API-coformer or API-API in case of drug-drug salt/cocrystal preparation). It is then concentrated by evaporating the solvent to allow crystal nucleation and

growth. This method is often used with the aim of harvesting large crystals suitable for single-crystal X-ray diffraction (SCXRD). In such a case, slow evaporation is usually preferred in order to promote crystal growth over nucleation (to reach less but bigger crystals). Solvent evaporation can be performed by evaporating the solvent upon ambient conditions, but it can also be assisted by rotary evaporation under vacuum or at elevated temperature. Rapid evaporation may be used to yield powder samples. For cocrystallization, if the two starting materials have different solubility in the selected solvent, non-equivalent concentrations of these components should be used to reach saturation. This method is relatively simple to set up, but it has some limitations. For example, crystallization of unwanted solvates or of starting materials (especially if these are less soluble than the cocrystal) can occur. [61, 62, 63, 64]

Slurry crystallization Slurry crystallization does not require full solubilization of the compounds (API-coformer or API-API in case of drug-drug salt/cocrystal). Instead, it involves suspending and stirring the components. This method requires that an excess solid remains throughout the experiment. This technique relies on the solution-mediated phase transformation process. The starting materials coming into contact with the solvent dissolve to some extent depending on their respective solubility. When the cocrystal starts to nucleate and grow, the starting materials dissolve again and the process continues. [60, 65, 64]

Sonocrystallization The application of ultrasound to a solution containing the raw materials increases the nucleation rate due to the cavitation energy resulting from ultrasonic waves. This often results in the crystallization of smaller crystals with a more homogeneous size distribution than is generally achievable by other methods. [66, 67]

Cooling crystallization This technique takes advantage of the temperature dependence of solubility. Indeed, cooling of a saturated solution usually leads to supersaturation, thus allowing crystal nucleation and growth. [68, 69, 64, 70]

Crystallization by the anti-solvent method This method consists in achieving supersaturation by adding a solvent (in which the product is sparingly soluble) into a solution of the starting materials (API-coformer or API-API). This technique requires finding a suitable antisolvent (in which the desired product has a low solubility) that is miscible with the selected solvent. [61, 71, 72].

Spray drying An undersaturated solution or a slurry of the starting materials is atomized (by dispersion through a nozzle for example) to yield fine droplets. The latter are ejected into a drying chamber to form dry particles by evaporation of moisture by a hot gas stream. This technique generally allows control of particle size, shape and density. It also has the advantage of allowing both low and large scale production. [73, 74, 75]

Freeze drying   A rapidly frozen solution is subjected to a high vacuum to allow solvent sublimation. This usually yields amorphous forms. If their glass transition temperature is at or below room temperature the amorphous forms can crystallize. On this basis, Eddleston et al. have successfully prepared cocrystals by freeze-drying. [76] Crystallization from an amorphous phase has the advantage that there is no crystalline seed of the starting material. However, crystalline forms of the starting materials can also be obtained from this amorphous phase. This can be the case if nucleation rate of the starting materials is higher than the one of the cocrystal. Solvents that can be used are however limited to those for which the apparatus is resistant. [76]

Supercritical fluid techniques   Supercritical fluids have properties of both gases and liquids and are obtained by compression and heating a gas, such as CO_2. Supercritical fluids may be used either as solvents, as antisolvents or as atomizing fluids in spray drying for example. In the first case, the starting materials are dissolved in the supercritical fluid and depressurization allow supersaturation, potentially leading to cocrystallization/salification. If the desired product is sparingly soluble in the supercritical fluid, the latter can be used as antisolvent and mixed with a solution containing the starting materials (in this case the supercritical fluid has to be miscible with the solvent). [64, 77]

1.5.4.2   Solid-state techniques

One of the best-known solid-state cocrystallization/salification methods is grinding which is itself diversified into neat, and liquid- or polymer-assisted grinding. In this section, these and other solid-state techniques are described such as contact cocrystallization/salification and methods derived from extrusion.

Contact method   Some cocrystals have been reported to form spontaneously upon mixing of their components. [78, 79, 80, 81] Grinding the components prior to mixing or exposing the reagents at higher temperature and relative humidity can increase the cocrystallization rate. [82, 83, 84]

Neat and liquid-/polymer-assisted grinding   Neat grinding (NG) consists of applying a pressure by grinding, either manually (with a mortar and a pestle) or mechanically (with a ball mill apparatus for example) on a dry solid consisting of a mixture of the API and its counter-ion/coformer. [85, 86, 87] Dry grinding may however yield (partial) amorphous content, or lead to incomplete conversion to the salt/cocrystal or to crystal defects. Usually, dry grinding is performed with stoichiometric amounts of the reactants as an excess of any one of them would require additional purification steps to isolate the cocrystal/salt. However, attempts are often performed in various molar ratios in order to explore the solid-state landscape (i.e., formation of other salts/cocrystals with different stoichiometry). Liquid-assisted grinding (LAG) involves adding a small amount of solvent, which plays a catalytic role. The addition of a few drops of solvent usually leads to increased formation kinetics (probably by wetting the solid and facilitating diffusion

of the components) and can also give salts/cocrystals in systems for which NG fails. [88] LAG also generally results in solid with higher crystallinity than NG but it can also lead to the formation of undesired solvates. [88, 89] Polymer-assisted grinding (PolAG), using either solid or liquid polymers, has been proposed as an alternative to LAG with the aim of avoiding solvate formation while positively influencing the properties of the salt/cocrystal as polymer can also be used for API formulation. [90] An advantage of the grinding techniques (NG, LAG or PolAG) is that a powder is obtained at the end of the process (it is not necessary to isolate the solid from a liquid phase as in solution-based method). This powder can then be directly analyzed by powder X-ray diffraction (PXRD) to determine if the process has yielded a crystalline or an amorphous phase and if the crystalline phase is new or not (by comparing the obtained pattern with the starting materials and their known polymorphs). This analysis can also provide information about partial conversion/excess amount of the reactants. This advantage may also be considered as a disadvantage if the crystal structure has to be determined by single-crystal X-ray diffraction, since in this case recrystallisation has to be performed (which requires solution-based techniques). [85] The powder obtained from grinding experiments can however be used as seeds for recrystallization.

Extrusion   Extrusion technology is a mechanical mixing procedure performed in a continuous process, which allows for easier scaling than grinding. [91, 92, 93] Distinction should be made between single/twin screw extrusion and hot melt extrusion. The former is carried out at a temperature at which the reactants do not melt whereas the latter requires the reactants to melt. [60] More particularly, single/twin screw extrusion consists in one/two rotating screw(s) in a barrel, allowing simultaneous mixing and movement of the reactants along the barrel. Hot melt extrusion is a similar technique combining melting and mixing of raw materials. [94] Liquid-assisted extrusion techniques in which a small amount of solvent is added during the process are also reported. [95] Similarly Boksa *et al.* reported matrix-assisted hot melt extrusion cocrystallization, in which a matrix is first mixed at the solid-state with the starting materials (API and coformer) and then subjected to extrusion. [96] The special feature is that the temperature is selected so that only the matrix becomes fluid during the extrusion process. The matrix thus acts as a solvent, improving mixing and reducing shear stresses, while producing matrix-embedded cocrystals. [96]

Crystallization from the melt   This method involves melting of the API and the coformer followed by slow cooling during which cocrystallization can occur. To improve mixing of the components, the starting compounds can be ground. Based on this, Zhou *et al.* investigated cocrystal stoichiometric diversity by differential scanning calorimetry performed at low heating rate and by hot stage microscopy. [97]

Sublimation   This technique consists in heating the starting materials to allow them to sublimate. As the starting materials can have very different sublimation temperatures, a special apparatus allowing different heating temperatures has to be used. For example a

glass system with two glass bulbs linked together by a U tube can be used to allow the vapours mixing and cocrystallization in different parts of the apparatus, depending on the sublimation temperature of the cocrystal. [98]

Spray congealing Consisting in a hybrid technology between hot melt extrusion and spray drying, spray congealing is performed by atomizing a melted mixture of the starting components (instead of a solution or slurry as in conventional spray drying). The droplets resulting from atomization are then cooled and the formed particles are then separated from the cooling gas and collected. Spray congealing has the advantage of being a scalable solvent-free method (unlike spray drying) that allows for particle engineering. However, as any melt-based method, care must be taken with heat sensitive compounds that may degrade at the temperature required for melting. [99]

NG, LAG and slurry techniques are usually preferred for rapid screening [14] and mechanochemistry (NG and LAG) is often recognized as being more efficient than solution and melt based methods for salt/cocrystal screening. [89].

1.5.5   Salts and cocrystals characterization techniques

Several analytical techniques can be used to characterize solids, including salts and cocrystals. These include microscopy, X-ray diffraction techniques (powder X-ray diffraction (PXRD) and single-crystal X-ray diffraction (SCXRD)), thermal and gravimetric analyses (differential scanning calorimetry (DSC), thermogravimetric analysis (TGA) and dynamic vapour sorption (DVS)) as well as vibrational (infra-red (IR) and Raman) and magnetic (solid-state nuclear magnetic resonance (ss-NMR)) spectroscopic methods.

1.5.5.1   Microscopy

Several microscopy techniques can be useful to characterize solid samples. Optical microscopy provides researchers with information on crystallite shape, size and colour (the colour of a salt/cocrystal can differ from the one of the starting materials). Birefringence can also be assessed using a polarizing microscope. This phenomenon can also be used between amorphous and crystalline content, as the amorphous sample does not cause birefringence. However, some crystals (e.g., cubic crystals) are isotropic and are not birefringent either. [40, 100]

Hot-stage microscopy (HSM)   combines thermal analysis and microscopy. In principle, the sample is heated at a predefined rate and a camera-microscope records images of the sample during the heating process. [40] This technique allows the detection of small changes and can be coupled with DSC and/or TGA data. HSM allows, among others, to observe desolvation, crystallization, phase transitions, melting, boiling and morphological changes during heating. [40] HSM is often used to identify cocrystallization or salt formation from the melt. In this particular context, the components screened for cocrystal/salt

formation are melted side-by-side and observed under polarized light. The identification of the formation of a new solid with a different melting point at the interface can indicate the presence of a salt or cocrystal. [100]

Scanning electron microscopy (SEM) is a microscopy technique relying on the scanning of a sample surface with an electron beam. The electron-atom interactions result in different signals giving information about surface morphology and composition of the sample. SEM is often used to visualize the morphology of salts and cocrystals. SEM also provides information on particle size and reaches dimensions not observable by optical microscopes.

1.5.5.2 X-ray diffraction

X-ray diffraction performed on either single-crystals (SCXRD) or powder samples (PXRD), is a technique of choice to study crystalline samples. The X-ray diffraction pattern is unique to a specific crystal form and this non-destructive technique is therefore suitable to characterize salts, cocrystals, polymorphs and solvates. [40, 100]

SCXRD is a technique of choice when well-diffracting single-crystals of suitable size (>100 µm) can be grown. SCXRD allows to locate atom positions and thus provides information on chemical structure and conformation, as well as on crystal packing, intermolecular interactions (e.g., H-bonds, stacking) and on the presence of solvent molecules. Information on thermal motion can also be retrieved from SCXRD data. In the particular case of chiral compounds, absolute configuration can also be determined from SCXRD if heavy atoms are present. [40, 100] The hydrogen atom diffracts weakly and the precision on its coordinates and its displacement parameters is therefore less good than for other heavier atoms. In most of the cases we have encountered, we have placed the hydrogen atoms (which are not involved in hydrogen bonds) in calculated positions.As the difference between a salt and a cocrystal depends only on H-atom transfer from one compound to another, the distinction between these two types of solids can be difficult. However, H-atom transfer can be indirectly assessed on the basis of bond lengths, angles and torsion angles. For example, for a carboxylic acid moiety, C-OH and C=O distances are around 1.3 and 1.2 Å, while bond lengths are usually almost equivalent for a carboxylate. [40, 100] Other techniques such as ss-NMR, IR and Raman are often used to distinguish between salts and cocrystals. Neutron diffraction is a technique that can accurately locate H atom position, because neutrons are scattered by the nuclei and not by the electron density, unlike X-rays. However, neutron diffraction facilities are not routinely accessible. [40, 100] Another limitation of SCXRD is that it requires single-crystals, which can be difficult to obtain (and which usually requires solution-mediated crystallization). In addition, several salt/cocrystal synthesis techniques, such as neat or liquid-assisted grinding, generally yield samples with crystallites that are not suitable for SCXRD structure determination. Solution crystallization with crystallites of the batch powder as seeds may result in single-crystals of suitable size for SCXRD. However, it is also possible that the crystal

does not correspond to the crystalline phase of the batch powder, as phase changes may occur in solution (e.g., polymorphic changes, crystallization of starting materials instead of a cocrystal, solvate formation). When single-crystals (or single-crystals corresponding to the batch powder) cannot be grown, structure solution from PXRD data can be an alternative to SCXRD. [100] This approach is however more complicated as explained in the next section.

PXRD is a powerful technique from which a lot of information can be retrieved, although it provides less structural information than SCXRD. PXRD patterns are unique to a crystalline phase. PXRD identification of a new crystalline phase can thus be achieved by comparison of the powder pattern with those retrieved from a database. Cocrystal or salt formation can also be assessed by PXRD, by comparing the experimental data with the PXRD patterns of the starting materials (and of their polymorphs/solvates). If a structure of the crystalline phase has been obtained, comparison of the calculated powder pattern from SCXRD data with the experimental PXRD pattern allows to conclude on the crystal structure of the batch powder. PXRD also provides information on cocrystal/salt yield and purity. Phase transition upon heating (variable-temperature powder X-ray diffraction (VT-PXRD)) or humidity exposure (variable-humidity powder X-ray diffraction (VH-PXRD)) can also be studied by equipping X-ray powder diffractometer with temperature or humidity controlled chambers. [100]

PXRD data can also be used for structure determination, but it is less straightforward and the success rate is lower than from SCXRD data. This can be attributed to the loss of information, as in a PXRD pattern, the three-dimensional information is compressed into one dimension. Peak overlapping may further complicate the situation. The quality of the powder sample (in terms of purity, crystallite size/preferred orientation) and the choice of instrument parameters (choice of radiation, wavelength and geometry) can have a significant impact on data quality and so on the success of structure determination. [101] Structure solution from PXRD data is often facilitated by the use of other techniques. For example, ss-NMR can provide information on the number of independent molecules in the unit cell, on disorder, on H-bond interactions and on the salt or cocrystal character of the solid. [40] Thermal methods such as TGA and DSC can also provide useful information about the presence of solvent or water molecules in the structure.

1.5.5.3 Thermal and/or gravimetric analysis

Thermal characterization methods measure the evolution of a property as a function of heating or cooling. TGA and DSC are two thermal analysis techniques often performed for solid sample characterization. DVS is often used in the pharmaceutical field to evaluate sample hygroscopicity.

TGA is a thermal and gravimetric method (measure of mass changes upon heating/cooling). This technique is often used to characterize solvates and hydrates. The amount of solvent or water present in a sample can be determined from the weight loss observed

upon heating. TGA can be coupled to SCXRD data to determine the stoichiometry of solvates/hydrates. Information on the strength of solvent/water interactions can also be deduced. For example, if some solvent/water molecules interact through strong H-bonds with the solid, a higher temperature of desolvation/dehydration can be expected in comparison to a solvate/hydrate in which solvent/water molecules are not strongly bound to the solid. TGA also provides information on sample degradation. TGA can be coupled to a mass spectrometer to identify the released volatile components. [102, 100]

DSC measures the difference in heat required to raise the temperature of a sample and a reference. The DSC curve therefore displays the endothermic and exothermic events (i.e., when the sample needs respectively more or less heat to raise its temperature compared to the reference). Exothermic and endothermic events are associated with phase transitions. For example, at its melting temperature, a sample will need more heat than the reference to reach the same temperature because it absorbs latent heat to melt. Some other transitions, such as crystallization, are exothermic and therefore require less heat than the reference to reach the same temperature. Melting, solvent evaporation, polymorphic transformations, (re)crystallization or decompositions are different processes that can be followed/identified by DSC. [100] Thermal properties of salts and cocrystals are often different from those of the starting materials. DSC analysis can be coupled with TGA, HSM, VT-PXRD to help in the interpretation of the endothermic and exothermic events observed on the DSC curve.

DVS is a gravimetric technique that measures the amount and kinetics of water (or solvent) absorption by a sample. The sample is exposed to a known vapor pressure of water (or solvent) at a constant temperature and the changes in sample mass are measured by a microbalance. The vapour pressure evolves in a stepwise manner and for each vapour pressure step a gravimetric equilibrium has to be reached before starting the next step (increase or decrease in vapor pressure). The isotherms are constructed by plotting the measured equilibrium masses against vapour pressure (or relative humidity if water is used as solvent). The plot of mass change (and vapour pressure) against time gives information on sorption kinetics. DVS can be used to study the stability conditions of hydrates or solvates as well as vapour-induced phase changes (crystallization, deliquescence). [103] Combination of DVS data with VH-PXRD can help to understand anhydrate-hydrate transformations. [104]

1.5.5.4 Spectroscopy

Infra-red (IR) and Raman are two vibrational spectroscopy techniques. IR measures the absorption of infra-red radiation while Raman spectroscopy measures its inelastic scattering. In both techniques a characteristic spectrum is obtained as a function of the bonds stretching and bending frequencies. Both IR and Raman spectroscopy are commonly used to study H-bonding and differentiate between a salt and a cocrystal because the vibrations are affected by proton transfer. [100, 40]

Solid-state nuclear magnetic resonance (ss-NMR) is a non-destructive spectroscopic technique that probes the electronic environments of the studied nuclei (^{13}C, ^{15}N, ^{19}F, ...). ss-NMR provides thus structural and dynamical information. However, ss-NMR can suffer from line broadening (and, depending on the studied nuclei, low sensitivity), resulting in a loss of resolution. The cross polarization/magic angle spinning solid-state nuclear magnetic resonance (CP/MAS ss-NMR), which overcomes these drawbacks, has made ss-NMR more popular for the physico-chemical characterization of solids. CP/MAS ss-NMR is often combined with PXRD for structure determination. [105, 100] ss-NMR can also be used to distinguish between salts and cocrystal, by studying ^{13}C or ^{15}N chemical shifts, for example, when the API has carboxylic and nitrogen containing functional groups. Indeed, ^{13}C signal of a carboxylic/carboxylate group shifts to higher frequencies upon $O-H\cdots N$ H-bond formation (3-7 ppm), with a maximum shift (6-7 ppm) for charge-assisted $N^+-H\cdots O^-$ H-bond. [40] Quite small ^{13}C shifts can however be observed between a neutral or a ionic state. This is particularly the case if, at the neutral state, the carboxylic group is involved in strong H-bonds (e.g., COOH dimers which typically have ^{13}C chemical shifts about 2 ppm lower than a carboxylate group). [40] ^{15}N chemical shifts are more sensitive to proton transfer than those of ^{13}C because nitrogen can be directly involved in the H-Bond (as donor or acceptor), unlike carbon, and also because nitrogen protonation leads to large chemical shifts (50 to 100 ppm lower frequencies for aromatic ^{15}N and up to 25 ppm for aliphatic ^{15}N). [40] However, its low magnetogyric ratio and low natural abundance, may result in long ^{15}N data acquisition time. In addition to chemical shift analysis, other technologies such as non quaternary suppression (NQS), which supresses signals of non-quaternary nuclei, are useful for the interpretation of ss-NMR spectra. ss-NMR also proves to be useful for solvate characterization as only the signals of bound solvents are detected under cross polarization conditions. [100]

1.5.6   Recently reported drug-drug crystalline complexes

From a publication point of view, as well as when considering currently marketed drugs, it appears that drug-drug cocrystals remain much rarer than pharmaceutical cocrystals (combining a drug and a GRAS compound). However, the approval of Entresto by both the FDA and EMA in 2015 may have well boosted the research for drug-drug cocrystals both in academia and in pharmaceutical companies.[106, 107] To date, Entresto (marketed by Novartis) is, to the best of our knowledge, the only drug-drug cocrystal approved by the authorities and on the market. This hydrated cocrystal combines the sodium salts of sacubitril and valsartan and is used to treat heart failure. The combination of the two drugs allows for a better biological response and the cocrystal form increases the bioavailability of valsartan (allowing a reduction of the administered dose). [107]

Drug-drug salts also seem to be quite rare despite the approval of dimenhydrinate before 1982. Dimenhydrinate is a drug-drug salt used for the treatment of motion sickness.

It combines diphenhydramine and 8-chlorotheophylline. Diphenhydramine is an antihistamine that induces sleepiness. This side effect is countered by the second component of dimenhydrinate, 8-chlorotheophylline, which is a stimulant.

In July 2019, FDA accepted to review a new drug application for a cocrystal of salt combining tramadol hydrochloride with celecoxib (Esteve). [108] This cocrystal, first reported in 2017 was discovered after thousands of experiments aiming at cocrystallizing potential pairs of drugs. [109, 108] It results in an increased intrinsic dissolution rate for celecoxib (which is currently the rate-limiting step for its absorption) and a slower tramadol release (which is believed to improve its tolerability). The improved pharmacokinetic profile of this cocrystal results in greater analgesic efficacy even at lower doses than those usually prescribed for these drugs. This recent new drug application illustrates the current interest in drug-drug cocrystals/salts.

In this section we report drug-drug salts and cocrystals that were recently published. Drugs constituting these salts/cocrystals as well as the change in properties resulting from the preparation of these solid forms are listed in Table 1.2.

TABLE 1.2: Drug-drug salts and cocrystals reported between 2018 and April 2021.
† Salt according to distances reported in crystallographic information file (but reported as cocrystal in the article). ‡ Hydrogen positioned at almost equal distance of acidic and basic sites. * Structure first reported before 2018 but further studied between 2018 and 2020. § No crystallographic data available (no 3D coordinates available).

Drug 1 - Drug 2	Property change	Salt or cocrystal?	Ref.
	Published in 2021		
Temozolomide (TEM) - Hesperetin (HES)	Improved hygroscopic stability of HES, improved tabletability of TEM and increased dissolution of HES and TEM	cocrystal	[113]
Carbamazepine (CBZ) - Emodin (EMO)	decreased CBZ solubility and intrinsic dissolution rate	cocrystal	[114]
Carbamazepine (CBZ) - Paenol (PAE)	increased CBZ solubility but decreased intrinsic dissolution rate	cocrystal	[114]
Lamotrigine (LTG) - Theophylline (THP)	slower LTG dissolution rate but increased hygroscopic stability	hydrated cocrystal	[115]
Sulfamethazine (SMA) - Diclofenac (DCF)	decreased SMA solubility	salt	[116]
Sulfamethazine (SMA) - Piperazine (PPZ)	no significant SMA solubility change	cocrystal	[116]
Diclofenac (DCF) - Metformin (MET)	improved DCF solubility, dissolution rate and permeability	salt	[117]

Drug 1 - Drug 2	Property change	Salt or cocrystal?	Ref.
Piroxicam (PXM) - Norfloxacin (NFX)	improved PXM solubility	solvated salt	[118]
Tenoxicam (TNX) - Ciprofloxacin (CIP)	improved TNX solubility	solvated salt	[118]
Meloxicam (MLX) - Ciprofloxacin (CIP)	improved MLX solubility	solvated salt	[118]
Lornoxicam (LNX) - Norfloxacin (NFX)	improved LNX solubility	hydrated solvated salt	[118]
Published in 2020			
Carvedilol (CAR) - hydrochlorothiazide (HCT)	improved CAR dissolution and solubility	cocrystal §	[119]
Erlotinib (ETB) - Furosemide (FSM)	increased FSM and decreased ETB solubility	salt†	[16]
Gefitinib (GTB) - Mefenamic acid (MFN)	increased MFN and decreased GTB solubility	cocrystal‡	[16]
Progesterone (PROG) - Phloroglucinol (SPF)	improved SPF hygroscopic stability and PROG solubility	cocrystal	[17]
Ethionamide (ETH) - Salicylic acid (SALA)	increased ETH dissolution rate	both reported	[120]
Trimethoprim (TMP) - Mefenamic acid (MFA)	improved TMP and MFA solubility	salt	[121]
Trimethoprim (TMP) - Tolfenamic acid (TFA)	improved TMP and TFA solubility	salt	[121]
Trimethoprim (TMP) - Flufenamic acid (FFA)	improved TMP solubility	salt	[121]
Sulfamethazine (SFZ) - Flufenamic acid (FFA)	improved SFZ and FFA solubility	cocrystal	[121]
Sulfamethazine (SFZ) - Niflumic acid (NFA)	no solubility improvement	cocrystal	[121]
Furosemide (FS) - Hexamethylenetetramine (HTEM)	improved FS solubility	salt	[122]
Furosemide (FS) - Amantadine (AMD)	improved FS solubility	salt	[122]
Furosemide (FS) - Isoniazid (INZ)	decreased FS solubility	cocrystal	[122]
Metformin (MET) - Salicylic acid (SALA)*	improved tabletability	cocrystal	[37, 123]
Metformin (MET) - Rosiglitazone (RSG)	improved RSG dissolution and anticancer activity (liver cells)	salt	[124]
Febuxostat (FBX) - Piroxicam (PXM)	improved PXM solubility, improved compressibility	cocrystal	[125]
Efavirenz (EFV) - Zidovudine (AZT)	improved EFV and AZT solubility	cocrystal§	[126]
Nevirapine (NVP) - Efavirenz (EFV)	improved NVP and EFV solubility	cocrystal§	[126]

Drug 1 - Drug 2	Property change	Salt or cocrystal?	Ref.
Olanzapine (OLN) - Nateglinide (NAT)	not determined	amorphous salt	[127]
Olanzapine (OLN) - Pyrazinoic acid (PZO)	improved solubility	salt	[127]
Sulfathiazole (SUZ) - Amantadine HCl (AMDH)	improved solubility, dissolution, permeability and antibacterial activity	cocrystal	[128]
Sulfathiazole (SUZ) - Amantadine (AMD)	improved solubility, dissolution, permeability and antibacterial activity	salt	[129]
Diflunisal (DIF) - Pyrazinamide (PZA)*	improved DIF solubility	cocrystal§	[130, 131]
Prothionamide (PRN) - Salicylic acid (SALA)	improved dissolution of PRN	cocrystal	[132]
Piperazine (PRZ)-Ferulic acid (FLA) - Pyrazinamide (PZA)	decreased dissolution rate and solubility of PRZ-FLA	cocrystal of salt	[133]
Nevirapine (NVP) - Salicylic acid (SALA)*	not determined	cocrystal	[134, 135]
Trimethoprim (TMP) - Nitrofurantoin (NFT)	improved NFT solubility and improved antibacterial activity (against *E. coli*)	anhydrous and solvated cocrystal and hydrated salt	[136]
Aripiprazole (APZ) - acetylsalicylic acid (ACS)	improved APZ dissolution rate	salt	[137]
Aripiprazole (APZ) - 4-aminosalicylic acid (PAS)	improved APZ dissolution rate but decreased solubility	salt	[137]
Furosemide (FSM) - 5-fluorocytosine (5FC)	improved FSM solubility, intrinsic dissolution rate and permeability	hydrated cocrystal	[138]
Published in 2019			
Olmesartan medoxomil (OLM) - Hydrochlorothiazide (HCTZ)§	OLM and HCTZ decreased dissolution rate	cocrystal	[139]
Glimepiride (GLI) - Metformin (MET)	improved MET stability and hygroscopicity, GLI solubility and dissolution rate	salt	[140]
Metaxalone (MTX) - Salicylamide (SLM)	not determined	cocrystal	[141]
Tolbutamide (TOL) - Metformin (MET)	improved MET stability and hygroscopicity, increased TOL solubility and dissolution rate	salt	[142]
Berberine chloride (BER) - Dihydromyricetin (DMY)	improved anticancer activity	cocrystal	[143]
Flurbiprofen (FBP) - Salicylamide (SLM)	decreased solubility at pH > 6.2	cocrystal	[144]

Drug 1 - Drug 2	Property change	Salt or cocrystal?	Ref.
Ciprofloxacin (CIP) - Salicylic acid (SALA)*	improved CIP solubility at pH 6.8	salt	[145, 146] [147]
Piroxicam (PXC) - Clonixin (CNX)	decreased PXC hygroscopicity	cocrystal	[148]
Carbamazepine (CBZ) - Aspirin (ASP)	not determined	cocrystal	[149, 150]
Famotidine (FAM) - Theophylline (THP)	improved FAM stability at pH 1.2	cocrystal	[151]
Levofloxacin (LVFX) - Metacetamol (MTM)	decreased LVFX hygroscopicity and photodegradation	cocrystal	[152]
5-Fluorocytosine (5FC) - 5-Fluorouracil (5FU)	Good stability at high relative humidity	cocrystal	[153, 154]
Mefenamic acid (MFA) - Piperazine (PPZ)	improved MFA dissolution and PPZ hygroscopicity	salt	[155]
Tolfenamic acid (TFA) - Piperazine (PPZ)	improved TFA dissolution and PPZ hygroscopicity	salt	[155]
Acetazolamide (ACZ) - Piperazine (PPZ)	improved ACZ solubility	salt	[156]
Acetazolamide (ACZ) - Theophylline (THP)	improved ACZ permeability	cocrystal	[156]
Metformin (MET) - Aspirin (ASP)	Improved MET hygroscopicity, decreased MET but increased ASP dissolution rates	salt	[157]
Published in 2018			
Tramadol (TRM) - Celecoxib (CXB)*	increased CXB and decreased TRM dissolution rate, synergistic antinociceptive effects	cocrystal	[38, 158] [159, 160] [161]
Sulfathiazole (SUZ)- Theophylline (THP)*	improved SUZ solubility at pH between 5.5 and 7	cocrystal	[162]
Sulfathiazole (SUZ)- Sulfanilamide (SNM)*	improved SUZ solubility	cocrystal	[162]
Apremilast (APR) - Aspirin (ASP)	improved solubility and dissolution at pH 2	cocrystal§	[163]
5-Fluorocytosine (5FC) - Isoniazid (INH)	improved stability against moisture	cocrystal	[164]
Theophylline (THP) - Pyridoxine HCl (PYR)	not determined	cocrystal of salt	[165]
Pyrazinamide (PZA) - Fumaric acid (FA) - Isoniazid (INH)	reduced INH but improved PZA solubility, improved pharmacokinetic properties	cocrystal	[166]
Theophylline (THP)- Acetazolamide (ACZ)	not determined	cocrystal	[167]
(S)-Ibuprofen (IBU) - Levetiracetam (LVT)	enantiospecific cocrystallization	cocrystal	[168]
Theophylline (THP) - Aspirin (ASP)	not determined	cocrystal	[169]

Drug 1 - Drug 2	Property change	Salt or cocrystal?	Ref.
Temozolomide (TMZ) - Baicalein (BAI)	improved TMZ chemical stability and improved pharmacokinetic properties	cocrystal	[170]
Emodin (EMD) - Berberine chloride (BER)	improved EMD pharmacokinetic properties and BER hygroscopicity	cocrystal of salt	[171]
Mefenamic acid (MEF) - Acetaminophen (ACM)*	improved MEF dissolution rate	cocrystal §	[172, 173]
Entacapone (ETP) - Acetamide (ACT)	Dissolution rate similar to the one of ETP	cocrystal	[174]
Entacapone (ETP) - Theophylline (THP)	improved ETP solubility	cocrystal hydrate	[174]
Entacapone (ETP) - Pyrazinamide (PZA)	improved ETP solubility	cocrystal	[174]
Entacapone (ETP) - Isoniazid (INH)	Dissolution rate similar to the one of ETP	cocrystal§	[174]
Norfloxacin (NOR) - Diclofenac (DCF)	improved NOR solubility and improved diffusion	salt	[175]
Norfloxacin (NOR) - Diflunisal (DIF)	improved NOR solubility	salt	[175]
Norfloxacin (NOR) - Mefenamic acid (MEF)	no solubility improvement	salt	[175]
Norfloxacin (NOR) - Indomethacin (IND)	improved NOR solubility and improved diffusion	salt hydrate	[175]

This search does not include patents on drug-drug cocrystals. A review of patents dealing with pharmaceutical cocrystals was carried out by Wouters *et al.*. [100] These authors report a few patents relating to drug-drug cocrystals prior to 2018 (association of temilsartan and beta blockers [110], duloxetine and naproxen [111], and patents related to Entresto [112]). As with any search, this one is certainly incomplete and some drug-drug cocrystals or salts published between 2018 and April 2021 may have been missed or omitted (e.g., due to the use of different terminology). However, the results of this search highlight the current interest in cocrystals and salts combining several APIs.

1.6 Challenges associated with the preparation of multidrug salts/cocrystals

One of the major challenges in the preparation of multidrug crystalline complexes is probably the proper selection of at least two drugs whose combination could provide pharmaceutical benefits. Indeed, just as additive/synergistic effects can be observed, it is also possible that antagonistic effects occur as a result of the combination of two drugs. Another difficulty that may be encountered is related to the pharmaceutical dose of the two APIs to be combined. [15, 38] Indeed salt formation and cocrystallization often result in complexes with defined molar ratio (often 1:1, 1:2, 2:1 molar ratios). Therefore, the

combination of two drugs that require administration at significantly different doses can be a problem. Another challenge associated with the occurrence of synergistic effects is the readjustment of the therapeutic dose that may be required. This may make it more difficult to predict the appropriate API ratio for salts/cocrystal preparation. [14] Therefore, the preparation of multidrug salts/cocrystals should ideally be done in several steps and in collaboration with pharmacologists in order to investigate drug interactions and manage potential dose adjustments.

The first step consisting of the preparation of multidrug salts/cocrystals and their physico-chemical characterizations (structure, solubility, thermal stability, stability against water sorption, ...) mainly concerns the solid-state and could be carried out by a chemist. Ideally, the choice of APIs to be combined should be based on pharmacological properties. This is to ensure a potential therapeutic application of the multicomponent crystalline complex. This selection may require the expertise of a pharmacologist. The second step is mainly related to the study of the biological effects of the combination (appearance of synergies, antagonisms, *in vivo* bioavailability assessment) and should preferably be performed by a pharmacologist. The results of these characterizations are crucial to determine if other adjustments at the solid-state are necessary.

This thesis will be devoted to the first step, i.e., the preparation and physico-chemical characterization of the salts/cocrystals. The APIs to combine will be chosen on the basis of literature data and in particular, compounds with potential interesting activities in the context of tuberculosis treatment will be selected.

1.7 System investigated in this work

At the beginning of this thesis, research on the serine pathway in the pathogen *Mycobacterium tuberculosis (M. tb)* was in progress in the laboratory. Thus, compounds involved in the treatment of this disease, including clofazimine (CFZ) which has been described as an inhibitor of the SerB2 enzyme of this pathogen [176], were selected for this work.

1.7.1 Tuberculosis and its treatment

It is estimated that, in 2019, 10 million people developed active tuberculosis (TB) and 1.4 million people died from this disease, ranking TB as the first cause of death from a single infectious agent and among the top ten causes of death worldwide. Tuberculosis is a disease that primilarily (but not exclusively) affects the lungs and is caused by *M. tb* (Koch bacilli). TB is spread by airborne pathogens and about a quarter of the world's population is infected. Although the infection remains latent in most people, it is estimated that 5-15% of infected people will develop the active form of the disease. [177] A number of factors increase the risk of developing TB, including human immunodeficiency virus (HIV) (18× higher risk), malnutrition (3× higher risk), alcohol abuse (3.3× higher risk), and smoking (1.6× higher risk). [178]

Preventive therapy (administration of isoniazid for 6 months) is available for population groups at higher risk of developing active TB (immunocompromised, people with household contacts with a person suffering from pulmonary tuberculosis). This therapy is not recommended for people with active TB as it may favour the emergence of drug resistance. [179] So far and since 1920s, only one vaccine, bacille Calmette-Guérin (BCG), is licensed for TB prevention. It is however only administered to children and does not prevent from all TB forms. People with TB who are infected with drug-susceptible strains of *M. tb* can be treated with a six-month regimen of first-line antibiotics. This consists of a two-month intensive phase during which four antibiotics are administered (isoniazid, rifampicin, pyrazinamide and ethambutol) followed by a four-month continuation phase during which isoniazid and rifampicin are prescribed (Figure 1.5A). [178] Resistant strains have however emerged and drug-resistant tuberculosis remains a global health issue, with 500,000 rifampicin resistant tuberculosis (RR-TB) new cases detected in 2019, including 390,000 multidrug resistant tuberculosis (MDR-TB) cases. [178] While the success rate is 85% for drug-susceptible TB (with first-line antibiotics), this rate drops to 57% for MDR-TB. These treatments are also longer (on average six to twenty months but it can be even longer), more toxic and more expensive than the first-line one. The duration, complexity, and toxicity of these therapies have deleterious effects on patient compliance. Drug-drug interactions between TB and acquired immune deficiency syndrome (AIDS) therapies further complicate the treatment of HIV positive people. In 2020 the World Health Organization (WHO) reports that twenty-two antitubercular drugs are in clinical trials, including thirteen new compounds, two drugs benefiting from accelerated approval (bedaquiline and delamanid), one recently FDA approved drug (pretomanid) and six already approved antimicrobials (clofazimine, levofloxacin, linezolid, moxifloxacin, high dose rifampicin and rifapentine).

WHO recommends to consider the following steps when elaborating a therapy for MDR-TB (Figure 1.6). Firstly, a latest generation fluoroquinolone (levofloxacin, moxifloxacin or gatifloxacin, Figure 1.5B) should be selected, plus a second-line injectable agent (amikacin, capreomycin or kanamycin, Figure 1.5C) and at least two other second-line agents (ethionamide or prothionamide, cycloserine or terizidone, linezolid and clofazimine, Figure 1.5D). Next, the addition of a first-line agent (pyrazinamide, high dose isoniazid or ethambutol, Figure 1.5A) should be considered if it can enhance the therapy. The next step is to add either bedaquiline or delamanid (Figure 1.5E) and finally, if the treatment cannot be made up in any other way (e.g., because of resistance), another agent among group D3 (4-aminosalicylic acid, imipenem + cilastatin, meropenem or amoxicillin + clavulanic acid, Figure 1.5F) should be selected (Figure 1.6). [180]

1.7.2 Drug repositioning for the treatment of tuberculosis

The emergence of resistant pathogens is due to their genetic evolution and this phenomenon is caused/accelerated by inadequate drug prescriptions or poor patient compliance. The treatment of tuberculosis is further complicated by the existence of different
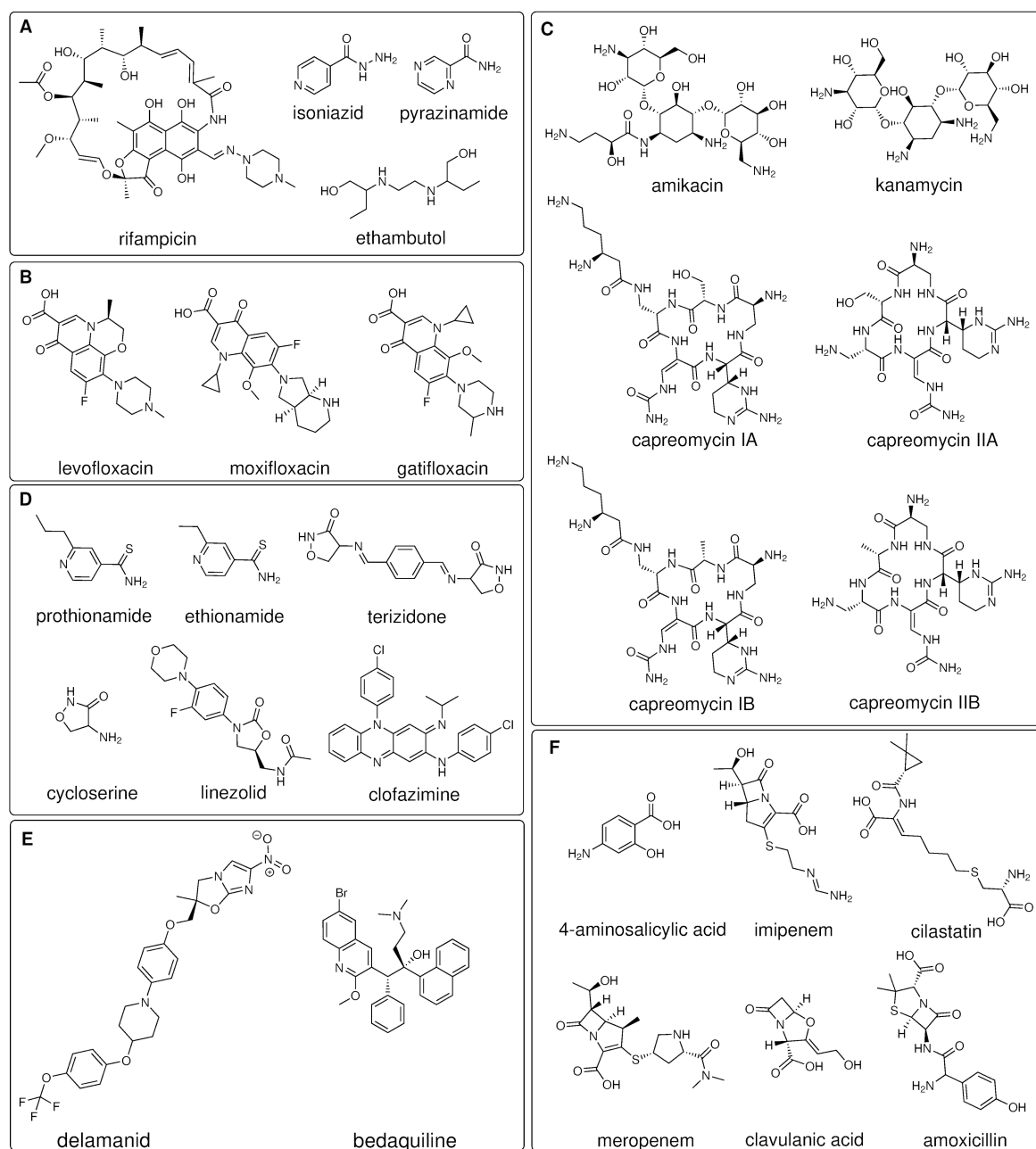
FIGURE 1.5: Chemical formula of selected TB drugs. A: first line drugs, B: last generation fluoro-quinolones, C: second-line injectable agents, D: other second-line agents, E: bedaquiline and delamanid and F: other agents recommended by the WHO.

forms of the disease: a dormant one and an active one. The problem is that the dormant bacilli are resistant to most standard therapies, which lengthens the duration of treatment since it is necessary for the dormant bacilli to enter the active phase in order to be killed. The long duration of tuberculosis therapy further complicates patient compliance. [181]
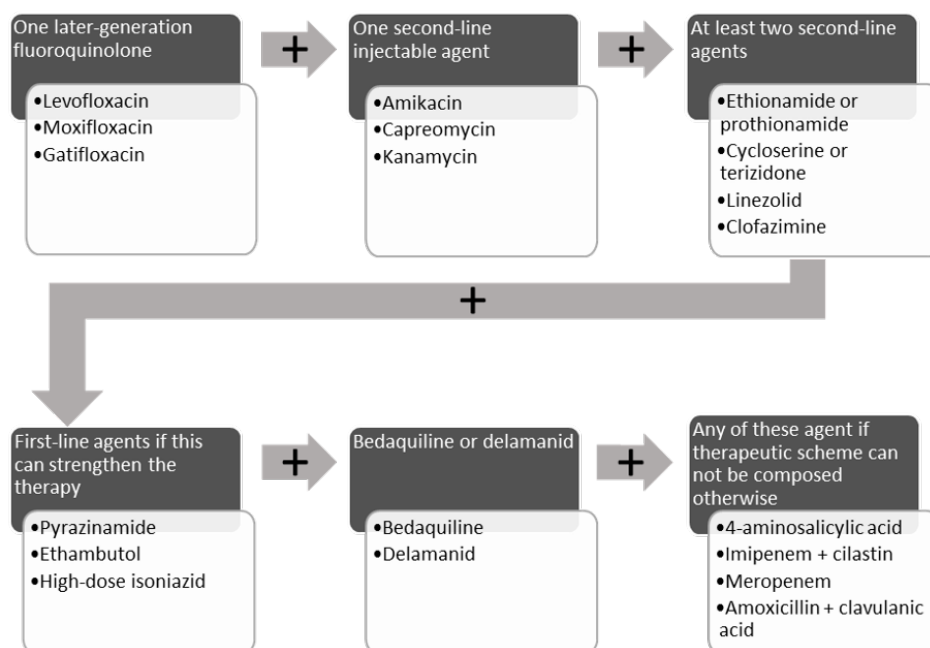
FIGURE 1.6: General workflow according to the WHO for MDR-TB treatment.

Drug repurposing could successfully complement new drug development in order to fight resistant mycobacteria. Host-pathogen interactions could be exploited for the implementation of adjunctive therapy. Drugs that are not themselves bactericidal could therefore be used to modulate host pathways that fight *M. tb*. This could also lead to a synergistic effect with anti-TB drugs. Host-directed therapies are attractive because they do not directly target the pathogen, making them insensitive to the development of resistance within the pathogen itself. [182]

1.7.2.1   Current antitubercular drugs resulting from repositioning

Drug repurposing has already proved to be successful in TB treatment. Fluoroquinolones, targeting topoisomerases and thus interfering with DNA replication, were used as broad-spectrum antibiotics and are currently recommended for TB treatment. Clofazimine (Figure 1.5D), primary used as antileprosy drug, has been repurposed for MDR-TB therapy. Common β-lactams, that were inactive against *M. tb* because of the bacilli β-lactamase, could be reprofiled for TB treatment in combination with clavulanate, a β-lactamase inhibitor (e.g., meropenem + clavulanic acid). Linezolid, originally used against Gram-positive bacteria, was shown to be also active against *M. tb*. [181] Attempts for drug repurposing could further help in the discovery of new anti-TB drugs. This is illustrated by the synthesis of nitroimidazopyrans (e.g., pretomanid) as analogues to nitroimidazofurans, initially developed for cancer therapy and proved active against *M. tb*, but unsuitable because of their mutagenicity. [181]

1.7.2.2   Other potential drugs for pathogen-directed adjunct therapies

Two drugs (entacapone and tolcapone, Figure 1.8) used as adjunctive therapy for the treatment of Parkinson's disease are active against Koch's bacilli at micromolar concentrations. [183] The anti-psychotic thioridazine as well as certain non-steroidal anti-inflammatory drugs (NSAIDs) inhibit mycobacterial growth. [184, 185, 186, 187, 188, 181] Verapamil (Figure 1.8), an antihypertensive agent, has been shown to inhibit efflux pumps of *M. tb* and to improve the activity of the first-line anti-TB drugs. [189, 190, 182, 191, 192] Avermectins, currently known as broad-spectrum antihelminthics have also shown *in vitro* antimicrobial properties. [193, 194]

Some sulfonamide-class antibiotics, such as sulfamethoxazole, have been successfully repositioned to treat MDR-TB, particularly in patients co-infected with HIV and MDR-TB. [195, 196] Sulfonamides are competitive inhibitors of dihydropteroate synthase (Figure 1.7). This enzyme is involved in the folic acid pathway and synthesizes folic acid from p-aminobenzoic acid. While micro-organisms are able to synthesize folic acid from p-aminobenzoic acid, in humans, folic acid is derived from food as we do not have a dihydropteroate synthase. The absence of this enzyme in humans therefore makes sulfonamides selective for micro-organisms. In both humans and micro-organisms, folic acid is then converted by dihydrofolate reductase to tetrahydrofolic acid (Figure 1.7). The latter is involved in several important biologic pathways including the conversion of serine to glycine and of deoxyuridine monophosphate to deoxythymidine monophosphate (itself further implicated in DNA synthesis). Synergism is often observed between sulfonamide and dihydrofolate reductase inhibitors such as trimethoprim or pyrimethamine (Figure 1.8). Actually, the sulfonamide used in the treatment of MDR-TB was prescribed as a fixed drug combination (trimethoprim - sulfamethoxazole, Figure 1.8). [197, 198]
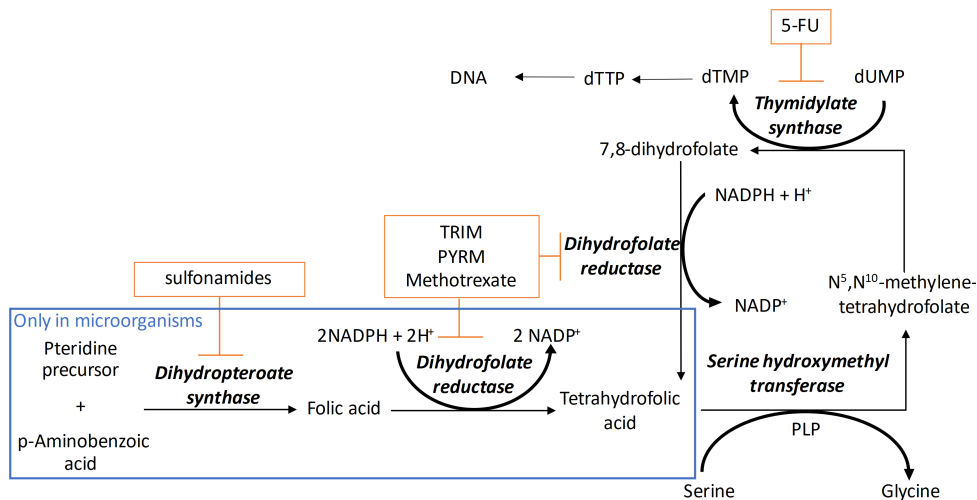
FIGURE 1.7: Effects of sulfonamides and dihydrofolate reductase inhibitors on the folate pathway. TRIM; trimethoprim, PYRM: pyrimethamine, 5-FU: 5-fluorouracil, PLP: pyridoxal 5'phosphate, dUMP: deoxyuridine monophosphate, dTMP: deoxythymidine monophosphate.

1.7.2.3   Potential drugs for host-directed adjunct therapies

Host-directed therapy (HDT), rather than targeting the pathogen, aim to modulate host responses to the bacilli. These therapies have the potential to prevent the emergence of resistance, shorten treatment duration and reduce lung damage. The latter are common and are caused, among others, by the host's inflammatory response. [199] There are two main approaches for HDT development: modulation the host inflammatory response (to reduce lung and tissue damage) and enhancement of the host immune response. [200]

A particularity of *M. tb* is that it can escape the immune response. In particular, after being phagocytozed by a macrophage, *M. tb* causes an arrest in the maturation of the phagosome by neutralizing reactive oxygen species (ROS) and preventing the fusion of the phagosome with the lysosome. These mechanisms prevent the death of the pathogen and increase the life span of the macrophage into which the pathogen has entered. The bacilli then use, among others, the cholesterol of the host to survive. [201] An alternative to conventional immunotherapy is to target pathways indirectly impacting the immune response. Several drugs have been investigated to be repurposed as HDT with this aim. Among these, imatinib, used to treat chronic myelogenous leukaemia [202], the anti-diabetic drug metformin [203, 204, 205] as well as two anticonvulsants (carbamazepine and valproic acid [206, 207, 208], Figure 1.8) have been shown to promote several beneficial host responses (i.e., phagosome maturation and acidification and macrophage autophagy), thereby reducing *M. tb* survival. [182, 199, 200] Another well-known class of drugs, the statins, has shown potential use against *M. tb*. When given in combinations with anti-TB drugs, statins such as simvastatin (Figure 1.8) significantly reduce the bacillary load in the lungs. These compounds act by modulating the intracellular environment in the macrophage, in particular by reducing lipid droplets accumulation and thus the amount of nutrients available for *M. tb*. [201, 209, 210]

In order to reduce the excessive host-inflammation, NSAIDs have been proposed as adjunct host-directed therapy. This is further supported by the fact that some molecules in this family exhibit anti-TB activity [191, 211, 212, 213]. Non-steroidal anti-inflammatory drugs are a family of compounds that inhibit cyclo-oxygenase (COX) enzymes. The latter are responsible for the synthesis of prostaglandin H_2 (PGH_2) from arachidonate in a 2-step reaction. PGH_2 can then be converted to other prostaglandins and thromboxanes. There are two cyclooxygenase isoforms in mammals: COX-1 and COX-2. COX-1 is responsible for the synthesis of prostaglandins that regulate gastric mucosal secretions whereas the prostaglandins that mediate inflammation are synthesized by COX-2. Inhibition of COX-2 helps to regulate inflammation but many NSAIDs are not selective (COX-1 and COX-2 have 60 to 65% amino acid sequence identity and only newer NSAIDs are COX-2 selective), resulting in their known gastric side effects. NSAIDs are also recommended by the WHO to relieve joint pain due to pyrazinamide. [214] Some compounds with anti-inflammatory properties and that have been reported to be of interest in the context of tuberculosis are presented hereafter. Some of these compounds further have pathogen-directed effects.

Diclofenac (Figure 1.8) has been shown to have bactericidal properties on Gram positive and negative bacteria as well as on drug-sensitive and drug-resistant strains of *M. tb*. The bactericidal activity of diclofenac (DCF) on *M. tb* has been demonstrated in both *in vitro* and *in vivo* tests. [215, 216] This molecule also has synergistic effects with streptomycin in a murine tuberculosis infection model. [215] Dutta *et al.* have shown that DCF antimycobacterial activity is further potentiated when administered in combination with other known antitubercular drugs. [215] Its mechanism of action against *M. tb* remains to be elucidated. It was however shown to inhibit DNA synthesis and to have membrane damaging effects on *Listeria*. [216]

Non-replicating forms of *M. tb* are inhibited by oxyphenbutazone (Figure 1.8). Such a compound could therefore potentially shorten the treatment duration as it is these latent forms that are generally more difficult to kill. [191] While oxyphenbutazone itself
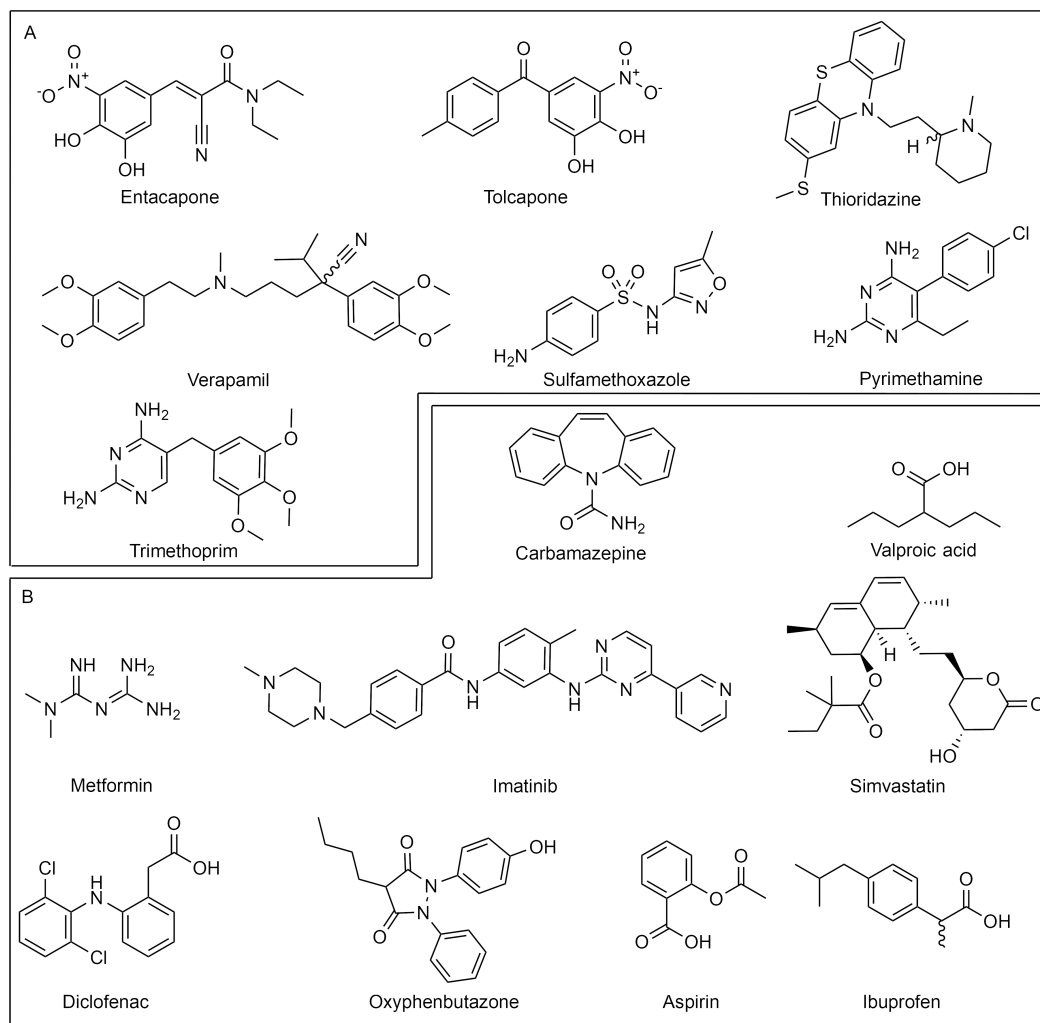
FIGURE 1.8: Potential drugs for: A pathogen-directed and B host-directed adjunct therapies.

has no effect on replicating pathogens, its potential *in vivo* hydroxylation alters its properties leading to the inhibition of both replicative and non-replicative pathogens. [217]. Oxyphenbutazone is not FDA approved and its use in human is limited due to the occurrence of fatal side effects. [191, 218]

Aspirin and ibuprofen (Figure 1.8) have been shown to increase the activity of pyrazinamide in a murine model. [219, 220, 221] Kroesen *et al.* have demonstrated that a low-dose of aspirin is beneficial in a murine model of TB. [222] This model is relevant for active but not latent tuberculosis and the authors suggest that low-dose aspirin should rather be administered to patients with a significant inflammatory response (which is usually the case at diagnosis, but not in patient with latent TB). [222] Inflammation is indeed beneficial in the early stages of the disease (as it helps to control and eliminate the pathogen) but then it becomes detrimental and must thus be controlled. Vilaplana *et al.* have shown that ibuprofen by itself (without other antitubercular drugs) can decrease lung lesions and bacillary load, resulting in improved survival in a murine model. [220] Guzman determined that the carboxylic acid functionality of ibuprofen is essential for its antituberculosis properties. [223] A phase II clinical trial evaluating the efficacy and safety of ibuprofen as adjunctive treatment in patients with extensively drug resistant tuberculosis (XDR-TB) began in 2016 (results not published yet). [224]

1.7.3   Focus on clofazimine

1.7.3.1   Clofazimine spectrum of action and use as an antitubercular drug

Clofazimine (CFZ) (Figure 1.9) is a riminophenazine initially synthesized in 1957 to treat tuberculosis. [225] The currently recommended first-line antibiotics, pyrazinamide discovered in 1952 and ethambutol in 1961, were however preferred to CFZ because of their better efficacy and lesser side effects. The anti-TB properties of the other first-line antibiotics, isoniazid and rifampicin, were discovered in 1950 and 1965 respectively. [226, 227] In 1981, CFZ was repurposed (and is still recommended by the WHO) for leprosy therapy thanks to its antimicrobial and anti-inflammatory properties. [228] The emergence of drug-resistant strains of *M. tb* has led to a renewed interest in this drug. CFZ is currently recommended as a group B agent for TB therapy and it is therefore recommended in the design of MDR-TB/RR-TB treatments. Its anti-tuberculosis effects are not yet well understood and pre-clinical studies are ongoing to investigate these properties. CFZ is further investigated in several phase II or III clinical trials. In particular, a phase III trial is underway in South-Africa to compare the safety and efficacy of a shortened 6-month regimen (including CFZ) to a standard 9-month regimen. [178, 229] The phase II CLO-FAST trial is investigating the ability of CFZ and rifapentine to shorten drug-sensitive TB treatment. [178, 230] CFZ is also included in the phase III endTB and endTB-Q trials aimed at shortening treatments of MDR-TB and fluoroquinolone-resistant MDR-TB. [178, 231, 232]
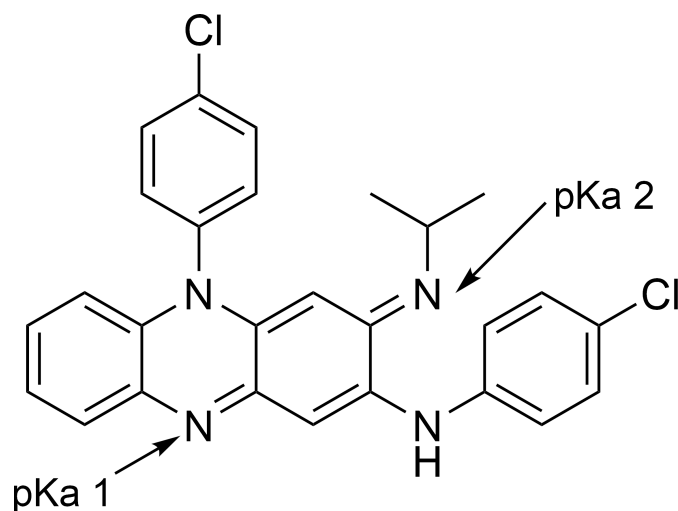
FIGURE 1.9: Chemical diagram of CFZ with its protonation sites depicted by the arrows (pKa 1 = 2.31, pKa 2 = 9.29). [233]

CFZ has been shown to be active against Gram-positive bacteria, several parasites (including *Plasmodium falciparum* and *Leishmania donovani*), and certain mycobacteria such as, *Mycobacterium leprae* and *Mycobacterium tuberculosis*. With regar to *M. tb*, clofazimine has bacteriostatic activity but has weak bactericidal properties. Synergistic effects have been demonstrated between CFZ and ethambutol, pyrazinamide, linezolid, bedaquiline and moxifloxacin. [234, 235, 236, 237]

Clofazimine is currently marketed by Novartis as Lamprene in soft capsules made of gelatine, glycerol, paramethoxyacetophenone and ethylvanillin. Lamprene, in addition to 50 or 100 mg CFZ (the active pharmaceutical ingredient), contains several excipients including butylated hydroxytoluene, propylene glycol, soy lecithin, hydrogenated soybean oil, sodium ethyl parahydroxybenzoate and sodium propyl parahydroxybenzoate, citric acid and rapeseed oil. To improve CFZ absorption it is recommended to take Lamprene with food or milk. [238]

1.7.3.2 Clofazimine modes of action against *Mycobacterium tuberculosis*

Several modes of action have been proposed for this compound. Yano *et al.* suggest that clofazimine is involved in a redox cycle in which it is first reduced by NADH-quinone mycobacterial oxidoreductase, which catalyzes the first event in the respiratory chain of *M. tb*. [239] The reduced form of CFZ is then non-enzymatically and spontaneously reoxydized by O_2, producing in this way ROS such as superoxide and hydrogen peroxide. [239, 228] This mechanistic hypothesis is further supported by the observation of an antagonistic effect between CFZ and high concentration of menaquinone, the natural substrate of NADH-quinone oxidoreductase in *M. tb*. [240, 228]

However, this mechanism does not explain the resistance of Gram-negative bacteria to CFZ and the observation of an only weak reduction of CFZ anti-TB activity at low oxygen concentration. [241] Other potential CFZ action modes have been proposed. First, membrane disrupting properties of CFZ were highlighted by Van Rensburg *et al.*. [242] because of its basicity, CFZ should exist as an amphilic cation *in vivo*. Such kind of molecule can disrupt the membrane of mycobacteria and Gram-positive bacteria and catalyze the acidic hydrolysis of the ester group of phospholipids. This results in the formation of fatty acids and lysophospholipids, both of which exhibit antimicrobial properties. [243, 244, 245] Membrane disruption is also thought to result in the inactivation of K^+ transporter, thus preventing K^+ uptake by the pathogen. [246, 245]

In 2016, Shree *et al.* showed that CFZ interacts with the SerB2 enzyme of *M. tb*. This phosphatase catalyzes the last step of the serine biosynthesis pathway (i.e., dephosphorylation of L-3-phosphoserine in L-serine). [176, 247] In humans, a phosphoserine phosphatase (hPSP), which is however not inhibited by CFZ, catalyzes the same reaction. In addition to its role in serine synthesis, which is essential for the pathogen survival, Shree *et al.* have demonstrated that the bacilli secrete SerB2 into the cytosol of host macrophages. This helps the pathogen to escape the host immune system. [176] Specifically, SerB2 can dephosphorylate cofilin, leading to a cytoskeletal remodelling within the host macrophages, which promotes pathogen invasion and survival. SerB2 also dephosphorylates MAPK p38 and NFκBp65 proteins, leading to a decrease in the expression of interleukin 8, a mediator of the immune response. None of the above-mentioned reactions were observed in the presence of CFZ, suggesting that this compound may have a role in mediating host-pathogen interactions. [176]

1.7.3.3 Crystallographic data related to clofazimine

On a crystallographic point of view, the first reported structure of clofazimine was a dimethylformamide solvate (Table 1.3). One year later, in 1985, structures of the two clofazimine polymorphs (CFZ (I) and CFZ (II), Table 1.3), crystallizing in triclinic and monoclinic space groups were reported. [248] The orthorhombic and high-temperature monoclinic polymorphs (CFZ (III) and CFZ (IV), Table 1.3) were reported in 2016. [249]. Bannigan *et al.* studied the solid-state properties and in particular the thermodynamic relationship of these polymorphs. [249] These authors suggest an order-disorder relationship between CFZ (II) and (IV). These two forms are further enantiotropically related, as CFZ (II) reversibly converts to CFZ (IV) upon heating. The other polymorphs are monotropically related. Bannigan *et al.* determined the relative thermodynamic stability of forms I to III, with form III being more stable than form II, which in turn is more stable than polymorph I. [249] In all polymorphs, no strong H-bonds are observed and the main intermolecular interactions are attributed to stacking.

TABLE 1.3: Selected crystallographic data of clofazimine or clofaziminium (solvated/hydrated) salts published structures.

Structure	Space group	a, b, c (Å); α, β, γ (°); V (Å³)	Z	CSD refcode	Refs
		Clofazimine polymorphs			
CFZ (I)	$P\bar{1}$	10.507(4), 12.852(12), 9.601(2); 95.95(4), 97.22(1), 69.73(6); 1204.0(13)	2	DAKXUI01	[248, 249]
CFZ (II)	$P2_1/a$	7.788(14), 22.960(13), 13.362(7); 90, 98.58(12), 90; 2363(5)	4	DAKXUI	[248, 249]
CFZ (III)	$Pbca$	23.2417(15), 8.1118(5), 25.5891(16); 90, 90, 90; 4824.4(5)	8	DAKXUI03	[249]
CFZ (IV)	$P2_1/c$	12.9083, 23.3031, 8.3092; 90, 95.1697, 90; 2489.27	4	DAKXUI02	[249]
		Clofazimine solvates			
CFZ-DMF	$P\bar{1}$	12.435(4), 12.807(5), 10.424(4); 111.74(3), 112.37(3), 90.90(3); 1402.0(10)	2	CEKTER	[250]
CFZ-Ace (1:1)	$P\bar{1}$	10.0842(13), 12.0695(16), 12.6613(16); 75.278(2), 66.588(2), 69.051(2); 1309.3(3)	2	GESHIX	[251]
		Clofaziminium solvated/hydrated salts			
CFZ-NH$^+$-H$_2$PO$_4^-$-H$_2$O (1:1:0.25)	$P\bar{1}$	14.3064 (9), 15.1345 (9), 27.9096 (17); 96.495 (2), 92.025 (2), 110.640 (2); 5600.4(6)	8	/	[252]
CFZ-NH$^+$-HSO$_4^-$-MeOH (1:1:1)	$C2/c$	18.9579(11), 15.4754(9), 20.0404(12); 90, 100.360(2), 90; 5783.6(6)	8	/	[252]
CFZ-NH$^+$-MSA$^-$-H$_2$O (1:1:1)	$P\bar{1}$	9.5945(12), 11.0456(12), 14.4628(11); 110.173(9), 95.859(9), 94.929(9); 1419.1(3)	2	GESHET	[251]
CFZ-NH$^+$-Cl$^-$-H$_2$O (1:1:0.13)	$Pbca$	10.2664(4), 19.8275(7), 24.1558(9); 90, 90, 90; 4917.1(3)	8	RAFHUE	[253]
		Clofaziminium salts			
CFZ-NH$^+$-Cl$^-$ (1:1)	$Pbca$	10.74739(15), 19.1763(4), 24.2362(3); 90, 90, 90; 4994.96(14)	8	LABQUD	[254]
CFZ-NH$^+$-MSA$^-$ (1:1)	$P2_1/n$	10.0229 (18), 17.772 (3), 15.592 (3); 90, 103.028 (4), 90; 2705.9(8)	4	GESGAO	[251]
CFZ-NH$^+$-MLE$^-$ (1:1)	$P2_1/n$	11.2549(19), 20.816(3), 12.519(2); 90, 103.413(17), 90; 2853.0(8)	4	GESHAP	[251]
CFZ-NH$^+$-INA$^-$ (1:1)	$P\bar{1}$	9.8153(9), 12.1738(10), 15.2122(10); 72.455(7), 77.844(7), 66.479(8); 1580.7(2)	2	GESGES	[251]

Structure	Space group	a, b, c (Å); α, β, γ (°); V (Å^3)	Z	CSD refcode	Refs
CFZ-NH$^+$-NA$^-$ (1:1)	$P\bar{1}$	11.6032(13), 15.361(2), 18.733(3); 111.337(14), 91.280(11), 109.295(11); 2896.5(8)	4	GESGIW	[251]
CFZ-NH$^+$-MLN$^-$ (1:1)	$P\bar{1}$	9.8401(8), 12.4069(10), 13.0576(10); 74.129(1), 70.300(1), 67.520(1); 1367.50(19)	2	GESGOC	[251]
CFZ-NH$^+$-SCL$^-$ (1:1)	$P\bar{1}$	10.8702(6), 11.2066(6), 13.8272(8); 82.354(5), 88.960(5), 63.492(6); 1492.31(17)	2	GESGUI	[251]
CFZ-NH$^+$-CIT$^-$ (1:1)	$P\bar{1}$	14.7409(6), 15.8211(6), 16.2514(7); 71.9280(10), 63.0410(10), 70.747(2); 3130.6(2)	4	NIKYOY	[252, 255]
CFZ-NH$^+$-PABA$^-$ (1:1)	$P\bar{1}$	11.5977(17), 15.5832(26), 18.9730(27); 111.386(11), 92.631(12), 106.136(13); 3025.24(89)	4	YUHHAN	[256]

DMF: *N*, *N*'-dimethylformamide; Ace: Acetone; MSA$^-$: methanesulfonate; MLE$^-$: maleate; INA$^-$: isonicotinate; NA$^-$: nicotinate; MLN$^-$: malonate; SCL$^-$: salycilate; CIT$^-$: citrate; PABA$^-$: para-aminobenzoate.

In 2012 Bolla *et al.* reported first clofaziminium salts (with methanesulfonate (hydrated and non-hydrated salt), maleate, isonicotinate, nicotinate, malonate and salicylate counter-anions) as well as a new acetone solvate of clofazimine. [251] The authors studied the solubility of the salts in a EtOH:water (60:40) medium and report solubility improvements ranging from 94-fold (clofaziminum methanesulfonate) to 2-fold (clofaziminium salicylate) compared to pure clofazimine. [251]

Concomitantly to this thesis, Bannigan *et al.* reported other clofaziminium salts with phosphate, sulfate, citrate, acetate, nitrate, formate and oxalate as counter-anion. [252] Only the crystallographic data of the phosphate, sulfate and citrate salts are however reported. These authors studied the solution behaviour of these salts, and more particularly their dissolution in water and simulated gastric and intestinal fluids. Bannigan *et al.* showed a better dissolution of the phosphate, sulfate and citrate salt in all three media compared to lamprene and CFZ (I). They reported instability of the salts in the simulated gastric fluid and precipitation of clofaziminium chloride when a supersaturated solution of CFZ (about 20 mg/L CFZ and above) is reached following dissolution of the salts. They also showed a lower concentration of clofazimine at a higher pH (i.e., in simulated intestinal fluid) than that obtained in simulated gastric fluid. [252] More recently, Sousa *et al.* have studied a clofaziminium salt combining clofazimine with para-aminobenzoic acid resulting in a 5-fold solubility improvement in an EtOH:water (60:40) medium.[256] These authors did not investigate the salt in simulated gastric or intestinal media. The supersaturation by dissolving the salts, as demonstrated by Bannigan *et al.* suggests that an improved bioavailability of CFZ could potentially be achieved. [252]

1.8   Objective of this thesis

The results of Bolla *et al.*, suggest that salt formation with clofazimine could be of interest to improve its solubility, despite the potential difficulties later pointed out by Bannigan *et al.*. [251, 252] No drug-drug salt involving clofazimine was reported prior to this thesis. Given that tuberculosis requires multidrug therapy to avoid the development of (or to circumvent) drug-resistance, we believe that the preparation of multidrug salts could be advantageous, particularly with regard to patient compliance and modulation of the physico-chemical properties of the parent drugs.

The objective of this thesis is articulated over three main steps. As limited crystallographic data were available at the beginning of this work, the first step is to study the ability of clofazimine to interact with different types of molecules. This study should allow identification of the most interesting synthons in order to select appropriate APIs to interact with clofazimine. The second step consists in preparing drug-drug crystalline complexes of clofazimine with other active pharmaceutical ingredients. The selection of drugs with different aqueous solubility may be of interest in order to investigate the impact of this parameter (counter-ion solubility) on CFZ solubility. During the final step, particular attention will be paid to the properties of the co-drugs in the solid state (crystallization of solvated *vs* non solvated forms, impact of salification/cocrystallization on the thermal properties of the parent drugs and on CFZ solubility).

Firstly, the ability of clofazimine to crystallize in different forms was assessed in the presence of compounds that do not exhibit drug-like properties. In particular, the ability of clofazimine to crystallize in the form of a solvate (Chapter 2) was studied. At the beginning of this thesis the number of structures involving clofazimine with other compounds was rather limited and therefore a structural study of clofaziminium salts was carried out (Chapter 3).

Clofazimine was then combined with active pharmaceutical ingredients having interesting properties in the context of tuberculosis treatment. Salts associating clofazimine with diclofenac (Chapter 4) and with 4-aminosalicylic acid (PAS) (Chapter 5) were crystallized and characterized. In Chapter 4, particular attention was paid to the choice of the recrystallization solvent and the possibility of modulating the API-API ratios in the solid state. A rational approach based on the molecular volume of the solvent and its (a)protic properties was implemented in order to study the crystallization of solvated and non-solvated salts. The ability of the system to accommodate and more particularly to interact with protic molecules was used to modulate the CFZ-DCF ratio in the solid state. In Chapter 5, the influence of salification on the physico-chemical properties of clofazimine and PAS was evaluated and more particularly the modulation (by salt formation) of the aqueous solubility of CFZ and of the thermal stability of PAS was investigated.

Bibliography

[1] M. A. Ator, J. P. Mallamo, and M. Williams. Overview of drug discovery and development. *Current protocols in pharmacology*, 35(1):9.9.1–9.9.26, 2006.

[2] S. Sinha and D. Vohora. Drug discovery and development: An overview. In *Pharmaceutical Medicine and Translational Clinical Research*, pages 19–32. Elsevier, 2018.

[3] M. Schenone, V. Dančík, B. K. Wagner, and P. A. Clemons. Target identification and mechanism of action in chemical biology and drug discovery. *Nature chemical biology*, 9(4):232, 2013.

[4] S. M. Paul, D. S. Mytelka, C. T. Dunwiddie, C. C. Persinger, B. H. Munos, S. R. Lindborg, and A. L. Schacht. How to improve R&D productivity: the pharmaceutical industry's grand challenge. *Nature reviews Drug discovery*, 9(3):203–214, 2010.

[5] K. C. Nicolaou. Advancing the drug discovery and development process. *Angewandte Chemie*, 126(35):9280–9292, 2014.

[6] N. Berdigaliyev and M. Aljofan. An overview of drug discovery and development. *Future Medicinal Chemistry*, 12(10):939–947, 2020.

[7] R. Thakuria and B. Sarma. Drug-drug and drug-nutraceutical cocrystal/salt as alternative medicine for combination therapy: a crystal engineering approach. *Crystals*, 8(2):101, 2018.

[8] M. N. Cayen, editor. *Early drug development: strategies and routes to first-in-human trials.* John Wiley & Sons, 2011.

[9] J. C. McWilliams and M. Guinn. Early phase API process development overview. In F. Giordanetto, editor, *Early Drug Development: Bringing a Preclinical Candidate to the Clinic*, volume 1, pages 11–30. John Wiley & Sons, 2018.

[10] W. Zheng, W. Sun, and A. Simeonov. Drug repurposing screens and synergistic drug-combinations for infectious diseases. *British journal of pharmacology*, 175(2):181–191, 2018.

[11] M. A. Farha and E. D. Brown. Drug repurposing for antimicrobial discovery. *Nature microbiology*, 4(4):565–577, 2019.

[12] T. I. Oprea and J. Mestres. Drug repurposing: far beyond new targets for old drugs. *The AAPS journal*, 14(4):759–763, 2012.

[13] S. Pushpakom, F. Iorio, P. A. Eyers, K. J. Escott, S. Hopper, A. Wells, A. Doig, T. Guilliams, J. Latimer, C. McNamee, et al. Drug repurposing: progress, challenges and recommendations. *Nature reviews Drug discovery*, 18(1):41–58, 2019.

[14] R. Thipparaboina, D. Kumar, R. B. Chavan, and N. R. Shastri. Multidrug co-crystals: towards the development of effective therapeutic hybrids. *Drug Discovery Today*, 21(3):481–490, 2016.

[15] X. Wang, S. Du, R. Zhang, X. Jia, T. Yang, and X. Zhang. Drug-drug cocrystals: Opportunities and challenges. *Asian Journal of Pharmaceutical Sciences*, 2020.

[16] C. P. George, S. H. Thorat, P. S. Shaligram, P. R. Suresha, and R. G. Gonnade. Drug-drug cocrystals of anticancer drugs erlotinib-furosemide and gefitinib-mefenamic acid for alternative multi-drug treatment. *CrystEngComm*, 22:6137–6151, 2020.

[17] C. Guo, Q. Zhang, B. Zhu, Z. Zhang, X. Ma, W. Dai, X. Gong, G. Ren, and X. Mei. Drug–drug cocrystals provide significant improvements of drug properties in treatment with progesterone. *Crystal Growth & Design*, 20(5):3053–3063, 2020.

[18] S.-W. Zhang, R. F. Dunn, and A. Y. Lee. Solid-state properties. In F. Gordanetto, editor, *Early Drug Development: Bringing a Preclinical Candidate to the Clinic*, volume 1, pages 203–228. Wiley Online Library, 2018.

[19] S. Aitipamula, R. Banerjee, A. K. Bansal, K. Biradha, M. L. Cheney, A. R. Choudhury, G. R. Desiraju, A. G. Dikundwar, R. Dubey, N. Duggirala, et al. Polymorphs, salts, and cocrystals: what's in a name? *Crystal Growth & Design*, 12(5):2147–2152, 2012.

[20] E. Grothe, H. Meekes, E. Vlieg, J. H. Ter Horst, and R. de Gelder. Solvates, salts, and cocrystals: a proposal for a feasible classification system. *Crystal Growth & Design*, 16(6):3237–3243, 2016.

[21] P. H. Karpinski. Polymorphism of active pharmaceutical ingredients. *Chemical Engineering & Technology: Industrial Chemistry-Plant Equipment-Process Engineering-Biotechnology*, 29(2):233–237, 2006.

[22] A. J. Cruz-Cabeza, S. M. Reutzel-Edens, and J. Bernstein. Facts and fictions about polymorphism. *Chemical Society Reviews*, 44(23):8619–8635, 2015.

[23] U.S. Department of Health and Human Services, Food and Drug Administration, and Center for Drug Evaluation and Research (CDER). Waiver of in vivo bioavailability and bioequivalence studies for immediate-release solid oral dosage forms based on a biopharmaceutics classification system guidance for industry, 2017.

[24] European Medicines Agency (EMA). ICH M9 guideline on biopharmaceutics classification system-base biowaivers, 2020.

[25] A. M. Thayer. Finding solutions. *Chemical & Engineering News*, 88(22):13–18, 2010.

[26] L. Di, E. H. Kerns, and T. Carter, Guy. Drug-like property concepts in pharmaceutical design. *Current pharmaceutical design*, 15(19):2184–2194, 2009.

[27] V. R. Vemula, V. Lagishetty, and S. Lingala. Solubility enhancement techniques. *International journal of pharmaceutical sciences review and research*, 5(1):41–51, 2010.

[28] A. Kumar, S. K. Sahoo, K. Padhee, P. S. Kochar, A. Sathapathy, and N. Pathak. Review on solubility enhancement techniques for hydrophobic drugs. *Pharmacie Globale*, 3(3):001–007, 2011.

[29] K. T. Savjani, A. K. Gajjar, and J. K. Savjani. Drug solubility: importance and enhancement techniques. *ISRN pharmaceutics*, 2012, 2012.

[30] S. Kadam, D. Shinkar, and R. Saudagar. Review on solubility enhancement techniques. *International Journal of Pharma and Bio Sciences*, 3(3):462–475, 2013.

[31] T. Patole and A. Deshpande. Co-crystallization-a technique for solubility enhancement. *Int J Pharm Sci Res*, 5(9):3566–3576, 2014.

[32] D. C. Vimalson, S. Parimalakrishnan, N. Jeganathan, and S. Anbazhagan. Techniques to enhance solubility of hydrophobic drugs: An overview. *Asian Journal of Pharmaceutics*, 10(2):S67, 2016.

[33] S. Jagtap, C. Magdum, D. Jadge, and R. Jagtap. Solubility enhancement technique: a review. *Journal of Pharmaceutical Sciences and Research*, 10(9):2205–2211, 2018.

[34] D. Singh, N. Bedi, and A. K. Tiwary. Enhancing solubility of poorly aqueous soluble drugs: Critical appraisal of techniques. *Journal of pharmaceutical investigation*, 48(5):509–526, 2018.

[35] A. R. Kale, S. Kakade, and A. Bhosale. A review on: Solubility enhancement techniques. *Journal of Current Pharma Research*, 10(2):3630–3647, 2020.

[36] M. A. Jahangir, S. S. Imam, A. Muheem, A. Chettupalli, F. A. Al-Abbasi, M. S. Nadeem, I. Kazmi, M. Afzal, and S. Alshehri. Nanocrystals: Characterization overview, applications in drug delivery, and their toxicity concerns. *Journal of Pharmaceutical Innovation*, 2020.

[37] J. Bhatt, D. Bahl, K. Morris, L. L. Stevens, and R. Haware. Structure-mechanics and improved tableting performance of the drug-drug cocrystal metformin: salicylic acid. *European Journal of Pharmaceutics and Biopharmaceutics*, 153:23–35, 2020.

[38] C. Almansa, C. S. Frampton, J. M. Vela, S. Whitelock, and C. R. Plata-Salamán. Co-crystals as a new approach to multimodal analgesia and the treatment of pain. *Journal of Pain Research*, 12:2679, 2019.

[39] A. Newman, C. Chen, and C. Sanrame. Salt and cocrystal screening. In F. Gordanetto, editor, *Early Drug Development: Bringing a Preclinical Candidate to the Clinic*, volume 1, pages 229–270. Wiley Online Library, 2018.

[40] P. C. Vioglio, M. R. Chierotti, and R. Gobetto. Pharmaceutical aspects of salt and cocrystal forms of APIs and characterization challenges. *Advanced drug delivery reviews*, 117:86–110, 2017.

[41] US Food and Drug Administration et al. Regulatory classification of pharmaceutical co-crystal guidance for industry, 2018.

[42] European Medicines Agency (EMA). Reflection paper on the use of cocrystals of active substances in medicinal products, 2015.

[43] P. Grobelny, A. Mukherjee, and G. R. Desiraju. Drug-drug co-crystals: Temperature-dependent proton mobility in the molecular complex of isoniazid with 4-aminosalicylic acid. *CrystEngComm*, 13(13):4358–4364, 2011.

[44] C. B. Aakeröy, M. E. Fasulo, and J. Desper. Cocrystal or salt: does it really matter? *Molecular Pharmaceutics*, 4(3):317–322, 2007.

[45] S. L. Childs, G. P. Stahly, and A. Park. The salt- cocrystal continuum: the influence of crystal structure on ionization state. *Molecular pharmaceutics*, 4(3):323–338, 2007.

[46] A. J. Cruz-Cabeza. Acid–base crystalline complexes and the pKa rule. *CrystEngComm*, 14(20):6362–6365, 2012.

[47] A. W. Newman, S. L. Childs, and B. A. Cowans. Salt and cocrystal form selection. In S. C. Gad, editor, *Pharmaceutical Sciences Encyclopedia: Drug Discovery, Development, and Manufacturing*, pages 1–28. Wiley Online Library, 2010.

[48] G. R. Desiraju. Supramolecular synthons in crystal engineering—a new organic synthesis. *Angewandte Chemie International Edition in English*, 34(21):2311–2327, 1995.

[49] L. Fábián. Cambridge structural database analysis of molecular complementarity in cocrystals. *Crystal Growth & Design*, 9(3):1436–1443, 2009.

[50] N. Sarkar, N. C. Gonnella, M. Krawiec, D. Xin, and C. B. Aakeröy. Evaluating the predictive abilities of protocols based on hydrogen-bond propensity, molecular complementarity, and hydrogen-bond energy for cocrystal screening. *Crystal Growth & Design*, 20(11):7320–7327, 2020.

[51] M. C. Etter. Encoding and decoding hydrogen-bond patterns of organic compounds. *Accounts of Chemical Research*, 23(4):120–126, 1990.

[52] N. Sarkar and C. B. Aakeröy. Evaluating hydrogen-bond propensity, hydrogen-bond coordination and hydrogen-bond energy as tools for predicting the outcome of attempted co-crystallisations. *Supramolecular Chemistry*, 32(2):81–90, 2020.

[53] P. T. Galek, J. A. Chisholm, E. Pidcock, and P. A. Wood. Hydrogen-bond coordination in organic crystal structures: statistics, predictions and applications. *Acta Crystallographica Section B: Structural Science, Crystal Engineering and Materials*, 70(1):91–105, 2014.

[54] P. T. Galek, L. Fabian, W. S. Motherwell, F. H. Allen, and N. Feeder. Knowledge-based model of hydrogen-bonding propensity in organic crystals. *Acta Crystallographica Section B: Structural Science*, 63(5):768–782, 2007.

[55] P. T. Galek, F. H. Allen, L. Fábián, and N. Feeder. Knowledge-based H-bond prediction to aid experimental polymorph screening. *CrystEngComm*, 11(12):2634–2639, 2009.

[56] P. T. Galek, L. Fábián, and F. H. Allen. Truly prospective prediction: inter-and intramolecular hydrogen bonding. *CrystEngComm*, 12(7):2091–2099, 2010.

[57] P. A. Wood, N. Feeder, M. Furlow, P. T. Galek, C. R. Groom, and E. Pidcock. Knowledge-based approaches to co-crystal design. *CrystEngComm*, 16(26):5839–5848, 2014.

[58] N. Sarkar, A. S. Sinha, and C. B. Aakeröy. Systematic investigation of hydrogen-bond propensities for informing co-crystal design and assembly. *CrystEngComm*, 21(40):6048–6055, 2019.

[59] A. Fernández Casares, W. M. Nap, G. Ten Figás, P. Huizenga, R. Groot, and M. Hoffmann. An evaluation of salt screening methodologies. *Journal of Pharmacy and Pharmacology*, 67(6):812–822, 2015.

[60] M. Karimi-Jafari, L. Padrela, G. M. Walker, and D. M. Croker. Creating cocrystals: a review of pharmaceutical cocrystal preparation routes and applications. *Crystal Growth & Design*, 18(10):6370–6387, 2018.

[61] E. Losev and E. Boldyreva. A salt or a co-crystal–when crystallization protocol matters. *CrystEngComm*, 20(16):2299–2305, 2018.

[62] A. V. Trask, W. S. Motherwell, and W. Jones. Pharmaceutical cocrystallization: engineering a remedy for caffeine hydration. *Crystal Growth & Design*, 5(3):1013–1021, 2005.

[63] P. P. Bag, M. Patni, and C. M. Reddy. A kinetically controlled crystallization process for identifying new co-crystal forms: fast evaporation of solvent from solutions to dryness. *CrystEngComm*, 13(19):5650–5652, 2011.

[64] M. Rodrigues, B. Baptista, J. A. Lopes, and M. C. Sarraguça. Pharmaceutical cocrystallization techniques. Advances and challenges. *International Journal of Pharmaceutics*, 547(1-2):404–420, 2018.

[65] N. Takata, K. Shiraki, R. Takano, Y. Hayashi, and K. Terada. Cocrystal screening of stanolone and mestanolone using slurry crystallization. *Crystal Growth and Design*, 8(8):3032–3037, 2008.

[66] P. P. Apshingekar, S. Aher, A. L. Kelly, E. C. Brown, and A. Paradkar. Synthesis of caffeine/maleic acid co-crystal by ultrasound-assisted slurry co-crystallization. *Journal of Pharmaceutical Sciences*, 106(1):66–70, 2017.

[67] H. N. Kim and K. S. Suslick. The effects of ultrasound on crystals: Sonocrystallization and sonofragmentation. *Crystals*, 8(7):280, 2018.

[68] A. Y. Sheikh, S. Abd Rahim, R. B. Hammond, and K. J. Roberts. Scalable solution cocrystallization: case of carbamazepine-nicotinamide I. *CrystEngComm*, 11(3):501–509, 2009.

[69] G. He, P. S. Chow, and R. B. Tan. Investigating the intermolecular interactions in concentration-dependent solution cocrystallization of caffeine and p-hydroxybenzoic acid. *Crystal Growth & Design*, 10(8):3763–3769, 2010.

[70] H.-H. Tung, E. L. Paul, M. Midler, and J. A. McCauley. *Crystallization of organic compounds: an industrial perspective.* John Wiley & Sons, 2009.

[71] I.-C. Wang, M.-J. Lee, S.-J. Sim, W.-S. Kim, N.-H. Chun, and G. J. Choi. Anti-solvent co-crystallization of carbamazepine and saccharin. *International journal of pharmaceutics*, 450(1-2):311–322, 2013.

[72] M.-J. Lee, I.-C. Wang, M.-J. Kim, P. Kim, K.-H. Song, N.-H. Chun, H.-G. Park, and G. J. Choi. Controlling the polymorphism of carbamazepine-saccharin cocrystals formed during antisolvent cocrystallization using kinetic parameters. *Korean Journal of Chemical Engineering*, 32(9):1910–1917, 2015.

[73] S. P. Patil, S. R. Modi, and A. K. Bansal. Generation of 1:1 carbamazepine: nicotinamide cocrystals by spray drying. *European Journal of Pharmaceutical Sciences*, 62:251–257, 2014.

[74] C. Grossjohann, D. R. Serrano, K. J. Paluch, P. O'Connell, L. Vella-Zarb, P. Manesiotis, T. Mccabe, L. Tajber, O. I. Corrigan, and A. M. Healy. Polymorphism in sulfadimidine/4-aminosalicylic acid cocrystals: solid-state characterization and physicochemical properties. *Journal of pharmaceutical sciences*, 104(4):1385–1398, 2015.

[75] J. Weng, S. N. Wong, X. Xu, B. Xuan, C. Wang, R. Chen, C. C. Sun, R. Lakerveld, P. C. L. Kwok, and S. F. Chow. Cocrystal engineering of itraconazole with suberic acid via rotary evaporation and spray drying. *Crystal Growth & Design*, 19(5):2736–2745, 2019.

[76] M. D. Eddleston, B. Patel, G. M. Day, and W. Jones. Cocrystallization by freeze-drying: preparation of novel multicomponent crystal forms. *Crystal Growth & Design*, 13(10):4599–4606, 2013.

[77] L. Padrela, M. A. Rodrigues, S. P. Velaga, H. A. Matos, and E. G. de Azevedo. Formation of indomethacin–saccharin cocrystals using supercritical fluid technology. *European Journal of Pharmaceutical Sciences*, 38(1):9–17, 2009.

[78] T. Ervasti, J. Aaltonen, and J. Ketolainen. Theophylline–nicotinamide cocrystal formation in physical mixture during storage. *International Journal of Pharmaceutics*, 486(1-2):121–130, 2015.

[79] I. Sarcevica, L. Orola, K. P. Nartowski, Y. Z. Khimyak, A. N. Round, and L. Fáabián. Mechanistic and kinetic insight into spontaneous cocrystallization of isoniazid and benzoic acid. *Molecular pharmaceutics*, 12(8):2981–2992, 2015.

[80] C. Ji, M. C. Hoffman, and M. A. Mehta. Catalytic effect of solvent vapors on the spontaneous formation of caffeine–malonic acid cocrystal. *Crystal Growth & Design*, 17(4):1456–1459, 2017.

[81] P. MacFhionnghaile, C. M. Crowley, P. McArdle, and A. Erxleben. Spontaneous solid-state cocrystallization of caffeine and urea. *Crystal Growth & Design*, 20(2):736–745, 2020.

[82] C. Maheshwari, A. Jayasankar, N. A. Khan, G. E. Amidon, and N. Rodríguez-Hornedo. Factors that influence the spontaneous formation of pharmaceutical cocrystals by simply mixing solid reactants. *CrystEngComm*, 11(3):493–500, 2009.

[83] A. Y. Ibrahim, R. T. Forbes, and N. Blagden. Spontaneous crystal growth of co-crystals: the contribution of particle size reduction and convection mixing of the co-formers. *CrystEngComm*, 13(4):1141–1152, 2011.

[84] K. Nartowski, Y. Khimyak, and D. Berry. Tuning the spontaneous formation kinetics of caffeine: malonic acid co-crystals. *CrystEngComm*, 18(15):2617–2620, 2016.

[85] A. V. Trask and W. Jones. Crystal engineering of organic cocrystals by the solid-state grinding approach. In *Organic solid state reactions*, pages 41–70. Springer, 2005.

[86] A. V. Trask, W. D. S. Motherwell, and W. Jones. Solvent-drop grinding: green polymorph control of cocrystallisation. *Chem. Commun.*, 40:890–891, 2004.

[87] A. V. Trask, J. van de Streek, W. S. Motherwell, and W. Jones. Achieving polymorphic and stoichiometric diversity in cocrystal formation: Importance of solid-state grinding, powder X-ray structure determination, and seeding. *Crystal Growth & Design*, 5(6):2233–2241, 2005.

[88] T. Friscíc and W. Jones. Recent advances in understanding the mechanism of cocrystal formation via grinding. *Crystal Growth & Design*, 9(3):1621–1637, 2009.

[89] S. L. James, C. J. Adams, C. Bolm, D. Braga, P. Collier, T. Friščić, F. Grepioni, K. D. Harris, G. Hyett, W. Jones, et al. Mechanochemistry: opportunities for new and cleaner synthesis. *Chemical Society Reviews*, 41(1):413–447, 2012.

[90] D. Hasa, G. Schneider Rauber, D. Voinovich, and W. Jones. Cocrystal formation through mechanochemistry: from neat and liquid-assisted grinding to polymer-assisted grinding. *Angewandte Chemie*, 127(25):7479–7483, 2015.

[91] C. Medina, D. Daurio, K. Nagapudi, and F. Alvarez-Nunez. Manufacture of pharmaceutical co-crystals using twin screw extrusion: A solvent-less and scalable process. *Journal of pharmaceutical sciences*, 99(4):1693–1696, 2010.

[92] T. Stolar, S. Lukin, M. Tireli, I. Sović, B. Karadeniz, I. Kereković, G. Matijasić, M. Gretić, Z. Katancić, I. Dejanović, et al. Control of pharmaceutical cocrystal polymorphism on various scales by mechanochemistry: Transfer from the laboratory batch to the large-scale extrusion processing. *ACS Sustainable Chemistry & Engineering*, 7(7):7102–7110, 2019.

[93] D. Daurio, K. Nagapudi, L. Li, P. Quan, and F.-A. Nunez. Application of twin screw extrusion to the manufacture of cocrystals: scale-up of AMG 517–sorbic acid cocrystal production. *Faraday discussions*, 170:235–249, 2014.

[94] H. L. Lee, J. M. Vasoya, M. d. L. Cirqueira, K. L. Yeh, T. Lee, and A. T. Serajuddin. Continuous preparation of 1:1 haloperidol–maleic acid salt by a novel solvent-free method using a twin screw melt extruder. *Molecular Pharmaceutics*, 14(4):1278–1291, 2017.

[95] D. Daurio, C. Medina, R. Saw, K. Nagapudi, and F. Alvarez-Núñez. Application of twin screw extrusion in the manufacture of cocrystals, part I: four case studies. *Pharmaceutics*, 3(3):582–600, 2011.

[96] K. Boksa, A. Otte, and R. Pinal. Matrix-assisted cocrystallization (MAC) simultaneous production and formulation of pharmaceutical cocrystals by hot-melt extrusion. *Journal of pharmaceutical sciences*, 103(9):2904–2910, 2014.

[97] Z. Zhou, H. M. Chan, H. H.-Y. Sung, H. H. Tong, and Y. Zheng. Identification of new cocrystal systems with stoichiometric diversity of salicylic acid using thermal methods. *Pharmaceutical research*, 33(4):1030–1039, 2016.

[98] T. Carstens, D. A. Haynes, and V. J. Smith. Cocrystals: Solution, mechanochemistry, and sublimation. *Crystal Growth & Design*, 20(2):1139–1149, 2019.

[99] Í. Duarte, R. Andrade, J. F. Pinto, and M. Temtem. Green production of cocrystals using a new solvent-free approach by spray congealing. *International Journal of Pharmaceutics*, 506(1-2):68–78, 2016.

[100] J. Wouters, D. Braga, F. Grepioni, L. Aerts, and L. Quéré. Alternative solid forms: co-crystals. In *Polymorphism in the Pharmaceutical Industry: Solid Form and Drug Development*, pages 61–90. Wiley-VCH Verlag GmbH & Co. KGaA, 2019.

[101] W. I. David, K. Shankland, L. B. McCusker, and C. Baerlocher. Structure determination from powder diffraction data. *IUCr monographs on crystallography*, 13, 2006.

[102] P. Gabbott. *Principles and applications of thermal analysis.* John Wiley & Sons, 2008.

[103] M. Allan and L. J. Mauer. RH-temperature phase diagrams of hydrate forming deliquescent crystalline ingredients. *Food chemistry*, 236:21–31, 2017.

[104] D. Raijada, A. D. Bond, F. H. Larsen, C. Cornett, H. Qu, and J. Rantanen. Exploring the solid-form landscape of pharmaceutical hydrates: transformation pathways of the sodium naproxen anhydrate-hydrate system. *Pharmaceutical research*, 30(1):280–289, 2013.

[105] T. Polenova, R. Gupta, and A. Goldbourt. Magic angle spinning NMR spectroscopy: a versatile technique for structural and dynamic analysis of solid-phase systems. *Analytical Chemistry*, 87(11):5458–5469, 2015.

[106] US Food and Drug Administration. Drug trials snapshot, 2020. [Accessed on 27th November 2020], Available at: https://www.ema.europa.eu/en/documents/assessment-report/entresto-epar-public-assessment-report_en.pdf.

[107] European Medicines Agency (EMA). Assessment report: Entresto, 2015.

[108] Esteve. CTC (44 mg tramadol and 56 mg celecoxib tablet) co-crystal of tramadol and celecoxib. In *Joint Meeting of the Anesthetic and Analgesic Drug Products Advisory Committeeand the Drug Safety and Risk Management Advisory Committee*, 2020. [Accessed on 27th November 2020], Available at : https://www.fda.gov/media/134129/download.

[109] C. Almansa, R. Merce, N. Tesson, J. Farran, J. Tomaás, and C. R. Plata-Salaman. Co-crystal of tramadol hydrochloride–celecoxib (CTC): a novel API–API co-crystal for the treatment of pain. *Crystal Growth & Design*, 17(4):1884–1892, 2017.

[110] C. Plata Salaman, N. Tesson, C. Jiménez Gonzales, and L. Vaiana. Crystalline forms of sartans like telmisartan with beta blockers. *EP/EP2649996*, 2013.

[111] H. H. Buschmann, L. Solà Carandell, J. Benet Buchholz, et al. Co-crystals of duloxetine and naproxen. *WO 2009/141144*, 2009.

[112] L. Feng, S. Godtfredsen, P. Karpinski, et al. Pharmaceutical combinations of an angiotensin receptor antagonist and an NEP inhibitor. *WO 2007/056546 A1*, 2007.

[113] J. Wang, X.-L. Dai, T.-B. Lu, and J.-M. Chen. Temozolomide–hesperetin drug–drug cocrystal with optimized performance in stability, dissolution, and tabletability. *Crystal Growth & Design*, 21(2):838–846, 2021.

[114] D. Huang, H. S. Chan, Y. Wu, L. Li, L. Zhang, Y. Lv, X. Yang, and Z. Zhou. Phase solubility investigation and theoretical calculations on drug-drug cocrystals of carbamazepine with Emodin, Paeonol. *Journal of Molecular Liquids*, 329:115604, 2021.

[115] W. Kuang, S. Ji, X. Wang, J. Zhang, and P. Lan. Relationship between crystal structures and physicochemical properties of lamotrigine cocrystal. *Powder Technology*, 380:18–25, 2021.

[116] R. Wang, P. Yuan, D. Yang, B. Zhang, L. Zhang, Y. Lu, and G. Du. Structural features and interactions of new sulfamethazine salt and cocrystal. *Journal of Molecular Structure*, 1229:129596, 2021.

[117] W.-Q. Feng, L.-Y. Wang, J. Gao, M.-Y. Zhao, Y.-T. Li, Z.-Y. Wu, and C.-W. Yan. Solid state and solubility study of a potential anticancer drug-drug molecular salt of diclofenac and metformin. *Journal of Molecular Structure*, 1234:130166, 2021.

[118] L.-T. Jiao, D.-z. Yang, L. Zhang, S.-y. Yang, G.-h. Du, and Y. Lu. Salt solvates of quinolones and oxicams: Theoretical computation, structural characterization and dissolution studies. *Journal of Molecular Structure*, 1223:128865, 2021.

[119] S. Eesam, J. S. Bhandaru, C. Naliganti, R. K. Bobbala, and R. R. Akkinepally. Solubility enhancement of carvedilol using drug–drug cocrystallization with hydrochlorothiazide. *Future Journal of Pharmaceutical Sciences*, 6(1):1–13, 2020.

[120] D. Bernasconi, S. Bordignon, F. Rossi, E. Priola, C. Nervi, R. Gobetto, D. Voinovich, D. Hasa, N. T. Duong, Y. Nishiyama, et al. Selective synthesis of a salt and a cocrystal of the ethionamide-salicylic acid system. *Crystal Growth & Design*, 20(2):906–915, 2020.

[121] B. Bhattacharya, S. Das, G. Lal, S. R. Soni, A. Ghosh, C. M. Reddy, and S. Ghosh. Screening, crystal structures and solubility studies of a series of multidrug salt hydrates and cocrystals of fenamic acids with trimethoprim and sulfamethazine. *Journal of Molecular Structure*, 1199:127028, 2020.

[122] H. Guan, Y. Wu, Y. Han, J. Liu, D. Huang, Z. Liang, Z. Zhou, and F. Guo. Furosemide adducts with hexamethylenetetramine, amantadine and isoniazid: A structural case that demonstrates the effect of carboxylic acid dimer and sulfonic acid dimer on the solubility. *Crystal Growth & Design*, 2020.

[123] R. Pérez-Fernández, N. Fresno, P. Goya, J. Elguero, L. Menéndez-Taboada, S. García-Granda, and C. Marco. Structure and thermodynamical properties of metformin salicylate. *Crystal growth & design*, 13(4):1780–1785, 2013.

[124] X. Bian, L. Jiang, J. Zhou, X. Guan, J. Wang, P. Xiang, J. Pan, and X. Hu. Improving dissolution and cytotoxicity by forming multidrug crystals. *Molecules*, 25(6):1343, 2020.

[125] S. Modani, A. Gunnam, B. Yadav, A. K. Nangia, and N. R. Shastri. Generation and evaluation of pharmacologically relevant drug–drug cocrystal for gout therapy. *Crystal Growth & Design*, 20(6):3577–3583, 2020.

[126] J. B. Ngilirabanga, P. P. Rosa, M. Aucamp, Y. Kippie, and H. Samsodien. Dual-drug co-crystal synthesis for synergistic in vitro effect of three key first-line antiretroviral drugs. *Journal of Drug Delivery Science and Technology*, page 101958, 2020.

[127] K. K. Sarmah, N. Nath, D. R. Rao, and R. Thakuria. Mechanochemical synthesis of drug–drug and drug–nutraceutical multicomponent solids of olanzapine. *CrystEngComm*, 22(6):1120–1130, 2020.

[128] L.-Y. Wang, F.-Z. Bu, Y.-T. Li, Z.-Y. Wu, and C.-W. Yan. A sulfathiazole–amantadine hydrochloride cocrystal: The first codrug simultaneously comprising antiviral and antibacterial components. *Crystal Growth & Design*, 20(5):3236–3246, 2020.

[129] L.-Y. Wang, Y.-M. Yu, M.-C. Yu, Y.-T. Li, Z.-Y. Wu, and C.-W. Yan. A crystalline solid adduct of sulfathiazole–amantadine: the first dual-drug molecular salt containing both antiviral and antibacterial ingredients. *CrystEngComm*, 22(22):3804–3813, 2020.

[130] X. Wu, Y. Wang, J. Xue, J. Liu, J. Qin, Z. Hong, and Y. Du. Solid phase drug-drug pharmaceutical co-crystal formed between pyrazinamide and diflunisal: Structural characterization based on terahertz/Raman spectroscopy combining with DFT calculation. *Spectrochimica Acta Part A: Molecular and Biomolecular Spectroscopy*, page 118265, 2020.

[131] A. O. Évora, R. A. Castro, T. M. Maria, M. T. Rosado, M. Ramos Silva, A. Matos Beja, J. Canotilho, and M. E. S. Eusébio. Pyrazinamide-diflunisal: a new dual-drug co-crystal. *Crystal growth & design*, 11(11):4780–4788, 2011.

[132] S. Amrutha, L. Giri, S. SeethaLekshmi, and S. Varughese. Enhanced aqueous solubility of the solid forms of a BCS class-II anti-tuberculosis drug, prothionamide. *Crystal Growth & Design*, 20(8):5086–5096, 2020.

[133] X.-Z. Yu, L.-Y. Wang, F. Liu, Y.-T. Li, Z.-Y. Wu, and C.-W. Yan. Sustained-release dual-drug ternary salt cocrystal of piperazine ferulate with pyrazinamide: Synthesis, structure, and Hirshfeld surface analysis. *Crystal Growth & Design*, 20(3):2064–2073, 2020.

[134] R. N. Costa, A. L. Reviglio, S. Siedler, S. G. Cardoso, Y. G. Linck, G. A. Monti, A. M. Carvalho, J. A. Resende, M. H. Chaves, H. V. Rocha, et al. New multicomponent forms of the antiretroviral Nevirapine with improved dissolution performance. *Crystal Growth & Design*, 20(2):688–698, 2020.

[135] M. R. Caira, S. A. Bourne, H. Samsodien, E. Engel, W. Liebenberg, N. Stieger, and M. Aucamp. Co-crystals of the antiretroviral nevirapine: crystal structures, thermal analysis and dissolution behaviour. *CrystEngComm*, 14(7):2541–2551, 2012.

[136] D. K. Maity, R. K. Paul, and G. R. Desiraju. Drug–drug binary solids of nitrofurantoin and trimethoprim: Crystal engineering and pharmaceutical properties. *Molecular Pharmaceutics*, 17(12):4435–4442, 2020.

[137] Y. Zhao, B. Sun, L. Jia, Y. Wang, M. Wang, H. Yang, Y. Qiao, J. Gong, and W. Tang. Tuning physicochemical properties of antipsychotic drug aripiprazole with multicomponent crystal strategy based on structure and property relationship. *Crystal Growth & Design*, 20(6):3747–3761, 2020.

[138] L. F. Diniz, P. S. Carvalho Jr, S. A. Pena, J. E. Gonçalves, M. A. Souza, J. D. de Souza Filho, L. F. Bomfim Filho, C. H. Franco, R. Diniz, and C. Fernandes. Enhancing the solubility and permeability of the diuretic drug furosemide via multicomponent crystal forms. *International Journal of Pharmaceutics*, 587:119694, 2020.

[139] M. M. Abdelquader, E. A. Essa, and G. M. El Maghraby. Inhibition of co-crystallization of olmesartan medoxomil and hydrochlorothiazide for enhanced dissolution rate in their fixed dose combination. *AAPS PharmSciTech*, 20(1):3, 2019.

[140] X. Bian, L. Jiang, Z. Gan, X. Guan, L. Zhang, L. Cai, and X. Hu. A glimepiride-metformin multidrug crystal: Synthesis, crystal structure analysis, and physicochemical properties. *Molecules*, 24(20):3786, 2019.

[141] S. V. Gohel, P. Sanphui, G. P. Singh, K. Bhat, and M. Prakash. Lower melting pharmaceutical cocrystals of metaxalone with carboxamide functionalities. *Journal of Molecular Structure*, 1178:479–490, 2019.

[142] L. Jia, S. Wu, and J. Gong. A tolbutamide–metformin salt based on antidiabetic drug combinations: synthesis, crystal structure analysis and pharmaceutical properties. *Acta Crystallographica Section C: Structural Chemistry*, 75(9), 2019.

[143] P. Li, T. Ramaiah, M. Zhang, Y. Zhang, Y. Huang, and B. Lou. Two cocrystals of berberine chloride with myricetin and dihydromyricetin: Crystal structures, characterization, and antitumor activities. *Crystal Growth & Design*, 20(1):157–166, 2019.

[144] A. O. Surov, A. N. Manin, A. P. Voronin, D. E. Boycov, O. V. Magdysyuk, and G. L. Perlovich. New pharmaceutical cocrystal forms of flurbiprofen: Structural, physicochemical, and thermodynamic characterization. *Crystal Growth & Design*, 19(10):5751–5761, 2019.

[145] R. Nagalapalli and S. Yaga Bheem. Synthesis, crystal structure, and Hirshfeld surface analysis of ciprofloxacin-salicylic acid molecular salt. *Journal of Crystallography*, 2014, 2014.

[146] A. O. Surov, N. A. Vasilev, A. V. Churakov, J. Stroh, F. Emmerling, and G. L. Perlovich. Solid forms of ciprofloxacin salicylate: Polymorphism, formation pathways, and thermodynamic stability. *Crystal Growth & Design*, 19(5):2979–2990, 2019.

[147] I. Nugrahani, B. Tjengal, T. Gusdinar, A. Horikawa, and H. Uekusa. A comprehensive study of a new 1.75 hydrate of ciprofloxacin salicylate: SCXRD structure determination,

solid characterization, water stability, solubility, and dissolution study. *Crystals*, 10(5):349, 2020.

[148] D. Li, J. Li, Z. Deng, and H. Zhang. Piroxicam–clonixin drug–drug cocrystal solvates with enhanced hydration stability. *CrystEngComm*, 21(28):4145–4149, 2019.

[149] B. Nicolaï, B. Fournier, S. Dahaoui, J.-M. Gillet, and N.-E. Ghermani. Crystal and electron properties of carbamazepine–aspirin co-crystal. *Crystal Growth & Design*, 19(2):1308–1321, 2019.

[150] P. Vishweshwar, J. A. McMahon, M. Oliveira, M. L. Peterson, and M. J. Zaworotko. The predictably elusive form II of aspirin. *Journal of the American Chemical Society*, 127(48):16802–16803, 2005.

[151] B. Saikia, N. Sultana, T. Kaushik, and B. Sarma. Engineering a remedy to improve phase stability of famotidine under physiological pH environments. *Crystal Growth & Design*, 19(11):6472–6481, 2019.

[152] T. Shinozaki, M. Ono, K. Higashi, and K. Moribe. A novel drug-drug cocrystal of levofloxacin and metacetamol: reduced hygroscopicity and improved photostability of levofloxacin. *Journal of Pharmaceutical Sciences*, 108(7):2383–2390, 2019.

[153] C. C. da Silva, R. d. Pepino, C. C. de Melo, J. C. Tenorio, and J. Ellena. Controlled synthesis of new 5-fluorocytosine cocrystals based on the pKa rule. *Crystal Growth & Design*, 14(9):4383–4393, 2014.

[154] C. C. da Silva, C. C. de Melo, M. S. Souza, L. F. Diniz, R. L. Carneiro, and J. Ellena. 5-fluorocytosine/5-fluorouracil drug-drug cocrystal: a new development route based on mechanochemical synthesis. *Journal of Pharmaceutical Innovation*, 14(1):50–56, 2019.

[155] X. Wang, S. Xu, L. Jia, Y. Yang, Y. Liu, J. Gong, and S. Wu. Drug–drug salts of mefenamic acid\tolfenamic acid and piperazine to improve physicochemical properties for potential veterinary use. *CrystEngComm*, 21(35):5284–5291, 2019.

[156] Y.-X. Zhang, L.-Y. Wang, J.-K. Dai, F. Liu, Y.-T. Li, Z.-Y. Wu, and C.-W. Yan. The comparative study of cocrystal/salt in simultaneously improving solubility and permeability of acetazolamide. *Journal of Molecular Structure*, 1184:225–232, 2019.

[157] W.-X. Zhou, H.-W. Zhao, H.-H. Chen, Z.-Y. Zhang, and D.-Y. Chen. Characterization of drug–drug salt forms of metformin and aspirin with improved physicochemical properties. *CrystEngComm*, 21(25):3770–3773, 2019.

[158] J. López-Cedrún, S. Videla, M. Burgueno, I. Juárez, S. Aboul-Hosn, R. Martín-Granizo, J. Grau, M. Puche, J.-L. Gil-Diez, J.-A. Hueto, et al. Co-crystal of tramadol–celecoxib in patients with moderate to severe acute post-surgical oral pain: a dose-finding, randomised, double-blind, placebo-and active-controlled, multicentre, phase II trial. *Drugs in R&D*, 18(2):137–148, 2018.

[159] H. Dooner, G. Mundin, S. Mersmann, C. Bennett, U. Lorch, M. Encabo, M. Escriche, G. Encina, and K. Smith. Pharmacokinetics of tramadol and celecoxib in japanese and caucasian subjects following administration of co-crystal of tramadol-celecoxib (CTC): A randomised, open-label study. *European journal of drug metabolism and pharmacokinetics*, 44(1):63–75, 2019.

[160] N. Gascon, C. Almansa, M. Merlos, J. Miguel Vela, G. Encina, A. Morte, K. Smith, and C. Plata-Salamán. Co-crystal of tramadol-celecoxib: preclinical and clinical evaluation of a novel analgesic. *Expert Opinion on Investigational Drugs*, 28(5):399–409, 2019.

[161] A. Port, C. Almansa, R. Enrech, M. Bordas, and C. R. Plata-Salamaán. Differential solution behavior of the new API–API co-crystal of tramadol–celecoxib (CTC) versus its constituents and their combination. *Crystal Growth & Design*, 19(6):3172–3182, 2019.

[162] K. L. Yeh and T. Lee. Intensified crystallization processes for 1: 1 drug–drug cocrystals of sulfathiazole–theophylline, and sulfathiazole–sulfanilamide. *Crystal Growth & Design*, 18(3):1339–1349, 2018.

[163] F.-Y. Wang, Q. Zhang, Z. Zhang, X. Gong, J.-R. Wang, and X. Mei. Solid-state characterization and solubility enhancement of apremilast drug–drug cocrystals. *CrystEngComm*, 20(39):5945–5948, 2018.

[164] M. S. Souza, L. F. Diniz, L. Vogt, P. S. Carvalho Jr, R. F. D'vries, and J. Ellena. Mechanochemical synthesis of a multicomponent solid form: the case of 5-fluorocytosine isoniazid codrug. *Crystal Growth & Design*, 18(9):5202–5209, 2018.

[165] F. Rossi, P. Cerreia Vioglio, S. Bordignon, V. Giorgio, C. Nervi, E. Priola, R. Gobetto, K. Yazawa, and M. R. Chierotti. Unraveling the hydrogen bond network in a theophylline–pyridoxine salt cocrystal by a combined X-ray diffraction, solid-state NMR, and computational approach. *Crystal Growth & Design*, 18(4):2225–2233, 2018.

[166] F. Liu, Y. Song, Y.-N. Liu, Y.-T. Li, Z.-Y. Wu, and C.-W. Yan. Drug-bridge-drug ternary cocrystallization strategy for antituberculosis drugs combination. *Crystal Growth & Design*, 18(3):1283–1286, 2018.

[167] S. Kakkar, B. Bhattacharya, C. M. Reddy, and S. Ghosh. Tuning mechanical behaviour by controlling the structure of a series of theophylline co-crystals. *CrystEngComm*, 20(8):1101–1109, 2018.

[168] B. Harmsen and T. Leyssens. Dual-drug chiral resolution: Enantiospecific cocrystallization of (S)-ibuprofen using levetiracetam. *Crystal Growth & Design*, 18(1):441–448, 2018.

[169] S. Darwish, J. Zeglinski, G. R. Krishna, R. Shaikh, M. Khraisheh, G. M. Walker, and D. M. Croker. A new 1:1 drug-drug cocrystal of theophylline and aspirin: Discovery, characterization, and construction of ternary phase diagrams. *Crystal Growth & Design*, 18(12):7526–7532, 2018.

[170] J.-M. Li, X.-L. Dai, G.-J. Li, T.-B. Lu, and J.-M. Chen. Constructing anti-glioma drug combination with optimized properties through cocrystallization. *Crystal Growth & Design*, 18(8):4270–4274, 2018.

[171] Y. Deng, Y. Zhang, Y. Huang, M. Zhang, and B. Lou. Preparation, crystal structures, and oral bioavailability of two cocrystals of emodin with berberine chloride. *Crystal Growth & Design*, 18(12):7481–7488, 2018.

[172] C. Pathak, K. Savjani, A. K. Gajjar, and J. K. Savjani. Cocrystal formation of paracetamol with indomethacin and mefenamic acid: An efficient approach to enhance solubility. *Int J Pharm Pharm Sci*, 5(4):414–419, 2013.

[173] N. Wichianphong and M. Charoenchaitrakool. Application of Box–Behnken design for processing of mefenamic acid–paracetamol cocrystals using gas anti-solvent (GAS) process. *Journal of CO2 Utilization*, 26:212–220, 2018.

[174] M. K. Bommaka, M. C. Mannava, K. Suresh, A. Gunnam, and A. Nangia. Entacapone: improving aqueous solubility, diffusion permeability, and cocrystal stability with theophylline. *Crystal Growth & Design*, 18(10):6061–6069, 2018.

[175] B. Bhattacharya, A. Mondal, S. R. Soni, S. Das, S. Bhunia, K. B. Raju, A. Ghosh, and C. M. Reddy. Multidrug salt forms of norfloxacin with non-steroidal anti-inflammatory drugs: solubility and membrane permeability studies. *CrystEngComm*, 20(41):6420–6429, 2018.

[176] S. Shree, A. K. Singh, R. Saxena, H. Kumar, A. Agarwal, V. K. Sharma, K. Srivastava, K. K. Srivastava, S. Sanyal, and R. Ramachandran. The M. tuberculosis HAD phosphatase (Rv3042c) interacts with host proteins and is inhibited by Clofazimine. *Cellular and molecular life sciences*, 73(17):3401–3417, 2016.

[177] World Health Organization. *Global tuberculosis report 2019*. World Health Organization, Geneva, 2019.

[178] World Health Organization. *Global tuberculosis report 2020*. World Health Organization, Geneva, 2020.

[179] World Health Organization et al. WHO consolidated guidelines on tuberculosis: module 1: prevention: tuberculosis preventive treatment. In *WHO consolidated guidelines on tuberculosis*. World Health Organization, 2020.

[180] World Health Organization et al. *Compendium of WHO guidelines and associated standards: ensuring optimum delivery of the cascade of care for patients with tuberculosis.* World Health Organization, 2018.

[181] A. Maitra, S. Bates, T. Kolvekar, P. V. Devarajan, J. D. Guzman, and S. Bhakta. Repurposing — a ray of hope in tackling extensively drug resistance in tuberculosis. *International Journal of Infectious Diseases*, 32:50–55, 2015.

[182] G. V. Rayasam and T. S. Balganesh. Exploring the potential of adjunct therapy in tuberculosis. *Trends in Pharmacological Sciences*, 36(8):506–513, 2015.

[183] S. L. Kinnings, N. Liu, N. Buchmeier, P. J. Tonge, L. Xie, and P. E. Bourne. Drug discovery using chemical systems biology: repositioning the safe medicine Comtan to treat multi-drug and extensively drug resistant tuberculosis. *PLoS Comput Biol*, 5(7):e1000423, 2009.

[184] L. Amaral, J. Kristiansen, L. Abebe, and W. Millett. Inhibition of the respiration of multi-drug resistant clinical isolates of Mycobacterium tuberculosis by thioridazine: potential use for initial therapy of freshly diagnosed tuberculosis. *Journal of Antimicrobial Chemotherapy*, 38(6):1049–1053, 1996.

[185] D. Ordway, M. Viveiros, C. Leandro, R. Bettencourt, J. Almeida, M. Martins, J. E. Kristiansen, J. Molnar, and L. Amaral. Clinical concentrations of thioridazine kill intracellular multidrug-resistant Mycobacterium tuberculosis. *Antimicrobial agents and chemotherapy*, 47(3):917–922, 2003.

[186] D. Van Soolingen, R. Hernandez-Pando, H. Orozco, D. Aguilar, C. Magis-Escurra, L. Amaral, J. Van Ingen, and M. J. Boeree. The antipsychotic thioridazine shows promising therapeutic activity in a mouse model of multidrug-resistant tuberculosis. *PloS one*, 5(9):e12640, 2010.

[187] L. Amaral and M. Viveiros. Why thioridazine in combination with antibiotics cures extensively drug-resistant Mycobacterium tuberculosis infections. *International journal of antimicrobial agents*, 39(5):376–380, 2012.

[188] E. Abbate, M. Vescovo, M. Natiello, M. Cufré, A. García, P. Gonzalez Montaner, M. Ambroggi, V. Ritacco, and D. van Soolingen. Successful alternative treatment of extensively drug-resistant tuberculosis in Argentina with a combination of linezolid, moxifloxacin and thioridazine. *Journal of antimicrobial chemotherapy*, 67(2):473–477, 2012.

[189] S. Gupta, S. Tyagi, D. V. Almeida, M. C. Maiga, N. C. Ammerman, and W. R. Bishai. Acceleration of tuberculosis treatment by adjunctive therapy with verapamil as an efflux inhibitor. *American journal of respiratory and critical care medicine*, 188(5):600–607, 2013.

[190] S. Gupta, K. A. Cohen, K. Winglee, M. Maiga, B. Diarra, and W. R. Bishai. Efflux inhibition with verapamil potentiates bedaquiline in Mycobacterium tuberculosis. *Antimicrobial agents and chemotherapy*, 58(1):574–576, 2014.

[191] A. Maitra, S. Bates, M. Shaik, D. Evangelopoulos, I. Abubakar, T. D. McHugh, M. Lipman, and S. Bhakta. Repurposing drugs for treatment of tuberculosis: a role for non-steroidal anti-inflammatory drugs. *British medical bulletin*, 118(1):138, 2016.

[192] J. Xu, R. Tasneen, C. A. Peloquin, D. V. Almeida, S.-Y. Li, K. Barnes-Boyle, Y. Lu, and E. Nuermberger. Verapamil increases the bioavailability and efficacy of bedaquiline but not clofazimine in a murine model of tuberculosis. *Antimicrobial agents and chemotherapy*, 62(1):e01692–17, 2018.

[193] L. E. Lim, C. Vilchèze, C. Ng, W. R. Jacobs, S. Ramón-García, and C. J. Thompson. Anthelmintic avermectins kill Mycobacterium tuberculosis, including multidrug-resistant clinical strains. *Antimicrobial agents and chemotherapy*, 57(2):1040–1046, 2013.

[194] O. Pacios, L. Blasco, I. Bleriot, L. Fernandez-Garcia, M. González Bardanca, A. Ambroa, M. López, G. Bou, and M. Tomás. Strategies to combat multidrug-resistant and persistent infectious diseases. *Antibiotics*, 9(2):65, 2020.

[195] S. M. Ameen and M. Drancourt. In vitro susceptibility of Mycobacterium tuberculosis to trimethoprim and sulfonamides in France. *Antimicrobial agents and chemotherapy*, 57(12):6370–6371, 2013.

[196] O. Oladimeji, P. Isaakidis, O. J. Obasanya, O. Eltayeb, M. Khogali, R. Van den Bergh, A. M. Kumar, S. G. Hinderaker, S. T. Abdurrahman, L. Lawson, et al. Intensive-phase treatment outcomes among hospitalized multidrug-resistant tuberculosis patients: results from a nationwide cohort in Nigeria. *PloS one*, 9(4):e94393, 2014.

[197] D. Sharma, Y. K. Dhuriya, N. Deo, and D. Bisht. Repurposing and revival of the drugs: a new approach to combat the drug resistant tuberculosis. *Frontiers in microbiology*, 8:2452, 2017.

[198] S. Cohen-Bacrie, I. B. Kahla, E. Botelho-Nevers, M. Million, P. Parola, P. Brouqui, and M. Drancourt. Imported extensively drug-resistant Mycobacterium tuberculosis Beijing genotype, Marseilles, France, 2011. *Eurosurveillance*, 16(16):19846, 2011.

[199] R. S. Wallis, M. Maeurer, P. Mwaba, J. Chakaya, R. Rustomjee, G. B. Migliori, B. Marais, M. Schito, G. Churchyard, S. Swaminathan, et al. Tuberculosis—advances in development of new drugs, treatment regimens, host-directed therapies, and biomarkers. *The Lancet infectious diseases*, 16(4):e34–e46, 2016.

[200] A. Zumla, J. Chakaya, M. Hoelscher, F. Ntoumi, R. Rustomjee, C. Vilaplana, D. Yeboah-Manu, V. Rasolofo, P. Munderi, N. Singh, et al. Towards host-directed therapies for tuberculosis. *Nature reviews Drug discovery*, 14(8):511–512, 2015.

[201] D. Banerjee and R. Bhattacharyya. Statin therapy may prevent development of tuberculosis in diabetic state. *Medical hypotheses*, 83(1):88–91, 2014.

[202] R. J. Napier, W. Rafi, M. Cheruvu, K. R. Powell, M. A. Zaunbrecher, W. Bornmann, P. Salgame, T. M. Shinnick, and D. Kalman. Imatinib-sensitive tyrosine kinases regulate mycobacterial pathogenesis and represent therapeutic targets against tuberculosis. *Cell host & microbe*, 10(5):475–485, 2011.

[203] A. Singhal, L. Jie, P. Kumar, G. S. Hong, M. K.-S. Leow, B. Paleja, L. Tsenova, N. Kurepina, J. Chen, F. Zolezzi, et al. Metformin as adjunct antituberculosis therapy. *Science translational medicine*, 6(263):263ra159, 2014.

[204] B. I. Restrepo. Metformin: candidate host-directed therapy for tuberculosis in diabetes and non-diabetes patients. *Tuberculosis*, 101:S69–S72, 2016.

[205] E. Lachmandas, C. Eckold, J. Böhme, V. A. Koeken, M. B. Marzuki, B. Blok, R. J. Arts, J. Chen, K. W. Teng, J. Ratter, et al. Metformin alters human host responses to Mycobacterium tuberculosis in healthy subjects. *The Journal of infectious diseases*, 220(1):139–150, 2019.

[206] M. Schiebler, K. Brown, K. Hegyi, S. M. Newton, M. Renna, L. Hepburn, C. Klapholz, S. Coulter, A. Obregón-Henao, M. Henao Tamayo, et al. Functional drug screening reveals anticonvulsants as enhancers of mTOR-independent autophagic killing of Mycobacterium tuberculosis through inositol depletion. *EMBO molecular medicine*, 7(2):127–139, 2015.

[207] M. Rao, D. Valentini, A. Zumla, and M. Maeurer. Evaluation of the efficacy of valproic acid and suberoylanilide hydroxamic acid (vorinostat) in enhancing the effects of first-line tuberculosis drugs against intracellular Mycobacterium tuberculosis. *International Journal of Infectious Diseases*, 69:78–84, 2018.

[208] E. Nieto-Patlán, J. Serafín-López, I. Wong-Baeza, S. M. Pérez-Tapia, L. Cobos-Marín, S. Estrada-Parra, I. Estrada-García, A. D. Chávez-Blanco, and R. Chacón-Salinas. Valproic acid promotes a decrease in mycobacterial survival by enhancing nitric oxide production in macrophages stimulated with IFN-γ. *Tuberculosis*, 114:123–126, 2019.

[209] S. P. Parihar, R. Guler, R. Khutlang, D. M. Lang, R. Hurdayal, M. M. Mhlanga, H. Suzuki, A. D. Marais, and F. Brombacher. Statin therapy reduces the mycobacterium tuberculosis burden in human macrophages and in mice by enhancing autophagy and phagosome maturation. *The Journal of infectious diseases*, 209(5):754–763, 2014.

[210] N. K. Dutta, N. Bruiners, M. L. Pinn, M. D. Zimmerman, B. Prideaux, V. Dartois, M. L. Gennaro, and P. C. Karakousis. Statin adjunctive therapy shortens the duration of TB treatment in mice. *Journal of Antimicrobial Chemotherapy*, 71(6):1570–1577, 2016.

[211] V. M. Kroesen, M. I. Gröschel, N. Martinson, A. Zumla, M. Maeurer, T. S. van der Werf, and C. Vilaplana. Non-steroidal anti-inflammatory drugs as host-directed therapy for tuberculosis: a systematic review. *Frontiers in immunology*, 8:772, 2017.

[212] J. Ivanyi and A. Zumla. Nonsteroidal anti-inflammatory drugs for adjunctive tuberculosis treatment. *The Journal of Infectious Diseases*, 208(2):185–188, 2013.

[213] T. Dallenga, L. Linnemann, B. Paudyal, U. Repnik, G. Griffiths, and U. E. Schaible. Targeting neutrophils for host-directed therapy to treat tuberculosis. *International Journal of Medical Microbiology*, 308(1):142–147, 2018.

[214] World Health Organization and Stop TB Initiative (World Health Organization). *Treatment of tuberculosis: guidelines*. World Health Organization, 2010.

[215] N. K. Dutta, S. G. Dastidar, A. Kumar, K. Mazumdar, R. Ray, and A. N. Chakrabarty. Antimycobacterial activity of the antiinflammatory agent diclofenac sodium, and its synergism with streptomycin. *Brazilian Journal of Microbiology*, 35(4):316–323, 2004.

[216] K. Mazumdar, S. Dastidar, J. Park, and N. Dutta. The anti-inflammatory non-antibiotic helper compound diclofenac: an antibacterial drug target. *European journal of clinical microbiology & infectious diseases*, 28(8):881, 2009.

[217] B. Gold, M. Pingle, S. J. Brickner, N. Shah, J. Roberts, M. Rundell, W. C. Bracken, T. Warrier, S. Somersan, A. Venugopal, et al. Nonsteroidal anti-inflammatory drug sensitizes Mycobacterium tuberculosis to endogenous and exogenous antimicrobials. *Proceedings of the National Academy of Sciences*, 109(40):16004–16011, 2012.

[218] J. S. Cavanaugh, R. Jou, M.-H. Wu, T. Dalton, E. Kurbatova, J. Ershova, J. P. Cegielski, and G. P. Investigators. Susceptibilities of MDR Mycobacterium tuberculosis isolates to unconventional drugs compared with their reported pharmacokinetic/pharmacodynamic parameters. *Journal of Antimicrobial Chemotherapy*, 72(6):1678–1687, 2017.

[219] S. T. Byrne, S. M. Denkin, and Y. Zhang. Aspirin and ibuprofen enhance pyrazinamide treatment of murine tuberculosis. *Journal of antimicrobial chemotherapy*, 59(2):313–316, 2006.

[220] C. Vilaplana, E. Marzo, G. Tapia, J. Diaz, V. Garcia, and P.-J. Cardona. Ibuprofen therapy resulted in significantly decreased tissue bacillary loads and increased survival in a new murine experimental model of active tuberculosis. *The Journal of infectious diseases*, 208(2):199–202, 2013.

[221] D. P. Eisen, E. S. McBryde, and A. Walduck. Low-dose aspirin and ibuprofen's sterilizing effects on mycobacterium tuberculosis suggest safe new adjuvant therapies for tuberculosis. *The Journal of infectious diseases*, 208(11):1925–1927, 2013.

[222] V. M. Kroesen, P. Rodríguez-Martínez, E. García, Y. Rosales, J. Díaz, M. Martín-Céspedes, G. Tapia, M. R. Sarrias, P.-J. Cardona, and C. Vilaplana. A beneficial effect of low-dose aspirin in a murine model of active tuberculosis. *Frontiers in immunology*, 9:798, 2018.

[223] J. D. Guzman, D. Evangelopoulos, A. Gupta, K. Birchall, S. Mwaigwisya, B. Saxty, T. D. McHugh, S. Gibbons, J. Malkinson, and S. Bhakta. Antitubercular specific activity of ibuprofen and the other 2-arylpropanoic acids using the HT-SPOTi whole-cell phenotypic assay. *BMJ open*, 3(6):e002672, 2013.

[224] U.S. National Library of Medicine. Potential efficacy and safety of using adjunctive ibuprofen for XDR-TB tuberculosis (NSAIDS-XDRTB). NCT02781909, 2016, September -. [Accessed on 19th November 2020], Available at: https://clinicaltrials.gov/ct2/show/NCT02781909.

[225] V. C. Barry, J. Belton, M. L. Conalty, J. M. Denneny, D. W. Edward, J. O'sullivan, D. Twomey, and F. Winder. A new series of phenazines (rimino-compounds) with high antituberculosis activity. *Nature*, 179(4568):1013–1015, 1957.

[226] S. Päuser, C. Mörgeli, U. B. Schaad, and N. Eric. Lifesavers for millions, 2012. [Accessed on 24th November 2020], Available at: https://www.roche.de/res/literatur/153/Lifesavers-for-millions-original-0e0c6031240f3e63ee17b4db61146b93.pdf.

[227] P. Sensi. History of the development of rifampin. *Reviews of infectious diseases*, 5(Supplement_3):S402–S406, 1983.

[228] M. C. Cholo, M. T. Mothiba, B. Fourie, and R. Anderson. Mechanisms of action and therapeutic efficacies of the lipophilic antimycobacterial agents clofazimine and bedaquiline. *Journal of Antimicrobial Chemotherapy*, 72:338–353, 2017.

[229] U.S. National Library of Medicine. Building evidence for advancing new treatment for rifampicin resistant tuberculosis (RR-TB) comparing a short course of treatment (containing bedaquiline, delamanid and linezolid) with the current South African standard of care. Identifier NCT04062201, 2019, August 22 -. [Accessed on 19th November 2020], Available at: https://clinicaltrials.gov/ct2/show/NCT04062201.

[230] U.S. National Library of Medicine. Clofazimine- and rifapentine-containing treatment shortening regimens in drug-susceptible tuberculosis: The CLO-FAST study. Identifier NCT04311502, 2020, November 2 -. [Accessed on 19th November 2020], Available at: https://clinicaltrials.gov/ct2/show/NCT04311502.

[231] U.S. National Library of Medicine. Evaluating newly approved drugs for multidrug-resistant TB (endTB). Identifier NCT02754765, 2016, April 28 -. [Accessed on 19th November 2020], Available at: https://clinicaltrials.gov/ct2/show/record/NCT02754765.

[232] U.S. National Library of Medicine. Evaluating newly approved drugs in combination regimens for multidrug-resistant TB with fluoroquinolone resistance (endTB-Q) (endTB-Q). Identifier NCT03896685, 2019, April 1 -. [Accessed on 19th November 2020], Available at: https://clinicaltrials.gov/ct2/show/NCT03896685.

[233] T. Woldemichael, R. K. Keswani, P. M. Rzeczycki, M. D. Murashov, V. LaLone, B. Gregorka, J. A. Swanson, K. A. Stringer, and G. R. Rosania. Reverse engineering the intracellular self-assembly of a functional mechanopharmaceutical device. *Scientific reports*, 8(1):1–16, 2018.

[234] K. Williams, A. Minkowski, O. Amoabeng, C. A. Peloquin, D. Taylor, K. Andries, R. S. Wallis, K. E. Mdluli, and E. L. Nuermberger. Sterilizing activities of novel combinations lacking first-and second-line drugs in a murine model of tuberculosis. *Antimicrobial agents and chemotherapy*, 56(6):3114–3120, 2012.

[235] Z. Zhang, T. Li, G. Qu, Y. Pang, and Y. Zhao. In vitro synergistic activity of clofazimine and other antituberculous drugs against multidrug-resistant Mycobacterium tuberculosis isolates. *International journal of antimicrobial agents*, 45(1):71–75, 2015.

[236] L. Zou, M. Liu, Y. Wang, J. Lu, and Y. Pang. Determination of in vitro synergy between linezolid and other antimicrobial agents against Mycobacterium tuberculosis isolates. *Tuberculosis*, 95(6):839–842, 2015.

[237] A. López-Gavín, G. Tudó, A. Vergara, J. C. Hurtado, and J. Gonzalez-Martín. In vitro activity against Mycobacterium tuberculosis of levofloxacin, moxifloxacin and UB-8902 in combination with clofazimine and pretomanid. *International journal of antimicrobial agents*, 46(5):582–585, 2015.

[238] Agence Nationale de sécurité du médicament et des produits de santé (ANSM), Haute autorité de la santé (HAS), and Union nationale des caisses d'assurance maladie (UNCAM). LAMPRENE 100mg, capsule molle - notice patient. [Accessed on 27th November 2020], Available at: http://base-donnees-publique.medicaments.gouv.fr/affichageDoc.php?specid=67132888&typedoc=N.

[239] T. Yano, S. Kassovska-Bratinova, J. S. Teh, J. Winkler, K. Sullivan, A. Isaacs, N. M. Schechter, and H. Rubin. Reduction of clofazimine by mycobacterial type 2 NADH: quinone oxidoreductase a pathway for the generation of bactericidal levels of reactive oxygen species. *Journal of Biological Chemistry*, 286(12):10276–10287, 2011.

[240] B. Lechartier and S. T. Cole. Mode of action of clofazimine and combination therapy with benzothiazinones against Mycobacterium tuberculosis. *Antimicrobial agents and chemotherapy*, 59(8):4457–4463, 2015.

[241] Y. Lu, M. Zheng, B. Wang, L. Fu, W. Zhao, P. Li, J. Xu, H. Zhu, H. Jin, D. Yin, et al. Clofazimine analogs with efficacy against experimental tuberculosis and reduced potential for accumulation. *Antimicrobial agents and chemotherapy*, 55(11):5185–5193, 2011.

[242] C. Van Rensburg, G. Joone, J. O'sullivan, and R. Anderson. Antimicrobial activities of clofazimine and B669 are mediated by lysophospholipids. *Antimicrobial agents and chemotherapy*, 36(12):2729–2735, 1992.

[243] M. Baciu, S. C. Sebai, O. Ces, X. Mulet, J. A. Clarke, G. C. Shearman, R. V. Law, R. H. Templer, C. Plisson, C. A. Parker, et al. Degradative transport of cationic amphiphilic drugs across phospholipid bilayers. *Philosophical Transactions of the Royal Society A: Mathematical, Physical and Engineering Sciences*, 364(1847):2597–2614, 2006.

[244] H. Steel, R. Cockeran, and R. Anderson. Platelet-activating factor and lyso-PAF possess direct antimicrobial properties in vitro. *Apmis*, 110(2):158–164, 2002.

[245] M. C. Cholo, H. C. Steel, P. B. Fourie, W. A. Germishuizen, and R. Anderson. Clofazimine: current status and future prospects. *Journal of antimicrobial chemotherapy*, 67(2):290–298, 2012.

[246] H. Steel, N. Matlola, and R. Anderson. Inhibition of potassium transport and growth of mycobacteria exposed to clofazimine and B669 is associated with a calcium-independent increase in microbial phospholipase A2 activity. *Journal of Antimicrobial Chemotherapy*, 44(2):209–216, 1999.

[247] M. Haufroid and J. Wouters. Targeting the serine pathway: A promising approach against tuberculosis? *Pharmaceuticals*, 12(2):66, 2019.

[248] U. Rychlewska, M. B. H. Broom, D. S. Eggleston, and D. J. Hodgson. Antileprosy dihydrophenazines. Structural characterization of two crystal forms of clofazimine and of isoclofazimine, B. 3857. *Journal of the American Chemical Society*, 107(16):4768–4772, 1985.

[249] P. Bannigan, J. Zeglinski, M. Lusi, J. O'Brien, and S. P. Hudson. Investigation into the solid and solution properties of known and novel polymorphs of the antimicrobial molecule clofazimine. *Crystal Growth & Design*, 16(12):7240–7250, 2016.

[250] D. S. Eggleston, W. E. Marsh, and D. J. Hodgson. Structures of the antileprosy phenazine derivatives clofazimine-N,N-dimethylformamide, C27H22C12N4.C3H7NO, and B 1912, C30H27ClN4. *Acta Crystallographica*, C40:288–292, 1984.

[251] G. Bolla and A. Nangia. Clofazimine mesylate: A high solubility stable salt. *Crystal Growth & Design*, 12(12):6250–6259, 2012.

[252] P. Bannigan, E. Durack, C. Madden, M. Lusi, and S. P. Hudson. Role of biorelevant dissolution media in the selection of optimal salt forms of oral drugs: Maximizing the gastrointestinal solubility and in vitro activity of the antimicrobial molecule, clofazimine. *ACS Omega*, 2(12):8969–8981, 2017.

[253] E. M. Horstman, R. K. Keswani, B. A. Frey, P. M. Rzeczycki, V. LaLone, J. A. Bertke, P. J. Kenis, and G. R. Rosania. Elasticity in macrophage-synthesized biocrystals. *Angewandte Chemie - International Edition*, 56(7):1815–1819, 2017.

[254] R. K. Keswani, J. Baik, L. Yeomans, C. Hitzman, A. M. Johnson, A. S. Pawate, P. J. Kenis, N. Rodriguez-Hornedo, K. A. Stringer, and G. R. Rosania. Chemical analysis of drug biocrystals: A role for counterion transport pathways in intracellular drug disposition. *Molecular Pharmaceutics*, 12(7):2528–2536, 2015.

[255] P. Bannigan, E. Durack, H. Mathur, M. C. Rea, R. P. Ross, and S. P. Hudson. Delivery of a hydrophobic drug into the lower gastrointestinal system via an endogenous enzyme-mediated carrier mechanism: An in vitro study. *European Journal of Pharmaceutics and Biopharmaceutics*, 133:12–19, 2018.

[256] M. L. Sousa, M. C. Sarraguça, A. O. dos Santos, J. M. G. Sarraguça, J. Lopes, and P. R. da Silva Ribeiro. A new salt of clofazimine to improve leprosy treatment. *Journal of Molecular Structure*, 1214:128226, 2020.

Chapter 2

Crystal structures of two solvates of the antileprosy and antitubercular compound clofazimine: clofazimine ethanol solvate and clofazimine ethylacetate solvate

Crystal structures of two solvates of the antileprosy and antitubercular compound clofazimine: clofazimine ethanol solvate and clofazimine ethyl acetate solvate

Laurie Bodart*, Nikolay Tumanov and Johan Wouters

Namur Medicine and Drug Innovation Center - Namur Research Institute for Life, Science (NAMEDIC-NARILIS), Namur Institute of Structured Matter (NISM), Department of Chemistry, University of Namur (UNamur), 61 Rue de Bruxelles, 5000 Namur, Belgium
Correspondence e-mail: laurie.bodart@unamur.be

Abstract. Two new solvates of clofazimine with ethanol ((3E)-N,5-bis(4-chlorophenyl)-3-[(propan-2-yl)imino]-3,5-dihydrophenazin-2-amine; ethanol, $C_{27}H_{22}Cl_2N_4$, C_2H_6O) and with ethyl acetate ((3E)-N,5-bis(4-chlorophenyl)-3-[(propan-2-yl)imino]-3,5-dihydrophenazin-2-amine; hemi(ethyl acetate), $C_{27}H_{22}Cl_2N_4$, $0.5(C_4H_8O_2)$) are identified. Both solvates crystallize in the same space group but in different ratios. Indeed, in the clofazimine ethyl acetate solvate structure, the disordered solvent molecule lies on an inversion center and the asymmetric unit contains one clofazimine molecule and half an ethyl acetate molecule. However, in ethanol solvated structure of clofazimine, ethanol is disordered over two positions but is not located on the inversion center and the asymmetric unit contains one molecule of each ethanol and clofazimine. Ethanol interacts with clofazimine through strong hydrogen bonds while only a weak $C-H\cdots O$ H-bond is observed between clofazimine and ethyl acetate. Despite these differences, solvent molecules are located in the same cavity than that of the already reported clofazimine solvates with N,N-dimethylformamide[1] and with propane-2-one [2].

2.1 Chemical context
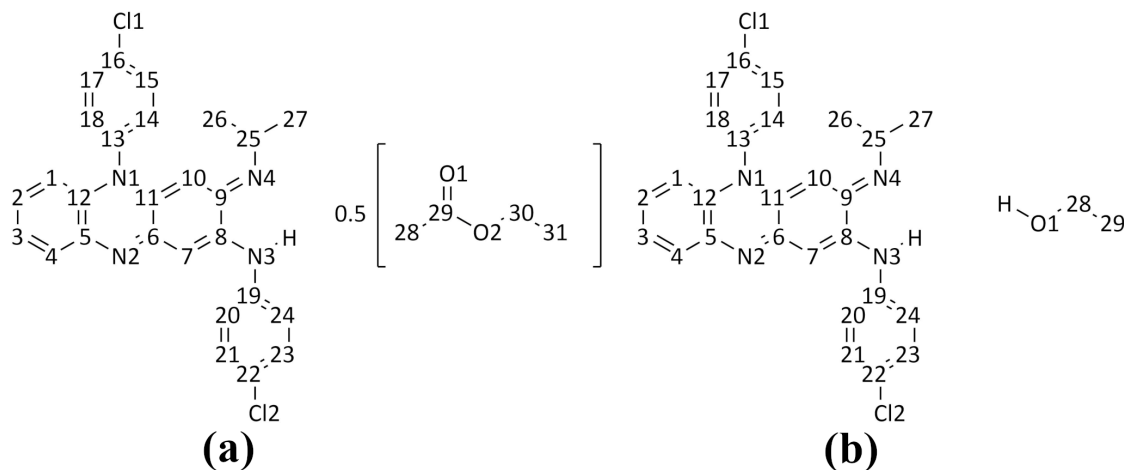
FIGURE 2.1: Labeling scheme of (a) ethyl acetate and (b) ethanol solvates of clofazimine.

Clofazimine (CFZ) is an iminophenazine compound first synthesized by Barry *et al.* [3] that is classified as an antileprosy and antituberculosis agent on the World Health Organisation List of Essential Medicines [4]. This agent was first synthesized as an antituberculosis drug [3] but was then repurposed to an antileprosy drug [5] due to the discovery of more potent compounds for tuberculosis treatment. Clofazimine is now recommended against multidrug resistant Mycobacterium tuberculosis. However, it has poor pharmacological properties because of its high lipophilicity [5, 6]. Because of the recent revival of interest in clofazimine as an antitubercular drug, several clofazimine preparations in the solid-state were investigated, including amorphous solid dispersion [7], inhalation suspensions [8], clofaziminium salts [9, 2, 10, 11, 12, 13] as well as clofazimine loading in nanocellulose hydrogels [14]. Bannigan *et al.* also investigated clofazimine polymorphism [15]. Here we report two new solvates of clofazimine with ethyl acetate, CFZ-EtOAc (1/0.5) and with ethanol, CFZ-EtOH (1/1) (Figures 2.1 and 2.2). These solvates were identified while studying the effect of solvents on clofazimine polymorphism during liquid-assisted grinding.

2.2 Structural commentary

Clofazimine was ground in the presence of seven solvents, namely, methanol, ethanol, butanol, acetonitrile, ethyl acetate, cyclohexane and toluene. Results of this solvent screening is presented in Table 2.1.

Crystals of CFZ-EtOAc (1/0.5) and of CFZ-EtOH (1/1) were obtained by recrystallization, in EtOAc or EtOH, of a CFZ powder ground in presence of EtOAc or EtOH respectively. The crystallization process was performed by solvent evaporation at room temperature (293-298K). Both solvates crystallize in space group $P\bar{1}$ (Table 2.2). In the
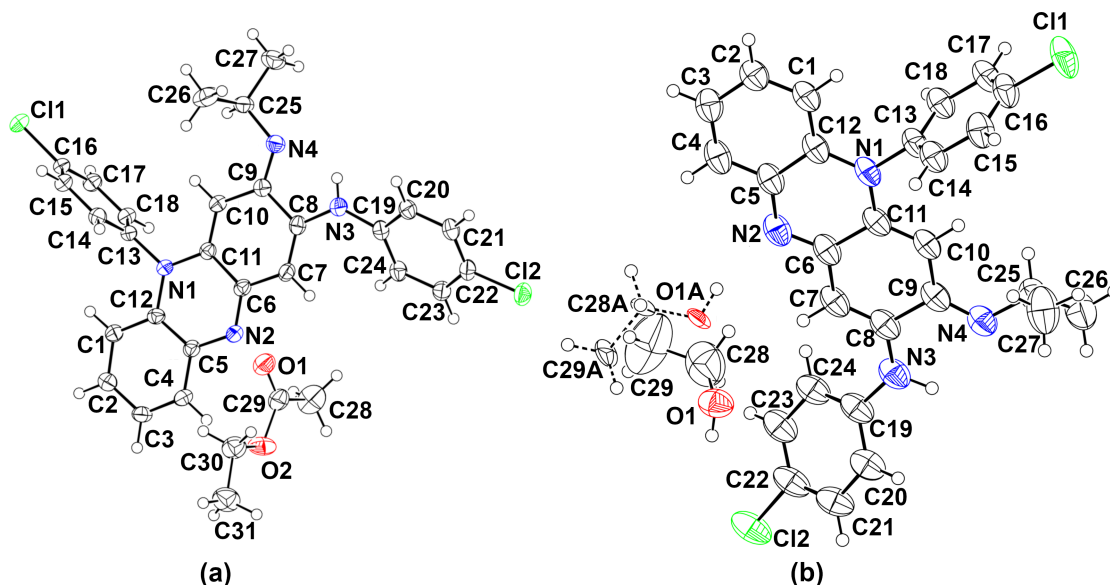
FIGURE 2.2: Structure and labeling scheme of (a) CFZ-EtOAc and (b) CFZ-EtOH. Displacement ellipsoids are drawn at the 50% probability level. Molecule with dashed bonds represents the second position of EtOH (disorder).

ethyl acetate solvate structure, the asymmetric unit contains one molecule of clofazimine and a half ethyl acetate molecule, located on an inversion center (Figure 2.2). A CFZ intramolecular H-bond (N3−H3N···N4, Table 2.3) as well as a weak H-bond [17, 18] between clofazimine and ethyl acetate (C15−H15···O1, Table 2.3) are observed. In the CFZ-EtOH solvate structure, the asymmetric unit contains one molecule of solvent and one molecule of clofazimine (Figure 2.2). Ethanol is disordered over two positions (refined occupancies: 0.771 (5) and 0.229 (5)) and interacts with clofazimine through strong H-bonds (N3−H3···O1 and O1−H1O···N4, as well as O1A−H1OA···N2, Table 2.3). A weak H bond similar to that observed between CFZ and EtOAc is also present between clofazimine and ethanol, C15−H15···O1 Table 2.3.

TABLE 2.1: Results of liquid-assisted grinding screening of clofazimine solid forms in presence of several solvents.
[a] References: Rychlewska *et al.* 1985 [16] and Bannigan *et al.* 2016 [15].

Solvent	Crystalline phase identified by PXRD	CCDC refcode[a]
No solvent	CFZ (I)	DAKXUI01
MeOH	CFZ (I and II)	DAKXUI01 and DAKXUI
EtOH	New pattern (CFZ-EtOH (1/1))	This work
ButOH	CFZ (II)	DAKXUI
MeCN	CFZ (II)	DAKXUI
EtOAc	New pattern (CFZ-EtOAc (1/0.5))	This work
Cyclohexane	CFZ (II)	DAKXUI
Toluene	CFZ (II)	DAKXUI

TABLE 2.2: Experimental details.
Experiments were carried out using an Xcalibur Ruby Gemini Ultra diffractometer. H atoms were treated by a mixture of independent and constrained refinement. Analytical numeric absorption correction using a multifaceted crystal model based on expressions derived by R.C. Clark & J.S. Reid. [19]. Empirical absorption correction using spherical harmonics, implemented in SCALE3 ABSPACK scaling algorithm. Computer programs: *CrysAlis PRO* 1.171.39.46 [20], *CrysAlis PRO* 1.171.40.53 [21], *SHELXT 2014/5* [22], *SHELXL2016/6* [23]. *Mercury*[24], *PublCIF*[25]

	CFZ-EtOAc (1/0.5)	CFZ-EtOH (1/1)
Crystal data		
Chemical formula	$C_{27}H_{22}Cl_2N_4 \cdot 0.5(C_4H_8O_2)$	$C_{27}H_{22}Cl_2N_4 \cdot C_2H_6O$
M_r	517.44	519.45
Crystal system, space group	Triclinic, $P\bar{1}$	Triclinic, $P\bar{1}$
Temperature (K)	100	100
a, b, c (Å)	10.3627(3), 12.0396(4), 12.5861(4)	10.1832(12), 12.0747(10), 12.7486(12)
α, β, γ (°)	87.459(3), 65.968(3), 65.930(3)	74.699(8), 66.689(11), 67.256(10)
V (Å^3)	1295.42(8)	1316.2(3)
Z	2	2
Radiation type	Cu Kα	Cu Kα
μ (mm^{-1})	2.49	2.45
Crystal size (mm)	$0.40 \times 0.10 \times 0.06$	$0.56 \times 0.12 \times 0.06$
Data collection		
Absorption correction	Analytical	Analytical
$T_{\min}$, $T_{\max}$	0.606, 0.871	0.519, 0.874
No. of measured, independent and observed [$I > 2\sigma(I)$] reflections	17752, 4595, 4129	11463, 4594, 3669
R_{int}	0.026	0.032
$(\sin(\theta/\lambda)_{\max}$ (Å^{-1})	0.597	0.598
Refinement		
R[F^2 > 2σ(F^2)], wR(F^2), S	0.031, 0.085, 1.05	0.061, 0.184, 1.05
No. of reflections	4595	4594
No. of parameters	359	363
No. of restraints	0	33
$\Delta\rho_{\max}$, $\Delta\rho_{\min}$ (e Å^{-3})	0.22, -0.23	0.44, -0.51

2.3 Supramolecular features

Despite the differences in H-bonds observed between clofazimine and solvent molecules in CFZ-EtOAc and in CFZ-EtOH, the crystal packing of these two solvates are very similar. Indeed, in both CFZ-EtOAc and CFZ-EtOH a weak C15−H15···O1 H-bond (Figures 2.3 and 2.4, Table 2.3) is observed between CFZ and the solvent molecule. Clofazimine molecules are stacked in a head-to-tail manner and this stacking is further stabilized by weak C18−H18···N2 H-bonds (Figures 2.3 and 2.4, Table 2.3). Crystal packing comparison performed with the 'Crystal-packing similarity'tool in *Mercury* [24] with a packing shell size of 15 molecules and a distance and angle tolerance of 20% revealed that clofazimine molecules have a similar conformation and that solvent molecules are located in the same cavity (Figure 2.5).

TABLE 2.3: Hydrogen-bond geometry.

D−H⋯A	D−H⋯A (Å)	D−H (Å)	H⋯A (Å)	D−H⋯A (°)
		CFZ-EtOAc (1/0.5)		
N3−H3N⋯N4	0.82(2)	2.14(2)	2.591(2)	115(2)
C4−H4⋯Cl1[1]	0.95	2.73	3.621(2)	156
C15−H15⋯O1^{ii}	0.95	2.49	3.386(3)	158
C18−H18⋯N2^{iii}	0.95	2.57	3.460(2)	156
		CFZ-EtOH (1/1)		
N3−H3⋯O1^{ii}	0.98(4)	2.08(4)	3.046(4)	169(3)
O1−H1O⋯N4^{ii}	0.84	2.12	2.906(4)	155
O1A−H1OA⋯N2	0.84	2.07	2.880(6)	163
N3−H3⋯N4	0.97(5)	2.22(5)	2.656(4)	106(4)
C15−H15⋯O1^{iv}	0.95	2.59	3.490(5)	159
C18−H18⋯N2^{v}	0.95	2.52	3.424(4)	159

Symmetry codes: (i) x+1, y, z-1; (ii) -x, -y+1, -z+1; (iii) -x+1, -y, -z+1; (iv) -x+1, -y+1, -z+1; (v) -x+1, -y, -z+1.

(a) **(b)**
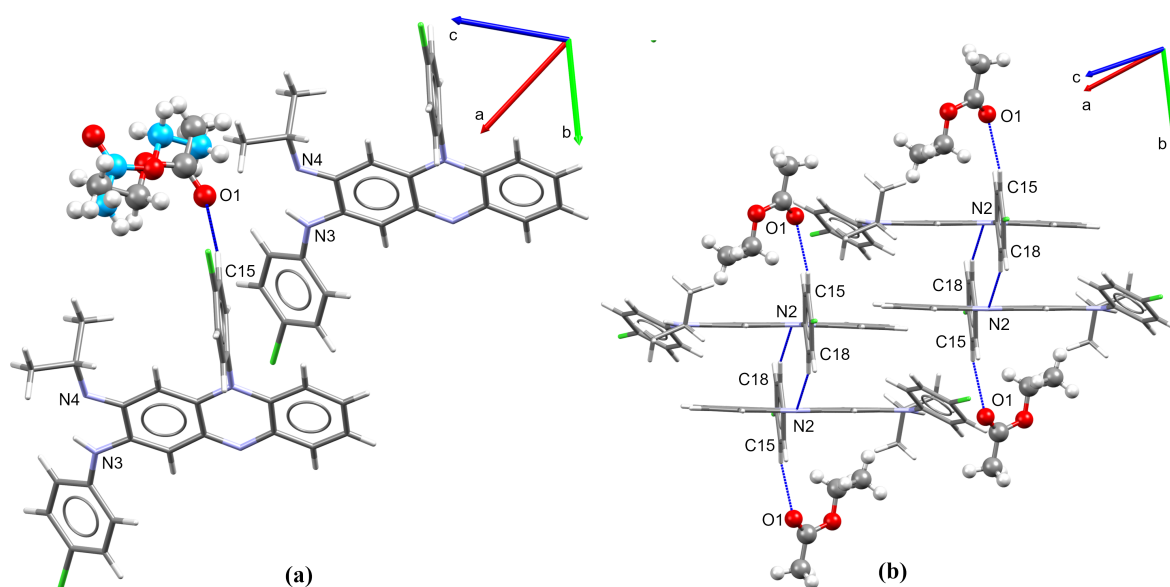
FIGURE 2.3: Weak C15−H⋯O1 H-bond between CFZ and EtOAc (a) and stacking of clofazimine molecules, further stabilized by C18−H⋯N2 H-bond (b) observed in the structure of CFZ-EtOAc (1/0.5). EtOAc molecules are in ball and stick representation (EtOAc molecules are on an inversion center and carbons were colored in grey and blue to allow differentiation of both position of EtOAc (a)). Disorder is not illustrated on Figure (b). H-bonds are illustrated by dark blue lines.
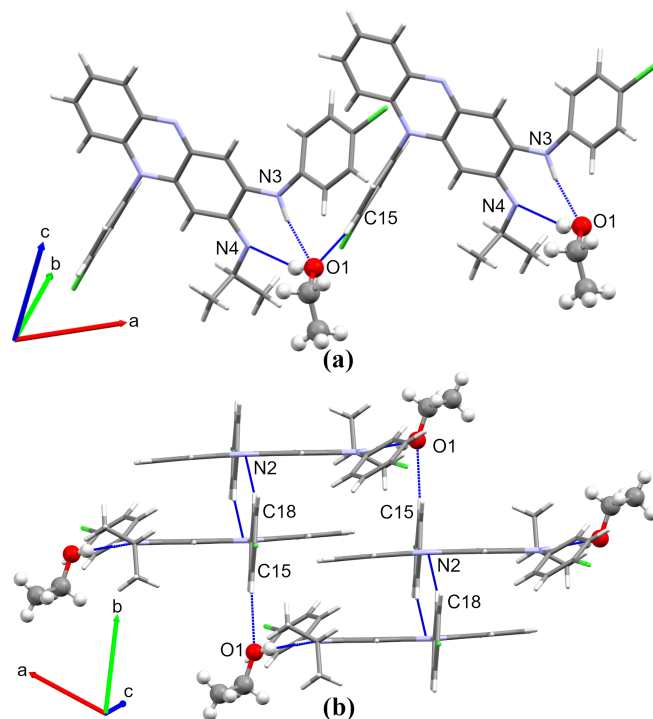
FIGURE 2.4: Weak C15−H···O1H-bond between CFZ and EtOH (a) and stacking of clofazimine molecules, further stabilized by C18−H···N2 H-bond (b) observed in the structure of CFZ-EtOH (1/1). EtOH molecules are represented in ball and stick model. Disorder of EtOH is not shown. H-bonds are illustrated by dark blue lines.
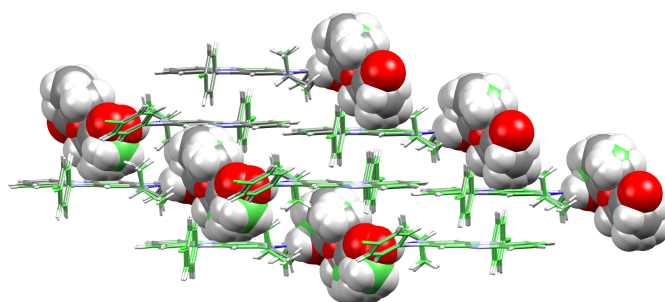
FIGURE 2.5: Crystal packing comparison between CFZ-EtOH (grey) and CFZ-EtOAc (green). Solvent molecules are represented in space fill model.

2.4 Database survey

A search of the Cambridge Structural Database (CSD version 5.42 [26]) performed using clofazimine structure search within ConQuest version 2020.3.0 [27] gave 38 hits, including 4 clofazimine polymorphs [16, 15], 16 anhydrous (cocrystal of) salts (and their polymorphs) [2, 28, 29, 10, 12, 11], 16 hydrated/solvated (cocrystal of) salts (and their polymorphs) [2, 30, 9, 10, 11]. Only two clofazimine solvates are reported with dimethyl-formamide (CFZ-DMF, CSD refcode: CEKTER [1] and with acetone (CFZ-ACE, CSD refcode GESHIX [2]). Crystal packing of CFZ-EtOAc and CFZ-EtOH were compared with those of CFZ-DMF and CFZ-ACE, using the 'Crystal-packing similarity'tool in Mercury (packing shell size of 15 molecules; distance and angle tolerance; 20%). This comparison revealed that in all solvate structures clofazimine has a similar conformation and that solvent molecules are located in the same cavity (Figure 2.6).

(a)

(b)
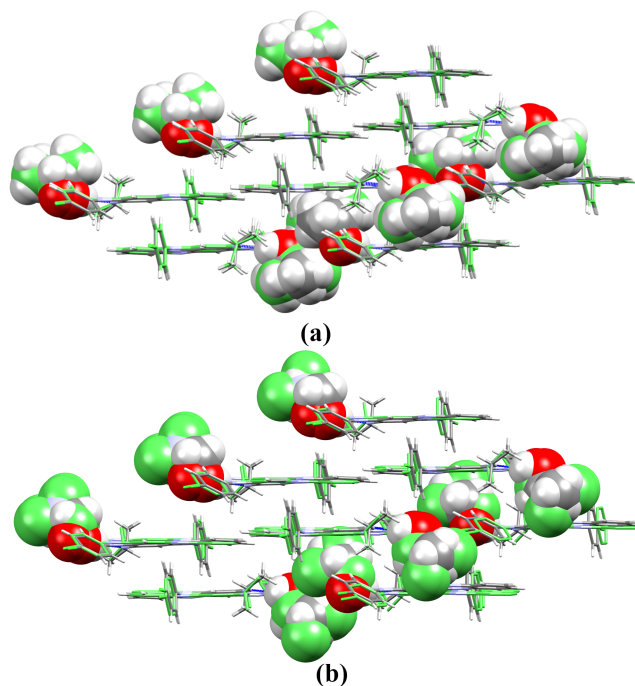
FIGURE 2.6: Crystal packing comparison between (a) CFZ-EtOH (grey) and CFZ-DMF (green) and (b) CFZ-EtOH (grey) and CFZ-ACE (green). Solvent molecules are represented in space fill model.

2.5 Synthesis and crystallization

CFZ-EtOAc and CFZ-EtOH powders were prepared by grinding clofazimine (75.0 mg, 0.158 mmol, purchased from TCI, Zwijndrecht, Belgium) in presence of 30 µL of EtOAc (Sigma-Aldrich, Schnelldorf, Germany) or EtOH (Merck, Overijse, Belgium). The powders were ground in 2 mL eppendorf tubes in presence of eight stainless steel grinding balls (seven balls with a diameter of 2 mm and one ball with a diameter of 3 mm) at

30 Hz during 90 minutes using a Retsch MM 400 Mixer mill apparatus. The crystals were grown by solvent evaporation at room temperature (293-298K) in ethyl acetate (for CFZ-EtOAc) or in ethanol (for CFZ-EtOH). The calculated and experimental powder patterns of CFZ-EtOH and CFZ-EtOAc are presented on Figure 2.7.

2.6   Refinement

Crystal data, data collection and structure refinement details are summarized in Table 2.2. In both structures, H atoms bound to carbon atoms were placed in calculated positions and refined using a riding model (C−H bond length of 0.95 Å for H located on aromatic carbons, 0.98 Å methyl groups, 0.99 Å for CH_2 and 1.0 Å for CH) and with $U_{iso}(H) = 1.2\ U_{eq}(C)$ (except for methyl groups $U_{iso}(H) = 1.5\ U_{eq}(C)$). The H-atom located on N3 of clofazimine was found and refined without constraint (except $U_{iso}(H) = 1.2\ U_{eq}(N)$). The refined N−H distance is 0.97 (4) Å in CFZ-EtOH and 0.82 (2) Å in CFZ-EtOAc, which is in agreement with N−H distance in clofazimine (0.986 Å, CSD refcode: DAKXUI01[16] and 0.80 (2) Å, CSD refcode: DAKXUI [16]).

In the structure of CFZ-EtOH, ethanol is disordered over two positions. Respective occupancies were refined to 0.771 (5) and 0.229 (5), the second position is indicated by the A label suffix for C and O atoms. The H-atom of ethanol alcohol group could not be freely refined and it was positioned at idealized coordinates for OH group, using a rotating group refinement with $U_{iso}(H) = 1.5\ U_{eq}(O)$. The atoms of the disordered ethanol molecule were restrained to have the same bond length, same 1,3 distances and same U_{ij} components (SIMU, standard deviation of 0.04). The parameter of anisotropic displacement in the direction of the bond of disordered ethanol were also restrained using DELU (standard deviation of 0.01).

Acknowledgements

Funding information
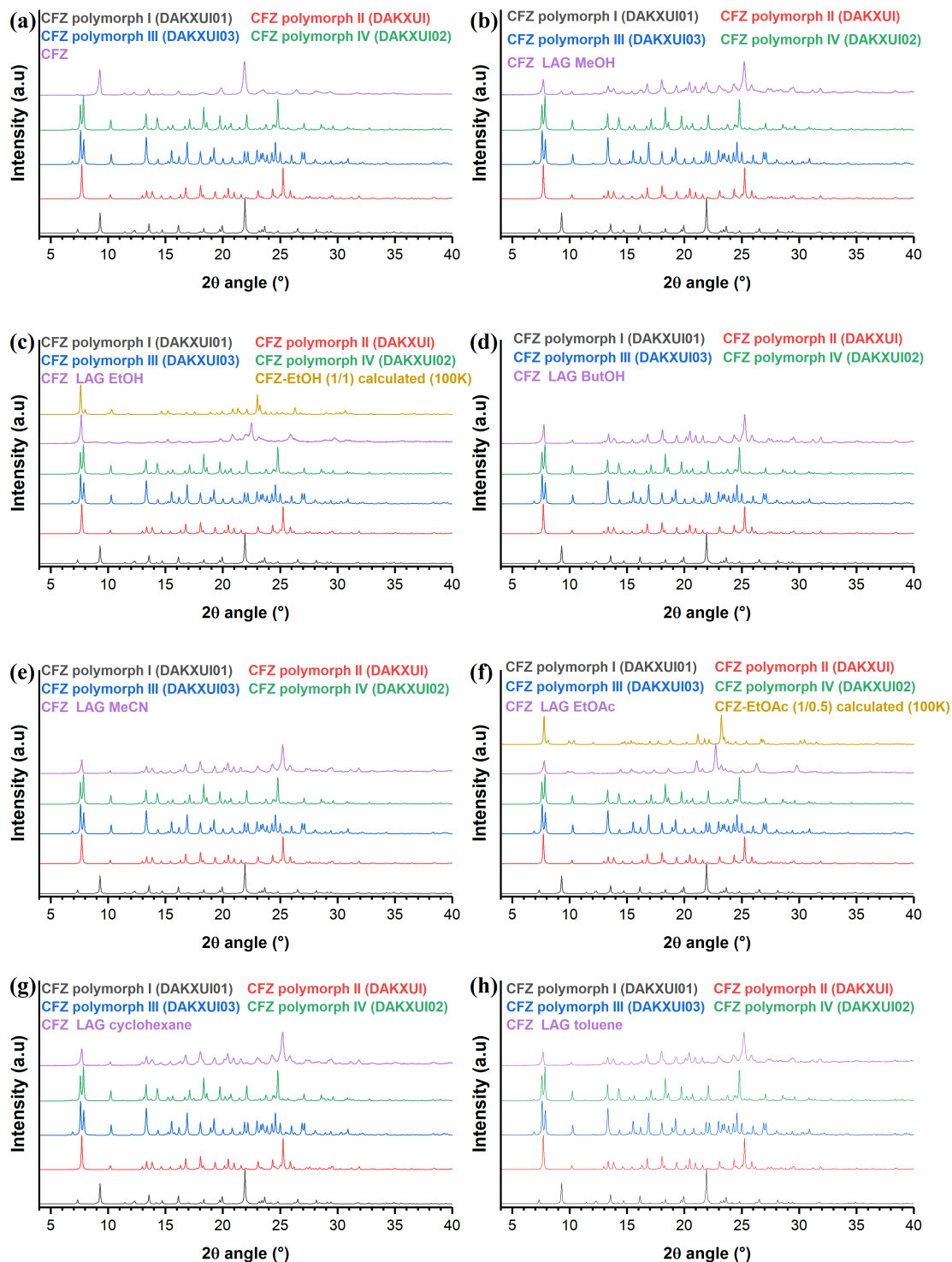
FIGURE 2.7: PXRD patterns of clofazimine polymorphs compared with the pattern of clofazimine commercial powder (a) and clofazimine powder ground in presence of: methanol (b), ethanol (and comparison with calculated pattern) (c), butanol (d), acetonitrile (e), ethyl acetate (and comparison with calculated pattern) (f), cyclohexane (g) and toluene (h).

Bibliography

[1] D. S. Eggleston, W. E. Marsh, and D. J. Hodgson. Structures of the Antileprosy Phenazine Derivatives Clofazimine-N,N- Dimethylformamide, C27H22C12N4.C3H7NO, and B 1912, C30H27ClN4. *Acta Crystallographica*, C40:288–292, 1984.

[2] G. Bolla and A. Nangia. Clofazimine mesylate: A high solubility stable salt. *Crystal Growth & Design*, 12(12):6250–6259, 2012.

[3] V. C. Barry, J. G. Belton, M. L. Conalty, J. M. Denneny, D. W. Edward, J. F. O'sullivan, D. Twomey, and F. Winder. A new series of phenazines (rimino-compounds) with high antituberculosis activity. *Nature*, 179(4568):1013–1015, 1957.

[4] World Health Organization. World health organization model list of essential medicines: 21st list 2019 (no. who/mvp/emp/iau/2019.06). Technical report, World Health Organization, 2019.

[5] M. C. Cholo, H. C. Steel, P. B. Fourie, W. A. Germishuizen, and R. Anderson. Clofazimine: current status and future prospects. *Journal of antimicrobial chemotherapy*, 67(2):290–298, 2012.

[6] C. E. Van Rensburg, G. K. Joone, J. F. O'sullivan, and R. Anderson. Antimicrobial activities of clofazimine and B669 are mediated by lysophospholipids. *Antimicrobial agents and chemotherapy*, 36(12):2729–2735, 1992.

[7] A. S. Narang and A. K. Srivastava. Evaluation of solid dispersions of clofazimine. *Drug Development and Industrial Pharmacy*, 28(8):1001–1013, 2002.

[8] B. Banaschewski, D. Verma, L. J. Pennings, M. Zimmerman, Q. Ye, J. Gadawa, V. Dartois, D. Ordway, J. van Ingen, S. Ufer, et al. Clofazimine inhalation suspension for the aerosol treatment of pulmonary nontuberculous mycobacterial infections. *Journal of Cystic Fibrosis*, 18(5):714–720, 2019.

[9] P. Bannigan, E. Durack, C. Madden, M. Lusi, and S. P. Hudson. Role of Biorelevant Dissolution Media in the Selection of Optimal Salt Forms of Oral Drugs: Maximizing the Gastrointestinal Solubility and in Vitro Activity of the Antimicrobial Molecule, Clofazimine. *ACS Omega*, 2(12):8969–8981, 2017.

[10] L. Bodart, N. Tumanov, and J. Wouters. Structural variety of clofaziminium salts: effect of the counter-ion on clofaziminium conformation and crystal packing. *Acta Crystallographica Section B: Structural Science, Crystal Engineering and Materials*, 75(4), 2019.

[11] L. Bodart, A. Derlet, X. Buol, T. Leyssens, N. Tumanov, and J. Wouters. Combining two antitubercular drugs, clofazimine and 4-aminosalicylic acid, in order to improve clofazimine aqueous solubility and 4-aminosalicylic acid thermal stability. *Journal of Pharmaceutical Sciences*, 109(12):3645–3652, 2020.

[12] M. L. Sousa, M. C. Sarraguça, A. O. dos Santos, J. M. G. Sarraguça, J. Lopes, and P. R. da Silva Ribeiro. A new salt of clofazimine to improve leprosy treatment. *Journal of Molecular Structure*, page 128226, 2020.

[13] L. Bodart, M. Prinzo, A. Derlet, N. Tumanov, and J. Wouters. Taking advantage of solvate formation to modulate drug–drug ratio in clofaziminium diclofenac salts. *CrystEngComm*, 23(1):185–201, 2021.

[14] C. Piotto and P. Bettotti. Surfactant mediated clofazimine release from nanocellulose-hydrogels. *Cellulose*, 26(7):4579–4587, 2019.

[15] P. Bannigan, J. Zeglinski, M. Lusi, J. O'Brien, and S. P. Hudson. Investigation into the Solid and Solution Properties of Known and Novel Polymorphs of the Antimicrobial Molecule Clofazimine. *Crystal Growth & Design*, 16(12):7240–7250, 2016.

[16] U. Rychlewska, M. B. H. Broom, D. S. Eggleston, and D. J. Hodgson. Antileprosy dihydrophenazines. Structural characterization of two crystal forms of clofazimine and of isoclofazimine, B. 3857. *Journal of the American Chemical Society*, 107(16):4768–4772, 1985.

[17] G. R. Desiraju et al. Distinction between the weak hydrogen bond and the van der waals interaction. *Chemical Communications*, (8):891–892, 1998.

[18] G. R. Desiraju and T. Steiner. *The weak hydrogen bond: in structural chemistry and biology*, volume 9. International Union of Crystallography, 2001.

[19] R. C. Clark and J. S. Reid. The Analytical Calculation of Absorption in Multifaceted Crystals. *Acta Crystallographica A*, 51:887–897, 1995.

[20] Rigaku Oxford Diffraction. CrysAlis PRO. Version 1.171.39.46. *CrysAlis PRO. Version 1.171.39.46*, pages Rigaku Oxford Diffraction Ltd, Yarnton, England, 2018.

[21] Rigaku Oxford Diffraction. CrysAlis PRO. Version 1.171.40.53. *CrysAlis PRO. Version 1.171.40.53*, pages Rigaku Oxford Diffraction Ltd, Yarnton, England, 2019.

[22] G. M. Sheldrick. SHELXT - Integrated space-group and crystal-structure determination. *Acta Crystallographica A*, 71(1):3–8, 2015.

[23] G. M. Sheldrick. Crystal structure refinement with SHELXL. *Acta Crystallographica C*, 71:3–8, 2015.

[24] C. F. Macrae, I. J. Bruno, J. A. Chisholm, P. R. Edgington, P. McCabe, E. Pidcock, L. Rodriguez-Monge, R. Taylor, J. Van De Streek, and P. A. Wood. Mercury CSD 2.0 - New features for the visualization and investigation of crystal structures. *Journal of Applied Crystallography*, 41(2):466–470, 2008.

[25] S. P. Westrip. publcif: software for editing, validating and formatting crystallographic information files. *Journal of Applied Crystallography*, 43(4):920–925, 2010.

[26] C. R. Groom, I. J. Bruno, M. P. Lightfoot, and S. C. Ward. The Cambridge Structural Database. *Acta Crystallographica B*, 72:171–179, 2016.

[27] I. J. Bruno, J. C. Cole, P. R. Edgington, M. Kessler, C. F. Macrae, P. McCabe, J. Pearson, and R. Taylor. New software for searching the cambridge structural database and visualizing crystal structures. *Acta Crystallographica Section B: Structural Science*, 58(3):389–397, 2002.

[28] R. K. Keswani, J. Baik, L. Yeomans, C. Hitzman, A. M. Johnson, A. S. Pawate, P. J. Kenis, N. Rodriguez-Hornedo, K. A. Stringer, and G. R. Rosania. Chemical Analysis of Drug Biocrystals: A Role for Counterion Transport Pathways in Intracellular Drug Disposition. *Molecular Pharmaceutics*, 12(7):2528–2536, 2015.

[29] P. Bannigan, E. Durack, H. Mathur, M. C. Rea, R. P. Ross, and S. P. Hudson. Delivery of a hydrophobic drug into the lower gastrointestinal system via an endogenous enzyme-mediated carrier mechanism: An in vitro study. *European Journal of Pharmaceutics and Biopharmaceutics*, 133:12–19, 2018.

[30] E. M. Horstman, R. K. Keswani, B. A. Frey, P. M. Rzeczycki, V. LaLone, J. A. Bertke, P. J. Kenis, and G. R. Rosania. Elasticity in Macrophage-Synthesized Biocrystals. *Angewandte Chemie - International Edition*, 56(7):1815–1819, 2017.

Chapter 3

Structural variety of clofaziminium salts: effect of the counter-ion on clofaziminium conformation and crystal packing†

Structural variety of clofaziminium salts: effect of the counter-ion on clofaziminium conformation and crystal packing

Laurie Bodart*, Nikolay Tumanov and Johan Wouters

Department of Chemistry, University of Namur, Rue de Bruxelles 61, Namur 5000, Belgium.
Correspondence e-mail: laurie.bodart@unamur.be

Keywords: clofazimine; salts; conformational comparison; crystal packing comparison; counter-ion effect on clofaziminium conformation; tuberculosis.

Abstract. Clofazimine is a water-insoluble antimycobacterial agent gaining attention as a treatment for multidrug resistant and extensively drug-resistant tuberculosis. Novel salts of clofazimine are reported with fumaric, succinic, 2,4-dihydroxybenzoic and terephthalic acids and with saccharin. The salt structures were obtained by single-crystal X-ray diffraction. The salts with 2,4-dihydroxybenzoic acid and with saccharin are solvated (methanol and acetonitrile, respectively). The reaction of clofazimine with terephthalic acid led to two salt cocrystals, one solvated and one non-solvated. These new clofaziminium salts are compared with the currently known ones in terms of crystal packing and clofazimine/ium conformation. Clofaziminium hydrogen succinate presents isostructurality with clofaziminium hydrogen malonate, an already described salt. In the structure of clofaziminium terephthalate terephthalic acid salt cocrystal, solvent evaporation leads to packing and hydrogen-bonding modifications. In all the new structures, the clofaziminium conformation is quite well conserved and steric hindrance is observed around the protonated site. Conformational optimization of clofaziminium reveals that this steric-hindrance energy penalty is compensated for by hydrogen-bond interactions with the salt counter-ions.

Chapter 3

3.1   Introduction

Clofazimine (CFZ) (Fig. 3.1) is an antimycobacterial and anti-inflammatory agent belonging to the family of riminophenazine. First synthesized by Barry and co-workers in 1957, clofazimine has been used worldwide in combination with dapsone and rifampicin as a treatment against leprosy thanks to its bactericidal effect against *Mycobacterium leprae* [1]. Besides its anti-leprotic properties, clofazimine is also a drug used to treat multidrug resistant tuberculosis (MDR-TB) [2]. Recently, the appearance of resistant strains of *Mycobacterium tuberculosis* (*M. tb*) has resulted in a renewal of interest in this drug, since clofazimine exhibits good *in vitro activity* against MDR-TB [3, 4]. However, clofazimine is a very lipophilic molecule, resulting in poor solubility and very long half-life (around 70 days in the human body [5]). This property is associated with undesirable effects such as recrystallization of the compound in the liver and in macrophages [6, 7] and bioaccumulation, resulting in strong side effects, skin discoloration [8] and poor compliance.

Currently, clofazimine has limited clinical use, probably because of its lack of bioavailability and thus its limited efficiency. Several methods have been investigated to increase clofazimine solubility, with varying degrees of success. Among these were, for example, clofazimine complexation in cyclodextrins [9], preparation of an amorphous solid dispersion [10] or clofazimine co-administration with lipid vehicles [11].

Because clofazimine is gaining attention as a treatment for MDR-TB and extensively drug resistant tuberculosis (XDR-TB), groups of researchers have recently tried new approaches to improve its pharmacological properties. As clofazimine is a weakly basic compound (pKa 9.29 [7]), a possible strategy to increase its solubility is salt formation. In 2012, Bolla and co-workers published eight structures of salts and one of these, clofazimine mesylate, was 99 times more soluble in 60% EtOH-water media than pure clofazimine [12]. In 2016, Bannigan and co-workers investigated clofazimine polymorphism [13] and more recently they studied the solubility of several clofaziminium salts [14]. Here, we report seven new structures: three salts [clofaziminium hydrogen fumarate, **CFZ-NH$^+$-FA$^+$ (1:1)**, clofaziminium hydrogen succinate, **CFZ-NH$^+$-SA$^-$ (1:1)**, and clofaziminium saccharinate, **CFZ-NH$^+$-SACC$^-$(1:1)**], two solvated salts [clofaziminium 2,4-dihydroxybenzoate methanol solvate, **CFZ-NH$^+$-2,4-DHBA$^-$-MeOH (1:1:1)**, and clofaziminium saccharinate acetonitrile solvate, **CFZ-NH$^+$-SACC$^-$-MeCN (1:1:1.4)**] and two salt cocrystals (with structures composed of one cation, one anion and a non-ionized molecule), one nonstoichiometrically solvated and the other non-solvated [clofaziminium terephthalate terephthalic acid solvate, **CFZ-NH$^+$-TRPTA^{2-}-TRPTA-solvent (1:0.5:0.5:x)**, and clofaziminium terephthalate terephthalic acid, **CFZ-NH$^+$-TRPTA^{2-}-TRPTA (1:0.5:0.5)**]. These new salts are compared with the currently known ones in terms of crystal packing and clofaziminium conformation.
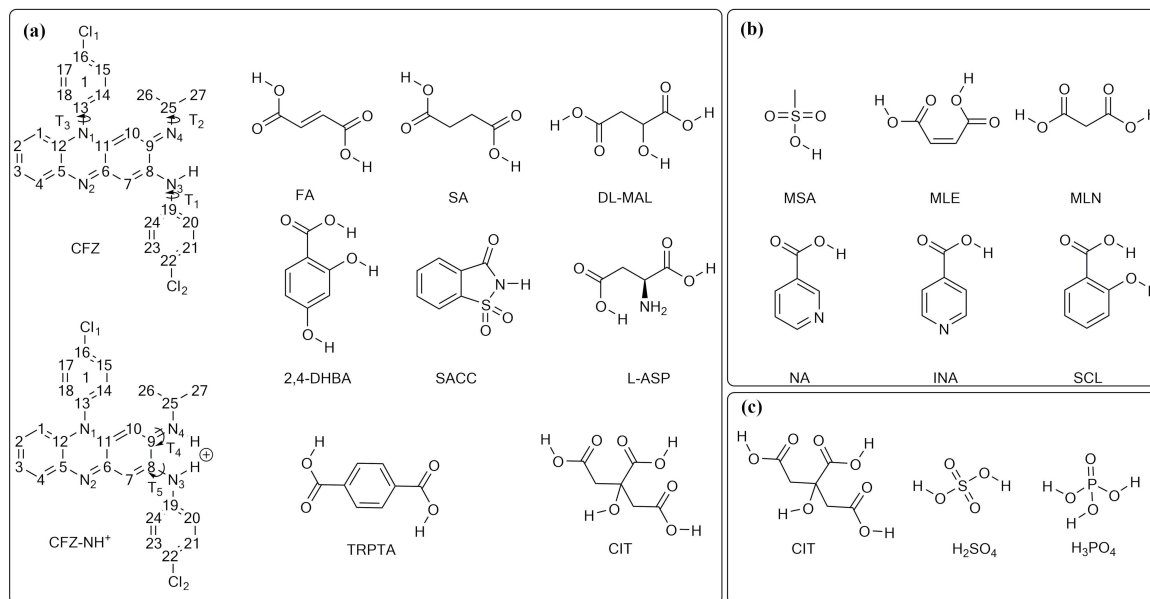
FIGURE 3.1: (a) The numbering scheme for clofazimine/ium (CFZ/CFZ-NH$^+$) (torsion angles: T1 C8-N3-C19-C20, T2 C9-N4-C25-C27, T3 C12-N1-C13-C18, T4 H-N4-C9-C8 and T5 H-N3-C8-C9) and selected acids in the present work: fumaric acid (FA), succinic acid (SA), DL-malic acid (DL-MAL), 2,4-dihydroxybenzoic acid (2,4-DHBA), saccharin (SACC), L-aspartic acid (L-ASP), terephthalic acid (TRPTA) and citric acid (CIT). (b) Acids crystallized with clofazimine by Bolla & Nangia (2012) [12]. (c) Acids crystallized with clofazimine by Bannigan et al. (2017) [14]. The CFZ-NH$^+$-CIT$^-$ (1:1) salt was previously described by Bannigan et al. (2017) [14]; in the present study, salt formation of CFZ/CIT in 2:1 and 3:1 molar ratios was attempted.

3.2 Experimental

3.2.1 Materials

Clofazimine was purchased from TCI Europe N.V. (Zwijndrecht, Belgium). Fumaric, 2,4-dihydroxybenzoic and terephthalic acids and saccharin were purchased from Sigma-Aldrich (Steinheim, Germany), while succinic acid was purchased from J. T. Baker Chemicals (Deventer, Holland). The crystallization solvents (acetonitrile, methanol, ethyl acetate and diethyl ether) are commercially available (Acros Organics, Geel, Belgium) and were used without further purification.

3.2.2 General routes for clofazimine salification

All samples were prepared by liquid-assisted grinding (LAG) [15, 16, 17, 18] using a Retsch MM 400 Mixer Mill apparatus with two grinding jars in which five 2 ml Eppendorf tubes can be installed. Each sample grinding was performed with around 100 mg of powder (75 mg of clofazimine and a corresponding mass of acid to respect the 1:1, 2:1 or 3:1 CFZ:acid molar ratios) in the presence of six to eight stainless steel grinding balls (2 mm diameter). The following solvents were used for liquid-assisted ball milling: acetonitrile (MeCN) for

CFZ/FA, CFZ/SA, CFZ/SACC, CFZ/L-ASP and CFZ/DL-MAL equimolar mixtures, and for CFZ/CIT 2:1 and 3:1 mixtures; methanol (MeOH) for CFZ/2,4-DHBA 1:1; and ethyl acetate (EtOAc) for CFZ/TRPTA. Powders leading to new diffraction patterns were then involved in crystallization assays by slow evaporation at room temperature (293-298K) in a mixture of MeCN and MeOH, except for the CFZ/TRPTA 1:1 powder for which EtOAc was used. For CFZ/DL-MAL, crystallization in diethyl ether (Et_2O) at 4 °C and in MeCN at room temperature was also attempted.

3.2.3 Single-crystal X-ray diffraction (SCXRD)

Selected crystals of suitable size were mounted on an Oxford Diffraction Gemini Ultra R system (four-circle kappa platform, Ruby CCD detector). By default Mo radiation was used for data collection, but if a crystal diffracted poorly then Cu radiation was used as it allows enhanced intensities with this Gemini system. In consequence, data were collected using Mo Kα ($\lambda = 0.71073$ Å) for **CFZ-NH$^+$-SA$^-$ (1:1)**, **CFZ-NH$^+$-TRPTA^{2-}-TRPTA-solvent (1:0.5:0.5:x)** and **CFZ-NH$^+$-TRPTA^{2-}-TRPTA (1:0.5:0.5)**, or Cu Kα ($\lambda = 1.54184$Å) for the other salts [**CFZ-NH$^+$-FA$^+$ (1:1)**, **CFZ-NH$^+$-2,4-DHBA$^-$-MeOH (1:1:1)**, **CFZ-NH$^+$-SACC$^-$(1:1)** and **CFZ-NH$^+$-SACC$^-$-MeCN (1:1:1.4)**].

Full data sets were collected either at 295 K [**CFZ-NH$^+$-FA$^+$ (1:1)**, **CFZ-NH$^+$-SA$^-$ (1:1)**, **CFZ-NH$^+$-SACC$^-$(1:1)**, **CFZ-NH$^+$-2,4-DHBA$^-$-MeOH (1:1:1)** and **CFZ-NH$^+$-TRPTA^{2-}-TRPTA (1:0.5:0.5)**] or at 100 K [**CFZ-NH$^+$-SACC$^-$-MeCN (1:1:1.4)** and **CFZ-NH$^+$-TRPTA^{2-}-TRPTA-solvent (1:0.5:0.5:x)**].

Analytical absorption correction was performed on SCXRD data for structures **CFZ-NH$^+$-FA$^+$ (1:1)**, **CFZ-NH$^+$-SA$^-$ (1:1)**, **CFZ-NH$^+$-TRPTA^{2-}-TRPTA-solvent (1:0.5:0.5:x)** and **CFZ-NH$^+$-TRPTA^{2-}-TRPTA (1:0.5:0.5)** using *CrysAlis PRO* [Versions 1.171.38.46 [19] and 1.171.39.46 [20]]. Analytical numerical absorption correction was implemented using a multifaceted crystal model based on expressions derived by Clark & Reid [21]. Empirical absorption correction was carried out using spherical harmonics [22] as implemented in the *SCALE3 ABSPACK* scaling algorithm. Gaussian absorption correction was performed on SCXRD data for structures **CFZ-NH$^+$-SACC$^-$-MeCN (1:1:1.4)** and **CFZ-NH$^+$-2,4-DHBA$^-$-MeOH (1:1:1)** using *CrysAlis PRO* (Version 1.171.39.46 [20]). Numerical absorption correction was carried out based on Gaussian integration over a multifaceted crystal model. Multi-scan absorption correction was performed on SCXRD data for structure **CFZ-NH$^+$-SACC$^-$(1:1)** (*CrysAlis PRO* Version 1.171.39.46 [20]).

Structures were solved by the dual-space method using *SHELXT* [23] and then refined by the least-squares method using *SHELXL-2018/1* [24] within *OLEX2* [25] and *SHELXLE* [26]. Non-H atoms were refined anisotropically. H atoms involved in strong hydrogen bonds were located in difference Fourier maps [except for disordered MeOH molecules in the structure of **CFZ-NH$^+$-2,4-DHBA$^-$-MeOH (1:1:1)**], while those not involved in hydrogen bonds were refined as riding atoms by fixing the displacement ellipsoids to 1.2 times that of the parent atom (or 1.5 for methyl groups).

Several structures are disordered, namely **CFZ-NH$^+$-SA$^-$ (1:1)** (atoms C29 and C30 of hydrogen succinate), **CFZ-NH$^+$-2,4-DHBA$^-$-MeOH (1:1:1)** (2,4-DHBA$^-$ and MeOH show minor disorder, but the H atom of the OH group of the disordered MeOH could not be located in the difference Fourier map), **CFZ-NH$^+$-SACC$^-$ (1:1)** (SACC$^-$ is disordered) and **CFZ-NH$^+$-SACC$^-$-MeCN (1:1:1.4)** (chlorophenyl ring 1 in Fig. 3.1, the isopropyl groups of clofazimine and the acetonitrile, which is disordered over three positions).

The structure of the salt cocrystal **CFZ-NH$^+$-TRPTA^{2-}-TRPTA-solvent (1:0.5:-0.5:x)** presents solvent-accessible voids forming channels but the solvent of crystallization could not be unambiguously assigned. Therefore, the original reflection file of **CFZ-NH$^+$-TRPTA^{2-}-TRPTA-solvent (1:0.5:0.5:x)** was submitted to the *PLATON* SQUEEZE procedure [27]. The total potential accessible void volume was determined as 489Å^3 with an electron count per cell of 141, which corresponds to 2.9 EtOAc molecules in the unit cell.

Only low-resolution data collection (up to 0.9Å) could be performed for the structure **CFZ-NH$^+$-SACC$^-$ (1:1)** because the crystals were obtained by desolvating crystals of **CFZ-NH$^+$-SACC$^-$-MeCN (1:1:1.4)** (other methods did not lead to unsolvated crystals).

3.2.4 Powder X-ray diffraction (PXRD)

Powder diffraction data were collected on a PANalytical X'PERT PRO Bragg-Brentano diffractometer with Cu Kα radiation (λ = 1.54184Å) at 45 kV and 30 mA with an X'Celerator linear detector. Data were collected at 2θ angles from 4 to 40° with a step size of 0.0167°. Variable-temperature measurements using an AntonPaar system were realized at 25 °C and then between 30 and 200 °C with data collection every 10 °C. Calculated powder patterns from the SCXRD data were generated with the program *Mercury* (Version 3.10.2 [28]).

3.2.5 Search of the Cambridge Structural Database (CSD)

The known structures of clofazimine and clofaziminium salts were retrieved from the Cambridge structural database (CSD) [29] using *ConQuest*. In total, 15 structures involving clofazimine were retrieved (clofazimine, clofaziminium salts and/or solvates). Three other clofaziminium salts [**CFZ-NH$^+$-CIT$^-$ (1:1)**, **CFZ-NH$^+$-H$_2$PO$_4$$^-$-H$_2$O (1:1:0.25)** and **CFZ-NH$^+$-HSO$_4^-$-MeOH (1:1:1)**] were available as supplementary data from the publication of Bannigan *et al.* (2017) [14]. All 18 of these structures were analysed further.

3.2.6 Structure visualization, void calculation and generation of full interaction maps (FIMs)

The structures were visualized using *Mercury* and images were generated using the same program. Figures illustrating voids were generated with the 'Display voids' option in *Mercury*, with a probe radius of 1.2 Å and a grid spacing of 0.1 Å. For the structures of **CFZ-NH$^+$-TRPTA^{2-}-TRPTA-solvent (1:0.5:0.5:x)** and **CFZ-NH$^+$-TRPTA^{2-}-TRPTA (1:0.5:0.5)**, the least-squares planes passing through atoms N1, C5 and C6 of clofaziminium were calculated with *Mercury* in order to compare the crystal packing of the two structures. Full interaction maps (FIMs) were generated within *Mercury*. The probes used for FIM generation were uncharged NH nitrogen, alcohol oxygen and carbonyl oxygen, with a contour level of 6.0. FIMs were generated using the coordinates of a clofazimine molecule (from the polymorph with CSD refcode DAKXUI03) [Fig. 3.2(a)], a clofaziminium ion [refcode GESHET, **CFZ-NH$^+$-MSA$^-$-H$_2$O (1:1:1)**] [Figs. 3.2(b) and 3.6(a)] and a clofaziminium ion from **CFZ-NH$^+$-CIT$^-$ (1:1)** [Fig. 3.6(b)] (for these salts, only clofaziminium was considered for FIM generation).

3.2.7 Crystal-packing comparison

Crystal-packing comparisons and overlays of the crystal structures were performed with the 'Crystal-packing similarity' tool in *Mercury*, with a packing shell size of 15 molecules and distance and angle tolerances of 30% and 30°, respectively. Molecular differences and structure inversion were allowed, while bond types, H-atom positions, an atom's hydrogen count and an atom's bond count were ignored. As multi-component systems with different counter-ions were analysed, the smallest molecular component was ignored for the packing overlays. Only **CFZ-NH$^+$-SA$^-$ (1:1)** showed a molecular overlay of 15 molecules out of 15 with **CFZ-NH$^+$-MLN$^-$ (1:1)** (GESGOC).

3.2.8 Melting-point measurement

The melting points of the non-solvated salts were determined visually using a Büchi B545 melting-point apparatus.

3.2.9 Clofazimine/clofaziminium overlay

For each structure of clofazimine/clofaziminium salt (the structures of this paper and these found in the literature), the coordinates of one molecule/ion of clofazimine/clofaziminium were selected from the asymmetric unit. All selected molecules/ions were overlaid using the 'Small-molecule overlay' tool in *Discovery Studio* (Version 18 in *BIOVIA* [30]). Neither rotatable bonds nor flexible torsions were allowed and the alignment by consensus was performed by a field that was 50% steric and 50% electrostatic.

3.2.10 Conformational analysis by quantum mechanics calculations

Optimization calculations of clofazimine and clofaziminium were performed using density functional theory (DFT) with the m06 functional [31] and the 6-311G(d) basis set [32]. To this end, the coordinates of the neutral form of clofazimine were extracted from the DAKXUI03 structure, while the coordinates of the protonated form (clofaziminium) were extracted from the crystal structure of **CFZ-NH$^+$-Cl$^-$ (1:1)** (LABQUD).

3.3 Results and discussion

Acidic compounds to react with clofazimine were selected after FIM analysis of clofazimine and clofaziminium. Salification assays were performed by liquid-assisted grinding, and powders leading to new diffraction patterns were used in crystallization experiments. In this section, the results obtained after the salification assays and PXRD measurements are first summarized. The new structures are then described and compared with the known ones in terms of interaction and crystal-packing similarity. Finally, the clofazimine and clofaziminium conformations are compared with each other and with the optimized conformations of clofazimine and clofaziminium (in the presence or absence of counterions).

3.3.1 FIM analysis of CFZ and CFZ-NH$^+$ and choice of acids to react with CFZ

FIMs were generated to investigate the propensity of clofazimine/clofaziminium to interact with uncharged NH nitrogen, alcohol oxygen and carbonyl oxygen. FIM calculations at the 6.0 contour level indicate two main sites of interaction, namely around atoms N3 and N4 for the first site and around N2 for the second site (Fig. 3.2). Both sites are common for clofazimine and clofaziminium. However, the interaction between the first site and carbonyl oxygen or OH probes is stronger in the case of clofaziminium [Figs. 3.2(a) and 3.2(b)]. From these FIM analyses, it can be assumed that clofazimine should be able to form salts with several carboxylic acids.

Clofaziminium salts with organic acids (methanesulfonic acid, maleic acid, isonicotinic acid, nicotinic acid, salicylic acid and malonic acid) were reported by Bolla & Nangia [12], while Bannigan and co-workers obtained clofaziminium salts by reacting clofazimine with organic and inorganic acids (hydrochloric, sulfuric, nitric, oxalic, phosphoric, citric, formic and acetic acids [14]). Here, other carboxylic acids (which should protonate atom N4 of CFZ) were selected to form new clofaziminium salts. 2,4-DHBA and DL-MAL were selected because of their alcohol functions, which could potentially interact with the N2 site of CFZ. L-ASP was chosen to assess the ability of clofazimine to react with amino acids. CIT was selected to be reacted with CFZ in 2:1 and 3:1 CFZ/CIT molar ratios to investigate the propensity of CIT to be unprotonated on multiple sites. The potential new structures of CFZ/CIT could be compared with the one obtained by Bannigan *et*
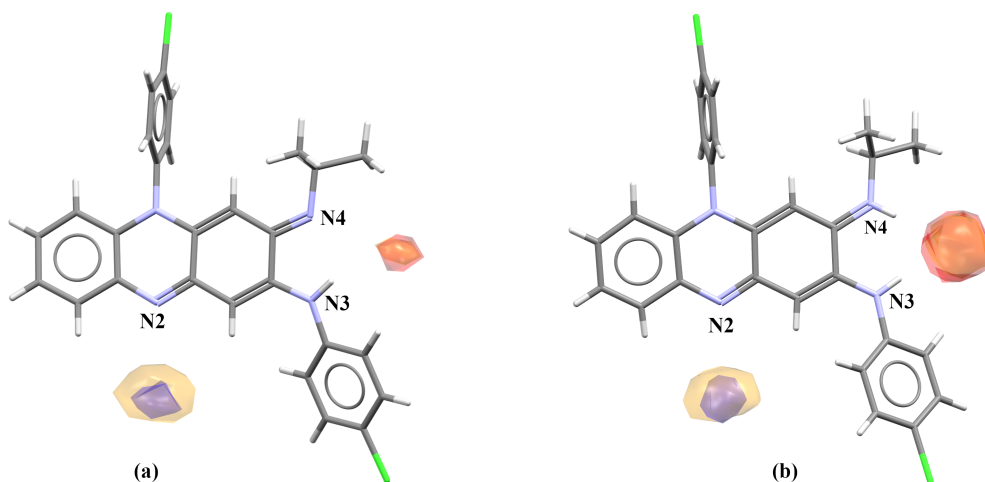
FIGURE 3.2: FIMs calculated around (a) clofazimine and (b) clofaziminium. Carbonyl oxygen, uncharged NH and alcohol OH probes are shown in red, blue and orange, respectively.

al. [14]. FA and SA were chosen for their similarity and so for their potential ability to form isostructural structures. TRPTA was selected to compare CFZ salts obtained with aliphatic *versus* aromatic dicarboxylic acids. Finally, saccharin was chosen to evaluate its propensity to react with clofazimine. Indeed, saccharin has acidic properties despite its lack of a carboxylic acid function.

Except for terephthalic acid and 2,4-dihydroxybenzoic acid, the selected compounds are classified either as food additives [33] or as generally regarded as safe (GRAS) [34].

3.3.2 CFZ salification assays and corresponding results

All liquid-assisted ball milling led to solids with new powder patterns except for CFZ/L-ASP 1/1 (Fig. A.2 in the supporting information). Crystallization assays of all powders except this one were attempted and only CFZ/DL-MAL did not crystallize under our conditions. Single-crystal X-ray diffraction data were collected on crystals of suitable size. Seven new clofaziminium salt structures were refined. Among these, three are salts [clofaziminium hydrogen fumarate, **CFZ-NH$^+$-FA$^-$ (1:1)**, clofaziminium hydrogen succinate, **CFZ-NH$^+$-SA$^-$ (1:1)**, and clofaziminium saccharinate, **CFZ-NH$^+$-SACC$^-$ (1:1)**], two are solvated salts [clofaziminium 2,4-dihydroxybenzoate methanol solvate, **CFZ-NH$^+$-2,4-DHBA$^-$-MeOH (1:1:1)**, and clofaziminium saccharinate acetonitrile solvate, **CFZ-NH$^+$-SACC$^-$-MeCN (1:1:1.4)**] and two are salt cocrystals (with structures composed of one cation, one anion and a non-ionized molecule), one nonstoichiometrically solvated and the other non-solvated [clofaziminium terephthalate terephthalic acid solvate, **CFZ-NH$^+$-TRPTA^{2-}-TRPTA-solvent (1:0.5:0.5:x)**, and clofaziminium terephthalate terephthalic acid, **CFZ-NH$^+$-TRPTA^{2-}-TRPTA (1:0.5:0.5)**]. The latter was obtained by slowly drying the corresponding solvated crystals at room temperature. Crystals of CFZ/CIT 2:1 were also obtained. However, the structure is intrinsically disordered and could not be refined, even using data collected at 100 K. Its

TABLE 3.1: Clofazimine salification assays and corresponding results.

Acid	pKas [35]	CFZ/Acid ratio	New PXRD?	Crystals?	Structure refined?
FA	3.02; 4.38	1/1	Yes	Yes	Yes
SA	4.21; 5.64	1/1	Yes	Yes	Yes
2,4-DHBA	3.11	1/1	Yes	Yes	Yes
DL-MAL	3.40; 5.11	1/1	Yes	No	No
SACC	1.94 [36]	1/1	Yes	Yes	Yes
L-ASP	1.99; 3.90	1/1	No	No	No
TRPTA	3.54; 4.34	1/1	Yes	Yes	Yes
CIT	3.13;	2/1	Yes	Yes	No§
	4.76; 6.40	3/1	Yes	Yes‡	No

§ Structure of **CFZ-NH$^+$-CIT$^-$ (2:1)** is intrinsically disordered. ‡ Crystallized as **CFZ-NH$^+$-CIT$^-$ (2:1)**.

cell parameters were determined [a = 19.2962 (5), b = 12.3140 (3) and c = 23.9105 (6)Å, and α = 90, β = 110.667 (3) and γ= 90°] and the powder pattern of the as-synthesized product matches the one calculated from single-crystal data (Fig. A.2).

Finally, CFZ/CIT 3:1 has a powder pattern very similar to the one obtained after grinding CFZ/CIT 2:1. However, some new peaks are observed (Fig. A.2). Crystallization assays of CFZ/CIT 3:1 led to crystals of CFZ/CIT 2:1. The results of the CFZ salification assays are summarized in Table 3.1.

3.3.3 Crystal-packing descriptions of the new CFZ salts

3.3.3.1 CFZ-NH$^+$-FA$^-$ (1:1) salt

Clofaziminium hydrogen fumarate salt [Fig. 3.3(a)] crystallizes in space group $P2_1/c$ (Table 3.2). Proton transfer between fumaric acid (O3) and the isopropyl imine of CFZ (N4) occurs. As already observed by Bannigan *et al.* [14], this proton transfer is accompanied by an increase in the iminium angle [C9-N4-C25 = 126.02 (18)°] compared with that of the uncharged clofazimine (C9-N4-C25 around 120°, Table A.3). An $R_2^1(7)$ hydrogen-bond motif is observed between FA$^-$ and CFZ-NH$^+$ (N4$^+$-H$\cdots$O3$^-$ and N3-H$\cdots$O3$^-$; Table A.2). Hydrogen fumarate forms chains along the a axis through hydrogen bonds [$C_1^1(7)$ motif, O1-H$\cdots$O3$^-$; Table A.2). A $D_1^1(2)$ motif is also present (N3-H$\cdots$O2; Table A.2). CFZ-NH$^+$ are stacked along the a axis in a head-to-tail fashion.

The PXRD pattern of the as-synthesized powder matches the one calculated from single-crystal data (Fig. A.1). The melting point of **CFZ-NH$^+$-FA$^-$ (1:1)** is 246 °C, which is much higher than that of the starting active pharmaceutical ingredient (API) (Table 3.3).

3.3.3.2 CFZ-NH$^+$-SA$^-$ (1:1) salt

Clofaziminium hydrogen succinate salt [Fig. 3.3(b)] crystallizes in the space group $P\bar{1}$ (Table 3.2). Proton transfer between succinic acid (O1) and the isopropyl imine of CFZ (N4) occurs, which is confirmed by bond distances reflecting resonance in the carboxylate

and by an increase in the iminium angle (Table A.3). An $R_2^1(7)$ hydrogen-bond motif is observed between SA$^-$ and CFZ-NH$^+$ (N4$^+$-H$\cdots$O1$^-$ and N3-H$\cdots$O1$^-$) and an intramolecular hydrogen bond is also present in the hydrogen succinate ion ($S_1^1(7)$ motif, O4-H$\cdots$O2$^-$; Table A.2). 2D sheets are formed through weak C-H$\cdots$O and C-H$\cdots$Cl hydrogen bonds (Table A.2).

The PXRD pattern of the as-synthesized product matches the one calculated from single-crystal data (Fig. A.1). This salt melts at 214 °C, 5 °C lower than that of the the starting API CFZ (Table 3.3).

3.3.3.3   CFZ-NH$^+$-SACC$^-$-MeCN (1:1:1.4) solvated salt

Clofaziminium saccharinate acetonitrile solvated salt [Fig. 3.3(c)] crystallizes in the space group $P\bar{1}$ (Table 3.2). Proton transfer between saccharin (N5) and the isopropyl imine of CFZ (N4) occurs and is confirmed by an increase in the iminium angle (Table A.3). The acetonitrile solvate is disordered over three positions (the occupancies of the first, second and third positions were refined to 0.4640, 0.4890 and 0.440, respectively). An $R_2^2(9)$ hydrogen-bond motif is observed between SACC$^-$ and CFZ-NH$^+$ (N4$^+$-H$\cdots$O3 and N3-H$\cdots$N5$^-$ [Fig. 3.3(c) and Table A.2]). Weak C-H$\cdots$O hydrogen-bonds stabilize the head-to-tail stacking of CFZ-NH$^+$ (Table A.2).

3.3.3.4   CFZ-NH$^+$-SACC$^-$ (1:1) salt

Clofaziminium saccharinate [Fig. 3.3(d)] was obtained by drying crystals of **CFZ-NH$^+$-SACC$^-$-MeCN (1:1:1.4)** at room temperature. The unsolvated salt [**CFZ-NH$^+$-SACC$^-$ (1:1)**] crystallizes in the space group $P\bar{1}$ (Table 3.2). Proton transfer between saccharin (N5) and the isopropyl imine of CFZ (N4) occurs and is confirmed by an increase in the iminium angle (Table A.3).

An $R_2^1(7)$ hydrogen-bond motif is observed between SACC$^-$ and CFZ-NH$^+$ (N4$^+$-H$\cdots$N5$^-$ and N3-H$\cdots$N5$^-$ [Fig. 3.3(c) and Table A.2]. Weak C-H$\cdots$O hydrogen bonds stabilize the head-to-tail stacking of CFZ-NH$^+$ (Table A.2).

It is interesting to note that the liquid-assisted grinding experiment leads to the unsolvated salt. Indeed, the powder pattern of the as-synthesized product (CFZ/SACC 1:1 LAG MeCN) matches that calculated from the SCXRD data of **CFZ-NH$^+$-SACC$^-$ (1:1)** and not that calculated from the SCXRD data of **CFZ-NH$^+$-SACC$^-$-MeCN (1:1:1.4)** (Fig. A.1).

TABLE 3.2: Experimental details.
Experiments were carried out using an Xcalibur Ruby Gemini Ultra diffractometer. H atoms were treated by a mixture of independent and constrained refinement. Computer programs: *CrysAlis PRO* 1.171.38.46 [19], *CrysAlis PRO* 1.171.39.46 [20], *SHELXT* [23], *SHELXT 2014/5* [23], *SHELXL2016/6* [24].

	CFZ-NH$^+$-FA$^-$ (1:1)		**CFZ-NH$^+$-SA$^-$ (1:1)**	
Crystal data				
Chemical formula	$C_{27}H_{23}Cl_2N_4^+ \cdot C_4H_3O_4^-$		$C_{27}H_{23}Cl_2N_4^+ \cdot C_4H_5O_4^-$	
M_r	589.46		591.47	
Crystal system, space group	Monoclinic, $P2_1/c$		Triclinic, $P\bar{1}$	
Temperature (°C)	22		22	
a, b, c (Å)	7.47882(9),	26.0041(3),	10.6376(6),	12.2781(5),
	14.78241(16)		12.7975(8)	
α, β, γ (°)	90, 102.5075(12), 90		90.079(4), 113.211(6), 108.284(4)	
V (Å^3)	2806.65(6)		1443.57(15)	
Z	4		2	
Radiation type	Cu Kα		Mo Kα	
μ (mm^{-1})	2.45		0.27	
Crystal size (mm)	0.57 × 0.13 × 0.04		0.57 × 0.42 × 0.03	
Data collection				
Absorption correction	Analytical		Analytical	
$T_{\min}, T_{\max}$	0.502, 0.915		0.897, 0.990	
No. of measured, independent and observed [$I > 2\sigma(I)$] reflections	15078, 4944, 4394		10778, 5090, 3520	
R_{int}	0.021		0.022	
$(\sin(\theta/\lambda))_{\max}$ (Å^{-1})	0.597		0.595	
Refinement				
R[F^2 > 2σ(F^2)], wR(F^2), S	0.049, 0.136, 1.01		0.045, 0.122, 1.03	
No. of reflections	4944		5090	
No. of parameters	383		412	
No. of restraints	0		4	
$\Delta\rho_{max}, \Delta\rho_{min}$ (e Å^{-3})	0.46, -0.51		0.24, -0.24	
	CFZ-NH$^+$-SACC$^-$-MeCN (1:1:1.4)		**CFZ-NH$^+$-SACC$^-$ (1:1)**	
Crystal data				
Chemical formula	$C_{27}H_{23}Cl_2N_4^+ \cdot C_7H_4NO_3S^- \cdot 1.393(C_2H_3N)$		$C_{27}H_{23}Cl_2N_4^+ \cdot C_7H_4NO_3S^-$	
M_r	713.78		656.56	
Crystal system, space group	Triclinic, $P\bar{1}$		Triclinic, $P\bar{1}$	
Temperature (°C)	-173		22	
a, b, c (Å)	7.9970(3), 13.5824(3), 16.6638(7)		8.2115(7), 13.5327(12),14.325(3)	
α, β, γ (°)	80.214(3), 80.034(4), 83.036(3)		89.04(1), 88.864(10), 83.781(7)	
V (Å^3)	1748.87(11)		1582.0(3)	
Z	2		2	
Radiation type	Cu Kα		Cu Kα	
μ (mm^{-1})	2.61		2.82	
Crystal size (mm)	0.70 × 0.26 × 0.05		0.54 × 0.29 × 0.05	
Data collection				
Absorption correction	Gaussian		Multi-scan	
$T_{\min}, T_{\max}$	0.295, 1.000		0.549, 1.000	

	CFZ-NH$^+$-SACC$^-$-MeCN (1:1:1.4)	CFZ-NH$^+$-SACC$^-$ (1:1)
No. of measured, independent and observed [$I > 2\sigma(I)$] reflections	17257, 6202, 5378	7488, 3783, 2265
R$_{int}$	0.033	0.038
$(\sin(\theta/\lambda))_{max}$ (Å^{-1})	0.598	0.526
Refinement		
R[F^2 > 2σ(F^2)], wR(F^2), S	0.053, 0.142, 1.05	0.064, 0.190, 1.08
No. of reflections	6202	3783
No. of parameters	594	525
No. of restraints	137	483
$\Delta\rho_{max}$, $\Delta\rho_{min}$ (e Å^{-3})	0.61, -0.67	0.23, -0.22

	CFZ-NH$^+$-2,4DHBA$^-$-MeOH (1:1:1)	CFZ-NH$^+$-TRPTA^{2-}-TRPTA-solvent (1:0.5:0.5:x)	CFZ-NH$^+$-TRPTA^{2-}-TRPTA (1:0.5:0.5)
Crystal data			
Chemical formula	C$_{27}$H$_{23}$Cl$_2$N$_4^+$ · C$_7$H$_5$O$_4^-$ · CH$_4$O	C$_{27}$H$_{23}$Cl$_2$N$_4^+$ · 0.5(C$_8$H$_4$O$_4^{2-}$) · 0.5(C$_8$H$_6$O$_4$)	C$_{27}$H$_{23}$Cl$_2$N$_4^+$ · 0.5(C$_8$H$_4$O$_4^{2-}$) · 0.5(C$_8$H$_6$O$_4$)
M_r	659.54	639.51	639.51
Crystal system, space group	Triclinic, $P\bar{1}$	Triclinic, $P\bar{1}$	Triclinic, $P\bar{1}$
Temperature (°C)	22	-173	22
a, b, c (Å)	9.4861(4), 12.5322(5), 15.3641(5)	11.7990(4), 12.0736(4), 14.6803(5)	10.4028(3), 10.8454(3), 15.4229(5)
α, β, γ (°)	98.415(3), 103.379(3), 110.450(4)	72.472(3), 80.688(3), 72.030(3)	71.183(3), 73.984(3), 76.148(2)
V (Å^3)	1612.41(12)	1891.44(12)	1561.33(9)
Z	2	2	2
Radiation type	Cu Kα	Mo Kα	Mo Kα
μ (mm^{-1})	2.22	0.21	0.25
Crystal size (mm)	0.49 × 0.12 × 0.06	0.57 × 0.39 × 0.26	0.72 × 0.48 × 0.41
Data collection			
Absorption correction	Gaussian	Analytical	Analytical
T_{min}, T_{max}	0.539, 0.991	0.917, 0.960	0.886, 0.921
No. of measured, independent and observed [$I > 2\sigma(I)$] reflections	15458, 5692, 4965	20823, 11543, 9100	13059, 5704, 4554
R$_{int}$	0.021	0.022	0.018
$(\sin(\theta/\lambda))_{max}$ (Å^{-1})	0.597	0.714	0.602
Refinement			
R[F^2 > 2σ(F^2)], wR(F^2), S	0.037, 0.111, 1.04	0.044, 0.118, 1.03	0.040, 0.109, 1.02
No. of reflections	5692	11543	5704
No. of parameters	555	420	420
No. of restraints	66	0	0
$\Delta\rho_{max}$, $\Delta\rho_{min}$ (e Å^{-3})	0.24, -0.32	0.41, -0.30	0.23, -0.27
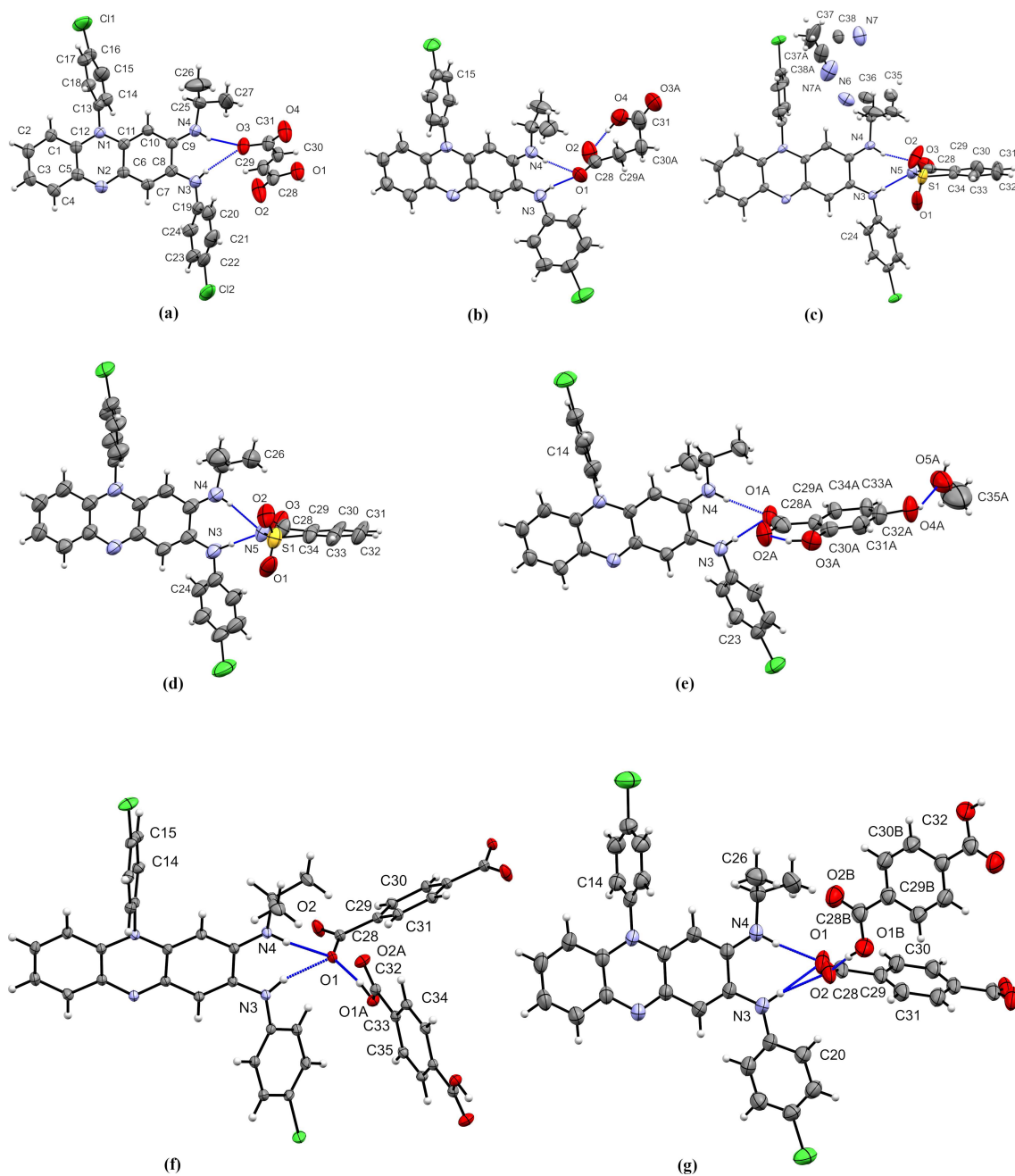
FIGURE 3.3: Hydrogen-bond interactions in the structures of (a) **CFZ-NH$^+$-FA$^-$ (1:1)**, (b) **CFZ-NH$^+$-SA$^-$ (1:1)**, (c) **CFZ-NH$^+$-SACC$^-$-MeCN (1:1:1.4)**, (d) **CFZ-NH$^+$-SACC$^-$ (1:1)**, (e) **CFZ-NH$^+$-2,4DHBA$^-$-MeOH (1:1:1)**, (f) **CFZ-NH$^+$-TRPTA^{2-}-TRPTA-solvent (1:0.5:0.5:x)** and (g) **CFZ-NH$^+$-TRPTA^{2-}-TRPTA (1:0.5:0.5)**. Ellipsoids are drawn at the 50% probability level.

TABLE 3.3: Melting points of non-solvated clofaziminium salts. † Sublimation

Compound analyzed	Melting point (°C)
CFZ (DAKXUI01)	219
Fumaric acid	210† [37]
Succinic acid	186.9
Saccharin	229.5 [38]
Terephthalic acid	276† [39]
CFZ-NH$^+$-FA$^-$ (1:1)	246
CFZ-NH$^+$-SA$^-$ (1:1)	214
CFZ-NH$^+$-SACC$^-$ (1:1)	252
CFZ-NH$^+$-TRPTA^{2-}-TRPTA (1:0.5:0.5)	240

3.3.3.5 CFZ-NH$^+$-2,4DHBA$^-$-MeOH (1:1:1) solvated salt

Clofaziminium 2,4-dihydroxybenzoate methanol solvated salt [Fig. 3.3(e)] crystallizes in the space group $P\bar{1}$ (Table 3.2). Proton transfer between 2,4-dihydroxybenzoic acid (O1) and the isopropyl imine of CFZ (N4) is confirmed by bond distances reflecting resonance in the carboxylate and by an increase in the iminium angle compared with the unprotonated form of clofazimine (Table A.3). MeOH and 2,4-DHBA$^-$ are slightly disordered.

An $R_2^1(7)$ hydrogen-bond motif is observed between 2,4-DHBA$^-$ and CFZ-NH$^+$ (N4$^+$-H···O1A$^-$ and N3-H···O1A$^-$, and N4$^+$-H···O1B$^-$ and N3-H···O1B$^-$; Table A.2). An
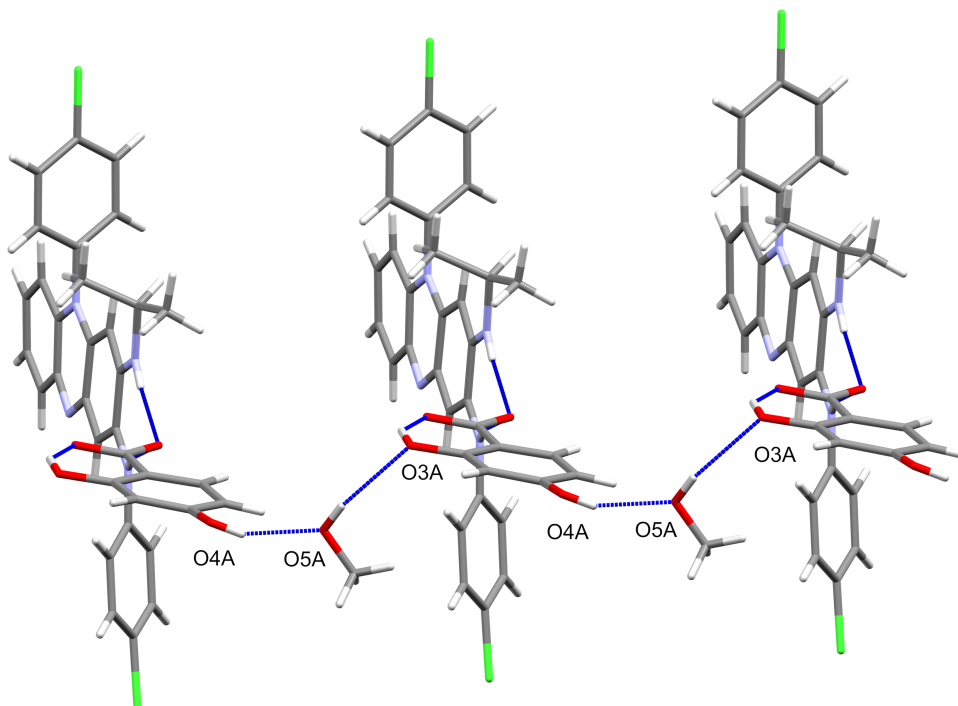
FIGURE 3.4: MeOH molecules serve as bridges between 2,4-DHBA$^-$ in the structure of **CFZ-NH$^+$-2,4DHBA$^-$-MeOH (1:1:1)**.

intramolecular hydrogen bond is also present in 2,4-dihydroxybenzoate [$S_1^1(6)$ motif, O3A-H$\cdots$O2A$^-$ and O3B-H$\cdots$O2B$^-$; Table A.2).

Methanol molecules serve as a bridge between two 2,4-DHBA$^-$ (Fig. 3.4) and a $C_2^2(8)$ motif (O4A-H$\cdots$O5A and O5A-H$\cdots$O3A) is observed (Table A.2, Fig. 3.4). In the second position of 2,4-DHBA$^-$ and MeOH (disordered), hydrogen-bond interactions form between O4B-H$\cdots$O5B and O5B-H$\cdots$O4B (Table A.2). CFZ-NH$^+$ are stacked in a head-to-tail fashion. This arrangement is further stabilized by weak C-H$\cdots$O hydrogen bonds (Table A.2).

The powder pattern of the as-synthesized product matches that calculated from single-crystal data (Fig. A.1).

3.3.3.6 CFZ-NH$^+$-TRPTA^{2-}-TRPTA-solvent (1:0.5:0.5:x) non-stoichiometrically solvated salt cocrystal.

Clofaziminium terephthalate terephthalic acid non-stoichiometrically solvated salt cocrystal crystallizes in the space group $P\bar{1}$ (Table 3.2). Its asymmetric unit is composed of one ion of clofaziminium with half a terephthalate ion and half a molecule of terephthalic acid [Fig. 3.3(f)]. Indeed, terephthalic acid and terephthalate are both positioned on an inversion centre. Proton transfer between terephthalate (O1) and the isopropyl imine of CFZ (N4) occurs and is confirmed by an increase in the iminium angle (Table A.3). Actually, the terephthalate anion serves as a linker between two clofaziminium cations, generating three-component CFZ-NH$^+$-TRPTA^{2-}-CFZ-NH$^+$ assemblies [Fig. 3.5(a)].

In these assemblies, an $R_2^1(7)$ hydrogen-bond motif is observed between TRPTA^{2-} and CFZ-NH$^+$ (N4$^+$-H$\cdots$O1$^-$ and N3-H$\cdots$O1$^-$; Table A.2). The three-component assemblies are interconnected through hydrogen bonds between terephthalate anions and terephthalic acid molecules [$D_1^1(2)$ hydrogen-bond motif, O1A-H$\cdots$O1$^-$; Fig. 3.5(a) and Table A.2]. Weak C-H$\cdots$O bonds are also present in the structure (Table A.2).

(a)	(b)	(c)	(d)

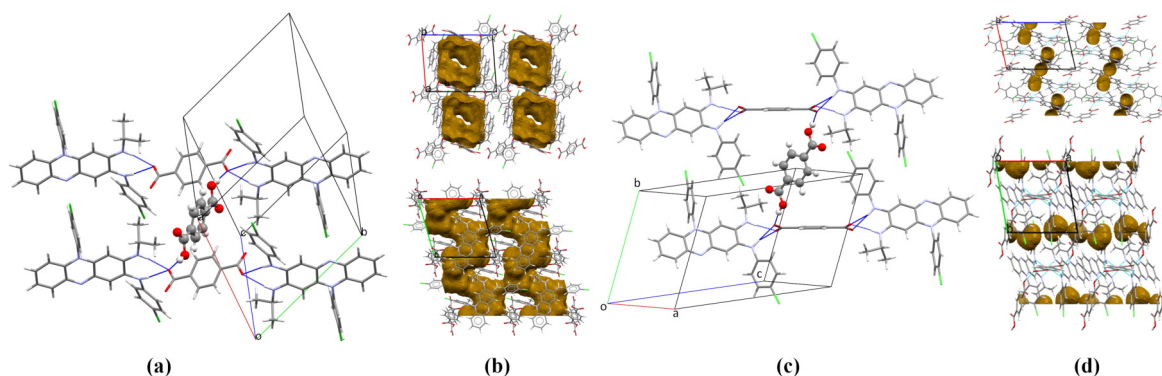FIGURE 3.5: Three-component assemblies (capped-stick representation) linked by terephthalic acid (ball-and-stick representation) of (a) **CFZ-NH$^+$-TRPTA^{2-}-TRPTA-solvent (1:0.5:0.5:x)** and (c) **CFZ-NH$^+$-TRPTA^{2-}-TRPTA (1:0.5:0.5)**. The voids formed along the *b* axis (top) and *c* axis (bottom) of (b) **CFZ-NH$^+$-TRPTA^{2-}-TRPTA-solvent (1:0.5:0.5:x)** and (d) **CFZ-NH$^+$-TRPTA^{2-}-TRPTA (1:0.5:0.5)**.

This arrangement results in solvent-accessible voids forming channels [Figs. 3.5(b) and A.4(a)]. Although one molecule of ethyl acetate could be located, high residual electron densities remained in the structure. As not all of the crystallization solvent molecules could be assigned unambiguously despite low-temperature measurement (-173 °C), the *PLATON* SQUEEZE [27] procedure was applied to the data.

3.3.3.7 CFZ-NH$^+$-TRPTA^{2-}-TRPTA (1:0.5:0.5) salt cocrystal

Clofaziminium terephthalate terephthalic acid salt cocrystal [Fig. 3.3(g)] was obtained by drying **CFZ-NH$^+$-TRPTA^{2-}-TRPTA-solvent (1:0.5:0.5:x)** at room temperature. **CFZ-NH$^+$-TRPTA^{2-}-TRPTA (1:0.5:0.5)** salt cocrystal crystallizes in the space group $P\bar{1}$ (Table 3.2). Its asymmetric unit is composed of one ion of clofaziminium with half a terephthalate ion and half a molecule of terephthalic acid [Fig. 3.3(g)]. Indeed, terephthalic acid and terephthalate are both positioned on an inversion centre. Proton transfer between terephthalate (O1) and the isopropyl imine of CFZ (N4) occurs and is confirmed by an increase in the iminium angle (Table A.3). Like in the solvated structure, the terephthalate anion serves as a linker between two clofaziminium cations, leading to three-component assemblies.

Bifurcated hydrogen bonds between TRPTA^{2-} and CFZ-NH$^+$ are observed [$R_2^2(9)$ motif, N4-H$^+$···O1$^-$ and N3-H···O2$^-$, in addition to $R_2^1(7)$, N4$^+$-H···O1$^-$ and N3-H···O1$^-$; Table A.2]. The three-component assemblies are interconnected through hydrogen bonds with terephthalic acid molecules [$D_1^1(2)$ hydrogen-bond motif, O1B-H···O2$^-$; Fig. 3.5(c), Table A.2].

Voids are present in the structure of **CFZ-NH$^+$-TRPTA^{2-}-TRPTA (1:0.5:0.5)**, but they are not interconnected and no channel is observed [Figs. 3.5(d) and A.4(b)]. Interestingly, as shown by variable-temperature powder X-ray diffraction, this non-solvated structure can be obtained by heating the batch powder synthesized by LAG with EtOAc as solvent (Fig. A.3).

3.3.4 CFZ-counter-ion interaction comparison

FIM analyses revealed two possible sites of interaction around clofazimine, namely near atoms N3 and N4 for the first site and around N2 for the second one. Analysis of the 18 known structures [15 in the CSD and three supplied as supplementary data to the article by Bannigan *et al.* [14]] and the seven new ones described in this paper reveals that the first site is involved in all salt structures while the second one is only involved in two structures. One structure is the hydrated salt **CFZ-NH$^+$-MSA$^-$-H$_2$O (1:1:1)**. Indeed, N2 interacts through hydrogen bonds with a water molecule [$D_1^1(2)$, 2.899 (4) Å and 173 (2)°; Fig. 3.6(a)]. In this case, the water molecule is placed at an optimal position (even for a contour level as high as 30). The second structure is **CFZ-NH$^+$-CIT$^-$ (1:1)**, in which N2 interacts through a hydrogen bond with one carboxylic acid group of the dihydrogen citrate ion [$D_1^1(2)$, 2.898 (4) Å and 161.6°; Fig. 3.6(b)]. In this structure, the OH from the carboxylic acid interacting with N2 is, however, less optimally placed. While hydrogen bonds between N2 from CFZ and OH from 2,4-DHBA or MeOH might
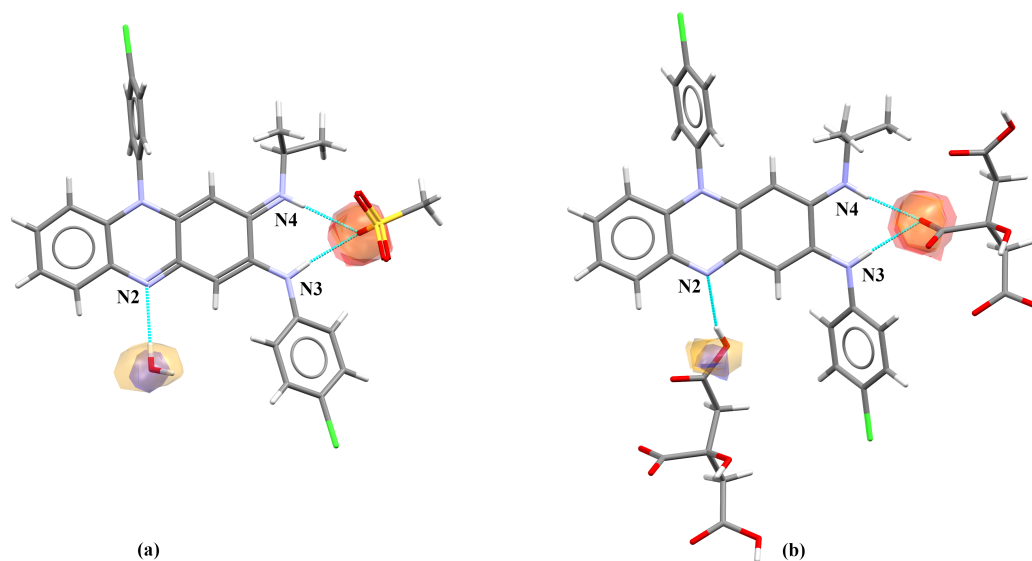
FIGURE 3.6: FIMs calculated around clofaziminium from (a) **CFZ-NH$^+$-MSA$^-$-H$_2$O (1:1:1)** and (b) CFZ-NH$^+$ of **CFZ-NH$^+$-CIT$^-$ (1:1)**. Carbonyl oxygen, uncharged NH and alcohol OH probes are shown in red, blue and orange, respectively.

have been expected, such an interaction is not observed in the structure of **CFZ-NH$^+$-2,4DHBA$^-$-MeOH (1:1:1)**.

Concerning clofaziminium salts obtained with aliphatic dicarboxylic acids, in the currently known structures, proton transfer has occurred from one carboxylic acid function while the other remained protonated. However, in the structures involving the aromatic dicarboxylic acid **CFZ-NH$^+$-TRPTA^{2-}-TRPTA (1:0.5:0.5)** and **CFZ-NH$^+$-TRPTA^{2-}-TRPTA-solvent (1:0.5:0.5:x)**), the terephthalate anion is fully unprotonated, leading to three-component assemblies (CFZ-NH$^+$-TRPTA^{2-}-CFZ-NH$^+$) bridged together by the remaining terephthalic acid molecule (CFZ and TRPTA were ball-milled in a 1:1 molar ratio). Double deprotonation of the terephthalic acid could eventually be explained by the two low pKa values for this compound (3.54 and 4.34 [35]). But interestingly, fumaric acid, which has a second pKa value similar to that of terephthalic acid (pKa of 3.02, and 4.38 for FA [35]), is unprotonated at only one site, thus forming a hydrogen fumarate salt of clofazimine. This observation could be explained by the longer distance between carboxylates in TRPTA compared with the COOH-COOH distance in FA [5.803 (3) Å in the structure of **CFZ-NH$^+$-TRPTA^{2-}-TRPTA (1:0.5:0.5)** *versus* 3.883 (3) Å in the structure of **CFZ-NH$^+$-FA$^-$ (1:1)**].

3.3.5 Crystal-packing comparison

All known clofaziminium salt structures, as well as those described in this paper, were compared by submitting them to the crystal-packing similarity tool in *Mercury*, with a packing shell size of 15 molecules and distance and angle tolerances of 30% and 30°, respectively. Only **CFZ-NH$^+$-SA$^-$ (1:1)** showed a molecular overlay of 15 molecules

out of 15 with **CFZ-NH$^+$-MLN$^-$ (1:1)** (GESGOC). This result was quite interesting. Indeed, isostructurality might have been expected between salts involving hydrogen succinate and hydrogen fumarate as counter-ion [as previously described by Galcera & Molins [40]]. However, a crystal-packing comparison of clofaziminium salts **CFZ-NH$^+$-FA$^-$ (1:1)** and **CFZ-NH$^+$-SA$^-$ (1:1)** indicates a lack of isostructurality. The negative charge on the carboxylate part of the hemisuccinate favours the formation of a strong intramolecular hydrogen bond at the expense of intermolecular hydrogen bonds [in contrast with what was observed in **CFZ-NH$^+$-FA$^-$ (1:1)**], preventing isostructurality with **CFZ-NH$^+$-FA$^-$ (1:1)**. This intramolecular hydrogen bond may be similar to the one observed in hydrogen maleate in the structure of **CFZ-NH$^+$-MLE$^-$ (1:1)** described by Bolla & Nangia [12]. However, no isostructurality is observed with **CFZ-NH$^+$-MLE$^-$ (1:1)**.

More surprisingly, **CFZ-NH$^+$-SA$^-$ (1:1)** presents isostructurality with **CFZ-NH$^+$-MLN$^-$ (1:1)**, a clofaziminium salt previously described by Bolla & Nangia [12]. The overlay between the crystal lattice of **CFZ-NH$^+$-SA$^-$ (1:1)** and that of **CFZ-NH$^+$-MLN$^-$ (1:1)** is illustrated in Fig. 3.7. Other crystal packings that are interesting to compare are those of **CFZ-NH$^+$-SACC$^-$-MeCN (1:1:1.4)** and **CFZ-NH$^+$-TRPTA^{2-}-TRPTA-solvent (1:0.5:0.5:x)** with their non-solvated analogues **CFZ-NH$^+$-SACC$^-$ (1:1)** and
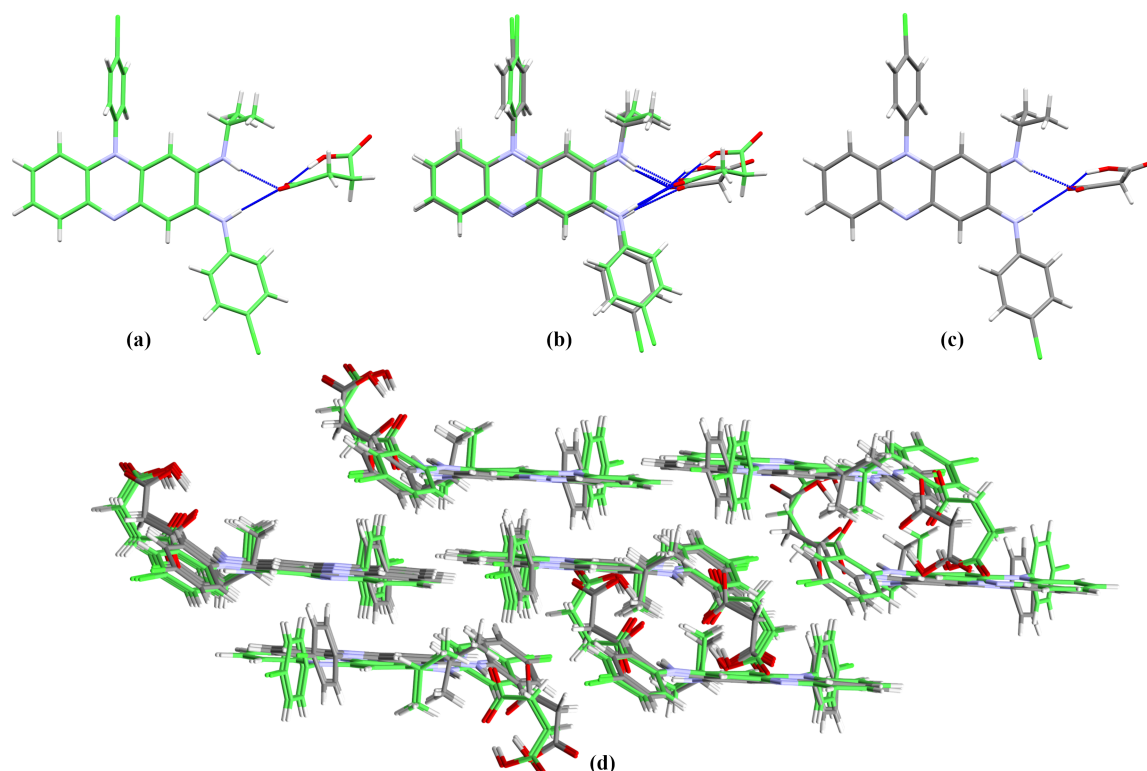
FIGURE 3.7: (a) The structure of salt **CFZ-NH$^+$-SA$^-$ (1:1)**. (b) An overlay between **CFZ-NH$^+$-SA$^-$ (1:1)** and **CFZ-NH$^+$-MLN$^-$ (1:1)**. (c) The structure of **CFZ-NH$^+$-MLN$^-$ (1:1)**. (d) A crystal-packing comparison of the salts **CFZ-NH$^+$-SA$^-$ (1:1)** (green) and **CFZ-NH$^+$-MLN$^-$ (1:1)** (grey).

CFZ-NH$^+$-TRPTA^{2-}-TRPTA (1:0.5:0.5). In terms of composition, these salts differ only in the presence or absence of solvent in the structure. However, this solvent may have a strong impact on the crystal packing. Indeed, in the non-solvated structure of **CFZ-NH$^+$-SACC$^-$**, an $R_2^1(7)$ hydrogen-bond motif is observed between SACC$^-$ and CFZ-NH$^+$ (N4$^+$-H$\cdots$N5$^-$ and N3-H$\cdots$N5$^-$), while in the solvated salt an $R_2^2(9)$ motif (N4$^+$-H$\cdots$O3 and N3-H$\cdots$N5$^-$) is observed. Such modification of the hydrogen bonds results in a slight shift in the position of SACC$^-$ (Fig. 3.8). However, both structures are quite similar, as 14 clofaziminium ions out of 15 overlay when the solvated and non-solvated structures are analysed by the crystal-packing similarity tool in *Mercury*.

More structural changes are observed between **CFZ-NH$^+$-TRPTA^{2-}-TRPTA-solvent (1:0.5:0.5:x)** and **CFZ-NH$^+$-TRPTA^{2-}-TRPTA (1:0.5:0.5)** [Fig. 3.9(c)]. In the non-solvated structure, hydrogen bonds observed between TRPTA^{2-} and CFZ-NH$^+$ are bifurcated, which is not the case in the solvated analogue. These bifurcated hydrogen bonds lead to major modifications in terms of the distance between the planes passing through the main core of CFZ-NH$^+$ (these planes were calculated by taking atoms N1, C5 and C6 of clofaziminium as reference). Indeed, while the inter-planar distance is 6.049 Å in the structure of **CFZ-NH$^+$-TRPTA^{2-}-TRPTA-solvent (1:0.5:0.5:x)** [labeled d in Fig. 3.9(a)], it is only 2.217 Å in the structure of **CFZ-NH$^+$-TRPTA^{2-}-TRPTA (1:0.5:0.5)** [d in Fig. 3.9(b)]. The differences in crystal packing observed between these two structures result in major changes in terms of (solvent-accessible) voids. Indeed, in the structure of **CFZ-NH$^+$-TRPTA^{2-}-TRPTA-solvent (1:0.5:0.5:x)**, solvent accessible voids form channels, as illustrated in Fig. 3.5(b), while in the structure of **CFZ-NH$^+$-TRPTA^{2-}-TRPTA (1:0.5:0.5)** the voids are not interconnected and no channel is observed [Fig. 3.5(d)].
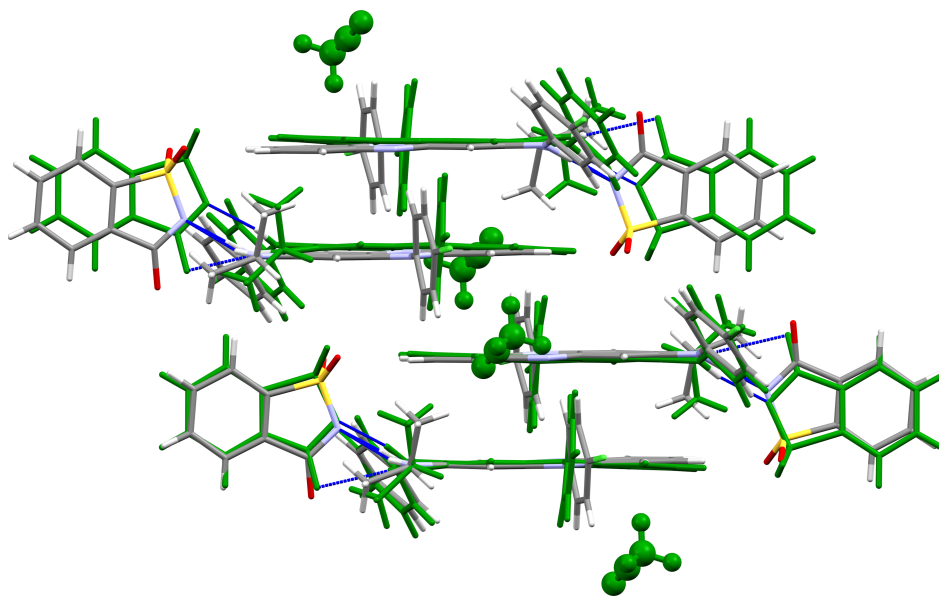
FIGURE 3.8: A crystal-packing overlay of the solvated (green) and non-solvated (grey) structures of clofaziminium saccharinate.
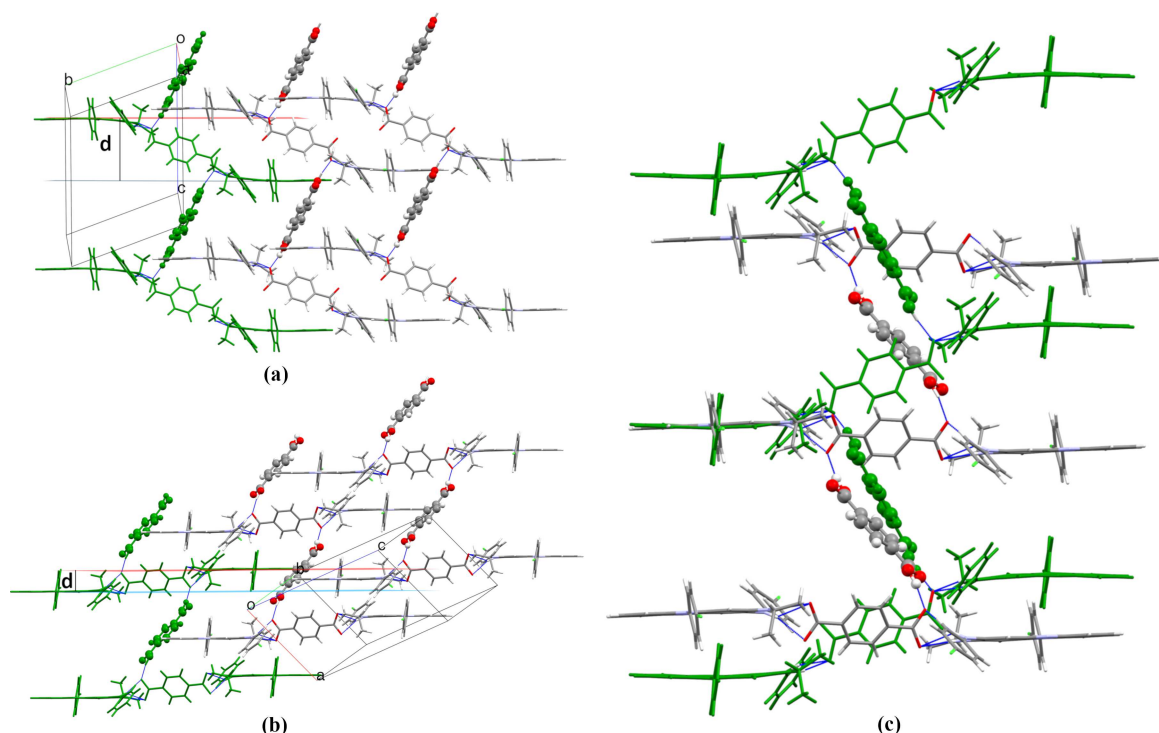
FIGURE 3.9: Distance, d, between the planes passing through the main core of CFZ-NH$^+$ in the structures of (a) **CFZ-NH$^+$-TRPTA^{2-}-TRPTA-solvent (1:0.5:0.5:x)** and (b) **CFZ-NH$^+$-TRPTA^{2-}-TRPTA (1:0.5:0.5)**. (c) A crystal-packing overlay of the solvated (green) and non-solvated (grey) structures.

3.3.6 Conformational analysis of clofazimine/clofaziminium

The clofazimine/clofaziminium conformation is quite constrained, but conformational changes could be expected around three main torsion angles (T1, T2 and T3; Fig. 3.1) for clofazimine and around four torsion angles (T1, T2, T4 and T5; Fig. 3.1) for clofaziminium. The T3 torsion angle (Fig.3.1) is expected to have values around 90° (because of steric hindrance that would result from T3 torsion-angle values different from 90°). To assess the conformational versatility of clofazimine(-ium), coordinates were extracted from known structures [from CSD data, and supplementary data from the article by Bannigan *et al.* [14]] and overlaid [Figs. 3.10(a) and 3.10(b)]. The results indicate similar conformations for all clofazimine molecules [Fig. 3.10(a)] which could be explained by the formation of an intramolecular hydrogen bond between N3-H and N4. The main differences are observed around the T1 and T2 torsion angles. T1 and T2 have values around 150 or -150° with two possible combinations: for negative T2 values, T1 can be either positive (CFZ I and II) or negative (see Table A.3).

Clofaziminium ions also adopt similar conformations [Fig. 3.10(b)]. The T1 torsion angle is quite well conserved in the salt structures, with the main values being in the range between 130 and 160°. However, flexibility is observed around T2. Indeed, the T2 torsion angle can adopt different values around 150-160°, 90-100° and 70-80°.

More surprising are the values of the T4 and T5 torsion angles. The T4 torsion angles
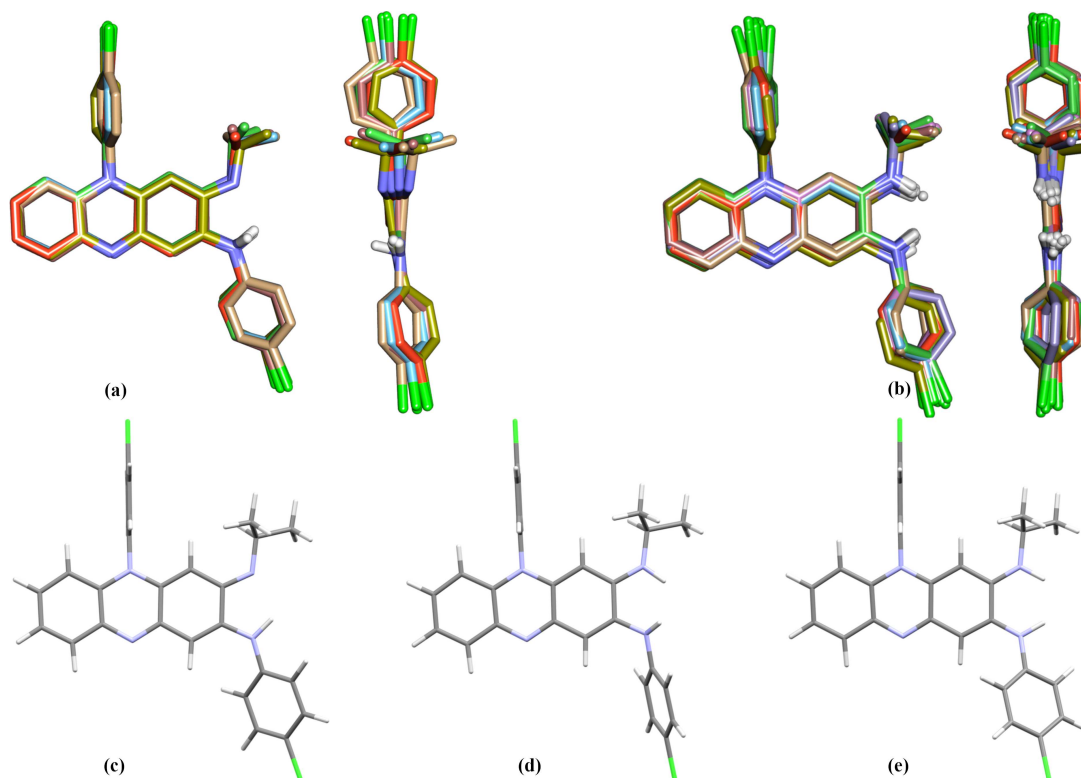
FIGURE 3.10: Front and side views after superimposition of (a) clofazimine and (b) clofaziminium conformations. (c)-(e) The optimized geometries of (c) clofazimine, (d) clofaziminium with no counter-ion, and (e) clofaziminium with Cl⁻ counter-ion.

are between 0 and 15°, while the T5 values are mainly between 0 and 20° in absolute value [there are a few exceptions: 38° in **CFZ-NH$^+$-SACC$^-$-MeCN (1:1:1.4)**, 31° in **CFZ-NH$^+$-SACC$^-$ (1:1)**, -28° **CFZ-NH$^+$-TRPTA^{2-}-TRPTA-solvent (1:0.5:0.5:x)** and 34° in **CFZ-NH$^+$-FA$^-$ (1:1)**]. Such values of T4 and T5 result in steric hindrance between the H atoms positioned on N3 and N4 (the distance around these H atoms is around 1.9 Å ; see Table A.3). Because of this steric effect, other values of T4 and T5 could be expected, indeed N3-H could be tilted outside the plane of clofazimine.

To assess the effect of the counter-ion on the CFZ-NH$^+$ conformation, optimization calculations were performed in the absence and presence of the counter-ion (Cl⁻), starting from the coordinates of clofaziminium chloride (LABQUD) [Figs. 3.10(d) and 3.10(e) and Tables A.5 and A.6]. Optimization of clofazimine was also performed [starting from the coordinates of DAKXUI03; Fig. 3.10(c) and Table A.4] for the sake of comparison. The optimized CFZ-NH$^+$ conformation confirms the hypothesis of possible higher T5 torsion-angle values (T4 = 15.40° and T5 = 51.35°). Such a high value of T5 is, however, never observed in crystal structures. This suggests quite a strong effect of the counter-ion on the clofaziminium conformation. Indeed, in the clofaziminium salt crystal structures, the H atom positioned on N3 remains almost in the plane of clofazimine. This could be explained by the presence of hydrogen bonds between CFZ-NH$^+$ and its counter-ion, which force the N3-H group to stay close to the clofaziminium plane and compensate for

the energy penalty due to steric hindrance. This assumption is supported by the fact that the optimized geometry of CFZ-NH$^+$ in the presence of the Cl$^-$ counter-ion results in T5 torsion values much closer, in absolute value, to those observed in actual crystal structures [T4 = -3.41° and T5 = -11.34° in optimized **CFZ-NH$^+$-Cl$^-$ (1:1)**; Fig. 3.10(e) compared with Fig. 3.10(b), and see also Table A.3].

3.4   Conclusions

Seven new (solvated/cocrystals of) salts of the drug clofazimine with fumaric, succinic, 2,4-dihydroxybenzoic and terephthalic acids and with saccharin are reported and compared with the currently known clofaziminium salt structures. Full interaction map analyses reveal two main sites of interaction around clofaziminium. Interaction between CFZ-NH$^+$ and its counter-ion mainly occurs at the first site located around N3 and N4. Interaction at the second site of clofaziminium is only observed in two structures [**CFZ-NH$^+$-CIT$^-$ (1:1)** and **CFZ-NH$^+$-MSA$^-$-H$_2$O (1:1:1)**] that were reported earlier.

   The acid/base reaction between clofazimine and dicarboxylic acids more often results in single proton transfer (one carboxylic acid function is unprotonated while the other remains protonated), except in the structures involving terephthalic acid (in which the COOH-COOH distance is longer than in the aliphatic dicarboxylic acids evaluated in the present work). In structures involving terephthalic acid, one terephthalate ion is fully unprotonated while the remaining terephthalic acid molecules serve as bridges between terephthalate anions.

   A crystal-packing comparison of all known structures revealed that **CFZ-NH$^+$-SA$^-$ (1:1)** and **CFZ-NH$^+$-MLN$^-$ (1:1)** are isostructural. **CFZ-NH$^+$-SACC$^-$-MeCN (1:1:1.4)** and **CFZ-NH$^+$-TRPTA^{2-}-TRPTA-solvent (1:0.5:0.5:x)** can be converted to **CFZ-NH$^+$-SACC$^-$ (1:1)** and **CFZ-NH$^+$-TRPTA^{2-}-TRPTA (1:0.5:0.5)**, respectively, by solvent evaporation. In both cases, solvent evaporation leads to structural changes and hydrogen-bond interactions modifications. The crystal-packing comparison of these two structures reveals that in clofaziminium saccharinate the anion position is slightly changed, while in clofaziminium terephthalate the solvent has a strong impact on the hydrogen-bond interactions and packing. Indeed, the hydrogen-bond interactions between CFZ-NH$^+$ and TRPTA^{2-} change upon drying, leading to the disappearance of solvent-accessible channels in favour of isolated voids.

   In all known structures, clofazimine and clofaziminium adopt similar conformations. The conformation observed in salt structures may be surprising at first glance because it results in steric hindrance around the protonated site. However, conformational optimization of clofaziminium shows the strong impact of the counter-ion on the CFZ-NH$^+$ conformation. Indeed, hydrogen bonds occurring between clofaziminium and the counter-ion compensate for the energy penalty due to the steric hindrance.

   Altogether, these results indicate that, despite its quite constrained conformation, clofazimine can crystallize as salts with a wide variety of packings, which could lead to different physicochemical and pharmacokinetic properties.

Acknowledgements

Funding information

Bibliography

[1] V. C. Barry, J. G. Belton, M. L. Conalty, J. M. Denneny, D. W. Edward, J. F. O'Sullivan, D. Twomey, and F. Winder. A New Series of Phenazines (Rimino-Compounds) With High Antituberculosis Activity. *Nature*, 179(4568):1013–1015, 1957.

[2] World Health Organization. Treatment of Tuberculosis: Guidelines, 2010, 2010.

[3] V. M. Reddy, J. F. O'Sullivan, and P. R. J. Gangadharam. Antimycobacterial activities of riminophenazines. *Journal of Antimicrobial Chemotherapy*, 43(5):615–623, 1999.

[4] M. C. Cholo, H. C. Steel, P. B. Fourie, W. A. Germishuizen, and R. Anderson. Clofazimine: Current status and future prospects. *Journal of Antimicrobial Chemotherapy*, 67(2):290–298, 2012.

[5] L. Levy. Pharmacologic Studies of Clofazimine. *The American Journal of Tropical Medicine and Hygiene*, 23(6):1097–1109, nov 1974.

[6] E. M. Horstman, R. K. Keswani, B. A. Frey, P. M. Rzeczycki, V. LaLone, J. A. Bertke, P. J. Kenis, and G. R. Rosania. Elasticity in Macrophage-Synthesized Biocrystals. *Angewandte Chemie - International Edition*, 56(7):1815–1819, 2017.

[7] R. K. Keswani, J. Baik, L. Yeomans, C. Hitzman, A. M. Johnson, A. S. Pawate, P. J. Kenis, N. Rodriguez-Hornedo, K. A. Stringer, and G. R. Rosania. Chemical Analysis of Drug Biocrystals: A Role for Counterion Transport Pathways in Intracellular Drug Disposition. *Molecular Pharmaceutics*, 12(7):2528–2536, 2015.

[8] C. K. Job, L. Yoder, R. R. Jacobson, and R. C. Hastings. Skin pigmentation from clofazimine therapy in leprosy patients: A reappraisal. *Journal of the American Academy of Dermatology*, 23(2):236–241, 1990.

[9] I. I. Salem, G. Steffan, and N. Düzgünes. Efficacy of clofazimine-modified cyclodextrin against Mycobacterium avium complex in human macrophages. *International Journal of Pharmaceutics*, 260(1):105–114, 2003.

[10] A. S. Narang and A. K. Srivastava. Evaluation of solid dispersions of clofazimine. *Drug Development and Industrial Pharmacy*, 28(8):1001–1013, 2002.

[11] J. R. O'Reilly, O. I. Corrigan, and C. M. O'Driscoll. The effect of simple micellar systems on the solubility and intestinal absorption of clofazimine (B663) in the anaesthetised rat. *International Journal of Pharmaceutics*, 105(2):137–146, 1994.

[12] G. Bolla and A. Nangia. Clofazimine mesylate: A high solubility stable salt. *Crystal Growth and Design*, 12(12):6250–6259, 2012.

[13] P. Bannigan, J. Zeglinski, M. Lusi, J. O'Brien, and S. P. Hudson. Investigation into the Solid and Solution Properties of Known and Novel Polymorphs of the Antimicrobial Molecule Clofazimine. *Crystal Growth and Design*, 16(12):7240–7250, 2016.

[14] P. Bannigan, E. Durack, C. Madden, M. Lusi, and S. P. Hudson. Role of Biorelevant Dissolution Media in the Selection of Optimal Salt Forms of Oral Drugs: Maximizing the Gastrointestinal Solubility and in Vitro Activity of the Antimicrobial Molecule, Clofazimine. *ACS Omega*, 2(12):8969–8981, 2017.

[15] T. Friščic, S. L. Childs, S. A. A. Rizvi, and W. Jones. The role of solvent in mechanochemical and sonochemical cocrystal formation: a solubility-based approach for predicting cocrystallisation outcome. *CrystEngComm*, 11(3):418–426, 2009.

[16] N. Shan, F. Toda, and W. Jones. Mechanochemistry and co-crystal formation: Effect of solvent on reaction kinetics. *Chemical Communications*, 2(20):2372–2373, 2002.

[17] A. V. Trask, W. D. S. Motherwell, and W. Jones. Solvent-drop grinding: green polymorph control of cocrystallisation. *Chemical Communications*, (7):890–891, 2004.

[18] S. L. James, C. J. Adams, C. Bolm, D. Braga, P. Collier, T. Friščic, F. Grepioni, K. D. Harris, G. Hyett, W. Jones, A. Krebs, J. Mack, L. Maini, A. G. Orpen, I. P. Parkin, W. C. Shearouse, J. W. Steed, and D. C. Waddell. Mechanochemistry: opportunities for new and cleaner synthesis. *Chemical Society Reviews*, 41(1):413–447, 2012.

[19] Rigaku Oxford Diffraction. CrysAlis PRO. Version 1.171.38.46. *CrysAlis PRO. Version 1.171.38.46*, pages Rigaku Oxford Diffraction Ltd, Yarnton, England, 2015.

[20] Rigaku Oxford Diffraction. CrysAlis PRO. Version 1.171.39.46. *CrysAlis PRO. Version 1.171.39.46*, pages Rigaku Oxford Diffraction Ltd, Yarnton, England, 2018.

[21] R. C. Clark and J. S. Reid. The Analytical Calculation of Absorption in Multifaceted Crystals. *Acta Crystallographica A*, 51:887–897, 1995.

[22] R. H. Blessing. An Empirical Correction for Absorption Anisotropy. *Acta Crystallographica A*, 51:33–38, 1995.

[23] G. M. Sheldrick. SHELXT - Integrated space-group and crystal-structure determination. *Acta Crystallographica A*, 71(1):3–8, 2015.

[24] G. M. Sheldrick. Crystal structure refinement with SHELXL. *Acta Crystallographica C*, 71:3–8, 2015.

[25] O. V. Dolomanov, L. J. Bourhis, R. J. Gildea, J. A. K. Howard, and H. Puschmann. OLEX2: A complete structure solution, refinement and analysis program. *Journal of Applied Crystallography*, 42(2):339–341, 2009.

[26] C. B. Hübschle, G. M. Sheldrick, and B. Dittrich. ShelXle : a Qt graphical user interface for SHELXL. *Journal of Applied Crystallography*, 44:1281–1284, 2011.

[27] A. L. Spek. PLATON SQUEEZE: A tool for the calculation of the disordered solvent contribution to the calculated structure factors. *Acta Crystallographica C*, 71:9–18, 2015.

[28] C. F. Macrae, I. J. Bruno, J. A. Chisholm, P. R. Edgington, P. McCabe, E. Pidcock, L. Rodriguez-Monge, R. Taylor, J. Van De Streek, and P. A. Wood. Mercury CSD 2.0 - New features for the visualization and investigation of crystal structures. *Journal of Applied Crystallography*, 41(2):466–470, 2008.

[29] C. R. Groom, I. J. Bruno, M. P. Lightfoot, and S. C. Ward. The Cambridge Structural Database. *Acta Crystallographica B*, 72:171–179, 2016.

[30] Dassault Systèmes (2016). *Discovery Studio Modeling Environment, Release 2017.* BIOVIA, Vélizy-Villacoublay, France, 2016.

[31] Y. Zhao and D. G. Truhlar. The M06 suite of density functionals for main group thermochemistry, thermochemical kinetics, noncovalent interactions, excited states, and transition elements: Two new functionals and systematic testing of four M06-class functionals and 12 other function. *Theoretical Chemistry Accounts*, 120:215–241, 2008.

[32] M. J. Frisch, G. W. Trucks, H. B. Schlegel, G. E. Scuseria, M. A. Robb, J. R. Cheesemen, G. Scalmani, V. Barone, G. A. Petersson, H. Nakatsuji, X. Li, M. Caricato, A. V. Marenich, J. Bloino, B. G. Janesco, R. Gomperts, B. Mennucci, H. P. Hratchian, J. V. Ortiz, A. F. Izmaylov, J. L. Sonnenberg, D. Williams-Young, F. Ding, F. Lipparini, F. Egidi, J. Goings, B. Peng, A. Petrone, T. Henderson, D. Ranasinghe, V. G. Zakrzewski, J. Gao, N. Rega, G. Zheng, W. Liang, M. Hada, M. Ehara, K. Toyota, R. Fukuda, J. Hasegawa, M. Ishida, T. Nakajima, Y. Honda, O. Kitao, H. Nakai, T. Vreven, K. Throssell, J. A. Montgomery, J. J. E. Peralta, F. Ogliaro, M. J. Bearpark, J. J. Heyd, E. N. Brothers, K. N. Kudin, V. N. Staroverov, T. A. Keith, R. Kobayashi, J. Normand, K. Raghavachari, A. P. Rendell, J. C. Burant, S. S. Iyengar, J. Tomasi, M. Cossi, J. M. Millam, M. Klene, C. Adamo, R. Cammi, J. W. Ochterski, R. L. Martin, K. Morokuma, O. Farkas, J. B. Foresman, and D. J. Fox. *Gaussian 16, Revision A.03.* Gaussian Inc., Wallingford, Connecticut, USA, Wallingford CT, 2016.

[33] M. Ash and I. Ash. *Handbook of Food Additives.* Synapse Information Resources, New-York, 3rd edition, 2008.

[34] Select Committee on GRAS substances (2018). GRAS Substances (SCOGS) Database, 2018.

[35] W. M. Haynes. *Handbook of Chemistry and Physics.* Boca Raton: CRC Press, Boca Raton: CRC Press, 95th edition, 2014.

[36] R. C. Rowe, P. J. Sheskey, and S. C. Owen. *Handbook of Pharmaceutical Excipients.* Pharmaceutical Press and American Pharmacists Association, London/Philadelphia /Washigton DC, 5th edition, 2006.

[37] I. Temesvári, G. Liptay, and E. Pungor. Determination of maleic acid and fumaric acid in the presence of each other by thermal analysis. *E. Journal of Thermal Analysis*, 3:293–295, 1971.

[38] S. Basavoju, D. Bostro, and S. Velaga. Indomethacin – Saccharin Cocrystal : Design , Synthesis and Preliminary Pharmaceutical Characterization. *Pharmaceutical Research*, 25(3):530–541, 2008.

[39] A. B. E. Kimyonok and M. Ulutürk. Determination of the Thermal Decomposition Products of Terephthalic Acid by Using Curie-Point Pyrolyzer. *Journal of Energetic Materials*, 34:113–122, 2016.

[40] J. Galcera and E. Molins. Effect of the Counterion on the Solubility of Isostructural & DESIGN 2009. *Crystal Growth & Design*, 9(1):327–334, 2009.

Chapter 4

Taking advantage of solvate formation to modulate drug-drug ratio in clofaziminium diclofenac salts†

Taking advantage of solvate formation to modulate drug-drug ratio in clofaziminium diclofenac salts

Laurie Bodart[*,a], Maria Prinzo[b], Amélie Derlet[a], Nikolay Tumanov[a] and Johan Wouters[a]

[a]University of Namur (UNamur) Namur Medicine and Drug Innovation Center - Namur Research Institute for Life Science (NAMEDIC-NARILIS), Namur Institute of Structured Matter (NISM), Department of Chemistry, University of Namur (UNamur), 61 Rue de Bruxelles, 5000 Namur, Belgium.
E-mail: laurie.bodart@unamur.be and johan.wouters@unamur.be
[b]Drug science department, University of Catania, Viale Andrea Doria 6, 95125 Catania, Italy.

Abstract. Non-steroidal anti-inflammatory drugs, such as diclofenac, are gaining attention as repurposed compounds for the treatment of multidrug resistant tuberculosis. In this study, salts combining diclofenac with clofazimine, are prepared by solvent crystallization and by liquid-assisted grinding. Diclofenac anion possesses an H-bond acceptor which can strongly interact with protic solvent molecules. In this context, selected solvents (protic, aprotic and solvents with increasing molecular volume) are screened in order to investigate solvent impact on crystallization of solvated or unsolvated salt of clofazimine with diclofenac in 1:1 ratio. Five solvated salts and one unsolvated salt were successfully crystallized. The ability of the diclofenac anion to interact with a protic molecule is also exploited in order to crystallize a cocrystal of salt with drug:drug ratio different from 1:1. Structures of two solvated cocrystal of salts (with acetonitrile and ethylacetate) and two polymorphs of an unsolvated cocrystal of salt combining clofazimine with diclofenac in 1:2 ratios are determined.

4.1   Introduction

Pharmaceutical compounds are often exposed to solvents (or their vapors) during manu-facturing (i.e. at the steps of crystallization, wet granulation, spray drying or lyophiliza-tion) [1, 2]. Organic compounds including pharmaceuticals are often found in the form of solvates [3, 4]. However, crystalline changes induced by solvate formation or solvent evap-oration from the structure can considerably affect the physico-chemical properties of the compounds. Although, in the pharmaceutical industry, solvate formation can sometimes be beneficial to the properties of drugs (e.g., indinavir shows better bioavailability when in the form of a sulfate ethanol solvated form [5, 1, 6]), in many other cases it is a nuisance: for instance, if the solvent is toxic or the solvated form exhibits undesired physicochemical and/or mechanical properties. Thus, selecting a proper solvent which would present a re-duced probability of solvate formation is of crucial importance for drug manufacturing [7].

Several factors have been investigated for their impact on solvate formation. The two most important ones have been identified as solvent-solute affinity and molecular size and shape of the solvent [8, 9]. The first parameter, among other factors, depends on hydrogen bonding and aromatic interaction abilities of the molecule. The second parameter is in correlation with the concept of packing efficiency, since solvent presenting low affinity for a compound can still be incoporated into its structure if it allows a better packing [8, 10]. While various solvents, depending on their molecular volume, size and shape, may lead to different crystal packings, it is also possible that bulky molecules of the compound itself fail to form efficient packing and thus may incorporate solvent molecules in order to improve it. The presence of hydrogen bonding groups tends to promote inclusion of polar solvents by strong and specific interactions [11]. Despite identification of certain factors contributing to solvate formation, theoretical solvate prediction is challenging and research in this area is still ongoing [9, 10].

In this study, we focus on the solvated salts of a drug-drug system comprising clofaz-imine and diclofenac. Clofazimine (CFZ), exhibits antimycobacterial and anti-inflamma-tory properties and has been recently reevaluated as a potential treatment for multidrug resistant tuberculosis [12, 13, 14, 15, 16, 17]. Diclofenac (DCF) belongs to the class of non-steroidal anti-inflammatory drugs (NSAIDs) that has been recently proposed as a host-directed therapy in the treatment of tuberculosis owing to its antitubercular proper-ties [18, 19, 20, 21, 22]. Several studies showing the ability of clofazimine (pKa: 9.29 [23]) to form salts with organic and inorganic acids [24, 25, 26, 27, 28] point that combining CFZ with DCF in a drug-drug salt should be achievable. Several solvates were previously reported for clofaziminium as well as diclofenac salts [26, 28] and strong H-bond interac-tion between DCF and solvent molecules have been reported [29]. Solvate formation is thus also expected with protic solvents during the preparation the drug-drug CFZ-DCF salts.
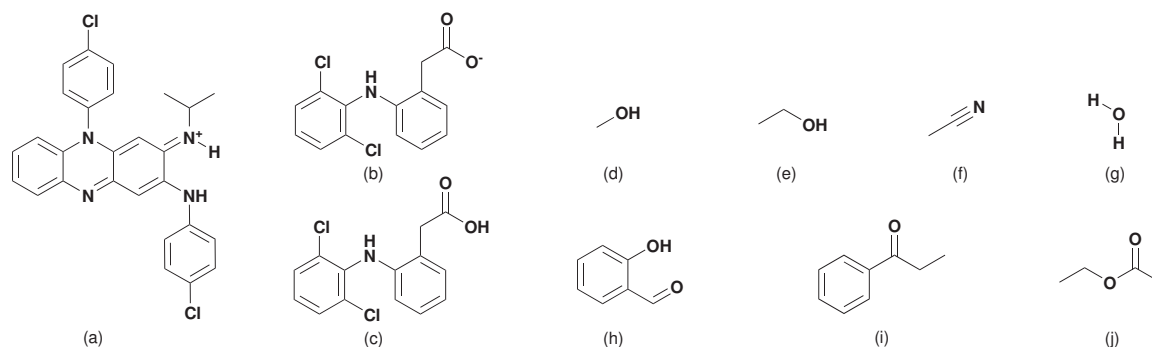
FIGURE 4.1: Scheme of the chemical species observed in the crystal structures of solvated and unsolvated salts/cocrystal of salts: (a) clofaziminium cation, (b) diclofenac anion, (c) diclofenac, (d) methanol, (e) ethanol, (f) acetonitrile, (g) water, (h) salicylaldehyde, (i) propiophenone and (j) ethylacetate.

In our experiments, as expected, diclofenac tended to bind protic solvents and incorporate them into structure, thereby resulting in the solvated form of the CFZ-DCF 1:1 salt. Our further hypothesis was that diclofenac molecule, being also protic, should be able to compete with the solvent molecule for that binding site and thus instead of a solvated 1:1 form lead to a 1:2 CFZ-DCF cocrystal of salt, with diclofenac molecule being connected to diclofenac anion. To verify this and also to see whether an unsolvated 1:1 salt can also be obtained, we have selected a number of aprotic solvents with increasing molecular volume, which due to their chemical nature should have a lower probability of binding to diclofenac. Experimenting with various solvents, we obtained in total five solvated 1:1 forms, two solvated 1:2 forms, one unsolvated 1:1 CFZ-DCF salt and two unsolvated 1:2 cocrystal of salt (Figure 4.1), thus proving that selecting a proper solvent is essential in crystallization processes and might be key to obtaining desired structures.

4.2   Materials and methods

4.2.1   Materials

Clofazimine and diclofenac were respectively purchased from TCI Europe N.V. (Zwijndrecht, Belgium) and Sigma Aldrich (Schnelldorf, Germany). Propiophenone (PPP), salicylaldehyde (SAL), ethyl acetate (EtOAc) (Sigma Aldrich, Schnelldorf, Germany), acetonitrile (MeCN) (Thermo Fisher Scientific, Geel, Belgium), methanol (MeOH) (Chem-Lab, Zedelgem, Belgium), ethanol (EtOH) (Merck, Overijse, Belgium), polyethylene glycol (PEO) of average MW 200 and *N, N*'-dimethylformamide (DMF) (Acros Organics, Geel, Belgium) were used without further purification as crystallization solvents.

4.2.2 (Solvated/hydrated) clofaziminium diclofenac salts preparation

4.2.2.1 Liquid-assisted grinding

CFZNH⁺-DCF⁻-MeOH (1:1:0.74), **CFZNH⁺-DCF⁻-EtOH (1:1:1)** and **CFZNH⁺-DCF⁻ (1:1)** can be obtained by grinding 75.0 mg, 0.158 mmol of CFZ with 46.9 mg, 0.158 mmol of DCF in presence of 30 µL of MeOH, EtOH and EtOAc respectively (liquid-assisted grinding (LAG)). **CFZNH⁺-DCF⁻-DCF (1:1:1)** (polymorph I), **CFZNH⁺-DCF⁻-DCF-MeCN (1:1:1:2)** and **CFZNH⁺-DCF⁻-DCF-EtOAc (1:1:1:1)** are prepared by grinding 75.0 mg (0.158 mmol) of CFZ with 93.8 mg (0.316 mmol) of DCF in presence of 30 µL of EtOH, MeCN and EtOAc respectively. Crystals of **CFZNH⁺-DCF⁻-DCF (1:1:1)** (polymorph I), **CFZNH⁺-DCF⁻-DCF-MeCN (1:1:1:2)** and **CFZNH⁺-DCF⁻-DCF-EtOAc (1:1:1:1)** were obtained by recrystallization of the corresponding powder (CFZ-DCF 1:2 LAG EtOH, LAG MeCN and LAG EtOAc) in ethanol, acetonitrile and ethylacetate respectively (Figure 4.2). All ball milling experiments were performed at 30 Hz, during 90 minutes (samples were homogenized each 30 minutes) with a Retsch MM 400 Mixer Mill apparatus. Powders were inserted in 2 mL Eppendorf tubes with eight stainless steel balls (7 balls of 2 mm diameter and 1 ball of 3 mm diameter) and were then placed in two grinding jars in which up to 5 Eppendorf tubes can be installed. Powder of **CFZNH⁺-DCF⁻-DCF (1:1:1)** (polymorph II) cocrystal of salt is obtained by desolvation (heating at 130 - 140 °C) of **CFZNH⁺-DCF⁻-DCF-MeCN (1:1:1:2)** or of **CFZNH⁺-DCF⁻-DCF-EtOAc (1:1:1:1)** (obtained by liquid-assisted grinding, Figure 4.2).

4.2.2.2 Solvent evaporation method

Powders consisting of an equimolar ratio of clofazimine (37.4 mg, 0.0790 mmol) and diclofenac acid (23.4 mg, 0.0790 mmol) were stirred in the selected solvent (MeCN, MeOH, EtOH, DMF) until complete dissolution and left for slow evaporation at room temperature (20 - 25 °C). Crystals of **CFZNH⁺-DCF⁻-MeOH (1:1:0.74)**, **CFZNH⁺-DCF⁻-EtOH (1:1:1)** and **CFZNH⁺-DCF⁻-MeCN-H₂O (1:1:1:2)** were obtained in MeOH, EtOH and MeCN respectively. Crystals of **CFZNH⁺-DCF⁻-DCF-MeCN (1:1:1:2)** and of **CFZNH⁺-DCF⁻-DCF (1:1:1)** (polymorph II) were obtained in MeCN and PEO 200 respectively, by the same method but from a powder consisting of clofazimine (37.4 mg, 0.0790 mmol) and diclofenac acid (46.8 mg, 0.158 mmol) in 1:2 molar ratio.

Given the low vapor pressure at room temperature (20 - 25 °C) of propiophenone and salicylaldehyde and the quite good solubility of CFZ and DCF in these solvents, crystallization by solvent evaporation is quite difficult. For this reason, the 1:1 powder mixture of CFZ and DCF was not fully dissolved in these solvent (i.e. an excess powder was placed in the solvent and left at room temperature for crystallization) to give **CFZNH⁺-DCF⁻-PPP (2:2:5)** and **CFZNH⁺-DCF⁻-SAL-H₂O (4:4:9:1)**.

4.2.3   Single-crystal X-ray diffraction (SCXRD)

Data collection was performed with an Oxford Diffraction Gemini Ultra R system equipped with a four-circle kappa platform and a Ruby CCD detector, using Cu $K\alpha$ ($\lambda = 1.54184$ Å) radiation. Full data sets were collected either at 295 K (**CFZNH$^+$-DCF$^-$-MeOH (1:1:0.74), CFZNH$^+$-DCF$^-$ (1:1), CFZNH$^+$-DCF$^-$-DCF-MeCN (1:1:1:2), CFZNH$^+$-DCF$^-$-DCF-EtOAc (1:1:1:1)** and **CFZNH$^+$-DCF$^-$-DCF (1:1:1)** (polymorphs I and II)), at 100 K (**CFZNH$^+$-DCF$^-$-MeCN-H$_2$O (1:1:1:2)** and **CFZNH$^+$-DCF$^-$-SAL-H$_2$O (4:4:9:1)**) or at both temperatures (**CFZNH$^+$-DCF$^-$-EtOH (1:1:1)** and **CFZNH$^+$-DCF$^-$-PPP (2:2:5)**)). Low-temperature data collection was necessary for **CFZNH$^+$-DCF$^-$-MeCN-H$_2$O (1:1:1:2)** because crystals are unstable at room temperature. Crystals of **CFZNH$^+$-DCF$^-$-SAL-H$_2$O (4:4:9:1)** were stable at room temperature but disorder in the structure could not be resolved without low-temperature data collection. First, analytical numerical absorption correction implemented using a multifaceted crystal model based on expressions derived by Clark & Reid [30] was performed using *CrysAlis PRO* [31]. Then, empirical absorption correction was applied, within *CrysAlis PRO*, using spherical harmonics [32] as implemented in the SCALE3 ABSPACK scaling algorithm. Dual-space method implemented within *SHELXT* [33] was used for structure solution. Refinement was performed within *Olex²* [34] and *ShelXle* [35] using the least-square method (*SHELXL-2016/6* [36]). Anisotropic refinement was performed for non hydrogen atoms. If not involved in strong H-bonds, hydrogen atoms were refined as riding atoms with displacement spheres fixed to 1.2 times that of the parent atom (1.5 for methyl groups). Positions of H atoms involved in strong H-bond were located in Fourier map and refined (except for disordered MeOH molecule in the structure of **CFZNH$^+$-DCF$^-$-MeOH (1:1:0.74)**, disordered EtOH molecule in the structure of **CFZNH$^+$-DCF$^-$-EtOH (1:1:1)** (data collected at 295 K) and for disordered salicylaldehyde molecules and the water molecule in **CFZNH$^+$-DCF$^-$-SAL-H$_2$O (4:4:9:1)**). The solvent molecules are disordered in several structures. More particularly, the methanol molecule in **CFZNH$^+$-DCF$^-$-MeOH (1:1:0.74)**; all solvent molecules in **CFZNH$^+$-DCF$^-$-PPP (2:2:5)** (data collected at 295 K); one molecule of propiophenone (which is located close to an inversion center) in **CFZNH$^+$-DCF$^-$-PPP (2:2:5)** (data collection at 100 K); five salicylaldehyde molecules (which are not involved in intermolecular H-bonds) in the structure of **CFZNH$^+$-DCF$^-$-SAL-H$_2$O (4:4:9:1)**; the ethanol molecule in the structure of **CFZNH$^+$-DCF$^-$-EtOH (1:1:1)** for which data were collected at 295 K and one MeCN molecule in **CFZNH$^+$-DCF$^-$-DCF-MeCN (1:1:1:2)** are disordered.

4.2.4   Powder X-ray diffraction (PXRD)

Powder diffraction data were collected with Cu $K\alpha$ radiation ($\lambda = 1.54184$ Å) from 4 to 40° 2θ angle (step size of 0.0167°) on a PANalytical X'PERT PRO Bragg-Brentano diffractometer with an X'Celerator linear detector. Tension and current of the generator were set to 45 kV and 30 mA for data collection.

Variable-temperature powder X-ray diffraction (VT-PXRD) experiments were conducted on the same diffractometer equipped with an Anton-Paar TTK 450 system. Data were collected at 25 °C and then from 30 °C to 140 °C with data collection every 10 °C.

4.2.5 Thermogravimetric analysis (TGA) and differential scanning calorimetry (DSC)

Thermal properties of powders obtained by liquid-assisted grinding and corresponding to determined structures were analysed using a Mettler Toledo TGA/DSC 3+ apparatus. Around 5 - 10 mg of solid samples were placed in 100 μL open aluminium pans. The analysis was performed from 25 °C to 250 °C with a heating rate of 10 °C/min and using nitrogen (60 mL/min) as purge gas. TGA/DSC results were analysed using the STARe software (version 16.20).

4.2.6 Structure visualization, crystal packing comparison and solvent molecular volume calculations

Structures and crystal packings were visualized and compared using *Mercury* [37]. Voids were calculated with the 'Voids' option within *Mercury* [37] with a probe radius of 1.2 Å and an approximated grid spacing of 0.1 Å. Images were generated with de same program. Crystal packings were more specifically compared using the 'Crystal packing similarity' tool in *Mercury* [37]. Packing shell size, distance and angle tolerance parameters were set to 15 molecules, 30% and 30° respectively. Moreover, molecular differences and structure inversion were allowed while bond types, H-atom position, atoms' hydrogen counts and atoms bond counts were ignored. As structures contain different solvents, smallest molecular component was ignored for crystal packing comparison. Solvent molecular volumes were determined with the free Molinspiration molecular property calculation service [38].

4.3 Results and discussion

The current work includes two parts. In the first part, we have investigated solvated and unsolvated forms of CFZ-DCF 1:1 salt. The second part is focused on the ability of a diclofenac anion to bind a diclofenac molecule instead of a solvent molecule (a phenomenon often observed in 1:1 salts) to obtain a 1:2 CFZ-DCF cocrystal of salt. To obtain drug-drug salts, clofazimine and diclofenac were subjected to solvent evaporation crystallization and liquid-assisted grinding (Figure 4.2). Below and for each part of the work, we will first present structural analysis of the new crystal structures combining clofazimine with diclofenac (Figure 4.1 and Figures B.1 and B.2 (labeling)) and discuss the impact of solvent selection on the crystallization outcome.
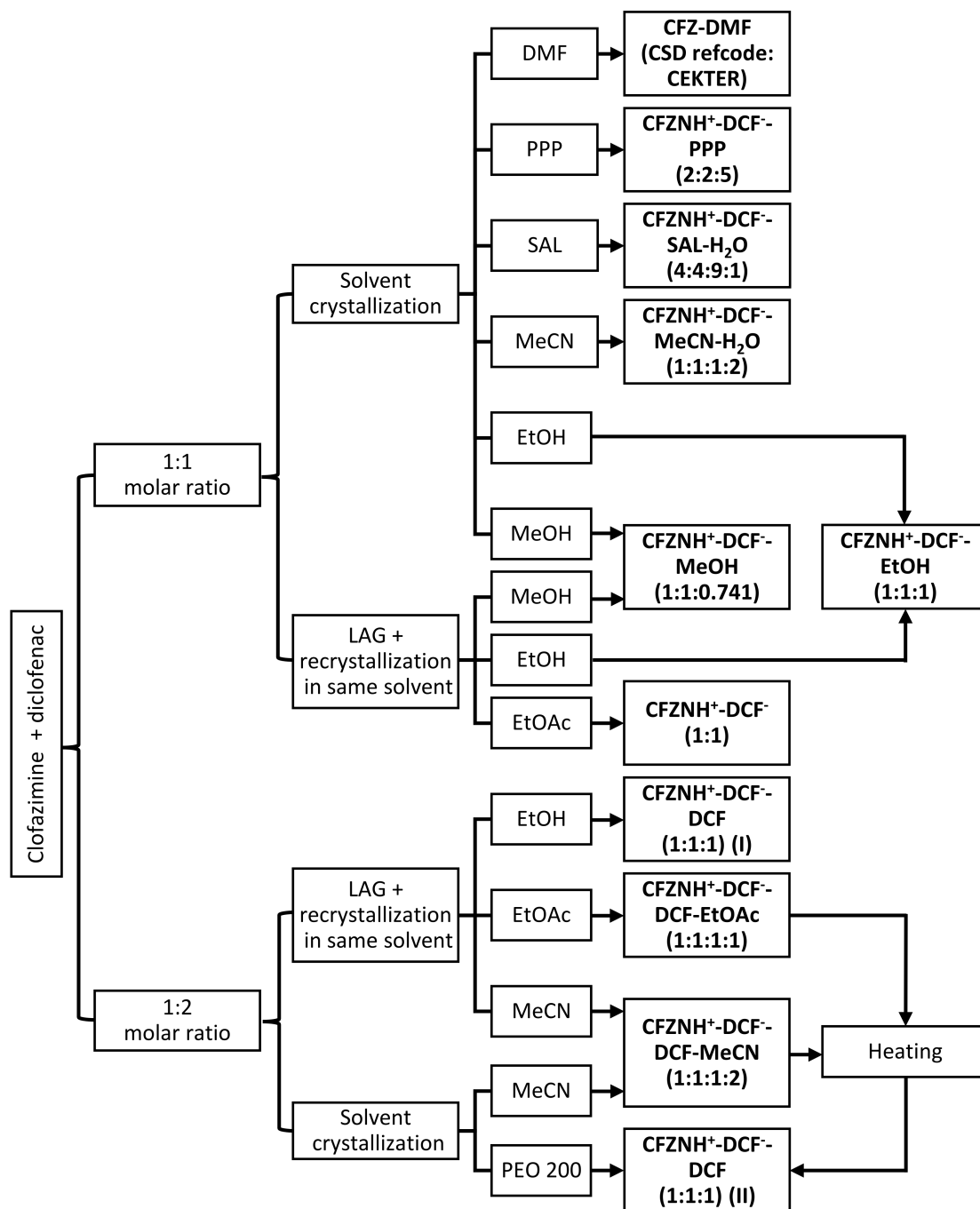
FIGURE 4.2: Summary of performed experiments and associated results. LAG: liquid-assisted grinding, DMF: *N, N'*-dimethylformamide, PPP: propiophenone, SAL: salicylaldehyde, MeCN: acetonitrile, EtOH: ethanol, MeOH: methanol, EtOAc: ethyl acetate, PEO: polyethylene glycol.

4.3.1 Investigation of CFZ-DCF 1:1 salts

The solvents used in the first part of this work were selected based on their ability to interact with the solute (CFZ cations and DCF anions) *via* hydrogen bonding or other weak interactions and on their molecular size and shape - two main parameters influencing the formation of solvates. First, we selected a series of protic solvents of increasing molecular volume (MeOH, EtOH, salicylaldehyde) in order to investigate the impact on solvate formation of those solvents that are capable of forming H-bond with diclofenac anion. In addition to H-bonds, the aromatic system of salicylaldehyde could also be involved in stacking interactions with clofaziminium cation and/or diclofenac anion. Second, we took aprotic solvents of variable molecular volume (MeCN, DMF, EtOAc, propiophenone) in order to study the effect of solvents that do not have the ability to interact with diclofenac anion through H-bond. Propiophenone, that could potentially interact with CFZNH$^+$ and DCF$^-$ through stacking has also been included among the selected aprotic solvents. Below we present structural analysis of the 1:1 solvated and unsolvated CFZ-DCF salts that were obtained using aforementioned solvents followed by the discussion of the solvent impact on crystallization outcome.

4.3.1.1 Structural analysis

CFZNH$^+$-DCF$^-$-MeOH (1:1:0.74) solvated salt crystallizes in $C2/c$ space group (Table 4.1). The asymmetric unit contains one clofaziminium cation, one diclofenac anion and methanol molecule, which is disordered over two positions (one position is located around $C2$ axis). A $R_2^1(7)$ motif is observed between clofazimine and diclofenac (N4−H4$\cdots$O1 and N3−H3$\cdots$O1 charge-assisted H-bonds, Figure 4.3 (a) and Table B.2). A weaker H-bond is also observed between **CFZNH$^+$** and **DCF$^-$** (N4−H4$\cdots$O2, Figure

(a)   (b)
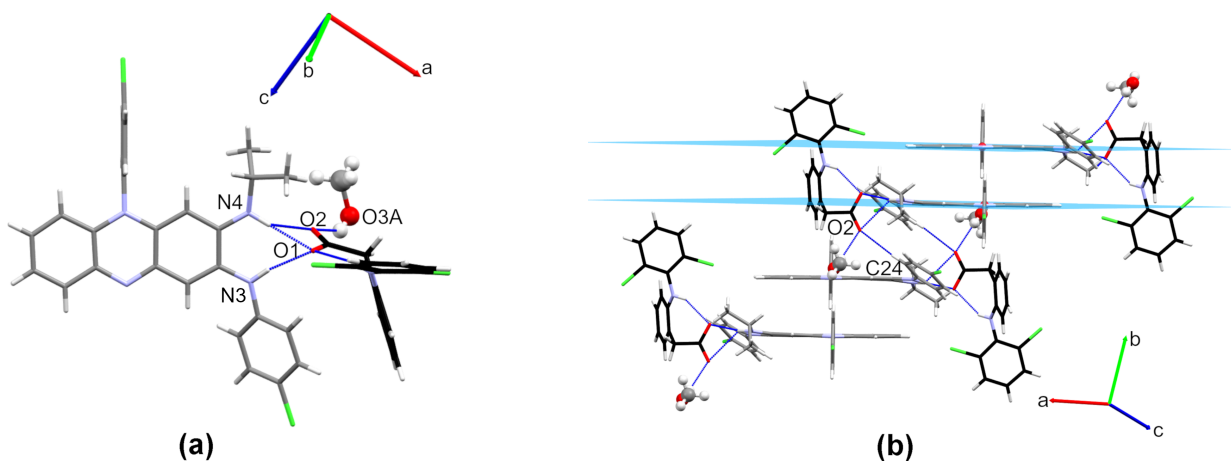
FIGURE 4.3: (a) H-bonds between clofaziminium, diclofenac and methanol in **CFZNH$^+$-DCF$^-$-MeOH (1:1:0.74)** (MeOH disorder not shown) and (b) weak C24−H24$\cdots$O2 H-bond stabilizing dimers of CFZNH$^+$-DCF$^-$-MeOH trimolecular assemblies and head-to-tail stacking of these assemblies (planes (light blue) and centroids (red) are calculated with C5 C6 C11 and C12 atoms). H-bonds are represented by blue dashed lines.

4.3 (a) and Table B.2). Methanol (position with an occupancy of 0.5) interacts with diclofenac through H-bond (O3A−H3OA$\cdots$O2, Figure 4.3 (a) and Table B.2). An intramolecular N5−H5$\cdots$O1 H-bond is also present within the diclofenac anion. A weak C24−H24$\cdots$O2 H-bond stabilizes dimers of CFZNH$^+$-DCF$^-$-MeOH trimolecular assemblies (Figure 4.3 (b)). These dimers are further stacked in a head-to-tail fashion (Figure 4.3 (b), centroid-centroid distance of 3.623(2) Å, orthogonal projection distance of 3.378(1) Å and horizontal displacement of 1.311 Å).

This salt can also be prepared by liquid-assisted grinding of CFZ with DCF (in 1:1 molar ratio) and with MeOH as solvent (Figure B.3(a)). TG/DSC analysis of the powder indicates a weight loss of 2.6% between 30 and 150 °C (calculated MeOH content: 2.99%) (Figure B.4). The powder of **CFZNH$^+$-DCF$^-$-MeOH (1:1:0.74)** melts at 118 °C (as confirmed by an analysis performed on a a Koffler apparatus). Complete desolvation is difficult to achieve before melting of the powder (at 100 °C, the solvate is still present) and the crystalline phase obtained upon heating of **CFZNH$^+$-DCF$^-$-MeOH (1:1:0.74)** at 110 °C could not be identified (Figure B.5).

CFZNH$^+$-DCF$^-$-EtOH (1:1:1) solvated salt crystallizes in $P\bar{1}$ triclinic space group (Table 4.1). The asymmetric unit consists of the clofaziminium cation, diclofenac anion and one solvent molecule (EtOH). This structure was determined at 295 and 100 K. At 295 K, EtOH molecule is disordered over two positions, both of which allow O3−H$\cdots$O1 interaction between EtOH and diclofenac anion while at 100 K the same interaction is observed but EtOH is not disordered. At both temperatures, diclofenac anion and clofaziminium interact through bifurcated charge-assisted H-bonds (N4−H4$\cdots$O2, N3−H3$\cdots$O2, N4−H4$\cdots$O1 and N3−H3$\cdots$O1, Table B.2 and Figure 4.4 (a)). A $D_1^1(2)$ motif between ethanol and diclofenac anion as well as an intramolecular H-bond ($S_1^1(7)$ motif) in diclofenac anion are also observed (O3−H3OB$\cdots$O1 and N5−H5$\cdots$O2 respectively, Table B.2 and Figure 4.4 (a)). Dimers of CFZNH$^+$-DCF$^-$-EtOH three-component assemblies are stabilized through weak H-bonds (C23−H23$\cdots$O2, Table B.2 and Figure 4.4 (b)).

PXRD pattern of the powder obtained by liquid-assisted grinding of CFZ with DCF (in 1:1 molar ratio) and with EtOH as solvent corresponds to the calculated pattern of **CFZNH$^+$-DCF$^-$-EtOH (1:1:1)** (Figure B.3(b)). This powder was analyzed by TG/DSC (Figure B.4) that revealed a weight loss of 5.6% which is consistent with calculated EtOH content (5.6%). Only one endothermic event, associated with salt melting and solvent evaporation was observed at 113 °C. Such a high temperature of desolvation suggests that EtOH is strongly bound to diclofenac anion (Figure B.4 and Table 4.2). This is in accordance with the O3$\cdots$O1 distance (between 2.672(3) and 2.82(1) Å) observed in the structure, which is characteristic of strong H-bond, as defined by Desiraju and Steiner [39].

TABLE 4.1: Experimental details.

	CFZNH$^+$-DCF$^-$-MeOH (1:1:0.74)	CFZNH$^+$-DCF$^-$-EtOH (1:1:1)	CFZNH$^+$-DCF$^-$-EtOH (1:1:1)
Chemical formula	$C_{27}H_{23}Cl_2N_4$·$C_{14}H_{10}Cl_2NO_2$·$0.741(CH_4O)$	$C_{27}H_{23}Cl_2N_4$·$C_{14}H_{10}Cl_2NO_2$·C_2H_6O	$C_{27}H_{23}Cl_2N_4$·$C_{14}H_{10}Cl_2NO_2$·C_2H_6O
Mr	793.42	815.59	815.59
Crystal system, space group	Monoclinic, $C2/c$	Triclinic, $P\bar{1}$	Triclinic, $P\bar{1}$
Temperature (K)	295(2)	295(2)	100(2)
a, b, c (Å)	16.7209(3), 17.2504(5), 27.8319(7)	12.5818(4), 13.4486(3), 13.5318(3)	12.5325(5), 13.1139(3), 13.1773(4)
α, β, γ (°)	90, 93.438(2), 90	80.291(2), 71.638(2), 71.710(2)	82.032(2), 71.833(3), 74.538(3)
V (Å^3)	8013.4(3)	2057.12(10)	1979.61(12)
Z	8	2	2
No. of measured, independent and observed [$I > 2\sigma(I)$] reflections	23679, 7080, 4722	27818, 7236, 6397	21176, 6977, 6386
R_{int}	0.040	0.024	0.046
$R[F^2 > 2\sigma(F^2)]$, $wR(F^2)$, S	0.059, 0.193, 1.02	0.050, 0.146, 1.06	0.057, 0.166, 1.07
CCDC number	2032488	2032489	2032490

	CFZNH$^+$-DCF$^-$-MeCN-H$_2$O (1:1:1:2)	CFZNH$^+$-DCF$^-$-SAL-H$_2$O (4:4:9:1)	CFZNH$^+$-DCF$^-$-PPP (2:2:5)
Chemical formula	$C_{27}H_{23}Cl_2N_4$·$C_{14}H_{10}Cl_2NO_2$·C_2H_3N· $2(H_2O)$	$4(C_{27}H_{23}Cl_2N_4)$·$4(C_{14}H_{10}Cl_2NO_2)$·$9(C_7H_6O_2)$· H_2O	$2(C_{27}H_{23}Cl_2N_4)$·$2(C_{14}H_{10}Cl_2NO_2)$·$5(C_9H_{10}O)$
Mr	846.61	4195.16	2209.89
Crystal system, space group	Triclinic, $P\bar{1}$	Triclinic, $P\bar{1}$	Triclinic, $P\bar{1}$
Temperature (K)	100(2)	100(2)	295(2)
a, b, c (Å)	11.6515(3), 11.7149(3), 16.0793(4)	10.4132(5), 21.2266(7), 25.0657(7)	10.7319(4), 13.6005(6), 21.5496(9)
α, β, γ (°)	103.558(2), 90.461(2), 105.250(2)	66.238(3), 89.969(3), 86.658(3)	73.502(4), 77.404(4), 73.540(4)
V (Å^3)	2052.78(9)	5060.5(3)	2859.7(2)
Z	2	1	1
No. of measured, independent and observed [$I > 2\sigma(I)$] reflections	18621, 7196, 6969	53166, 17765, 13730	28672, 10049, 6767
R_{int}	0.019	0.069	0.051
$R[F^2 > 2\sigma(F^2)]$, $wR(F^2)$, S	0.031, 0.080, 1.03	0.060, 0.171, 1.03	0.052, 0.160, 1.02
CCDC number	2032491	2032492	2032493

	CFZNH$^+$-DCF$^-$-PPP (2:2:5)	CFZNH$^+$-DCF$^-$ (1:1)	CFZNH$^+$-DCF$^-$-DCF (1:1:1) (I)
Chemical formula	$2(C_{27}H_{23}Cl_2N_4)$·$2(C_{14}H_{10}Cl_2NO_2)$·$5(C_9H_{10}O)$	$(C_{27}H_{23}Cl_2N_4)$·$(C_{14}H_{10}Cl_2NO_2)$	$C_{27}H_{23}Cl_2N_4$·$C_{14}H_{10}Cl_2NO_2$·$C_{14}H_{11}Cl_2NO_2$

	CFZNH$^+$-DCF$^-$-PPP (2:2:5)	CFZNH$^+$-DCF$^-$ (1:1)	CFZNH$^+$-DCF$^-$-DCF (1:1:1) (I)
Mr	2209.89	769.52	1065.66
Crystal system, space group Triclinic, $P\bar{1}$	Triclinic, $P\bar{1}$	Triclinic, $P\bar{1}$	
Temperature (K)	100(2)	295(2)	295(2)
a, b, c (Å)	10.5086(4), 13.4783(5), 21.4224(8)	12.4461(6), 13.2751(5), 13.3667(6)	10.8837(2), 14.4737(3), 17.7519(4)
α, β, γ (°)	73.629(3), 76.913(3), 73.271(3)	84.423(3), 67.963(4), 66.662(4)	101.568(2), 105.173(2), 94.286(2)
V (Å^3)	2752.92(19)	1876.21(16)	2620.06(10)
Z	1	2	2
No. of measured, independent and observed [$I > 2\sigma(I)$] reflections	28107, 9723, 7857	17078, 6630, 5192	26706, 9218, 8043
R_{int}	0.038	0.037	0.022
$R[F^2 > 2\sigma(F^2)]$, $wR(F^2)$, S	0.035, 0.090, 1.03	0.048, 0.141, 1.03	0.050, 0.141, 1.05
CCDC number	2032494	2032495	2032496

	CFZNH$^+$-DCF$^-$-DCF-MeCN (1:1:1:2)	CFZNH$^+$-DCF$^-$-DCF-EtOAc (1:1:1:1)	CFZNH$^+$-DCF$^-$-DCF (1:1:1) (II)
Chemical formula	$C_{27}H_{23}Cl_2N_4$· $C_{14}H_{10}Cl_2NO_2$· $C_{14}H_{11}Cl_2NO_2$· $2(C_2H_3N)$	$C_{27}H_{23}Cl_2N_4$· $C_{14}H_{10}Cl_2NO_2$· $C_{14}H_{11}Cl_2NO_2$· $C_4H_8O_2$	$C_{27}H_{23}Cl_2N_4$· $C_{14}H_{10}Cl_2NO_2$· $C_{14}H_{11}Cl_2NO_2$
Mr	1147.77	1153.76	1065.66
Crystal system, space group	Triclinic, $P\bar{1}$	Triclinic, $P\bar{1}$	Triclinic, $P\bar{1}$
Temperature (K)	295(2)	295(2)	295(2)
a, b, c (Å)	15.0694(11), 15.2735(10), 15.5991(13)	15.0569(4), 15.3773(4), 15.4247(4)	11.9326(3), 15.2549(4), 16.0042(4)
α, β, γ (°)	74.882(7), 61.685(8), 64.227(7)	76.043(2), 61.975(3), 63.541(3)	89.161(2), 70.570(2), 69.693(2)
V (Å^3)	2839.6(4)	2820.07(16)	2559.79(12)
Z	2	2	2
No. of measured, independent and observed [$I > 2\sigma(I)$] reflections	27894, 10010, 7543	27162, 9942, 8898	25042, 9036, 7679
R_{int}	0.032	0.022	0.025
$R[F^2 > 2\sigma(F^2)]$, $wR(F^2)$, S	0.050, 0.159, 1.08	0.042, 0.122, 1.05	0.045, 0.129, 1.04
CCDC number	2032497	2032498	2032499
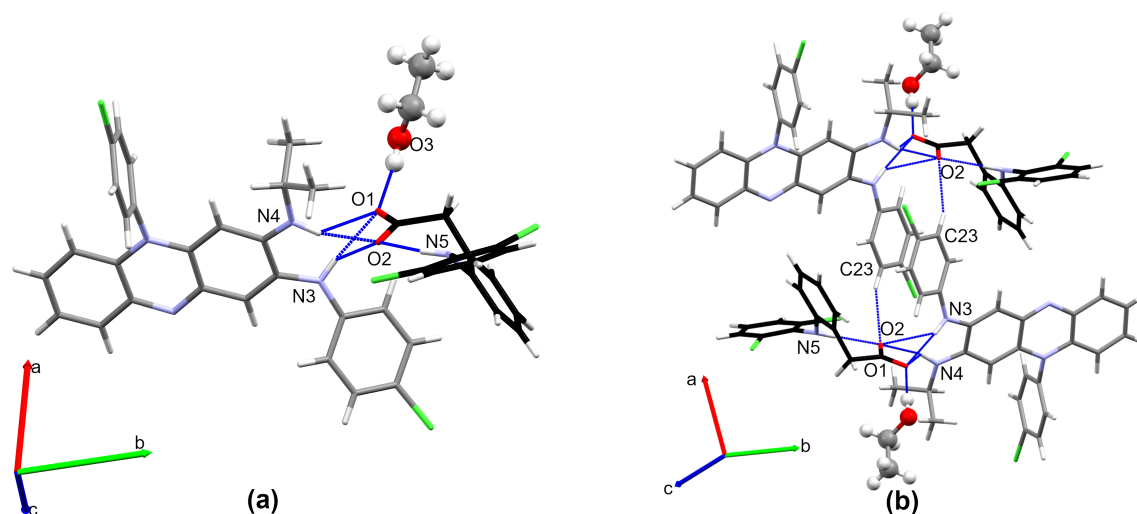
FIGURE 4.4: (a) H-bonds between clofaziminium, diclofenac anion and ethanol in the structure of **CFZNH$^+$-DCF$^-$-EtOH (1:1:1)** solvated salt. (b) Weak C23$-$H23$\cdots$O2 H-bonds stabilizing dimers of CFZNH$^+$-DCF$^-$-EtOH three-component assemblies. Ethanol molecules are in ball and stick model, carbon atoms of diclofenac anion are in black and H-bonds are represented by blue dashed lines.

TABLE 4.2: Melting point temperatures of reported crystalline phases. Powders were obtained by LAG. *Value obtained from desolvated powder of **CFZNH$^+$-DCF$^-$-DCF-MeCN (1:1:1:2)**.

Compound	Transition onset (°C)	Melting onset (°C)
CFZ	/	218
DCF	/	177
CFZNH$^+$-DCF$^-$-EtOH (1:1:1)	Desolvation at melting	113
CFZNH$^+$-DCF$^-$ (1:1)	/	186
CFZNH$^+$-DCF$^-$-DCF (1:1:1) (polymorph I)	/	171
CFZNH$^+$-DCF$^-$-DCF-MeCN (1:1:1:2)	93	157
CFZNH$^+$-DCF$^-$-DCF-EtOAc (1:1:1:1)	93	157
CFZNH$^+$-DCF$^-$-DCF (1:1:1) (polymorph II)	/	157*

CFZNH$^+$-DCF$^-$-MeCN-H$_2$O (1:1:1:2) solvated dihydrated salt crystallizes in space group $P\bar{1}$ (Tables 4.1 and B.1). One clofaziminium cation, one diclofenac anion, two water and one acetonitrile molecules constitute the asymmetric unit. A $R_2^1(7)$ motif is observed between clofaziminium and diclofenac (N4$-$H4$\cdots$O1 and N3$-$H3$\cdots$O1 charge-assisted H-bonds, Table B.2, Figure 4.5 (a)). An intramolecular N5$-$H5$\cdots$O1 H-bond is also present within the diclofenac anion. Water molecules bridge diclofenac anion and clofaziminium through O3$-$H3OA$\cdots$O2, O3$-$H3OB$\cdots$O4 and O4$-$H4OA$\cdots$N2 H-bonds (Table B.2), forming 8-component clusters (2 clofaziminium cations, 2 diclofenac anions and 4 water molecules, Figure 4.5 (b) and (c)). These 8-component clusters are
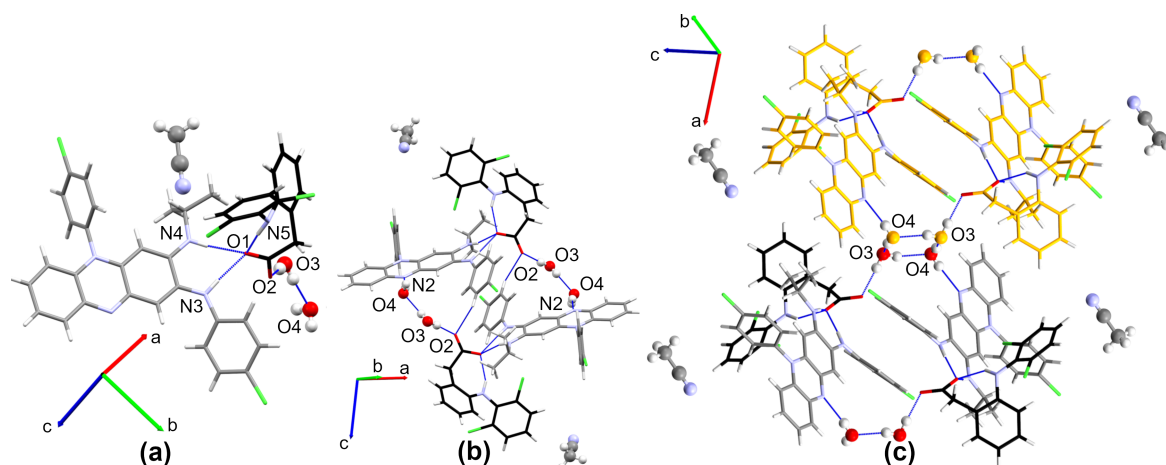
FIGURE 4.5: (a) H-bonds between clofaziminium, diclofenac and water in **CFZNH$^+$-DCF$^-$-MeCN-H$_2$O (1:1:1:2)**, (b) 8-component clusters stabilized by O3−H3OA···O2, O4−H4OB···O3 and O4−H4OA···N2 H-bonds and (c) chains of 8-component clusters along *a*-axis (one 8-component cluster is colored in orange). H-bonds are represented by blue dashed lines.

extended along *a*-axis thanks to water tetramers (R$_4^4$ (8) motif, O3−H3OB···O4 and O4−H4OB···O3, Table B.2, Figure 4.5 (c)).

CFZNH$^+$-DCF$^-$-SAL-H$_2$O (4:4:9:1) solvated hydrated salt crystallizes in $P\bar{1}$ space group (Tables 4.1 and B.1). The asymmetric unit contains two clofaziminium cations, two diclofenac anions, 4.5 salicylaldehyde and a half water molecules (one salicylaldehyde and the water are located on an inversion center). Clofaziminium cations interact with diclofenac anions through charge-assisted H-bonds ($R_2^1(7)$ motif, N4−H4···O1 and N3−H3···O1, as well as N8−H8···O3 and N9−H9···O3, Table B.2 and Figure 4.6 (a)).

Intramolecular H-bonds are observed within diclofenac anions (N5−H5···O1 and N10−H10 ···O3, Table B.2). Two salicylaldehyde molecules are H-bonded, through their phenol moiety, to diclofenac anion (O5S−H5OS···O2 as well as O7T−H7OT···O4, Table B.2 and Figure 4.6 (a)). Other solvent molecules are disordered and have their phenol moiety oriented to allow intramolecular H-bonds (O9U−H9OU···O10U, O9V−H9OV···O10V; O11W−H11W···O12W, O11X−H11X···O12X and O13Y−H13Y···O14Y, Table B.2 and Figure 4.6 (b)). The water molecule interacts with the salicylaldehyde molecule located on an inversion center through O15−H15O···O13Y (Table B.2), which is H-bonded to diclofenac anion (C29−H29B···O13Y, Table B.2). Chains along *a*-axis are stabilized by weak H-bonds between diclofenac anions (C38−H38···O2 and C79−H79···O4, Table B.2 and Figure 4.6 (c)). Several weak H-bonds are also observed between clofazimine and salicylaldehyde molecules (C1−H1···O12W, C18−H18···O6S, C55−H55···O8T, C61−H61A···O7T and C28W−H28W···O5S, Table B.2). Weak H-bonds are also observed between two CFZNH$^+$ cations (C14−H14···N2, C25−H25··· Cl6, C59−H59···N7 and C66−H66···Cl2, Table B.2).

FIGURE 4.6: (a) H-bonds between clofaziminium, diclofenac anion and salicylaldehyde molecules. H atoms not involved in strong H-bonds are omitted for clarity. Salicylaldehyde molecules are in ball and stick model, carbon atoms of the salicylaldehyde molecule located on an inversion center are coloured in cyan (other disordered SAL molecule are omitted). (b) Labeling of atoms involved in weak H-bonds in the structure of **CFZNH$^+$-DCF$^-$-SAL-H$_2$O (4:4:9:1)** (salicylaldehyde molecules are represented in wireframe model and H atoms not involved in strong H-bonds are omitted for clarity). (c) Weak H-bonds between diclofenac anions (C38−H38···O2 and C79−H79···O4) stabilize chains along *a*-axis (salicylaldehyde molecules are omitted for clarity). Carbon atoms of diclofenac anion are in black and H-bonds are represented by blue dashed lines.

CFZNH$^+$-DCF$^-$-PPP (2:2:5) solvated salt crystallizes in $P\bar{1}$ space group (Tables 4.1 and B.1). The asymmetric unit contains one clofaziminium cation, one diclofenac anion, and 2.5 propiophenone molecules (one PPP is located on an inversion center). The structure of this solvated salt was determined at 295 K and at 100 K. Same interactions are observed at both temperatures, but PPP molecules are disordered at 295 K. Clofaziminium cation and diclofenac anion interact through N3−H3···O1 and N4−H4···O1 charge-assisted H-bonds (Table B.2 and Figure 4.7 (a)). Two propiophenone molecules interact with clofaziminium through weak H-bonds (C15−H15···O3 and C18−H18···O4, Table B.2 and Figure 4.7(a)). Clofaziminium cations are stacked in a head-to-tail fashion (centroid-centroid distance of 3.519(1) Å, interplanar distance of 3.430(1) Å and horizontal displacement of 0.788 Å (planes and centroids were calculated using atoms C5 C6 C11 C12)). Moreover, a cation-π interaction is observed between iminium moiety of CFZNH$^+$ and one propiophenone molecule (vertical distance: 3.719 Å (between N4$^+$ and the plane passing through C54 C55 C56 C57 C58 and C59) and horizontal displacement of 0.837 Å, Figure 4.7(b)).
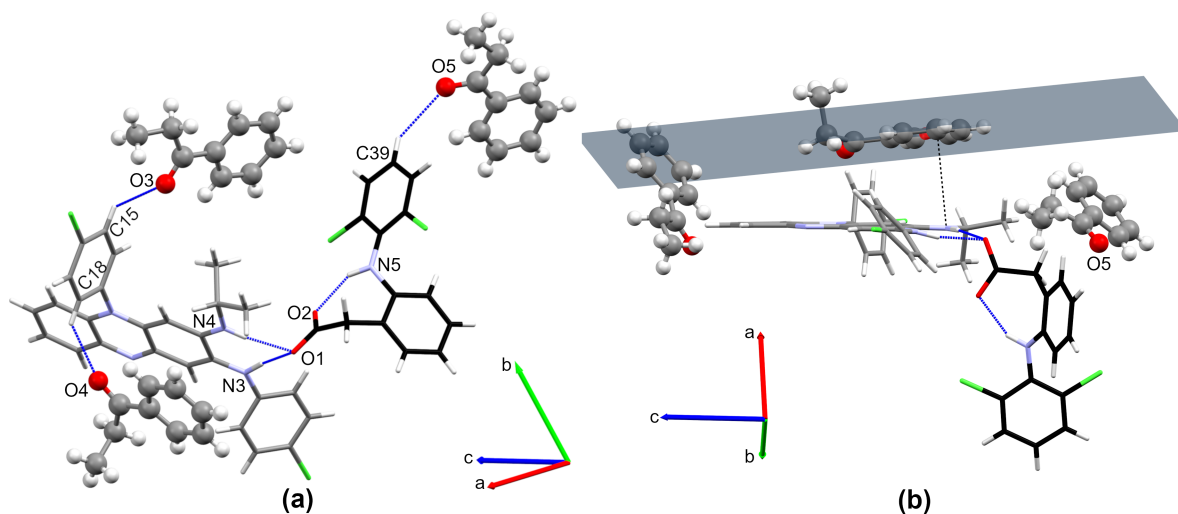
FIGURE 4.7: (a) H-bonds (blue dashed lines) between clofaziminium, diclofenac anion and propiophenone molecules (PPP whose oxygen atom is labeled O5 is located on an inversion center) and (b) π-cation interaction (black dashed line) between clofazimine and PPP (centroid in red and plane in blue). PPP molecules are in ball and stick model, carbon atoms of diclofenac anion are in black.

CFZNH$^+$-DCF$^-$ (1:1) salt crystallizes in space group $P\bar{1}$ (Tables 4.1 and B.1) with one clofaziminium cation and one diclofenac anion in the asymmetric unit. Clofaziminium interacts with diclofenac anion through charge-assisted H-bond ($R_2^1(7)$ motif, N4−H4···O1 and N3−H3···O1, Table B.2, Figure 4.8). An intramolecular H-bond is observed N5−H5···O2, Table B.2 within diclofenac anion. Interestingly, in this structure, the carboxylate of diclofenac anion is almost coplanar to the iminophenazine moiety of clofazimine (angle between planes passing through N4-C9-C8-N3 and O1-C28-O2-C29 is only 14.3°, Table 4.3) which is not the case in solvated structures (angles between the same planes are comprised between 83.2° and 62.5°, Table 4.3). This orientation results in a supplementary H-bond between clofaziminium and diclofenac (N3−H3···O2 Table B.2, Figure 4.8).

Clofaziminium cations are stacked in a head-to-tail fashion (Figure 4.8, centroid-centroid distance: 3.592(2) Å, orthogonal projection distance: 3.443(1) Å and horizontal offset of 1.026 Å, with centroids and planes calculated from C5 C6 C11 and C12 atoms). This crystalline phase can also be obtained by liquid-assisted grinding of CFZ with DCF (in 1:1 molar ratio) with EtOAc as solvent (Figure B.3(c)).

Melting point of this unsolvated salt was determined as 186 °C by DSC analysis (Figure B.4 and Table 4.2). Interestingly, this unsolvated salt has a smaller packing coefficient than the solvated 1:1 salts (Table 4.3). This is in accordance with the presence of voids (15.41 Å^3, 0.8% of the unit cell volume). This lower packing efficiency could explain solvent insertion (and so solvate crystallization) when diclofenac anion-solvent or clofaziminium cation-solvent interactions are possible.
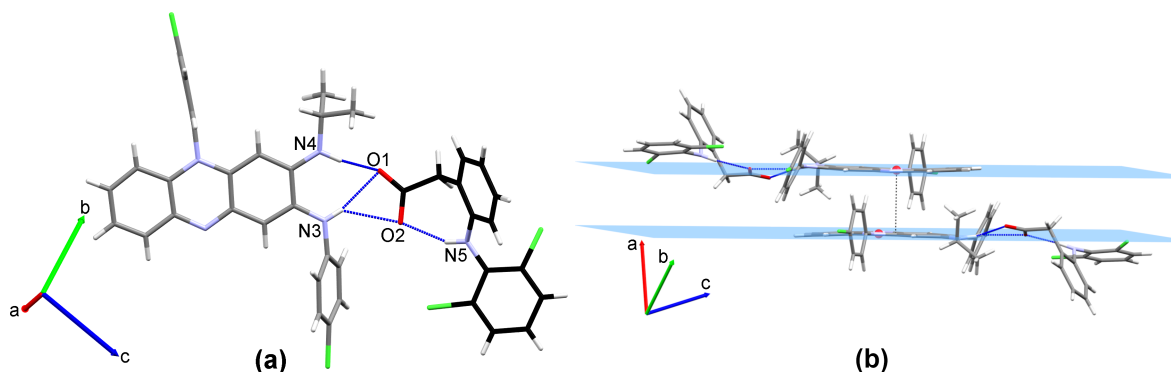
FIGURE 4.8: (a) H-bonds between clofaziminium and diclofenac anion in **CFZNH$^+$-DCF$^-$ (1:1)** and (b) π-π stacking between clofaziminium (centroids in red and planes in blue). Carbon atoms of diclofenac anion are in black. H-bonds are represented by blue dashed lines.

TABLE 4.3: Packing coefficient of the determined structures (at 295 K unless stated otherwise in the table) and angles between planes passing through N4-C9-C8-N3 atoms of clofaziminium cations and O1-C28-O2-C29 atoms of diclofenac anions.*Angle between planes passing through N8-C49-C50-N9 atoms of second clofaziminium cation and O3-C69-O4-C70 atoms of second diclofenac anion.

Structure	Packing coefficient	Angle between N4-C9-C8-N3 and O1-C28-O2-C29 planes (°)
CFZNH$^+$-DCF$^-$-MeOH (1:1:0.74)	0.661	83.0
CFZNH$^+$-DCF$^-$-EtOH (1:1:1)	0.658	73.3
CFZNH$^+$-DCF$^-$-EtOH (1:1:1) (100 K)	0.675	72.2
CFZNH$^+$-DCF$^-$-MeCN-H$_2$O (1:1:1:2) (100 K)	0.677	64.9
CFZNH$^+$-DCF$^-$-SAL-H$_2$O (4:4:9:1) (100 K)	0.700	74.5; 83.2*
CFZNH$^+$-DCF$^-$-PPP (2:2:5)	0.698	81.3
CFZNH$^+$-DCF$^-$-PPP (2:2:5) (100 K)	0.696	80.9
CFZNH$^+$-DCF$^-$ (1:1)	0.653	14.3
CFZNH$^+$-DCF$^-$-DCF (1:1:1) (polymorph I)	0.642	66.8
CFZNH$^+$-DCF$^-$-DCF-MeCN (1:1:1:2)	0.665	63.4
CFZNH$^+$-DCF$^-$-DCF-EtOAc (1:1:1:1)	0.657	62.5
CFZNH$^+$-DCF$^-$-DCF (1:1:1) (polymorph II)	0.660	46.4

4.3.1.2 Impact of solvent on crystallization of 1:1 salts

Salts combining clofazimine with diclofenac are, as initially expected, prone to solvate formation as indicated by the majority of the structures described in this work. First determined structure (**CFZNH$^+$-DCF$^-$-MeOH (1:1:0.74)**) contains the toxic solvent MeOH, which is H-bonded to the diclofenac anion.

To avoid presence of toxic solvent, several options can be considered. The most evident ones, would be salt preparation without solvent (neat grinding) or with non-toxic/pharmaceutically accepted solvents (water, ethanol [40]) or desolvation of solvated salts. Grinding clofazimine with diclofenac in 1:1 molar ratio in absence of solvent as well as in presence of water (LAG H$_2$O) resulted in a physical mixture of clofazimine with diclofenac

(Figure B.3(h)), thus not yielding any reaction. Moreover, crystallization experiment in only water as solvent was unsuccessful because of the low aqueous solubility of clofazimine. Since water as a solvent turned out to be unsuccessful and complete desolvation of **CFZNH$^+$-DCF$^-$-MeOH (1:1:0.74)** is difficult to achieve before melting of the powder, another pharmaceutically accepted solvent, namely ethanol, was chosen. In this case, solvent crystallization experiment as well as liquid-assisted ball milling, led to the same solvated salt: **CFZNH$^+$-DCF$^-$-EtOH (1:1:1)**, in which, as expected, ethanol interacted with DCF$^-$ through H-bond.

To further investigate the parameters influencing the crystallization of (un)solvated salts, another protic solvent of higher molecular volume, salicylaldehyde (111 Å^3 [38]) was selected. Despite their high molecular volume, salicylaldehyde molecules are included in the structure of **CFZNH$^+$-DCF$^-$-SAL-H$_2$O (4:4:9:1)**. Interestingly more than one salicylaldehyde molecule as well as one water molecule have been accommodated in the structure probably to allow a good packing (this structure turned to have the best packing coefficient, Table 4.3). The existence of this solvate proves that the ability of solvent to interact with solute via weak interactions may be one of the factors explaining why even bulky solvents can still be trapped in the crystal.

High molecular volume did not hamper solvent insertion in the structure, at least for protic solvents that are able to interact with the solute through H-bond. We then focused on aprotic solvents. First, we selected acetonitrile (molecular volume of 46 Å^3 [38]). However crystals obtained in these conditions corresponded to **CFZNH$^+$-DCF$^-$-MeCN-H$_2$O (1:1:1:2)**, a solvated hydrated salt, unstable at room temperature. Three other aprotic solvents (N,N-dimethylformamide, 78 Å^3, ethylacetate, 91 Å^3 and propiophenone, 136 Å^3 [38]) with larger molecular volumes were then selected to perform crystallization experiments of CFZ and DCF in 1:1 molar ratio. A larger molecular volume could potentially hamper solvent inclusion in the structure. However, we still observed solvate formation: crystals obtained from DMF corresponded to the known clofazimine solvate **CFZ-DMF** (CSD refcode: CEKTER [41]); crystallization experiments performed in propiophenone led to a solvated salt, **CFZNH$^+$-DCF$^-$-PPP (2:2:5)**, despite the absence of H-bond donor on propiophenone. The formation of the propiophenone solvate highlights again the fact that the molecular volume is not the only parameter affecting solvate formation, and that the interactions between the solvent and the solute are of crucial importance as well. In this case, propiophenone interacts with clofaziminium through π-cation interaction. Crystals of **CFZNH$^+$-DCF$^-$ (1:1)** unsolvated salt could however be obtained in ethylacetate, an aprotic molecule with a smaller molecular volume than propiophenone. The absence of the aromatic ring in ethylacetate, in contrast to propiophenone, results in a smaller number of potential interactions that it can form with clofazimine and thus may explain why ethylacetate is not incorporated into the structure. This unsolvated salt does not correspond to the crystalline phase appearing upon desolvation of **CFZNH$^+$-DCF$^-$-MeOH (1:1:0.74)**, which could indicate the existence of another polymorph of **CFZNH$^+$-DCF$^-$ (1:1)**.

4.3.2   Investigation of CFZ-DCF 1:2 cocrystal of salts

The second part of this work is dedicated to studying whether diclofenac molecule can bind diclofenac anion instead of the solvent molecule via O-H$\cdots$O bond. We followed the same solvent selection criteria as in the first part and chose the solvents that would be less likely to be incorporated into the structure. The addition of a second diclofenac molecule in the system is expected to generate other types of crystal packings than those obtained for salts in a 1:1 molar ratio. Therefore, solvents leading to unsolvated form(s) in the case of 1:1 salts could potentially lead to solvated salts in a 1:2 molar ratio and *vice versa*. The solvents selected for this second part of the study were therefore restricted to low-boiling aprotic (EtOAc and MeCN) and non-toxic protic (EtOH) solvents. Indeed, MeCN and EtOAc could potentially be included in the system if they allow a more efficient packing, however these two solvents should not normally interact with the solute (CFZNH$^+$, DCF$^-$ and DCF) through H-bond or stacking. These solvents should therefore not be strongly bound within the crystal structure and, due to their low boiling point, may easily evaporate from the solvated structure if the latter is formed. When a diclofenac molecule is available in the solution, it should compete with protic solvents for the diclofenac anion binding site, potentially leading to 1:2 CFZ-DCF forms. However, inclusion of a protic solvent could still be possible (if its shape and size can be accommodated in the crystal packing) because DCF molecule also possesses H-bond acceptor. Although, the potential O-H$\cdots$O interaction between DCF molecule and the solvent would be expected to be less strong with diclofenac molecule than with the anion.

4.3.2.1   Structural analysis

CFZNH$^+$-DCF$^-$-DCF (1:1:1) cocrystal of salt (polymorph I)   crystallizes in $P\bar{1}$ space group (Tables 4.1 and B.1). The asymmetric unit comprises one clofaziminium cation, one diclofenac anion and one diclofenac molecule. Clofaziminium interacts with diclofenac anion through charge-assisted H-bond ($R_2^2(9)$ motif, N4$-$H4$\cdots$O1 and N3$-$H3$\cdots$O2, Table B.2, Figure 4.9 (a)). Intramolecular H-bonds are observed within diclofenac anion and molecule (N5$-$H5$\cdots$O1 and N6$-$H6$\cdots$O4, Table B.2, Figure 4.9 (a)). Diclofenac anion and molecule interact together through O3$-$H3O$\cdots$O2 H-bond (Table B.2). This interaction is very similar to the one between diclofenac anion and ethanol in **CFZNH$^+$-DCF$^-$-EtOH (1:1:1)**. Indeed, even if these two structures are not isostructural, when clofaziminium and diclofenac anion are overlaid it can be observed that EtOH has a conformation similar to the first atoms (H3O, O3, C42 and C43) of diclofenac molecule (Figure 4.9 (d)).

All previously described interactions stabilize CFZNH$^+$-DCF$^-$-DCF assemblies. Two types of dimers of these assemblies, which are respectively stabilized by C31$-$H31$\cdots$O3 and C3$-$H3A $\cdots$O3 weak H-bonds (Table B.2, Figure 4.9 (b) and (c)), are also observed in the structure of **CFZNH$^+$-DCF$^-$-DCF (1:1:1)** cocrystal of salt. π-π stacking interactions are also observed between clofaziminium cations. The first one occurs between the phenazine core of two CFZNH$^+$, with a centroid-centroid distance of 3.669(1) Å, an
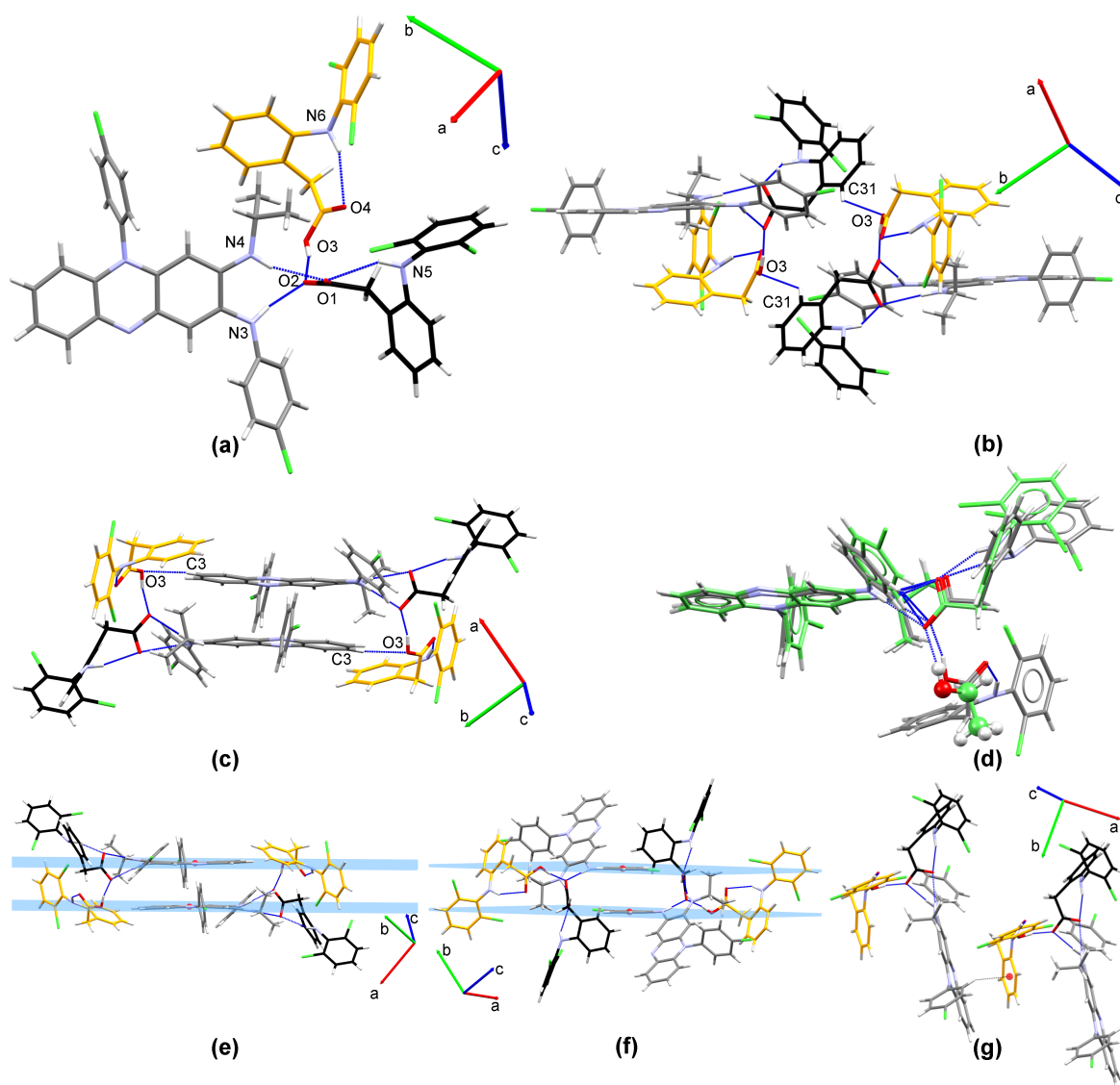
FIGURE 4.9: H-bonds between clofaziminium, diclofenac anion and diclofenac molecule in **CFZNH$^+$-DCF$^-$-DCF (1:1:1)** polymorph I (a), dimers of CFZNH$^+$-DCF$^-$-DCF assemblies stabilized through C31−H31···O3 (b) and through C3−H3A···O3 (c). Interaction between DCF molecule and DCF anion in **CFZNH$^+$-DCF$^-$-DCF (1:1:1)** polymorph I (grey) is similar to the one between DCF anion and EtOH in **CFZNH$^+$-DCF$^-$-EtOH (1:1:1)** (green) (d). π-π stacking between clofaziminium cations (e) and (f) and C−H···π interaction between CFZNH$^+$ and DCF molecule (g). Carbon atoms of diclofenac anion are in black while those of diclofenac molecule are in orange. H-bonds are represented by blue dashed lines.

orthogonal projection distance of 3.413(1) Å and an horizontal offset of 1.345 Å (planes and centroid calculated using C5 C6 C11 and C12 atoms, Figure 4.9 (e)). This stacking is further stabilized by C3−H3A···O3 (Figure 4.9 (c)) weak H-bonds. A second π-π stacking interaction is also observed between two C19 C20 C21 C22 C23 C24 aromatic rings of clofaziminium with a centroid-centroid distance of 3.801(1) Å, an orthogonal projection distance of 3.357(1) Å and an horizontal offset of 1.781 Å (Figure 4.9 (f)).

Finally a C−H⋯π interaction is observed between C18−H18 of clofaziminium and diclofenac molecule (C44 C45 C46 C47 C48 C49) with a H⋯centroid distance of 2.59 Å, a C⋯centroid distance of 3.443(3) Å and a C−H⋯centroid angle of 153° (Figure 4.9 (g)).

The powder pattern calculated from SCXRD data corresponds to the one of the batch powder prepared by LAG EtOH (Figure B.3(d)). This cocrystal of salt melts at 171 °C (Figure B.4 and Table 4.2).

CFZNH$^+$-DCF$^-$-DCF-MeCN (1:1:1:2) solvated cocrystal of salt also crystallizes in space group $P\bar{1}$ (Tables 4.1 and B.1). The asymmetric unit contains one clofaziminium cation, one diclofenac anion, one diclofenac molecule and two acetonitrile molecules (one MeCN molecule is disordered). Clofaziminium and diclofenac anion interact through charge-assisted H-bonds ($R_2^1(7)$ motif, N4−H4⋯O1 and N3−H3⋯O1, Table B.2, Figure 4.10 (a)). In both diclofenac (anion and molecule) an intramolecular H-bond is observed (N5−H5⋯O2 and N6−H6⋯O4, Table B.2). Molecular diclofenac and diclofenac anion interact through O3−H3B⋯O2 H-bond (Table B.2, Figure 4.10 (a)). Such H-bonds (N4−H4⋯O1, N3−H3⋯ O1 and O3−H3B⋯O2) stabilize CFZNH$^+$-DCF$^-$-DCF assemblies, which further form dimers through C38−H38⋯O4 (Figure 4.10 (b)). A weak H-bond, stabilizing chains along *a*-axis, is also observed between diclofenac molecules (C43−H43A⋯O3, Figure 4.10 (c) and (d)). This crystalline phase can also be obtained from liquid-assisted grinding of CFZ and DCF in 1:2 molar ratio and with MeCN as solvent (LAG) (Figure B.3(e)).

 TG/DSC analysis of **CFZNH$^+$-DCF$^-$-DCF-MeCN (1:1:1:2)** (powder obtained by liquid-assisted grinding experiment) reveals a 6.2% weight loss between 50 and 140 °C on the TG curve (Figure B.4) which is associated with an endothermic event on the DSC curve (onset: 93 °C) (Figure B.4 and Table 4.2). These events can be attributed to desolvation (calculated MeCN content of 7.2% in **CFZNH$^+$-DCF$^-$-DCF-MeCN (1:1:1:2)**). The endothermic event observed at 157 °C corresponds to the melting of the desolvated phase and suggests the formation of either an eutectic mixture or of an unsolvated crystalline phase combining CFZ and DCF (Figure B.4 and Table 4.2). A variable-temperature powder X-ray diffraction (VT-PXRD) experiment performed on **CFZNH$^+$-DCF$^-$-DCF-MeCN (1:1:1:2)** confirmed the formation of a new crystalline phase upon heating which does not correspond to **CFZNH$^+$-DCF$^-$-DCF (1:1:1)** polymorph I (Figure B.6). Results from VT-PXRD experiment and TG/DSC analyses suggest the formation of a second polymorph of **CFZNH$^+$-DCF$^-$-DCF (1:1:1)**.

CFZNH$^+$-DCF$^-$-DCF-EtOAc (1:1:1:1) solvated cocrystal of salt crystallizes in $P\bar{1}$ space group (Tables 4.1 and B.1). The asymmetric unit contains one clofaziminium cation, one diclofenac anion, one diclofenac molecule and one ethylacetate molecule. **CFZNH$^+$-DCF$^-$-DCF-EtOAc (1:1:1:1)** is isostructural to **CFZNH$^+$-DCF$^-$-DCF-MeCN (1:1:1:2)** and the same interactions are observed in both structures (Figure 4.10(e) and (f)). **CFZNH$^+$-DCF$^-$-DCF-EtOAc (1:1:1:1)** is prepared by ball-milling CFZ and DCF in 1:2 molar ratio in presence of few drops of EtOAc (Figure B.3(f)).

FIGURE 4.10: (a) H-bonds between clofaziminium, diclofenac anion and diclofenac molecule in **CFZNH$^+$-DCF$^-$-DCF-MeCN (1:1:1:2)**, (b) dimers of CFZNH$^+$-DCF$^-$-DCF assemblies (c) diclofenac molecules interact through C43−H43A···O3 H-bond and (d) C43−H43A···O3 H-bond between diclofenac molecules stabilizes chains along *a*-axis, (e) H-bonds between clofaziminium, diclofenac anion and diclofenac molecule in **CFZNH$^+$-DCF$^-$-DCF-EtOAc (1:1:1:1)**, (f)**CFZNH$^+$-DCF$^-$-DCF-EtOAc (1:1:1:1)** and **CFZNH$^+$-DCF$^-$-DCF-MeCN (1:1:1:2)** are isostructural (carbon atoms of **CFZNH$^+$-DCF$^-$-DCF-MeCN (1:1:1:2)** are in green). Carbon atoms of diclofenac anion are in black while those of diclofenac molecule are in orange (except in part (f)). Solvent is in ball and stick model (in space-fill model in part (f)). H-Bonds are represented by blue dashed lines.

TG/DSC analysis of the CFZ-DCF 1:2 LAG EtOAc powder reveals a 5.6% weight loss between 50 and 140 °C, associated to an endothermic event on the DSC curve (onset: 73 °C), indicating desolvation of **CFZNH$^+$-DCF$^-$-DCF-EtOAc (1:1:1:1)** (expected solvent content from SCXRD data: 7.6%). The single endothermic event observed at

157 °C corresponds to the melting of the desolvated phase (Figure B.4 and Table 4.2). A PXRD experiment performed on heated powder (130 °C) of **CFZNH$^+$-DCF$^-$-DCF-EtOAc (1:1:1:1)** confirmed the formation of a new crystalline phase, identical to the one obtained by heating **CFZNH$^+$-DCF$^-$-DCF-MeCN (1:1:1:2)** (Figure B.3(g)).

CFZNH$^+$-DCF$^-$-DCF (1:1:1) cocrystal of salt (polymorph II) crystallizes in triclinic $P\bar{1}$ space group (Tables 4.1 and B.1). Single-crystals of this unsolvated cocrystal of salt were obtained by recrystallization of CFZ-DCF 1:2 powder (physical mixture) in PEO 200. Charge-assisted H-bonds ($R_2^1(7)$, N3−H3$\cdots$O1 and N4−H4$\cdots$O1, Table B.2) are observed between clofaziminium and diclofenac anion. The second oxygen atom of DCF$^-$ is involved in a $D_1^1(2)$ H-bond with diclofenac molecule (O3−H3O$\cdots$O2, Table B.2). These H-bonds ($R_2^1(7)$ and $D_1^1(2)$) stabilize CFZNH$^+$-DCF$^-$-DCF assemblies (Figure 4.11 (a)). Weak H-bonds between CFZNH$^+$ and DCF molecule (C4−H4$\cdots$O3, Table B.2) stabilize dimers of CFZNH$^+$-DCF$^-$-DCF assemblies (Figure 4.11 (b)). A second type of such dimers is stabilized by a weak H-bond between DCF$^-$ and DCF molecule (C38−H38$\cdots$O4, Table B.2 and Figure 4.11 (c)). Intramolecular H-bonds in DCF$^-$ and DCF are also observed (N5−H5$\cdots$O2 and N6−H6$\cdots$O4, Table B.2 and Figure 4.11 (a)). In comparison with **CFZNH$^+$-DCF$^-$-DCF (1:1:1)** polymorph I, π-π stacking contribution to crystal packing stabilization is less important as there is no stacking between clofaziminium nor C−H$\cdots\pi$ interactions between clofaziminium and diclofenac molecule. There is however one π-π stacking interaction between two diclofenac anions with a centroid-centroid distance of 3.506(1) Å, an orthogonal projection distance of 3.355(1) Å and an horizontal offset of 1.017 Å (Figure 4.11(d), planes and centroids calculated with C36 C37 C38 C39 C40 and C41).

Despite a quite good overlay of the molecules constituting their asymmetric unit (Figure 4.11 (e)), **CFZNH$^+$-DCF$^-$-DCF-MeCN (1:1:1:2)** and **CFZNH$^+$-DCF$^-$-DCF (1:1:1)** are not isostructural as revealed by the crystal packing comparison performed with *Mercury* (only 9 molecules over 15 overlay despite distance and angle tolerance of 30% and 30°). Diclofenac anion orientation is slightly modified in the unsolvated cocrystal of salt in comparison to the one observed in **CFZNH$^+$-DCF$^-$-DCF-MeCN (1:1:1:2)**. Indeed, the angle between the planes passing through N4-C9-C8-N3 atoms of CFZNH$^+$ and through O1-C28-O2-C29 of DCF$^-$ is different in the two structures (63.44° in **CFZNH$^+$-DCF$^-$-DCF-MeCN (1:1:1:2)** *vs.* 46.41° in **CFZNH$^+$-DCF$^-$-DCF (1:1:1)**).

VT-PXRD and PXRD data measured after heating **CFZNH$^+$-DCF$^-$-DCF-MeCN (1:1:1:2)** and **CFZNH$^+$-DCF$^-$-DCF-EtOAc (1:1:1:1)** indicate a phase transformation from the solvated cocrystal of salts to the **CFZNH$^+$-DCF$^-$-DCF (1:1:1)** unsolvated cocrystal of salt (polymorph II) (Figures B.3(g) and B.6). TG/DSC data obtained from **CFZNH$^+$-DCF$^-$-DCF-MeCN (1:1:1:2)** indicate that **CFZNH$^+$-DCF$^-$-DCF (1:1:1)** polymorph II melts at 157 °C (Figure B.4 and Table 4.2). The difference in melting point observed between polymorph I (171 °C) and polymorph II (157 °C), can be partially explained by the fact that there are more π interactions in polymorph I while intermolecular H-bonds are of comparable strength in both polymorphs. It is interesting to notice that polymorph II has however a better packing (higher density) than polymorph
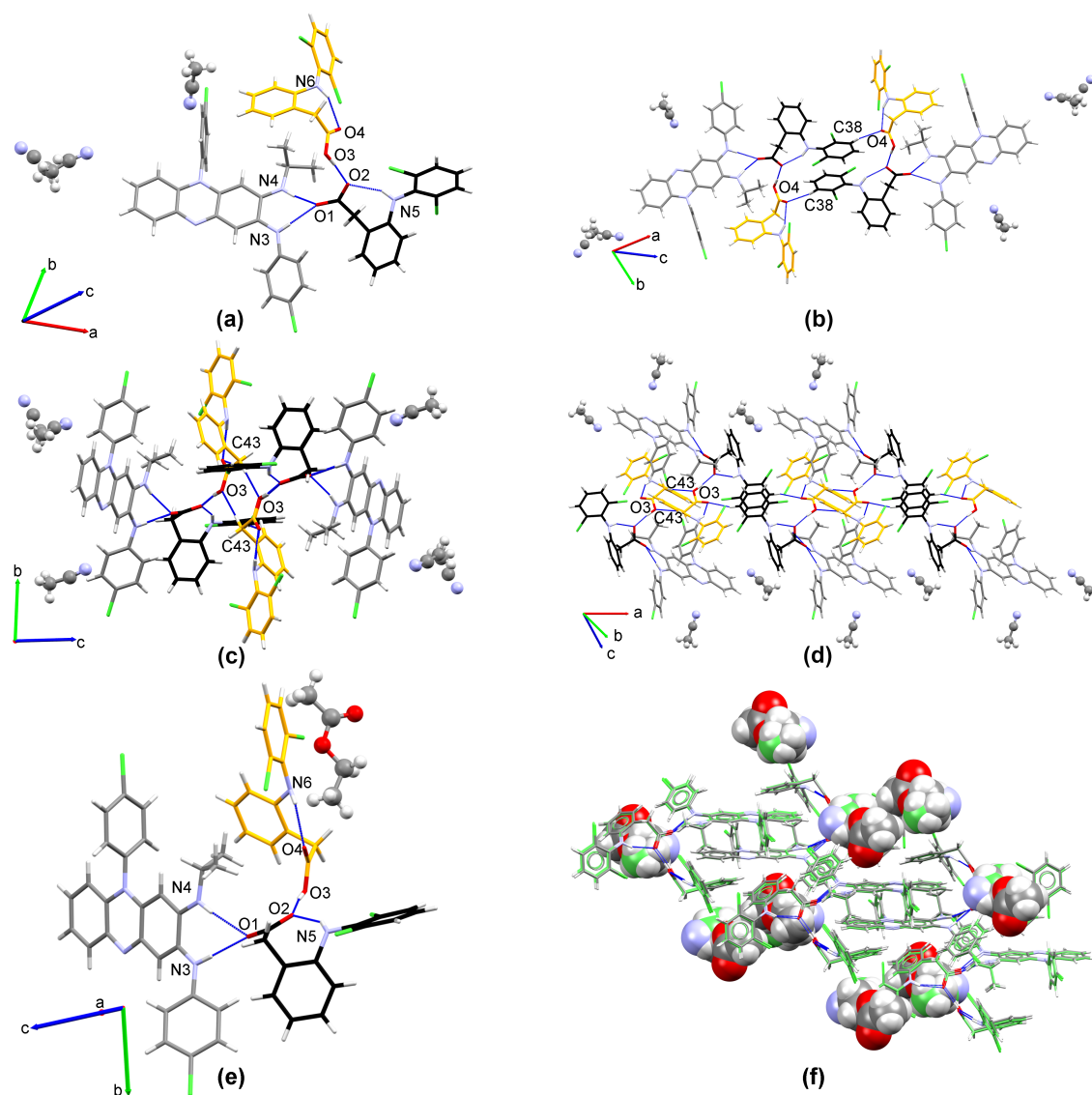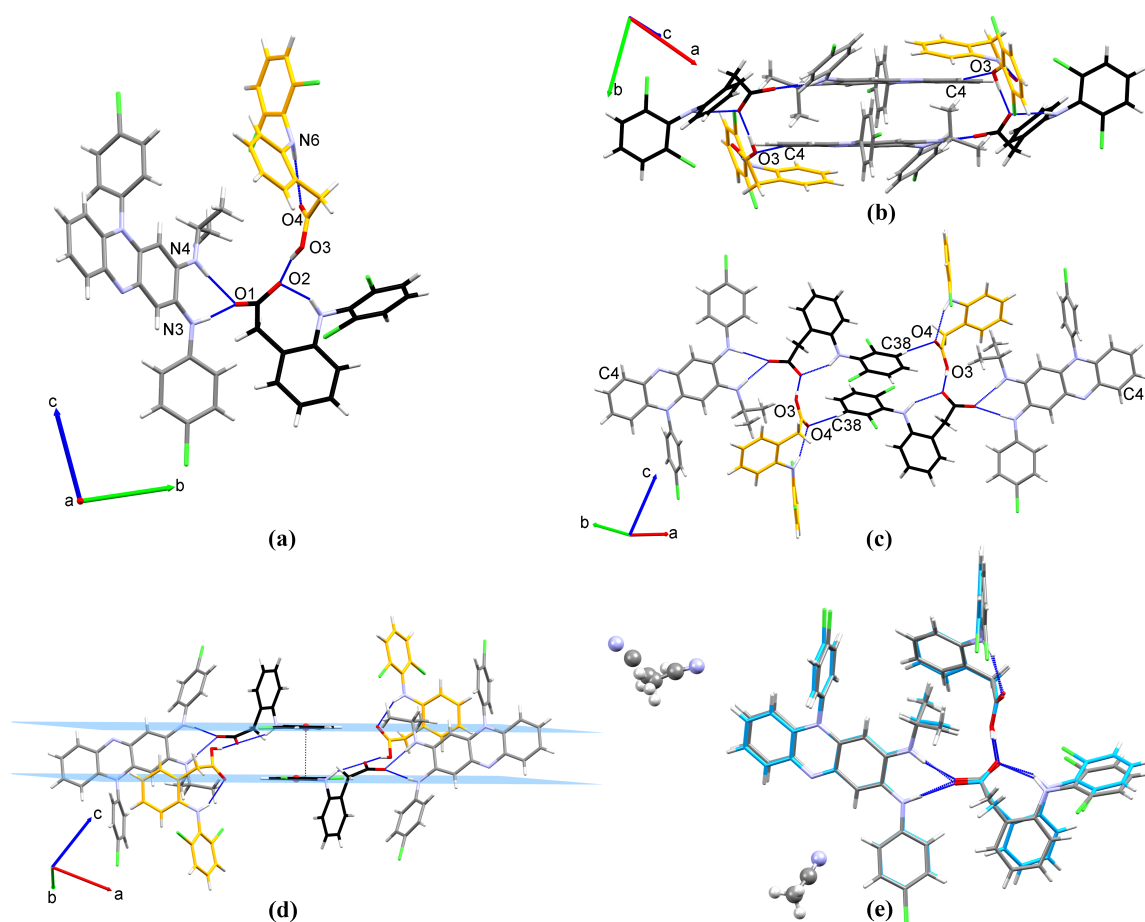
FIGURE 4.11: (a) H-bonds between clofaziminium, diclofenac anion and diclofenac molecule in **CFZNH$^+$-DCF$^-$-DCF (1:1:1)** (polymorph II), (b) clofaziminium and diclofenac molecule interact through C4−H4···O3, stabilizing a dimer of CFZNH$^+$-DCF$^-$-DCF assemblies (c) diclofenac anion and diclofenac molecule assemblies and (d) π-π stacking between two DCF$^-$ anions. (e) Asymmetric unit overlay of **CFZNH$^+$-DCF$^-$-DCF (1:1:1)** (carbon atoms in blue) and of **CFZNH$^+$-DCF$^-$-DCF-MeCN (1:1:1:2)** (carbons atoms in grey). Carbon atoms of diclofenac anion are in black while those of diclofenac molecule are in orange (except for part (e) of the Figure). H-bonds are represented by blue dashed lines.

I (packing coefficient of 0.660 *vs.* 0.642, density of 1.383 g.cm^{-3} *vs.* 1.351 g.cm^{-3} (data collected at 295 K for both structures)) (Table 4.3).

4.3.2.2 Impact of solvent on crystallization of 1:2 cocrystal of salts

Changing the clofazimine-diclofenac molecular ratio during crystallization experiment allowed the crystallization of a 1:2 unsolvated cocrystal of salt in EtOH, while this solvent previously led to a solvated 1:1 salt. This result indicates that diclofenac molecule can succesfully compete with the solvent for the interaction site with diclofenac anion. However, preparation of 1:2 cocrystal of salts did not completely rule out crystallization of solvated forms, as two solvated phases were obtained in acetonitrile and ethylacetate.

Interestingly, crystallization of a 1:2 cocrystal of salt in EtOAc leads to a solvated form while the same solvent previously lead to an unsolvated **CFZNH$^+$-DCF$^-$ (1:1)** salt. EtOAc and MeCN both have a small molecular volume that can be accommodated in the structure if packing allows. However, as expected no strong interactions exist between EtOAc or MeCN and the solutes (CFZNH$^+$, DCF$^-$ and DCF).

TG/DSC analysis of these two solvated cocrystal of salts (**CFZNH$^+$-DCF$^-$-DCF-MeCN (1:1:1:2)**, **CFZNH$^+$-DCF$^-$-DCF-EtOAc (1:1:1:1)**) revealed a weight loss between 50 and 100 °C and a melting point around 157 °C (Figure B.4). A phase transformation, probably associated with desolvation (and formation of an unsolvated cocrystal of salt combining CFZ and DCF), was identified by PXRD experiments (Figures B.6 and B.3(g)). The powder diffraction pattern obtained after desolvation of **CFZNH$^+$-DCF$^-$-DCF-MeCN (1:1:1:2)** or **CFZNH$^+$-DCF$^-$-DCF-EtOAc (1:1:1:1)** does not correspond to the one of **CFZNH$^+$-DCF$^-$-DCF (1:1:1)** (polymorph I) (Figures B.6 and B.3(g)), which could be the indication of the existence of a second polymorph of **CFZNH$^+$-DCF$^-$-DCF (1:1:1)**. To verify this hypothesis, we have tried to obtain single-crystals of this new unsolvated crystalline phase using other solvents that cannot be incorporated into the structure. We selected short chain polymers such as PEO (average MW: 200 g/mol and 400 g/mol) and polycaprolactone triol (average MW: 300 g/mol) as recrystallization solvents because of their higher molecular weight and also because of their molecular 'flexibility' in comparison to salicylaldehyde and propiophenone which previously led to solvated salts. Few single-crystals of **CFZNH$^+$-DCF$^-$-DCF (1:1:1)** (polymorph II) cocrystal of salt were obtained in PEO (average MW: 200 g/mol). Comparison of the calculated powder pattern of **CFZNH$^+$-DCF$^-$-DCF (1:1:1)** (polymorph II) with the one obtained after VT-PXRD experiment performed on **CFZNH$^+$-DCF$^-$-DCF-MeCN (1:1:1:2)** confirmed desolvation and phase transformation that were inferred from VT-PXRD and TG/DSC experiments.

4.4   Conclusions

Clofaziminium : diclofenac system is a great example of structural variety that can be reached when a clever solvent selection is applied to explore various crystalline forms. As expected, diclofenac anion is able to interact with protic solvent molecules through H-bonds, leading to the crystallization of solvated drug-drug salts of clofazimine and diclofenac. Protic and aprotic solvents of increasing molecular volumes were taken in order to understand how solvent impacts crystallization of clofazimine and diclofenac.

When facing probable solvate formation, the potential solute-solvent interactions can be more relevant than the size of the solvent. For example, the unsolvated **CFZNH$^+$-DCF$^-$ (1:1)** salt crystallized only in ethylacetate, an aprotic solvent having a lower molecular volume than another selected solvent, propiophenone. Despite its high molecular volume, propiophenone was incorporated into the structure owing to π interactions, resulting in the corresponding solvated salt. A particular feature of the **CFZNH$^+$-DCF$^-$ (1:1)** unsolvated structure is that the carboxylate of DCF$^-$ is almost coplanar to CFZNH$^+$. It is, to the best of our knowledge, the first time that this specific carboxylate orientation

is reported in a clofaziminium salt. These results highlight the importance of considering potential solute-solvent interactions not only in terms of H-bond interactions, but also other weak interactions such as probable π interactions.

Changing the clofazimine to diclofenac ratio from 1:1 to 1:2 allowed an extra diclofenac molecule to compete for the binding site with the protic solvent molecules. More particularly, diclofenac anion succesfully beated EtOH for the H-bond interaction on diclofenac anion resulting in an unsolvated cocrystal of salt (**CFZNH$^+$-DCF$^-$-DCF (1:1:1)** polymorph I) with the 1:2 clofazimine to diclofenac molar ratio. The second polymorph of **CFZNH$^+$-DCF$^-$-DCF (1:1:1)** emerged from desolvation of **CFZNH$^+$-DCF$^-$-DCF-MeCN (1:1:1:2)** and **CFZNH$^+$-DCF$^-$-DCF-EtOAc (1:1:1:1)**. The latter underlines that undesired solvated forms can potentially give access to other desired structures. Recrystallization using unconventional solvents such as short chain polymers exhibiting good fluidity, high molecular flexibility and high molecular weight can also be an option to avoid solvent inclusion into the structure, as illustrated by the successful growth of **CFZNH$^+$-DCF$^-$-DCF (1:1:1)** (polymorph II) in PEO 200.

Changing the drug:drug ratio in the structure expectedly affects the physico-chemical properties of the corresponding solid forms, for instance, the melting point of **CFZNH$^+$-DCF$^-$ (1:1)** is 186 °C whereas those of **CFZNH$^+$-DCF$^-$-DCF (1:1:1)** polymorphs I and II are 171 °C and 157 °C respectively.

Conflicts of interest

There are no conflicts to declare. The European Commission's support for the production of this publication does not constitute an endorsement of the contents, which reflect the views only of the authors, and the Commission cannot be held responsible for any use which may be made of the information contained therein.

Acknowledgements

Chapter 4

Bibliography

[1] U. J. Griesser. The importance of solvates. In R. Hilfiker, editor, *Polymorphism: in the Pharmaceutical Industry*, chapter 8, pages 211–233. Wiley Online Library, 2006.

[2] Ö. Almarsson and M. J. Zaworotko. Crystal engineering of the composition of pharmaceutical phases. do pharmaceutical co-crystals represent a new path to improved medicines? *Chemical communications*, (17):1889–1896, 2004.

[3] H. D. Clarke, K. K. Arora, H. Bass, P. Kavuru, T. T. Ong, T. Pujari, L. Wojtas, and M. J. Zaworotko. Structure- stability relationships in cocrystal hydrates: Does the promiscuity of water make crystalline hydrates the nemesis of crystal engineering? *Crystal growth & design*, 10(5):2152–2167, 2010.

[4] E. Grothe, H. Meekes, E. Vlieg, J. H. Ter Horst, and R. de Gelder. Solvates, salts, and cocrystals: a proposal for a feasible classification system. *Crystal Growth & Design*, 16(6):3237–3243, 2016.

[5] B. D. Johnson, A. Howard, R. Varsolona, J. McCauley, and D. K. Ellison. Indinavir sulfate. In *Analytical profiles of drug substances and excipients*, volume 26, pages 319–357. Elsevier, 1999.

[6] M. L. Peterson, M. B. Hickey, M. J. Zaworotko, and Ö. Almarsson. Expanding the scope of crystal form evaluation in pharmaceutical science. *J. Pharm. Pharm. Sci*, 9(3):317–326, 2006.

[7] C. Loschen and A. Klamt. Computational screening of drug solvates. *Pharmaceutical research*, 33(11):2794–2804, 2016.

[8] S. Boothroyd, A. Kerridge, A. Broo, D. Buttar, and J. Anwar. Why do some molecules form hydrates or solvates? *Crystal Growth & Design*, 18(3):1903–1908, 2018.

[9] A. Bērziņš, A. Kons, K. Saršūns, S. Belyakov, and A. Actiņš. On the rationalization of formation of solvates: Experimental and computational study of solid forms of several nitrobenzoic acid derivatives. *Crystal Growth & Design*, 20(9):5767–5784, 2020.

[10] K. Smokrović and V. Stilinović. Stoichiometry of adamantylamine–trinitrophloroglucinol salts controlled by solvate formation. *CrystEngComm*, 22(10):1822–1833, 2020.

[11] K. Takieddin, Y. Z. Khimyak, and L. Fabian. Prediction of hydrate and solvate formation using statistical models. *Crystal Growth & Design*, 16(1):70–81, 2016.

[12] M. C. Cholo, H. C. Steel, P. B. Fourie, W. A. Germishuizen, and R. Anderson. Clofazimine: Current status and future prospects. *Journal of Antimicrobial Chemotherapy*, 67(2):290–298, 2012.

[13] S. Tyagi, N. C. Ammerman, S.-Y. Li, J. Adamson, R. V. Converse, P. J.and Swanson, D. V. Almeida, and J. H. Grosset. Clofazimine shortens the duration of the first-line treatment regimen for experimental chemotherapy of tuberculosis. *Proceedings of the National Academy of Sciences*, 112(3):869–874, 2015.

[14] D. R. Silva, M. Dalcolmo, S. Tiberi, M. A. Arbex, M. Munoz-Torrico, R. Duarte, L. D'Ambrosio, D. Visca, A. Rendon, M. Gaga, et al. New and repurposed drugs to treat multidrug-and extensively drug-resistant tuberculosis. *Jornal Brasileiro de Pneumologia*, 44(2):153–160, 2018.

[15] S. Zhang, W. Shi, J. Feng, W. Zhang, and Y. Zhang. Varying effects of common tuberculosis drugs on enhancing clofazimine activity in vitro. *Emerging microbes & infections*, 6(4):e28, 2017.

[16] G. Sotgiu, S. Tiberi, R. Centis, L. D. Ambrosio, Z. Fuentes, A. Zumla, and G. Battista. International Journal of Infectious Diseases Applicability of the shorter ' Bangladesh regimen ' in high multidrug-resistant tuberculosis settings §. *International Journal of Infectious Diseases*, 56:190–193, 2017.

[17] C. Lange, D. Chesov, and J. Heyckendorf. Clofazimine for the treatment of multidrug-resistant tuberculosis. *Clinical Microbiology and Infection*, 25(2):128–130, 2019.

[18] N. K. Dutta, S. G. Dastidar, A. Kumar, K. Mazumdar, R. Ray, and A. N. Chakrabarty. Antimycobacterial activity of the antiinflammatory agent diclofenac sodium, and its synergism with streptomycin. *Brazilian Journal of Microbiology*, 35(4):316–323, 2004.

[19] K. Mazumdar, S. G. Dastidar, J. H. Park, and N. K. Dutta. The anti-inflammatory non-antibiotic helper compound diclofenac: an antibacterial drug target. *European journal of clinical microbiology & infectious diseases*, 28(8):881, 2009.

[20] A. Maitra, S. Bates, M. Shaik, D. Evangelopoulos, and I. Abubakar. Repurposing drugs for treatment of tuberculosis : a role for non-steroidal anti-in fl ammatory drugs. *British Medical Bulletin*, 118(May):145–155, 2016.

[21] V. M. Kroesen, M. I. Gröschel, N. Martinson, A. Zumla, M. Maeurer, T. van der Werf, and C. Vilaplana. Non-steroidal anti-inflammatory drugs as host-directed therapy for tuberculosis: a systematic review. *Frontiers in immunology*, 8:772, 2017.

[22] J. Ivanyi and A. Zumla. Nonsteroidal Antiin fl ammatory Drugs for Adjunctive Tuberculosis Treatment. *The Journal of Infectious Diseases*, 208(2):185–188, 2013.

[23] R. K. Keswani, J. Baik, L. Yeomans, C. Hitzman, A. M. Johnson, A. S. Pawate, P. J. A. Kenis, N. Rodriguez-Hornedo, K. A. Stringer, and G. R. Rosania. Chemical analysis of drug biocrystals: a role for counterion transport pathways in intracellular drug disposition. *Molecular pharmaceutics*, 12(7):2528–2536, 2015.

[24] G. Bolla and A. Nangia. Clofazimine mesylate: a high solubility stable salt. *Crystal growth & design*, 12(12):6250–6259, 2012.

[25] P. Bannigan, E. Durack, C. Madden, M. Lusi, and S. P. Hudson. Role of biorelevant dissolution media in the selection of optimal salt forms of oral drugs: maximizing the gastrointestinal solubility and in vitro activity of the antimicrobial molecule, clofazimine. *ACS omega*, 2(12):8969–8981, 2017.

[26] L. Bodart, N. Tumanov, and J. Wouters. Structural variety of clofaziminium salts: effect of the counter-ion on clofaziminium conformation and crystal packing. *Acta Crystallographica Section B: Structural Science, Crystal Engineering and Materials*, 75(4):674–686, 2019.

[27] M. L. Sousa, M. C. Sarraguça, A. O. dos Santos, J. M. G. Sarraguça, J. Lopes, and P. R. da Silva Ribeiro. A new salt of clofazimine to improve leprosy treatment. *Journal of Molecular Structure*, 1214:128226, 2020.

[28] L. Bodart, A. Derlet, X. Buol, T. Leyssens, N. Tumanov, and J. Wouters. Combining two antitubercular drugs, clofazimine and 4-aminosalicylic acid, in order to improve clofazimine aqueous solubility and 4-aminosalicylic acid thermal stability. *Journal of Pharmaceutical Sciences*, 109:3645–3652, 2020.

[29] W. Sun, L. Zuo, T. Zhao, Z. Zhu, and G. Shan. Five solvates of a multicomponent pharmaceutical salt formed by berberine and diclofenac. *Acta Crystallographica Section C: Structural Chemistry*, 75(12):1644–1651, 2019.

[30] R. C. Clark and J. S. Reid. The Analytical Calculation of Absorption in Multifaceted Crystals. *Acta Crystallographica A*, 51:887–897, 1995.

[31] Rigaku Oxford Diffraction. CrysAlis PRO. *CrysAlis PRO*, pages Rigaku Oxford Diffraction Ltd, Yarnton, England, 2019.

[32] R. H. Blessing. An Empirical Correction for Absorption Anisotropy. *Acta Crystallographica A*, 51:33–38, 1995.

[33] G. M. Sheldrick. SHELXT - Integrated space-group and crystal-structure determination. *Acta Crystallographica A*, 71(1):3–8, 2015.

[34] O. V. Dolomanov, L. J. Bourhis, R. J. Gildea, J. A. K. Howard, and H. Puschmann. OLEX2: A complete structure solution, refinement and analysis program. *Journal of Applied Crystallography*, 42(2):339–341, 2009.

[35] C. B. Hübschle, G. M. Sheldrick, and B. Dittrich. ShelXle : a Qt graphical user interface for SHELXL. *Journal of Applied Crystallography*, 44:1281–1284, 2011.

[36] G. M. Sheldrick. Crystal structure refinement with SHELXL. *Acta Crystallographica C*, 71:3–8, 2015.

[37] C. F. Macrae, I. Sovago, S. J. Cottrell, P. T. A. Galek, P. McCabe, E. Pidcock, M. Platings, G. P. Shields, J. S. Stevens, M. Towler, et al. Mercury 4.0: from visualization to analysis, design and prediction. *Journal of Applied Crystallography*, 53:226–235, 2020.

[38] M. Cheminformatics. Molinspiration [internet], accessed on 21-02-2020.

[39] G. R. Desiraju and T. Steiner. *The weak hydrogen bond: in structural chemistry and biology*, volume 9. International Union of Crystal, 2001.

[40] European Medicinal Agency (EMA). *Information for the package leaflet regarding ethanol used as an excipient in medicinal products for human use*. European Medicinal Agency (EMA), 2019.

[41] D. S. Eggleston, W. E. Marsh, and D. J. Hodgson. Structures of the antileprosy phenazine derivatives clofazimine-N, N-dimethylformamide, C27H22Cl2N4. C3H7NO, and B1912, C30H27ClN4. *Acta Crystallographica Section C: Crystal Structure Communications*, 40(2):288–292, 1984.

4.5 Additional data on CFZNH$^+$-DCF$^-$ salts: aqueous solubility evaluation

4.5.1 HPLC method for solubility evaluation

Solubility of CFZ, DCF, **CFZNH$^+$-DCF$^-$-EtOH (1:1:1)**, **CFZNH$^+$-DCF$^-$ (1:1)** salts and **CFZNH$^+$-DCF$^-$-DCF (1:1:1)** cocrystal of salt polymorphs I and II was evaluated in type I water, at 25 °C (Heidolf incubator 1000) and under agitation at 900 rpm (Heidolf titramax 1000 platform shaker), by wetting an excess amount of powder (15 - 20 mg) in 2.0 mL type I water. Experiments were performed in triplicate. After 20 hours, the samples were centrifuged at 13000 rpm (eppendorf centrifuge 5430R, equipped with a FA-45-24-11 rotor) for 15 minutes, the supernatant was recovered and centrifuged again (15 minutes, 13000 rpm). After second centrifugation, the supernatant was diluted twice with MeCN. Solubility was evaluated by a high-performance liquid chromatography (HPLC) method performed with a Zorbax SB C18 (3.5 μm, 3 x 100 mm) column heated to 40 °C and connected on an Agilent 1100 series HPLC system using UV detection at 280 and 490 nm. Gradient elution was performed with mobile phase A (trifluoroacetic acid 0.1%) and mobile phase B (MeCN) at a flow rate of 0.5 mL/min. Gradient started at 50% B for 4 minutes and then ramped up to 80% B in 0.5 minute. This solvent ratio was maintained for 2.5 minutes before returning to 50% B for 6 minutes to re-equilibrate the column. The injection volume was 5 μL. Calibration was performed with samples prepared in MeCN/water 1:1 (in volume) with concentrations ranging from 9 to 0.07 μg/mL for CFZ and from 45 to 0.7 μg/mL for DCF. pH of the salt solutions was measured after first centrifugation and, in all cases, it was comprised between 5.1 and 5.8.

4.5.1.1 Results of aqueous solubility evaluation

Unexpected elution peaks, possibly indicating degradation, were observed at 1.7 min for samples of **CFZNH$^+$-DCF$^-$-DCF (1:1:1)** cocrystal of salt (polymorph I and II) (Fig. 4.12) and their solubility was thus not determined. Aqueous solubility could however be determined for **CFZNH$^+$-DCF$^-$-EtOH (1:1:1)** and **CFZNH$^+$-DCF$^-$ (1:1)** salt.

The solubilized amount of CFZ and DCF from the pure APIs and from the solvated and non solvated salts are presented in Table 4.4. An 11-fold CFZ solubility improvement is thus observed for the solvated salt, but no improvement is observed for **CFZNH$^+$-DCF$^-$ (1:1)** salt. The increased amount of solubilized clofazimine (CFZ) could be attributed to the presence of EtOH, which could protentially diffuse in water, helping CFZ solubilization. Solubility improvement that is observed for the solvated salt remains however small and could only be detected by an HPLC method.
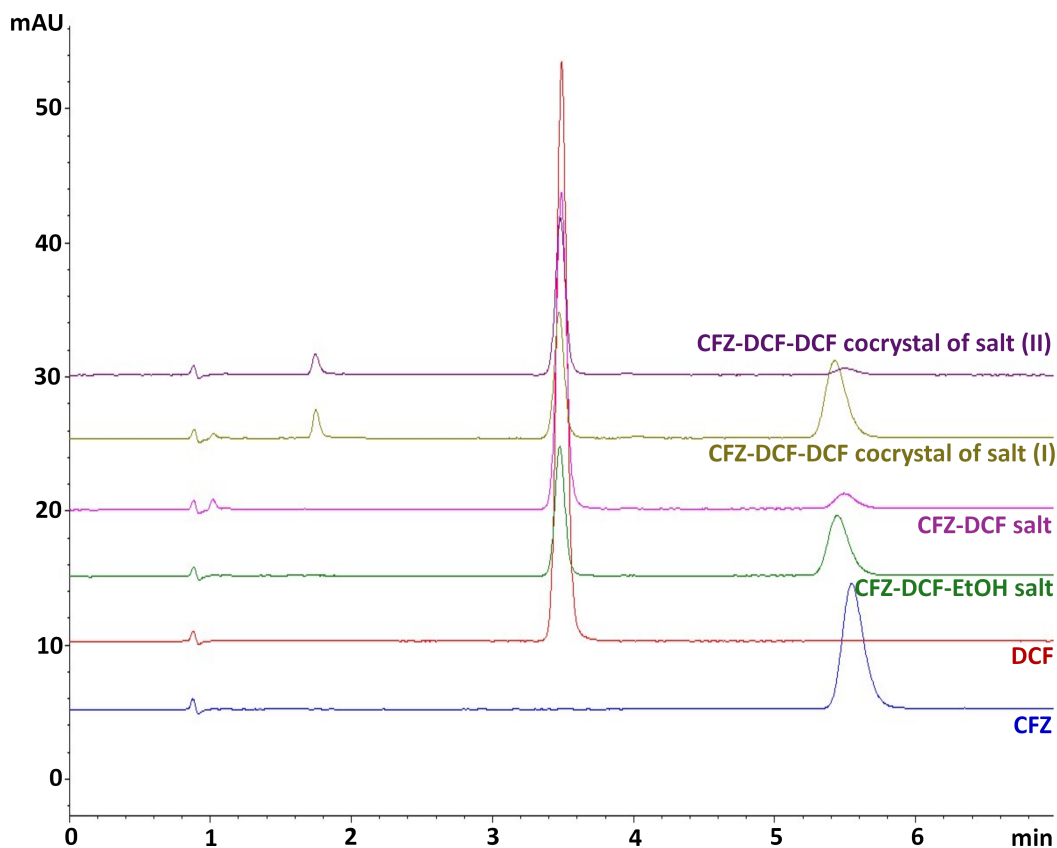
FIGURE 4.12: Typical HPLC chromatograms of, from bottom to top, CFZ (from calibration curve), DCF (from calibration curve), **CFZNH$^+$-DCF$^-$-EtOH (1:1:1)**, **CFZNH$^+$-DCF$^-$ (1:1)**, **CFZNH$^+$-DCF$^-$-DCF (1:1:1)** polymorphs I and II.

TABLE 4.4: Amount of CFZ and DCF released after 20h in water from CFZ, DCF, **CFZNH$^+$-DCF$^-$ (1:1)** and **CFZNH$^+$-DCF$^-$-EtOH (1:1:1)**.

Salt or API	Solubilized CFZ (µg/mL)	Solubilized DCF (µg/mL)
CFZ	0.20 ± 0.03	
DCF		8.05 ± 0.02
CFZNH$^+$-DCF$^-$-EtOH (1:1:1)	2.23 ± 0.30	5.60 ± 0.52
CFZNH$^+$-DCF$^-$ (1:1)	0.32 ± 0.16	11.59 ± 0.78

PXRD data collected after solubility evaluation do not indicate any phase change (Fig. 4.13) and the identification of the nature of the unexpected peak observed on HPLC chromatograms for **CFZNH$^+$-DCF$^-$-DCF (1:1:1)** cocrystal of salt (polymorph I and II) is thus not possible. This could indicate that the product eluting at 1.7 min is either in small quantity, higly soluble in water or amorphous.
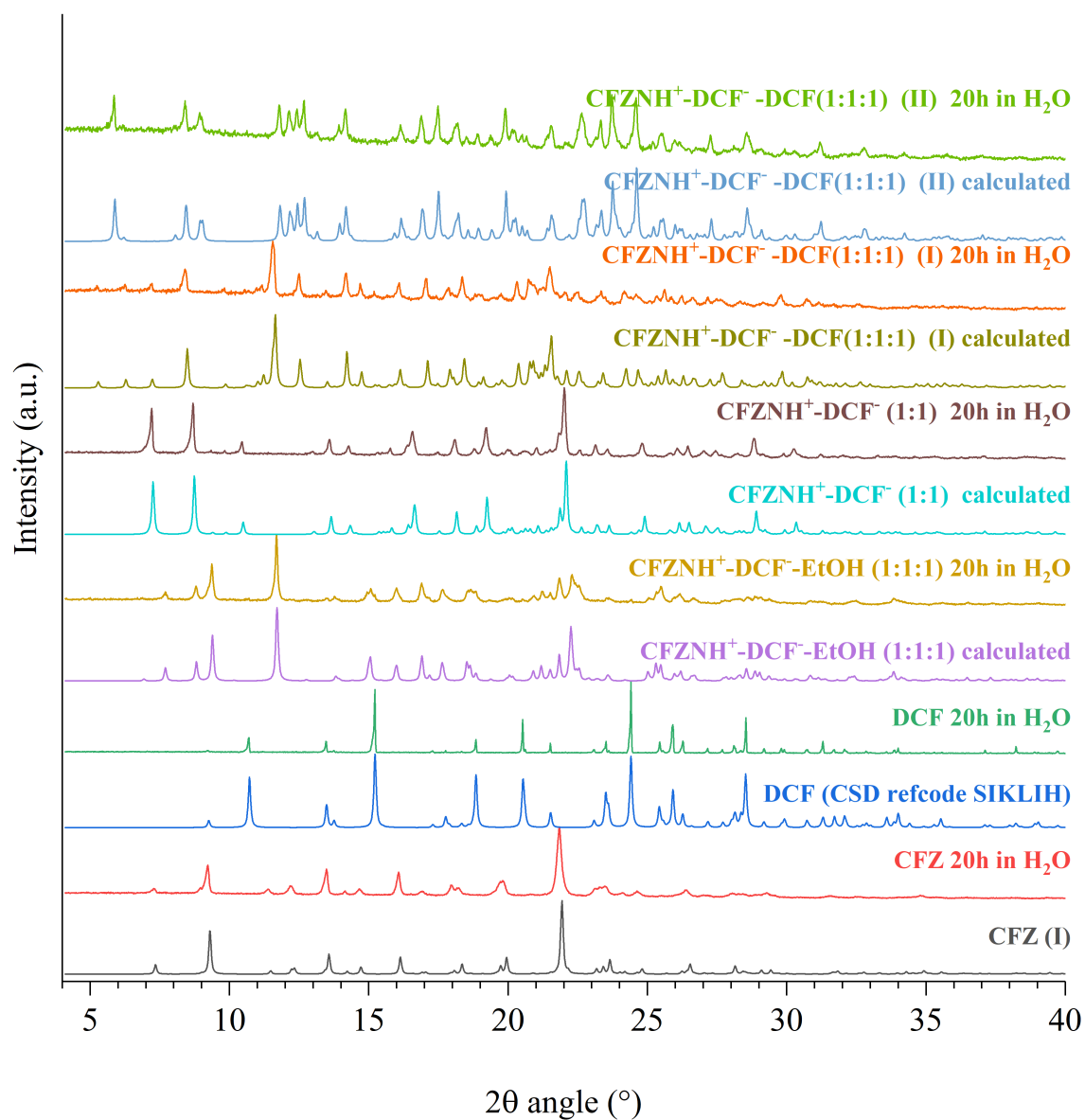
FIGURE 4.13: PXRD patterns of CFZ, DCF, **CFZNH$^+$-DCF$^-$-EtOH (1:1:1)**, **CFZNH$^+$-DCF$^-$ (1:1)**, and **CFZNH$^+$-DCF$^-$-DCF (1:1:1)** cocrystal of salt (polymorph I and II) before and after dispersion in water.

Chapter 5

Combining two antitubercular drugs, clofazimine and 4-aminosalicylic acid, in order to improve clofazimine aqueous solubility and 4-aminosalicylic acid thermal stability†

Combining two antitubercular drugs, clofazimine and 4-aminosalicylic acid, in order to improve clofazimine aqueous solubility and 4-aminosalicylic acid thermal stability

Laurie Bodart[*,a], Amelie Derlet[a], Xavier Buol[b], Tom Leyssens[b], Nikolay Tumanov[a] and Johan Wouters[*,a]

[a]Namur Medicine and Drug Innovation Center - Namur Research Institute for Life Science (NAMEDIC-NARILIS), Namur Institute of Structured Matter (NISM), Department of Chemistry, University of Namur (UNamur), 61 Rue de Bruxelles, 5000 Namur, Belgium.
[b]Institute of Condensed Matter and Nanosciences, UCLouvain, 1 Place Louis Pasteur, B-1348 Louvain-la-Neuve, Belgium.
[*]Correspondence to: Bodart Laurie (Telephone: +32 (0)81724569) and Johan Wouters (Telephone: +32 (0)81724550).
email addresses: laurie.bodart@unamur.be, johan.wouters@unamur.be.

Abstract. Four forms of a salt combining two antitubercular drugs, clofazimine and 4-aminosalicylic acid, are reported and the crystal structure of two of these forms are described. TG/DSC analysis of all four forms demonstrate an increase in the temperature at which degradation (upon decarboxylation) occurs in comparison to pure 4-aminosalicylic acid. Water solubility evaluation indicates a significant increase of the amount of clofazimine detected in water (10.26 ± 0.52 µg/mL for form I, 12.27 ± 0.32 µg/mL for form II, 7.15 ± 0.43 µg/mL for form III and 8.50 ± 1.24 µg/mL for form IV) in comparison to pure clofazimine (0.20 ± 0.03 µg/mL).

5.1 Introduction

Tuberculosis (TB) is an infectious disease caused by *Mycobacterium tuberculosis* (*M. tb*) which is still among the top causes of death worldwide [1]. Even if drug susceptible tuberculosis is curable with a two months treatment comprising four first-line antibiotics (rifampicin, isoniazid, pyrazinamide and ethambutol) followed by four months continuation phase with isoniazid and rifampicin [2], multidrug resistant tuberculosis (MDR-TB) and extensively drug resistant tuberculosis (XDR-TB) strains of *M. tb* have emerged because of bad compliance or inappropriate use of antitubercular drugs.

In this context, N,5-bis(4-chlorophenyl)-3-propan-2-yliminophenazin-2-amine (clofazimine (CFZ) Fig. 5.1(a)), an antimicrobial and anti-inflammatory agent has been selected to be part of the shortened Bangladesh regimen against multidrug resistant tuberculosis (MDR-TB) [3, 4]. Clofazimine is also recommended by the World Health Organization (WHO) as a group B agent for the treatment of MDR-TB and XDR-TB [5]. Belonging to the biopharmaceutics Classification System (BCS) class II, clofazimine bioavailability is however limited by its low aqueous solubility (<0.001 mg/mL [6, 7]). Several strategies have been adopted to improve clofazimine solubility e.g. the preparation of inclusion complexes with cyclodextrins or cucurbit[7]uril [8, 9, 10], of nanoparticules or nanosuspensions [11, 12], of amorphous solid dispersion [13] or co-administration with lipid vehicles [14]). Another alternative is to take advantage of the basicity of CFZ to prepare salts [15, 16, 17, 18].
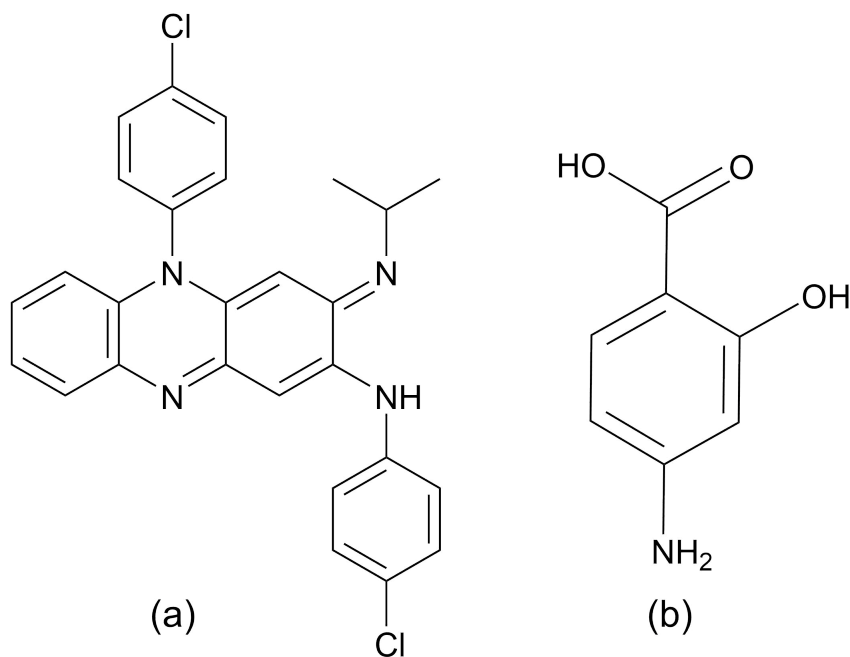
FIGURE 5.1: Molecular diagram of (a) clofazimine (CFZ) and (b) 4-aminosalicylic acid (PAS).

According to the WHO, 4-amino-2-hydroxybenzoic acid (4-aminosalicylic acid (PAS), Fig. 5.1(b)) is classified as a group C drug for the treatment of multidrug resistant tuberculosis [5]. This compound is a prodrug mimicking 4-aminobenzoic acid, the substrate of dihydropteroate synthase [19]. PAS is a BCS class III [20] compound with a reported aqueous solubility of 3.216 g/L at 30 °C [6]. It is however known to be unstable at low pH as it can decarboxylate to 3-aminophenol [21] through the formation of the PAS zwitterion (isoelectric point of 2.71) [21]. In the solid-state, the crystalline powder can also decompose under exposition to moisture or heat [22, 23]. The sodium and calcium salts of PAS are however reported to be more stable than the free acid [24]. Moreover PAS salts have also been reported to reduce the gastro-intestinal (GI) side effects associated to PAS [25, 26]. More recently, gastro-resistant caps avoiding PAS exposition to the gastric acidic medium and aiming at further diminishing these GI effects have been commercialized [26].

The association of CFZ and PAS is reported for the treatment of XDR-TB [27, 28]. Zhang et al. [29] have further shown that PAS enhanced CFZ activity in vitro and Lu et al. [30] have even shown a synergistic effect between both drugs. Similarly, an alternative formulation consisting of salts combining CFZ with PAS could potentially improve CFZ solubility and PAS stability. The present study reports on the preparation of $CFZNH^+$-PAS^- salts that were characterized in terms of thermal stability and aqueous solubility.

5.2 Materials and methods

5.2.1 Materials

Clofazimine and 4-aminosalicylic acid were purchased from TCI Europe and Sigma Aldrich respectively. Acetonitrile (MeCN), ethanol (EtOH) and ethyl acetate (EtOAc) were used without further purification as crystallization solvents. FaSSIF/FeSSIF/FaSSGF powder was purchased from Biorelevant (London, UK).

5.2.2 Salts preparation

Clofaziminium - 4-aminosalicylate (form I, II and III) were prepared by liquid-assisted grinding (LAG) of equimolar amount of CFZ (75.0 mg, 0.158 mmol) and PAS (24.3 mg, 0.158 mmol) in presence of 30 µL of MeCN (CFZ/PAS 1/1 LAG MeCN) (form I obtained after drying the powder), EtOH (CFZ/PAS 1/1 LAG EtOH, form II) or EtOAc (CFZ/PAS 1/1 LAG EtOAc form III). See Appendix C for comment about the choice of the solvents. Grinding experiments were performed in 2 mL Eppendorf tubes, filled with seven stainless steel balls of 1 mm diameter and one ball of 3 mm diameter. Ball milling was performed for 90 minutes at 30 Hz using a Retsch Mixer Mill 400 apparatus and samples were homogenized every 30 minutes. Single-crystals were obtained by recrystallization, at room temperature (293-298 K), of the CFZ/PAS 1:1 ground product with MeCN (CFZ/PAS

1/1 LAG MeCN) in a mixture of MeCN and MeOH (for form I) or in MeCN (for CFZNH$^+$-PAS$^-$-MeCN (1:1:1) solvate). Form IV is obtained by slurrying equimolar amount of CFZ (75.0 mg, 0.158 mmol) and PAS (24.3 mg, 0.158 mmol) in water (powder was recovered by centrifugation and then oven-dried at 60 °C for one night).

5.2.3   Single-crystal X-ray diffraction (SCXRD)

SCXRD data were collected with an Oxford Diffraction Gemini Ultra R equipped with a Ruby CCD detector. Full data sets were collected with Cu Kα (λ = 1.54184 Å) radiation at 295 and 100 K for form I and at 100 K for CFZNH$^+$-PAS$^-$-MeCN (1:1:1) solvate. Analytical numeric absorption correction (using a multifaceted crystal model based on expressions derived by R.C. Clark & J.S. Reid [31]), followed by empirical absorption correction (using spherical harmonics, implemented in SCALE3 ABSPACK scaling algorithm) were performed within *CrysAlis PRO* [32]. Structures were solved by the dual-space method implemented by *SHELXT* [33] within *Olex2* [34]. Refinement by the least-square method implemented by *SHELXL* [35] was performed within *ShelXle* [36]. Non hydrogen atoms were refined anisotropically while hydrogen atoms were refined as riding atoms with isotropic displacement parameter set to 1.2 times that of the parent atom (1.5 times for methyl and OH groups). In the structures determined at 100 K, hydrogen atoms implied in strong H-bonds were located in Fourier map and refined (except for H atoms of PAS$^-$ in the structure of form I because this anion is disordered over three positions). Structure visualization was performed within *Mercury* [37].

5.2.4   High-resolution powder X-ray diffraction and structure solution

High-resolution PXRD pattern of form II was collected at 295 K in transmission mode with a STOE MP diffractometer (Cu Kα_1 radiation, λ = 1.54059 Å) between 4 and 40° 2θ angle, with a step size of 0.15°. Sample was filled in a 0.7 mm diameter thin-wall glass capillary. Indexation was performed within F.O.X version 2017.2 [38]. Intensities were extracted by the Le Bail method implemented within F.O.X. and structure solution was performed by a direct-space method within the same program using clofaziminium and 4-aminosalicylate geometries extracted from SCXRD data. Structure was refined within TOPAS V6 [39], using rigid body approach.

PXRD data were collected with the same diffractometer in transmission mode (transmission scan mode) from 4 to 40° 2θ angle after solubility and slurry experiments.

5.2.5   Powder X-ray diffraction (PXRD)

PXRD data were collected with a PANalytical X'PERT PRO Bragg-Brentano diffractometer, using Cu Kα (λ = 1.54184 Å) radiation (2θ angle ranging from 4 to 40° with a

step size of 0.0167°).

Variable-temperature powder X-ray diffraction (VT-PXRD) data were collected at 25 °C, from 30 to 150 °C (data collected every 10 °C), at 175 and at 200 °C with the same diffractometer equipped with an Anton-Paar TTK 450 heating system.

5.2.6 Thermogravimetric analysis (TGA)/ differential scanning calorimetry DSC

Thermal stability of the four forms was evaluated with a TGA/DSC3+ apparatus (Mettler Toledo). Solid samples were analysed in open aluminium pans (100 µL) from 25 to 300 °C (at a 10 °C/min scanning rate) under a nitrogen flow (80 mL/min). Results were analyzed with the STARe software (version 16.20).

5.2.7 Solubility evaluation

Solubility of CFZ, PAS and CFZNH$^+$-PAS$^-$ salt (forms I to IV) was evaluated in type I water, by wetting an excess amount of powder (10 - 20 mg) in 2.0 mL type I water at 25 °C (Heidolf incubator 1000) and under agitation at 900 rpm (Heidolf titramax 1000 platform shaker). Experiments were performed in triplicate. After 24 hours, the samples were centrifuged at 13000 rpm (eppendorf centrifuge 5430R, equipped with a FA-45-24-11 rotor) for 15 minutes, the supernatant was recovered and centrifuged again (15 minutes, 13000 rpm). After second centrifugation, the supernatant was diluted twice with MeCN. Solubility was evaluated by a high-performance liquid chromatography (HPLC) method performed with a Zorbax SB C18 (3.5 µm, 3 x 100 mm) column heated to 40 °C and connected on an Agilent 1100 series HPLC system using UV detection at 280 and 490 nm. Gradient elution was performed with mobile phase A (trifluoroacetic acid 0.1%) and mobile phase B (MeCN) at a flow rate of 0.5 mL/min. Gradient started at 15% B and ramped up to 70% B in 0.5 minute. This solvent ratio was maintained for 6.5 minutes before returning to 15% B for 6 minutes to re-equilibrate the column. The injection volume was 5 µL. Calibration was performed with samples prepared in MeCN/water 1:1 (in volume) with concentrations ranging from 16.6 to 0.06 µg/mL for CFZ and from 80 to 1.25 µg/mL for PAS. pH of the salt solutions (forms I, II, III and IV) was measured after first centrifugation and, in all cases, it was comprised between 4.5 and 4.9.

5.2.8 Stability in Fasted-state simulated gastric fluid (FaSSGF)

Propensity of CFZNH$^+$-PAS$^-$ to undergo anion exchange in gastric fluid was evaluated by dispersing an excess amount of each form in FaSSGF. After 30 minutes, the PXRD pattern of the remaining solid was collected with a STOE MP diffractometer. Fasted-state simulated gastric fluid was prepared by solubilisation of 0.0597 g of FaSSIF/FeSSIF/FaSSGF powder in 1.0 L of a NaCl (1.999 g/L) solution adjusted with HCl at pH 1.6.

5.2.9   Relative stability of the four forms

Relative stability of the four forms was evaluated by competitive slurry experiments in water at 22 °C. Mixtures of two forms (I and II, I and III, I and IV, II and III, II and IV and III and IV) were suspended in water for 14 days. The solid phase was then recovered and analyzed in PXRD.

5.2.10   Evaluation of CFZNH$^+$-PAS$^-$ salts hygroscopicity

Dynamic vapour sorption (DVS) analyses were performed on a Q5000 SA apparatus (TA instruments) at 25 °C with nitrogen as flow gas (50 mL/min). Solid samples (7 - 15 mg) were placed in platinum crucible (empty crucible used as a reference) and inserted in a temperature and humidity controlled chamber. Samples were first dried at 40 °C for 1 hour and then exposed to variable relative humidity (10 to 90%) at 25 °C. Equilibrium was considered to be reached when no weight change is observed for two hours of exposure or if it is less than 0.010 mg/min.

5.3   Results

Forms I to III of CFZNH$^+$-PAS$^-$ salt were prepared by liquid-assisted grinding. PXRD patterns of the ground powders were compared to the one of the starting materials and in each case a new crystalline phase was identified (Fig. 5.2).

Single-crystals were obtained for form I (data were collected at 295 K and 100 K) and for a solvated salt (CFZNH$^+$-PAS$^-$-MeCN (1:1:1), data collected at 100 K). Structure of form II was determined from powder data. Both forms (I and II) crystallize in $P\bar{1}$ triclinic space group and their asymmetric units contain one clofaziminium cation (CFZNH$^+$) and one 4-aminosalicylate anion (PAS$^-$) (Table C.1).

Form III was first identified during competitive slurry of forms I and II in water and could be successfully obtained by liquid-assisted grinding of clofazimine with 4-aminosalicylic acid in presence of EtOAc. Form IV was first identified after solubility evaluation of form I and could be obtained by slurrying clofazimine and 4-aminosalicylic acid in water (Fig. 5.2). Despite several attempts, up to now, structures of forms III and IV could not be determined.

5.3.1   Polymorph I

Crystals were dried at room temperature before SCXRD data collection. PAS$^-$ is disordered over 3 positions with respective occupancy (at 100 K) of 0.493, 0.199 and 0.307 (disorder identified by letters A, B and C in atom labeling). Strong charge-assisted hydrogen bonds are observed between CFZNH$^+$ cation and PAS$^-$ anion (N4$^+$-H$\cdots$O1A$^-$, N3-H$\cdots$O2A$^-$, Fig. 5.3(a) and Table C.2). Other H-bonds interactions are presented in Table C.2.
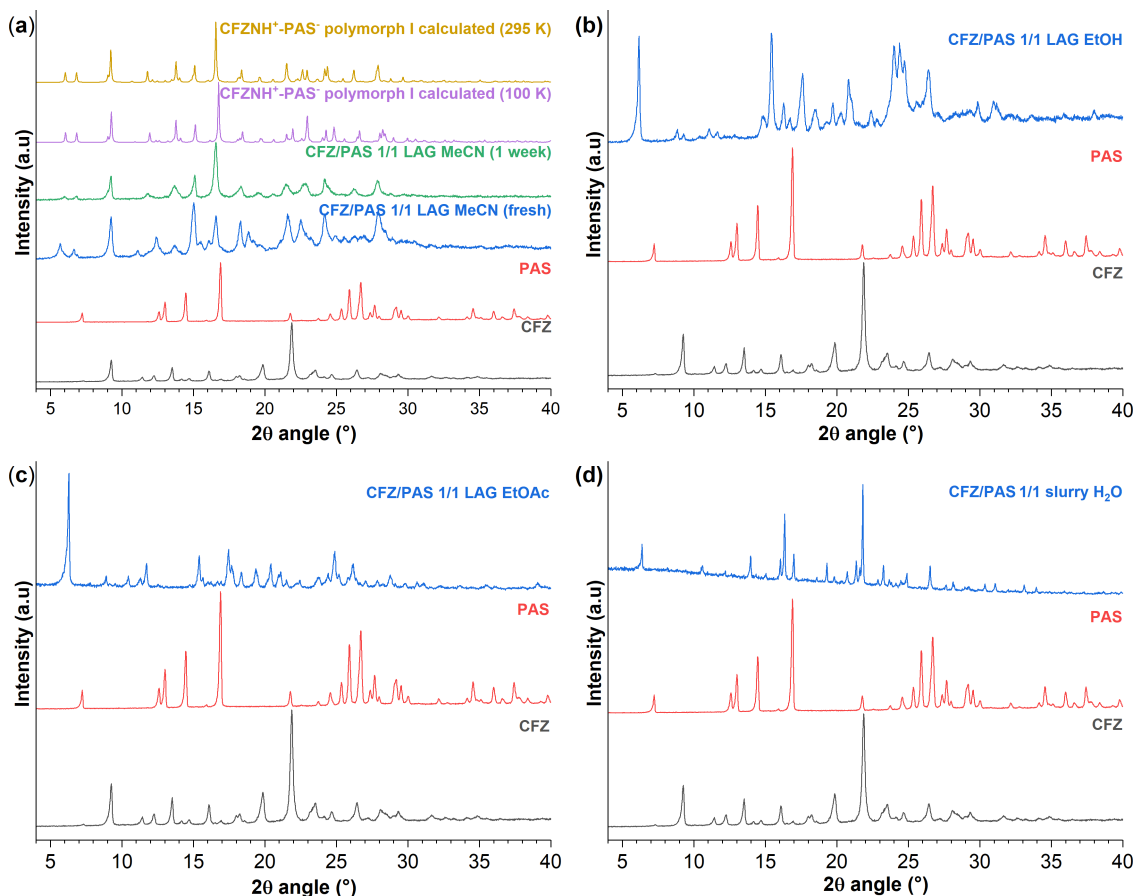
FIGURE 5.2: PXRD pattern of, from bottom to top: CFZ, PAS and (a) CFZ/PAS 1/1 LAG MeCN and calculated pattern of CFZNH$^+$-PAS$^-$ polymorph I at 100K and 295K, (b) CFZ/PAS 1/1 LAG EtOH, (c) CFZ/PAS 1/1 LAG EtOAc and (d) CFZ/PAS 1/1 slurry H$_2$O.

Clofaziminium cations are stacked in a head to tail fashion (centroid-centroid distance of 3.672(2) Å, orthogonal projection distance of 3.519(1) Å and horizontal displacement of 1.046 Å, Fig. 5.3(b)). C-H$\cdots\pi$ interactions are further observed between CFZNH$^+$ cation and PAS$^-$ anion (H26C$\cdots$centroid distance of 2.68 Å, orthogonal projection distance of 2.68 Å, C26$\cdots$centroid distance of 3.643(9) Å and C26-H26C$\cdots\pi$ angle of 78 °, Fig. 5.3(c)). Interestingly powder obtained just after LAG in presence of MeCN does not correspond to CFZNH$^+$-PAS$^-$ form I. This phase is however unstable at room temperature and spontaneously converts to form I as indicated by PXRD pattern measured on freshly prepared powder and after one week of storage at room temperature (Fig. 5.2).

5.3.2 Polymorph II

CFZNH$^+$ and PAS$^-$ interact through charge-assisted H-bonds (N4$^+$-H$\cdots$O1A$^-$, N3-H$\cdots$O1A$^-$, Fig. 5.3(d) and Table C.2). Clofaziminium cations are stacked in a head to tail fashion (centroid-centroid distance of 3.760(16) Å, orthogonal projection distance

of 3.682(13) Å and horizontal displacement of 0.767 Å, Fig. 5.3(e)). Two C-H···π interactions are observed between CFZNH$^+$ cation and PAS$^-$ anion (H26B···centroid distance of 2.95(9) Å, orthogonal projection distance of 2.81 Å, C26···centroid distance of 3.85(8) Å and C26-H26B···π angle of 78° as well as H4···centroid distance of 2.63(8) Å, orthogonal projection distance of 2.44 Å, C4···centroid distance of 3.48(8) Å and C4-H4···π angle of 84°, Fig. 5.3(f)). Structure of this second form of CFZNH$^+$-PAS$^-$ was determined from PXRD data collected on a powder of CFZ/PAS 1/1 LAG EtOH (Table C.1). Observed, calculated and difference patterns are shown in supplementary information (Fig. C.1).
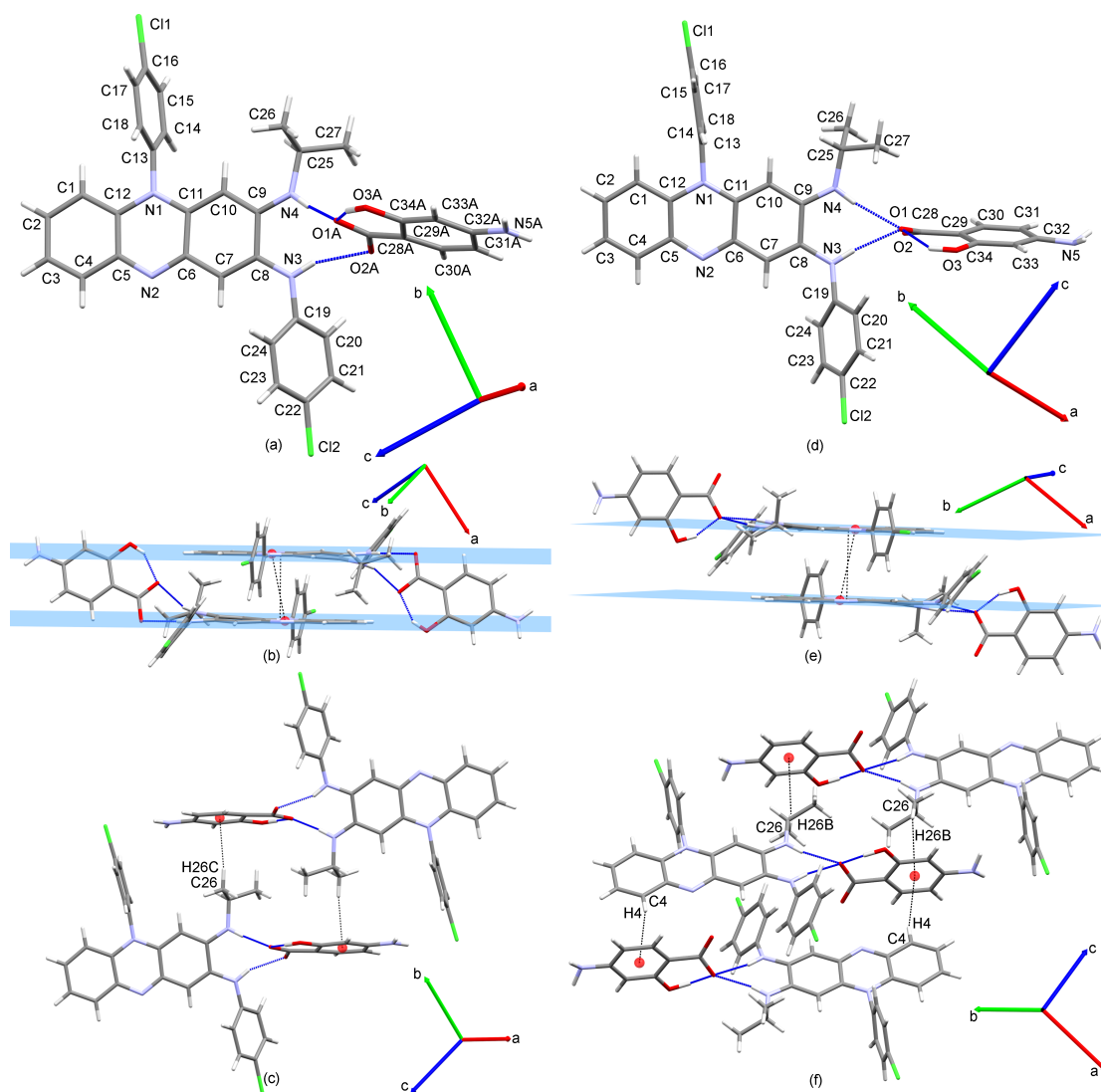
FIGURE 5.3: Crystal structures of CFZNH$^+$-PAS$^-$ forms I (left) and II (right). Asymmetric unit and labeling. (top, (a) and (d)), stacking of CFZNH$^+$ cations (centroids (red) and planes (blue) calculated with C5, C6, N1, N2, C11 and C12 atoms) (middle, (b) and (e)) and C-H···π interaction between CFZNH$^+$ and PAS$^-$ (centroids calculated with C29, C30, C31, C32, C33 and C34 atoms (position A of PAS considered in form I) (bottom, (c) and (f)).

5.3.3 Thermal analysis

TG/DSC analysis performed on a freshly prepared powder of CFZ/PAS 1/1 LAG MeCN (Fig. 5.4(a)) suggests that this phase is solvated as a weight loss (associated with a wide endotherm on the DSC curve (onset 51 °C)) is observed from 25 °C to around 95 °C. This assumption has been confirmed by the determination of the crystal structure of $CFZNH^+$-PAS^--MeCN (1:1:1) solvate (Fig. C.2 and Tables C.1 and C.2). A small exothermic event, not associated with any weight loss, is observed at 129 °C and, at 215 °C melting occurs, immediately followed by degradation (probably associated with PAS decarboxylation).

A VT-PXRD experiment performed on freshly prepared powder of CFZ/PAS 1/1 LAG MeCN indicates the formation of $CFZNH^+$-PAS^- form I upon heating (Fig. C.3). Then, between 130 and 150 °C a transformation occurs. Actually, a partial conversion of form I to form II is observed upon heating. A kinetically controlled process is suspected for this conversion and exact condition of conversion could not be determined (Figs. C.3 and C.4).
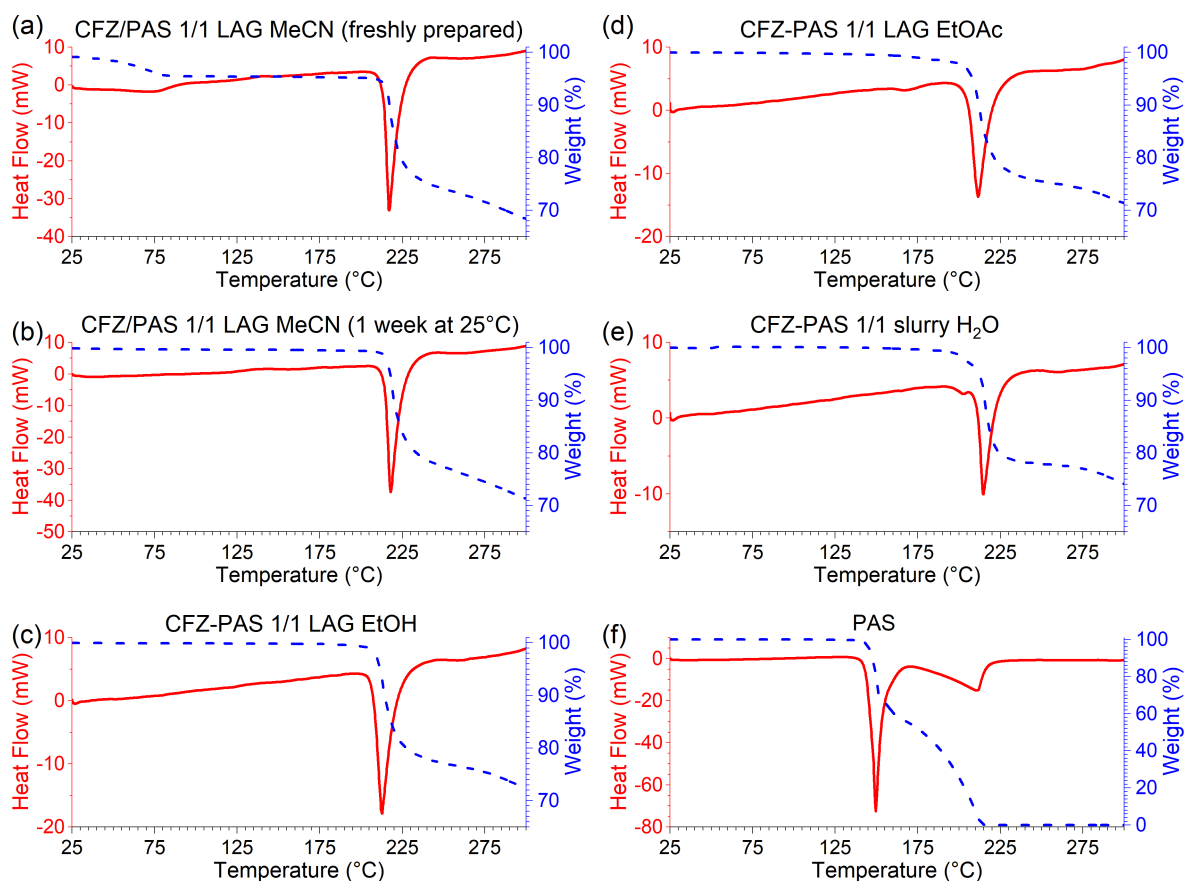
FIGURE 5.4: TGA (dashed blue) and DSC (plain red) curves of (a) CFZ/PAS 1/1 LAG MeCN (powder freshly prepared), (b) $CFZNH^+$-PAS^- form I, (c) $CFZNH^+$-PAS^- form II and (d) CFZ/PAS 1/1 LAG EtOAc (form III), (e) CFZ/PAS 1/1 slurry H_2o (form IV) and (f) PAS.

A new TG/DSC analysis (Fig. 5.4(b)) performed on powder corresponding to form I (CFZ/PAS LAG MeCN after one week of storage at room temperature) does not present any weight loss between 25 and 95 °C confirming complete phase transformation from a solvate to form I in these conditions. A small exothermic event is observed at 126°C (consistent with phase transformations identified by VT-PXRD) before melting and degradation at 217 °C.

In Fig. 5.4(c), thermal stability of form II was evaluated by TGA/DSC. Results indicated that this form is stable up to 210 °C, temperature at which melting and degradation occur.

Thermal analysis of form III (Fig. 5.4d) reveals an endothermic event (162 °C), corresponding to a phase conversion from form III to form II (Fig. C.5), before melting and degradation at 209 °C. TG/DSC analysis of form IV reveals the presence of a small endotherm at 202 °C (associated to a 4% weight loss). This event is followed by a second endotherm associated to melting and further degradation of the phase at 214 °C.

5.3.4 CFZNH$^+$-PAS$^-$ behaviour in solution

Solubility of CFZ, PAS and CFZNH$^+$-PAS$^-$ (forms I to IV) was studied in water at 25 °C by an HPLC method. Results indicate that after 24h of dispersion in water, only 0.20 ± 0.03 µg/mL of clofazimine is released in solution (Fig. 5.5).

PAS solubility could not be determined because PAS degrades in water (two peaks are observed on the chromatogram (Fig. C.6)). Such degradation is not observed for CFZNH$^+$-PAS$^-$ salts (forms I to IV).

All four forms present a significant increase of CFZ solubility after 24h in water (Fig. 5.5). Indeed, the amount of solubilized CFZ reaches 10.26 ± 0.52 µg/mL (50-fold improvement), 12.27 ± 0.32 µg/mL (60-fold solubility improvement), 7.15 ± 0.43 µg/mL
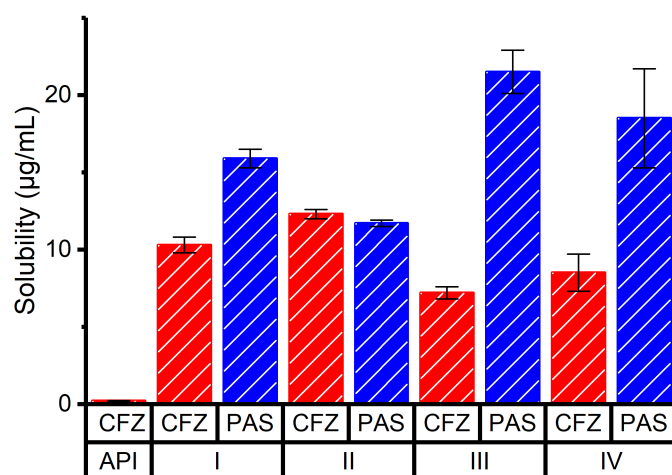
FIGURE 5.5: (a) Amount of CFZ (red) and PAS (blue) released after 24h in water from CFZ and the four salts (forms I to IV).
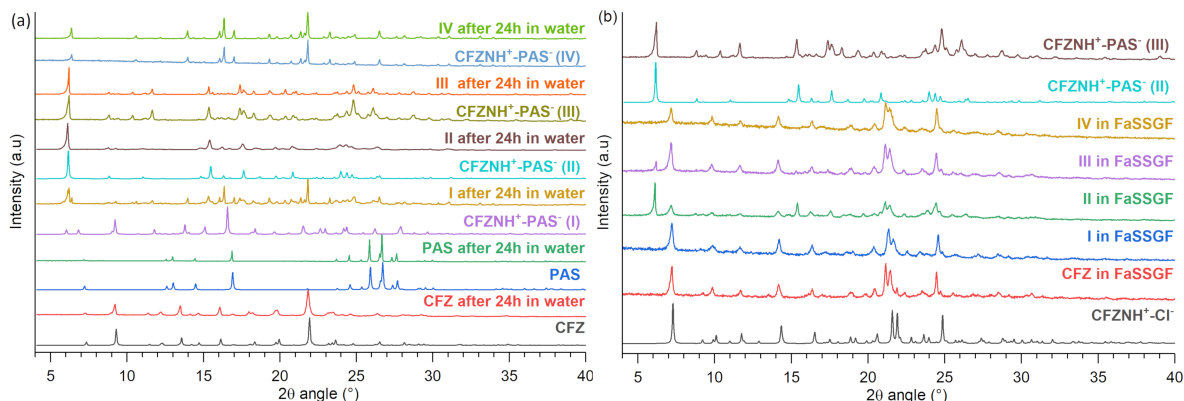
FIGURE 5.6: PXRD patterns, (a) of CFZ, PAS, CFZNH$^+$-PAS$^-$ forms I, II, III and IV before and after dispersion in water and (b) of CFZNH$^+$-Cl$^-$ (calculated pattern), CFZ, CFZNH$^+$-PAS$^-$ (forms I to IV) after dispersion in FaSSGF, and powder patterns of CFZNH$^+$-PAS$^-$ (II, calculated) and of form III.

(36-fold improvement) and 8.50 ± 1.24 µg/mL (42-fold improvement) from CFZNH$^+$-PAS$^-$ forms I to IV respectively. The amount of solubilized PAS is 15.94 ± 0.55 µg/mL, 11.70 ± 0.17 µg/mL, 21.47 ± 1.37 µg/mL and 18.47 ± 3.15 µg/mL from forms I to IV respectively.

PXRD analysis of the remaining powder (after 24h dispersion in water) indicates that CFZ does not undergo any crystalline phase change, CFZNH$^+$-PAS$^-$ forms II, III and IV remain stable in water for 24h, while form I converts to a mixture of form III and form IV. PAS degradation is not observed on PXRD pattern collected after solubility evaluation of PAS (Fig5.6(a)). This could be explained by the high aqueous solubility (26.29 g/L at 20 °C [6]) of the PAS degradation product, 3-aminophenol, in water.

Bannigan *et al.* [16] reported anion exchange and CFZNH$^+$Cl$^-$ precipitation after dispersion of CFZ salts in simulated gastric fluids. The propensity of CFZNH$^+$-PAS$^-$ for anion exchange was investigated by a slurry experiment of all four forms in FaSSGF. Powders recovered after dispersion of form I or IV correspond to CFZNH$^+$Cl$^-$, while the ones recovered after dispersion of form II or III in FaSSGF correspond to a mixture of CFZNH$^+$Cl$^-$ with CFZNH$^+$-PAS$^-$ (form II or III respectively) (Fig. 5.6(b)). Those data are consistent with what is reported in literature [16] and indicate rapid anion exchange and precipitation of the hydrochloride salt of clofazimine.

5.3.5 Relative stability of the four forms

Competitive slurry experiments of forms I and II, of forms I and III as well as of forms II and III lead to form III (Fig. 5.7). This indicates that both forms I and II are less stable than form III. Relative stability of forms I and II could not be determined as both are metastable (conversion to form III is already achieved after 48 h). All competitive slurry experiments implying form IV lead to form IV indicating that this is the most stable one (Fig. 5.7). The relative stability at 22 °C can thus be established as CFZNH$^+$-PAS$^-$ (I), CFZNH$^+$-PAS$^-$ (II) < CFZNH$^+$-PAS$^-$ (III) < CFZNH$^+$-PAS$^-$ (IV).
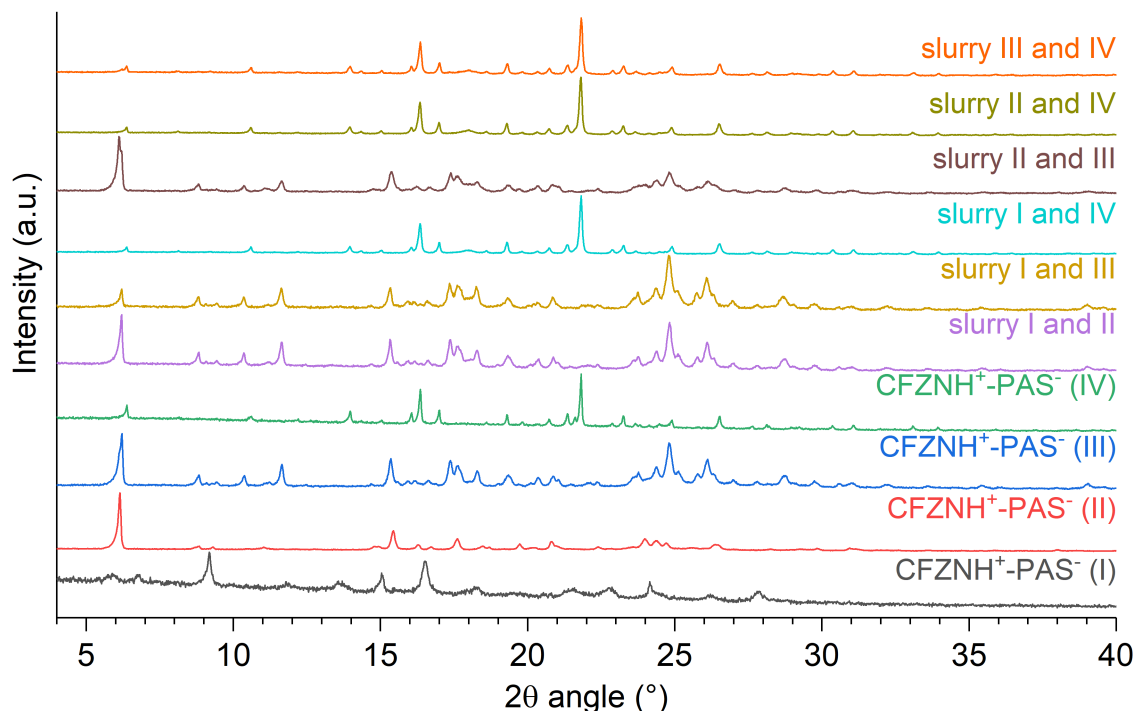
FIGURE 5.7: PXRD patterns of the solid phases recovered after 14 days of competitive slurry experiments of forms I and II, forms I and III, forms I and IV, forms II and III, forms II and IV and of forms III and IV compared to the powder patterns of forms I, II, III and IV.

5.3.6 Evaluation of CFZNH$^+$-PAS$^-$ salts water sorption

Dynamic vapour sorption (DVS) analyses were performed on the four forms identified. No deliquescence or significant water uptake was observed (Fig. 5.8) except for form I that reversibly absorbs around 3%water at 90% humidity (Fig. 5.8(a)). Such a 3% water absorption may correspond to a monohydrated (calculated water content of 2.8%) form of the salt. The isotherm hysteresis (Fig. 5.8(a)))is in line with the hypothesis of a hydrated form of CFZNH$^+$-PAS$^-$ (I).

5.4 Discussion

Thermal analyses of the four identified forms indicate that form I undergoes a phase conversion (between 120 and 150 °C), followed by melting at 215 °C. Form III converts to form II, which melts at 209 °C, upon heating. Thermal behaviour of form IV is more complicated as a small endotherm associated to a 4% weight loss is observed at 202 °C before melting at 214 °C. A 2.9% weight loss would be expected for a monohydrate, however the high temperature at which the 4% weight loss is observed suggests that this phase does not correspond to an hydrated form of a clofaziminium 4-aminosalicylate salt.
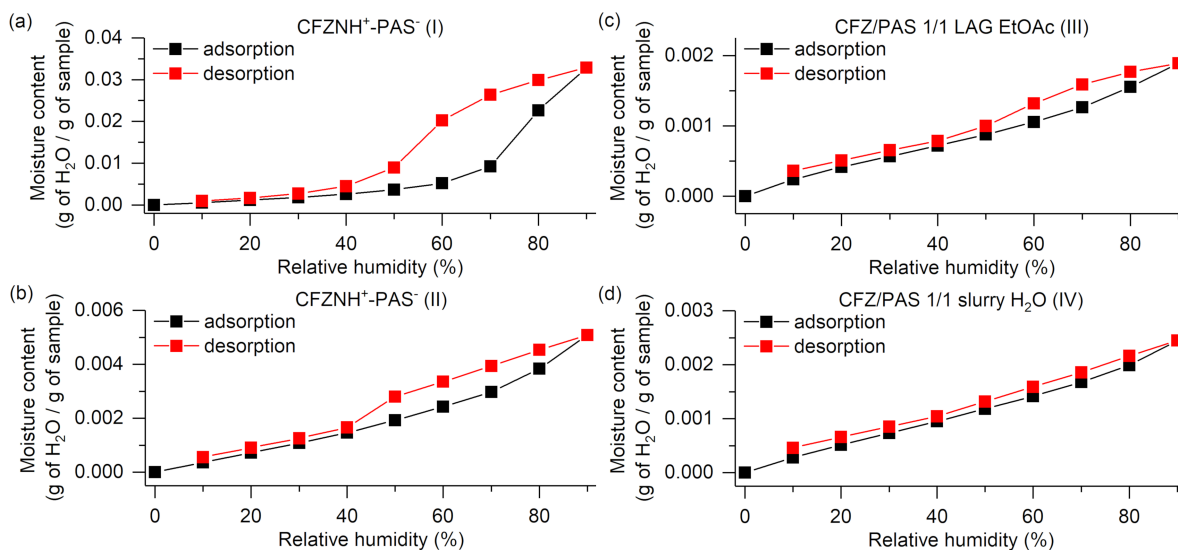
FIGURE 5.8: Sorption isotherms (adsorption and desorption) of CFZNH$^+$-PAS$^-$ form I (a), form II (b), form III (c) and form IV (d).

For all forms identified, melting is immediately followed by degradation, most probably through decarboxylation of PAS. CFZNH$^+$-PAS$^-$ salts present an increased thermal stability in comparison to pure PAS (which decarboxylates at 145 °C). Decarboxylation of pure PAS can however occur at lower temperature but with longer induction period (59h at 74 °C, 12.2h at 78 °C, 5h at 90 °C [24]). The increased thermal stability observed for all the four forms could probably be attributed to the presence of strong interactions (charged-assisted H-bonds, as observed in the structures of polymorphs I and II) between clofaziminium and the carboxylate of PAS. These interactions would probably prevent CO_2 release from PAS before melting of the salt. Such kind of interaction between clofaziminium and carboxylate was already reported in several studies [15, 17, 40]. More particularly improved solubility was observed for a clofaziminium mesylate salt presenting the same type of interaction [15]. Furthermore, such kind of strong interaction was also shown to improve physical stability of amorphous solid dispersion of clofazimine and hypromellose phthalate [40].

Pure PAS also decarboxylates in water, however decarboxylation of its sodium salt occurs to a lesser extent in water thanks to the higher pH of the PAS·Na solution in comparison to the PAS solution. We believe that the preparation of CFZNH$^+$-PAS$^-$ could potentially have a similar effect and that it could be beneficial for compound storage (moisture accelerates PAS decarboxylation and higher pH could slower the reaction). This hypothesis is supported by the absence of PAS degradation peak on the HPLC chromatograms measured after a 24h dispersion of CFZNH$^+$-PAS$^-$ salts in water.

Solubility study performed in water indicates a significant increase of solubilized CFZ (10.26 ± 0.52 μg/mL (form I), 12.27 ± 0.32 μg/mL (form II), 7.15 ± 0.43 μg/mL (form III) and 8.50 ± 1.24 μg/mL (form IV)) from CFZNH$^+$-PAS$^-$ salts in comparison to pure

CFZ (0.20 ± 0.03 µg/mL). Interestingly, forms III and IV have very similar solubility in water (same value within experimental errors). Furthermore, $CFZNH^+$-PAS^- salt preparation prevents PAS decarboxylation in water as indicated by the absence of degradation peak on the HPLC chromatogram.

Slurry of all four forms in FaSSGF has shown anion exchange and formation of $CFZNH^+Cl^-$. In consequence, CFZ bioavailability could be reduced because of the formation of $CFZNH^+Cl^-$ in the stomach. Preparation of gastro-resistant caps of $CFZNH^+$-PAS^- could be an alternative, among others, that could potentially avoid or reduce PAS decarboxylation and $CFZNH^+Cl^-$ formation in the stomach while maintaining an improved solubility profile for $CFZNH^+$-PAS^-.

Competitive slurry experiments performed at 22 °C have shown both the forms I and II are less stable than form III which is in accordance with the fact that the latter is less soluble than forms I and II in water. The most stable form is form IV. DVS analyses have shown that none of the four presented forms is deliquescent. A reversible 3% water sorption is however observed for form I, which could correspond to the formation of a monohydrated form. Water desorption suggests however that this potential hydrated form is not stable at low relative humidity. For all the other forms, measured water sorption is less than 1% even at 90% relative humidity exposure.

5.5 Conclusion

Four forms of a salt combining clofazimine and 4-aminosalicylic acid, two antitubercular drugs susceptible to be co-administered in patients suffering from XDR-TB, were identified by liquid-assisted grinding. Forms I and II have been structurally described and their thermal properties have been investigated by TGA/DSC. Two other forms for which structure could not be determined were also discovered. The preparation of these four forms resulted in an improved thermal stability towards PAS decarboxylation in comparison to pure PAS. This stabilization is also observed in water and it can probably be attributed to weak basicity of CFZ which increases pH of the solution and thus slows down the PAS decarboxylation.

Preparation of $CFZNH^+$-PAS^- salt resulted in an important increase of solubilized CFZ (50-fold and 60-fold CFZ solubility improvement from $CFZNH^+$-PAS^- forms I and II and around 40-fold improvement from forms III and IV which have same solubility within experimental errors). During the solubility test of $CFZNH^+$-PAS^- form I, a phase transformation in water has been observed with this polymorphic form while no phase transformation is observed during solubility evaluation for the three other forms.

Competitive slurry experiments have shown that form IV is the most stable one at 22 °C. Form II is more water soluble than forms III and IV but the latter two are more stable.

DVS analyses have shown a 3% water sorption at 90% relative humidity exposure for form I. The three other forms present a good stability regarding hygroscopicity as no significant water sorption is observed during DVS analyses. The phase transformation and the reversible water sorption observed for form I suggest that this phase could be more challenging for further development. The three other forms (II, III and IV) are interesting for further investigation but care has to be taken regarding phase transformation as several forms of $CFZNH^+$-PAS^- salts were identified.

If such combinations of CFZ with PAS could lead to improved bioavailability in vivo remains to be determined. A gastro-resistant formulation of $CFZNH^+$-PAS^- would probably be necessary in order to avoid PAS decarboxylation and $CFZNH^+Cl^-$ precipitation in the stomach. However, the present study suggests that salification of CFZ (BCS II) with PAS (BCS III drug) could lead to improved physico-chemical properties of both parent APIs.

Conflict of interest

There is no conflict to declare.

Acknowledgements

Bibliography

[1] World Health Organization. *Global tuberculosis report 2019.* World Health Organization, Geneva, 2019.

[2] World Health Organization. *Guidelines for treatment of drug-susceptible tuberculosis and patient care.* World Health Organization, Geneva, 2017.

[3] G. Sotgiu, S. Tiberi, R. Centis, L. D. Ambrosio, Z. Fuentes, A. Zumla, and G. Battista. International Journal of Infectious Diseases Applicability of the shorter ' Bangladesh regimen ' in high multidrug-resistant tuberculosis settings. *International Journal of Infectious Diseases*, 56:190–193, 2017.

[4] C. Lange, D. Chesov, and J. Heyckendorf. Clofazimine for the treatment of multidrug-resistant tuberculosis. *Clinical Microbiology and Infection*, 25(2):128–130, 2019.

[5] World Health Organization. *WHO consolidated guidelines on drug-resistant tuberculosis treatment.* World Health Organization, 2019.

[6] S. H. Yalkowsky, Y. He, and P. Jain. *Handbook of aqueous solubility data.* CRC press, 2016.

[7] C. D. Bevan and R. S. Lloyd. A high-throughput screening method for the determination of aqueous drug solubility using laser nephelometry in microtiter plates. *Analytical chemistry*, 72(8):1781–1787, 2000.

[8] P. Schwinté, M. Ramphul, R. Darcy, and J. F. O'sullivan. Amphiphilic cyclodextrin complexation of clofazimine. *Journal of inclusion phenomena and macrocyclic chemistry*, 47(3-4):109–112, 2003.

[9] I. I. Salem, G. Steffan, and N. Düzgünes. Efficacy of clofazimine-modified cyclodextrin against Mycobacterium avium complex in human macrophages. *International Journal of Pharmaceutics*, 260(1):105–114, 2003.

[10] S. Li, J. Y.-W. Chan, Y. Li, D. Bardelang, J. Zheng, W. W. Yew, D. P.-C. Chan, S. M. Y. Lee, and R. Wang. Complexation of clofazimine by macrocyclic cucurbit [7] uril reduced its cardiotoxicity without affecting the antimycobacterial efficacy. *Organic & biomolecular chemistry*, 14(31):7563–7569, 2016.

[11] Y. Zhang, J. Feng, S. A. McManus, H. D. Lu, K. D. Ristroph, E. J. Cho, E. L. Dobrijevic, H.-K. Chan, and R. K. Prud'homme. Design and solidification of fast-releasing clofazimine nanoparticles for treatment of cryptosporidiosis. *Molecular pharmaceutics*, 14(10):3480–3488, 2017.

[12] V. R. Patel and Y. K. Agrawal. Nanosuspension: An approach to enhance solubility of drugs. *Journal of advanced pharmaceutical technology & research*, 2(2):81, 2011.

[13] A. S. Narang and A. K. Srivastava. Evaluation of solid dispersions of clofazimine. *Drug Development and Industrial Pharmacy*, 28(8):1001–1013, 2002.

[14] J. R. O'Reilly, O. I. Corrigan, and C. M. O'Driscoll. The effect of simple micellar systems on the solubility and intestinal absorption of clofazimine (B663) in the anaesthetised rat. *International Journal of Pharmaceutics*, 105(2):137–146, 1994.

[15] G. Bolla and A. Nangia. Clofazimine mesylate: A high solubility stable salt. *Crystal Growth and Design*, 12(12):6250–6259, 2012.

[16] P. Bannigan, E. Durack, C. Madden, M. Lusi, and S. P. Hudson. Role of Biorelevant Dissolution Media in the Selection of Optimal Salt Forms of Oral Drugs: Maximizing the Gastrointestinal Solubility and in Vitro Activity of the Antimicrobial Molecule, Clofazimine. *ACS Omega*, 2(12):8969–8981, 2017.

[17] L. Bodart, N. Tumanov, and J. Wouters. Structural variety of clofaziminium salts: effect of the counter-ion on clofaziminium conformation and crystal packing. *Acta Crystallographica Section B: Structural Science, Crystal Engineering and Materials*, 75(4), 2019.

[18] M. L. Sousa, M. C. Sarraguça, A. O. dos Santos, J. M. G. Sarraguça, J. Lopes, and P. R. da Silva Ribeiro. A new salt of clofazimine to improve leprosy treatment. *Journal of Molecular Structure*, page 128226, 2020.

[19] J. Zheng, E. J. Rubin, P. Bifani, V. Mathys, V. Lim, M. Au, J. Jang, J. Nam, T. Dick, J. R. Walker, et al. para-Aminosalicylic acid is a prodrug targeting dihydrofolate reductase in Mycobacterium tuberculosis. *Journal of Biological Chemistry*, 288(32):23447–23456, 2013.

[20] J.-M. del Moral-Sanchez, I. Gonzalez-Alvarez, M. Gonzalez-Alvarez, A. Navarro, M. Bermejo, et al. Classification of WHO Essential Oral Medicines for Children Applying a Provisional Pediatric Biopharmaceutics Classification System. *Pharmaceutics*, 11(11):567, 2019.

[21] R. F. Rekker and W. T. Nauta. The UV Absorption Spectra of p-Aminosalicylic Acid and some Related Compounds–IV. The Ampholytic Forms of p-Aminosalicylic Aicd and some Structurally Related Compounds and their Decarboxylation. *Journal of Medicinal Chemistry*, 2(3):281–297, 1959.

[22] S. S. Kornblum and B. J. Sciarrone. Decarboxylation of p-aminosalicylic acid in the solid state. *Journal of pharmaceutical sciences*, 53(8):935–941, 1964.

[23] M. Rotich, B. Glass, and M. Brown. Thermal studies on some substituted aminobenzoic acids. *Journal of thermal analysis and calorimetry*, 64(2):681–688, 2001.

[24] M. Wesolowski. The decarboxylation and thermal stability of p-amino-salicylic acid and its salts. *Thermochimica Acta*, 21(2):243–253, 1977.

[25] E. L. Way, P. K. Smith, D. L. Howie, R. Weiss, and R. Swanson. The absorption, distribution, excretion and fate of para-aminosalicylic acid. *Journal of Pharmacology and Experimental Therapeutics*, 93(3):368–382, 1948.

[26] European Medicines Agency, EMA. Assessment report Para-aminosalicylic acid Lucane. Technical report, European Medicines Agency, EMA, 2014.

[27] World Health Organization. *Companion handbook to the WHO guidelines for the programmatic management of drug-resistant tuberculosis.* World Health Organization, 2014.

[28] H.-B. Xu, R.-H. Jiang, and H.-P. Xiao. Clofazimine in the treatment of multidrug-resistant tuberculosis. *Clinical Microbiology and Infection*, 18(11):1104–1110, 2012.

[29] S. Zhang, W. Shi, J. Feng, W. Zhang, and Y. Zhang. Varying effects of common tuberculosis drugs on enhancing clofazimine activity in vitro. *Emerging microbes & infections*, 6(4):e28, 2017.

[30] Y. Lu, B. Wang, W. J. Zhao, M. Q. Zheng, P. Li, L. Fu, and B. W. Liang. A study on the activity of clofazimine with antituberculous drugs against Mycobacterium tuberculosis. *Chinese journal of tuberculosis and respiratory diseases*, 33(9):675–678, 2010.

[31] R. C. Clark and J. S. Reid. The Analytical Calculation of Absorption in Multifaceted Crystals. *Acta Crystallographica A*, 51:887–897, 1995.

[32] Rigaku Oxford Diffraction. CrysAlis PRO. Version 1.171.40.67a. *CrysAlis PRO.*, pages Rigaku Oxford Diffraction Ltd, Yarnton, England, 2019.

[33] G. M. Sheldrick. SHELXT - Integrated space-group and crystal-structure determination. *Acta Crystallographica Section A: Foundations of Crystallography*, 71(1):3–8, 2015.

[34] O. V. Dolomanov, L. J. Bourhis, R. J. Gildea, J. A. K. Howard, and H. Puschmann. OLEX2: A complete structure solution, refinement and analysis program. *Journal of Applied Crystallography*, 42(2):339–341, 2009.

[35] G. M. Sheldrick. Crystal structure refinement with SHELXL. *Acta Crystallographica Section C: Structural Chemistry*, 71:3–8, 2015.

[36] C. B. Hübschle, G. M. Sheldrick, and B. Dittrich. ShelXle : a Qt graphical user interface for SHELXL. *Journal of Applied Crystallography*, 44:1281–1284, 2011.

[37] C. F. Macrae, I. Sovago, S. J. Cottrell, P. T. A. Galek, P. McCabe, E. Pidcock, M. Platings, G. P. Shields, J. S. Stevens, M. Towler, et al. Mercury 4.0: from visualization to analysis, design and prediction. *Journal of Applied Crystallography*, 2020.

[38] V. Favre-Nicolin and R. Cerny. FOX , ' free objects for crystallography ': a modular approach to ab initio structure determination from powder diffraction. *Journal of Applied Crystallography*, 35:734–743, 2002.

[39] A. A. Coelho. TOPAS and TOPAS-Academic : an optimization program integrating computer algebra and crystallographic objects written in C ++. *Journal of Applied Crystallography*, 51:210–218, 2018.

[40] H. Nie, Y. Su, M. Zhang, Y. Song, A. Leone, L. S. Taylor, P. J. Marsac, T. Li, and S. R. Byrn. Solid-state spectroscopic investigation of molecular interactions between clofazimine and hypromellose phthalate in amorphous solid dispersions. *Molecular pharmaceutics*, 13(11):3964–3975, 2016.

Chapter 6

General discussion, conclusions and perspectives

6.1 General discussion and conclusions

In this work, we first studied the solid-state transformations of clofazimine under liquid-assisted grinding conditions. This study showed that clofazimine is prone to solvate formation, as indicated by the two new solvates (with ethanol and ethyl acetate, Figure 6.1) presented in Chapter 2 and by the solvates (with DMF and acetone) already identified before the beginning of this thesis and presented in the introduction.
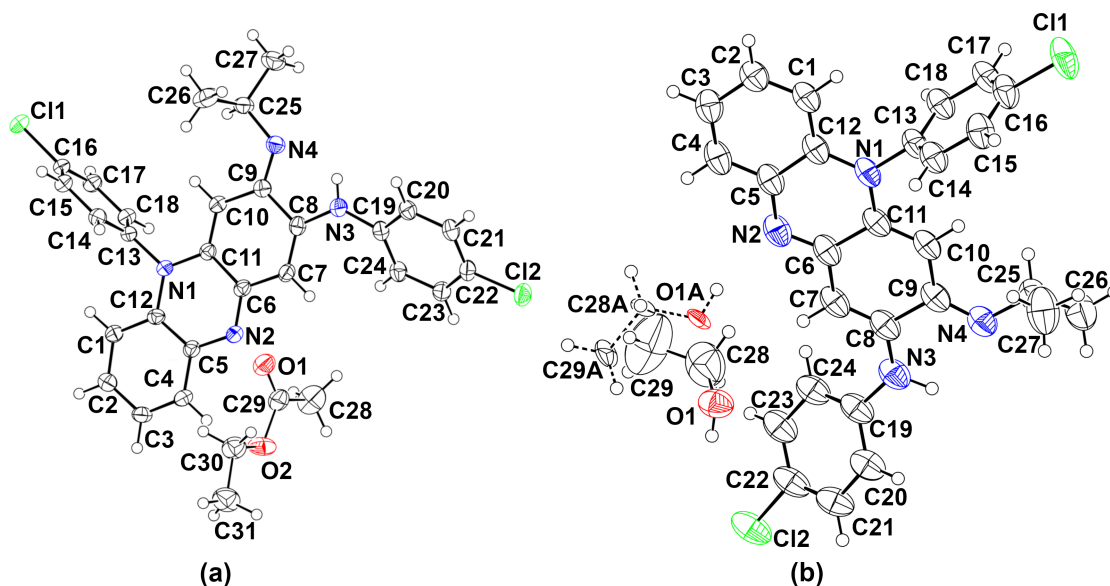
FIGURE 6.1: Structure and labeling scheme of (a) CFZ-EtOAc and (b) CFZ-EtOH. Displacement ellipsoids are drawn at the 50% probability level. Molecule with dashed bonds represents the second position of EtOH (disorder).

Considering the basic character of clofazimine, in Chapter 3, we studied the ability of this compound to interact with different molecules with acid and/or alcohol functions. The main objective was to identify the possible interaction sites for the preparation of drug-drug salts. Two main sites were shown to be involved in clofazimine interaction with other compounds. The first interaction site (around the imino group of CFZ), which corresponds to the protonation site of CFZ, is more often involved in H-bond interactions than the second (interaction with the phenazine group of CFZ). It appears, from this study, that clofazimine reacts well with carboxylic (and other) acid functions. Of the eight potential counterions tested, seven led to a new powder pattern after liquid-assisted grinding (Table 6.1).

Seven structures could be determined by SCXRD (two structures (one solvated and one non-solvated) were obtained with saccharin and terephthalic acid respectively). Dicarboxylic acids can interact with two molecules of clofazimine. This however requires a sufficient distance between these acid functions, as indicated by the double deprotonation of terephthalic acid, whereas only one proton transfer takes place between CFZ and fumaric acid (Figure 6.2).
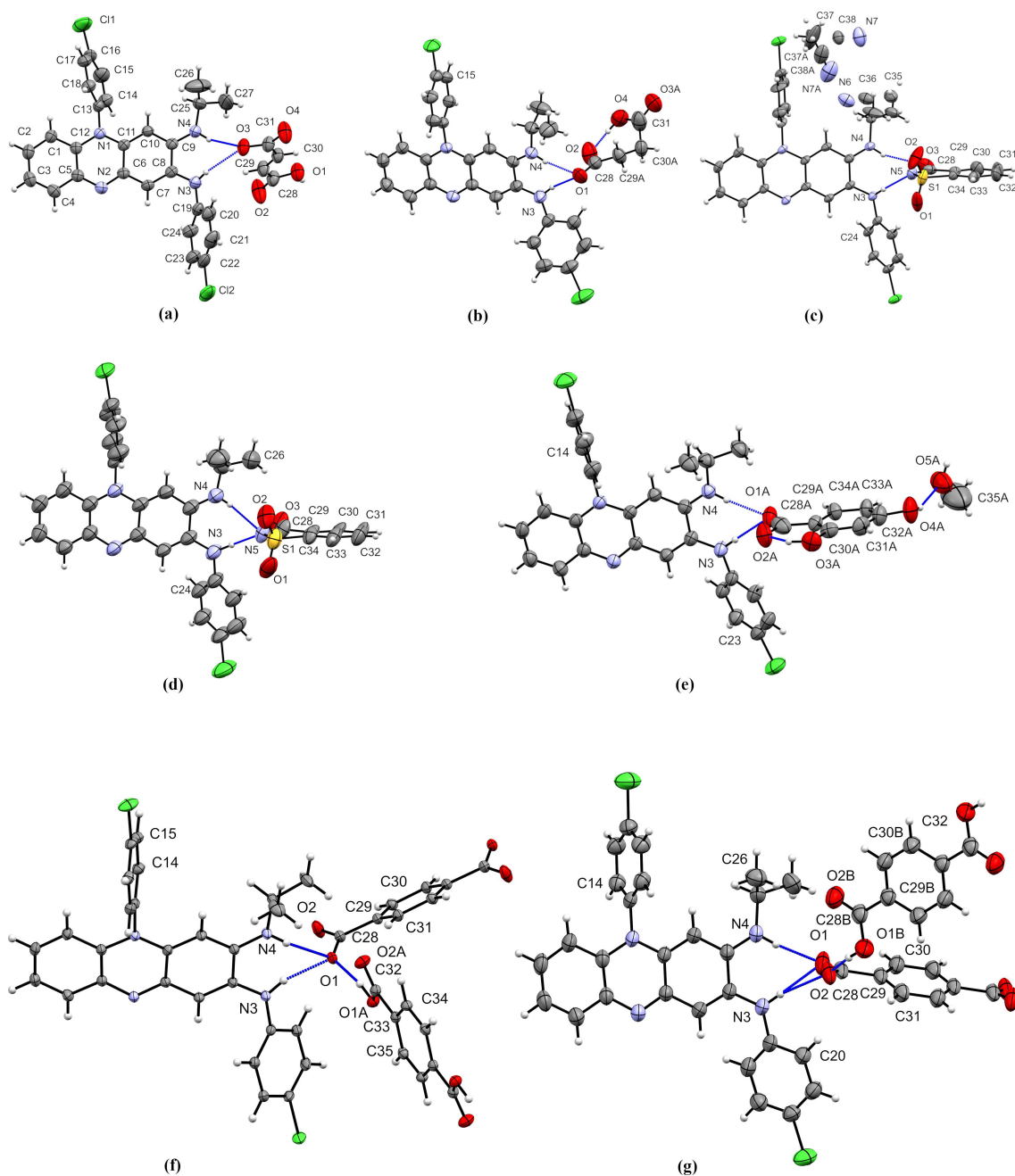
FIGURE 6.2: Hydrogen-bond interactions in the structures of (a) CFZ-NH$^+$-FA$^-$ (1:1), (b) CFZ-NH$^+$-SA$^-$ (1:1), (c) CFZ-NH$^+$-SACC$^-$-MeCN (1:1:1.4), (d) CFZ-NH$^+$-SACC$^-$ (1:1), (e) CFZ-NH$^+$-2,4DHBA$^-$-MeOH (1:1:1), (f) CFZ-NH$^+$-TRPTA^{2-}-TRPTA-solvent (1:0.5:0.5:x) and (g) CFZ-NH$^+$-TRPTA^{2-}-TRPTA (1:0.5:0.5). Ellipsoids are drawn at the 50% probability level.

The presence of an acidic function does not, however, guarantee salt formation with CFZ despite its pKa of 9.29 [3]. Indeed, in this work we did not identify any clofaziminium aspartate salt. The ΔpKa between CFZ and L-ASP is higher than 4, but no salt is observed, indicating that the ΔpKa rule alone does not guarantee salt formation. When

TABLE 6.1: Clofazimine salification assays and corresponding results.[§] Structure of **CFZ-NH+-CIT−** **(2:1)** is intrinsically disordered. [‡] Crystallized as **CFZ-NH+-CIT− (2:1)**.

Acid	pKas [1]	CFZ/Acid ratio	New PXRD?	Crystals?	Structure refined?
FA	3.02; 4.38	1/1	Yes	Yes	Yes
SA	4.21; 5.64	1/1	Yes	Yes	Yes
2,4-DHBA	3.11	1/1	Yes	Yes	Yes
DL-MAL	3.40; 5.11	1/1	Yes	No	No
SACC	1.94 [2]	1/1	Yes	Yes	Yes
L-ASP	1.99; 3.90	1/1	No	No	No
TRPTA	3.54; 4.34	1/1	Yes	Yes	Yes
CIT	3.13;	2/1	Yes	Yes	No[§]
	4.76; 6.40	3/1	Yes	Yes[‡]	No

the ΔpKa is used to predict the formation of salts, it is important to keep in mind that these pKa values are generally determined in water and that the use of organic solvents can have a significant impact on these. Therefore, although in water the difference in pKa between CFZ and L-ASP may be sufficient to form a salt, this may not be the case in MeCN or other organic solvents. Furthermore, the ΔpKa does not explain the absence of a new crystalline phase. Both molecules (CFZ and L-ASP) have functional groups that could still interact in the absence of proton transfer, and thus result in a cocrystal. The difficulty in obtaining new crystalline phase combining these two compounds could potentially be explained by an incompatibility of the molecules. Molecule geometry, as well as their size and shapes impact the crystal packing that can be formed and sometimes the inclusion of other molecules (solvent) can be necessary to form an efficient packing. Solvent inclusion may however be unsuitable in the pharmaceutical field (toxicity concerns, instability of solvated forms). Inclusion of solvent molecules and their implication in the crystal structure (in terms of H-bond or channel filling) have been illustrated in Chapter 3 and more specifically in Chapter 4. It is further reported that the crystalline environment (and so crystal packing) in itself can impact the ionization state in the solid-state.[4]

Based on the results presented in Chapter 3 drugs with carboxylic acid groups were selected to prepare drug-drug salts. Diclofenac and 4-aminosalicylic acid were selected as a NSAID that could be useful for host-directed therapy and as an anti-tubercular drug respectively. These two compounds were also selected because of their different aqueous solubility ($3.5 \pm 0.3 \cdot 10^{-3}$ g/L for DCF at 32 °C [5] [1] and 1.664 g/L for PAS [7] [2]) in order to allow an investigation of the effect of counter-ion solubility on CFZ aqueous solubility.

In Chapter 3 we observed hydrogen bond formation between carboxylate and a hydrogen bond donor that is not present on the CFZNH+ cation (i.e., with solvent molecule,

---

[1]its sodium salt has a reported aqueous solubility of 1.113 g/L [6]

[2]temperature is not stated but a solubility of 1.685 g/L is reported at 23 °C. Its sodium salt is reported to be around 100-fold (estimated from a graph) more soluble than its neutral form [8]. Because of PAS instability in water, only apparent solubility data are available.
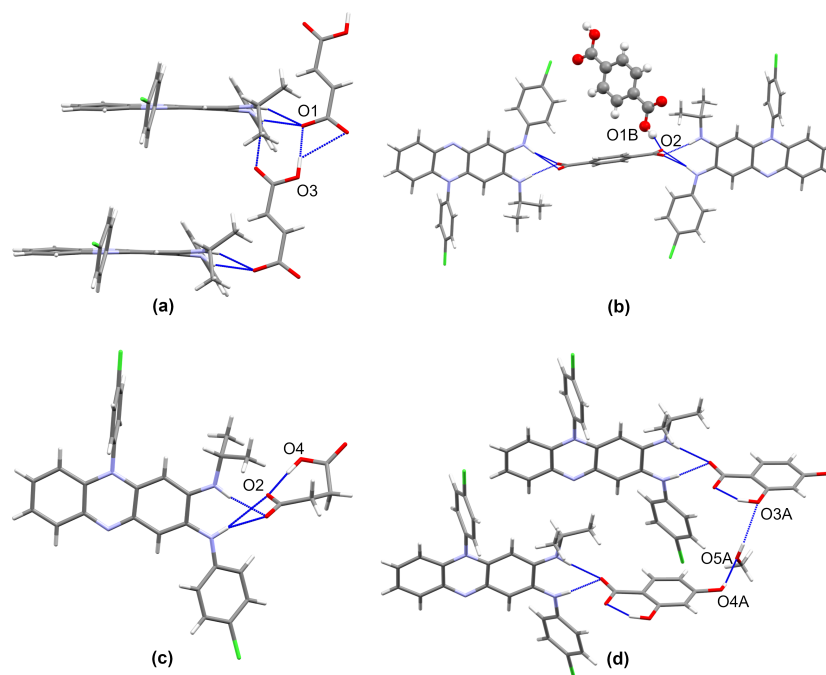
FIGURE 6.3: Hydrogen-bond involving carboxylate moiety in (a) CFZNH$^+$-FA$^-$ (1/1), (b) CFZNH$^+$-TRPTA^{2-}-TRPTA (1/0.5/0.5), (c) CFZNH$^+$-SA$^-$ (1/1) and (d) CFZNH$^+$-2,4-DHBA$^-$-MeOH (1/1/1) salts.

a second coformer molecule or intramolecular H-bond within the anion). This is a common feature of salts structures combining clofaziminium with a counterion bearing a carboxylate function and presented in Chapter 3. In the CFZNH$^+$-FA$^-$ salt, hemifumarate chains are stabilized by interactions of the O$-$H$\cdots$O$^-$ type. The salt cocrystal CFZNH$^+$-TRPTA^{2-}-TRPTA (1/0.5/0.5) also shows such interactions between the terephthalate anion and the terephthalic acid molecule. Intramolecular O$-$H$\cdots$O$^-$ hydrogen bonds are further observed in the structures of CFZNH$^+$-SA$^-$ and CFZNH$^+$-2,4-DHBA$^-$-MeOH salts (Figure 6.3). In the latter, the presence of a second H-bond donor (O-H group) results in the incorporation of a solvent molecule.

Carboxylate moiety of DCF$^-$ is also reported to strongly interact with solvent molecules through H-bonds [9]. In Chapter 4, dedicated to CFZ-DCF salts, we mainly studied factors affecting solvate formation. In this study we considered the protic or aprotic nature of the solvent, the possible solute-solvent interactions and solvent molecular volume.

First part of the work was dedicated to the crystallization of clofaziminium diclofenac salt in 1/1 molar ratio (Figure 6.4). Liquid-assisted grinding in presence of water did not allow salt formation and organic solvents were required. Solvent of relatively high molecular volume like salicylaldehyde (protic) or propiophenone (aprotic) could be accommodated in the structure. In both structures weak solvent-solute interactions were present, which could explain why such bulky solvents could be incorporated in the crystal (Figure 6.5).

FIGURE 6.4: Study of factors affecting solvate formation in CFZ-DCF salts: summary of performed experiments and associated results. LAG: liquid-assisted grinding, DMF: *N, N'*-dimethylformamide(78 Å^3 [10]), PPP: propiophenone (136 Å^3 [10]), SAL: salicylaldehyde (111 Å^3 [10]), MeCN: acetonitrile (46 Å^3 [10]), EtOH: ethanol (54 Å^3 [10]), MeOH: methanol (37 Å^3 [10]), EtOAc: ethyl acetate (91 Å^3 [10]), PEO: polyethylene glycol.
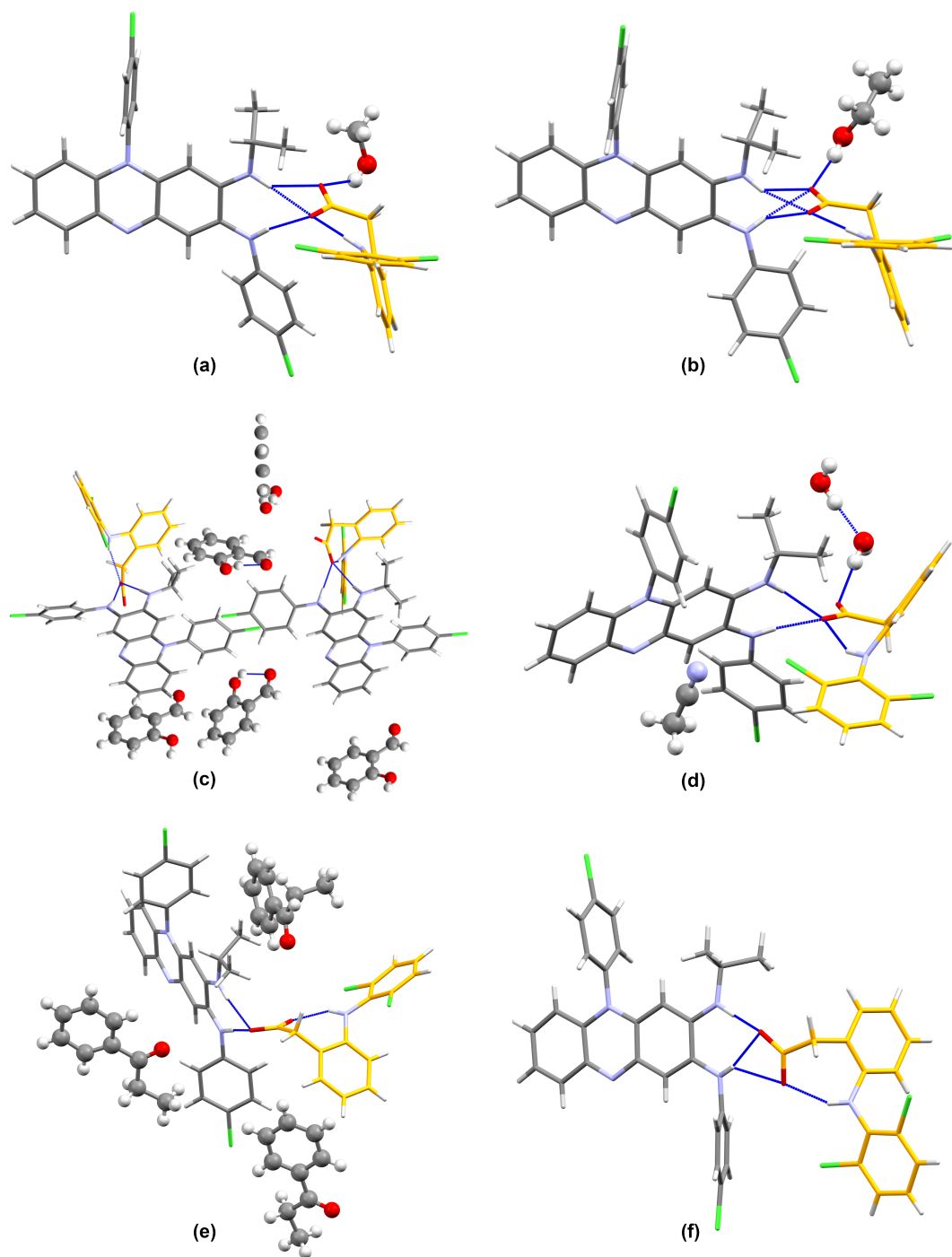
FIGURE 6.5: CFZNH$^+$-DCF$^-$ salts: (a) CFZNH$^+$-DCF$^-$-MeOH (1:1:0.741), (b) CFZNH$^+$-DCF$^-$-EtOH (1:1:1), (c) CFZNH$^+$-DCF$^-$-SAL-H$_2$O (4:4:9:1), (d) CFZNH$^+$-DCF$^-$MeCN-H$_2$O (1:1:1:2), (e) CFZNH$^+$-DCF$^-$PPP (2:2:5) and (f) CFZNH$^+$-DCF$^-$ (1:1). Solvent molecules are in ball and stick model and carbon of DCF$^-$ anion are in yellow.

We demonstrated that a rational solvent selection can yield crystallization of non-solvated salts even for compounds that do not allow efficient packing, as illustrated by

the lower packing coefficient (0.653) of the CFZNH$^+$-DCF$^-$ (1:1) salt in comparison to its solvated analogues. This non-solvated salt crystallized in ethyl acetate, an aprotic solvent having a calculated molecular volume of 91 Å^3.

As a second step, as diclofenac was shown to interact with protic compounds (solvent) and because DCF is a protic molecule, the CFZ to DCF molar ratio was successfully modulated from 1:1 to 1:2. In this second part of the work we firstly demonstrated that DCF molecule could successfully beat a protic solvent (EtOH) for the interaction site on diclofenac anion. Secondly, we showed that, despite their ability to be incorporated in the structure, solvents that do not present chemical function to strongly interact with the solute, and that have a low boiling point (in this study, MeCN or EtOAc), can be eliminated to yield non-solvated cocrystal of salt of CFZNH$^+$-DCF$^-$-DCF (Figure 6.6).
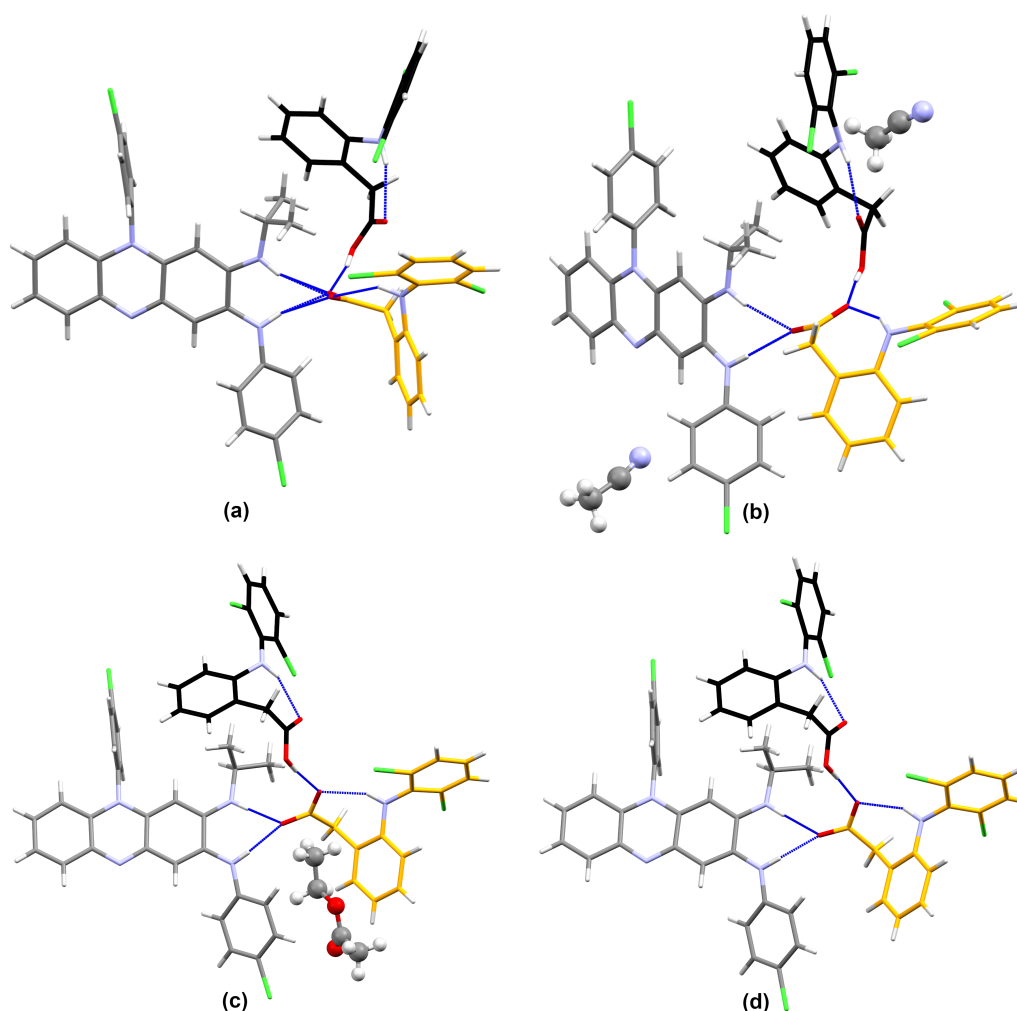
FIGURE 6.6: CFZNH$^+$-DCF$^-$-DCF cocrystal of salts: (a) CFZNH$^+$-DCF$^-$-DCF (1:1:1) polymorph I (obtained in EtOH), (b) CFZNH$^+$-DCF$^-$-DCF-MeCN (1:1:1:2), (c) CFZNH$^+$-DCF$^-$-DCF-EtOAc (1:1:1:1) and (d) CFZNH$^+$-DCF$^-$-DCF (1:1:1) polymorph II (from desolvation of MeCN or EtOAc solvates). Solvent molecules are in ball and stick model and carbon of DCF$^-$ anion and DCF molecule are in yellow and black respectively.

Finally, we demonstrated that unconventional solvents (short chain polymers) presenting good fluidity, high molecular flexibility and high molecular weight can be useful to avoid solvent inclusion during crystallization. This is illustrated by the crystallization of $CFZNH^+$-DCF^--DCF (1:1:1) polymorph II in PEO 200.

Regarding the aqueous solubility, only the salt $CFZNH^+$-DCF^--EtOH (1:1:1) allows the detection of an increase in the amount of solubilized CFZ. However, this increase remains small.

In order to determine whether the use of a more soluble counter-ion could increase the aqueous solubility of CFZ, in Chapter 5 we present salts combining it with another antituberculosis drug, PAS. Four forms have been identified and all resulted in an increase of the CFZ solubility in water (Figure 6.7). However, tests in simulated gastric fluid (FaSSGF) have shown that an anion exchange takes place in this media. None of the four identified polymorphs is deliquescent. However, a 3% water sorption occurs at 90% relative humidity for polymorph I.
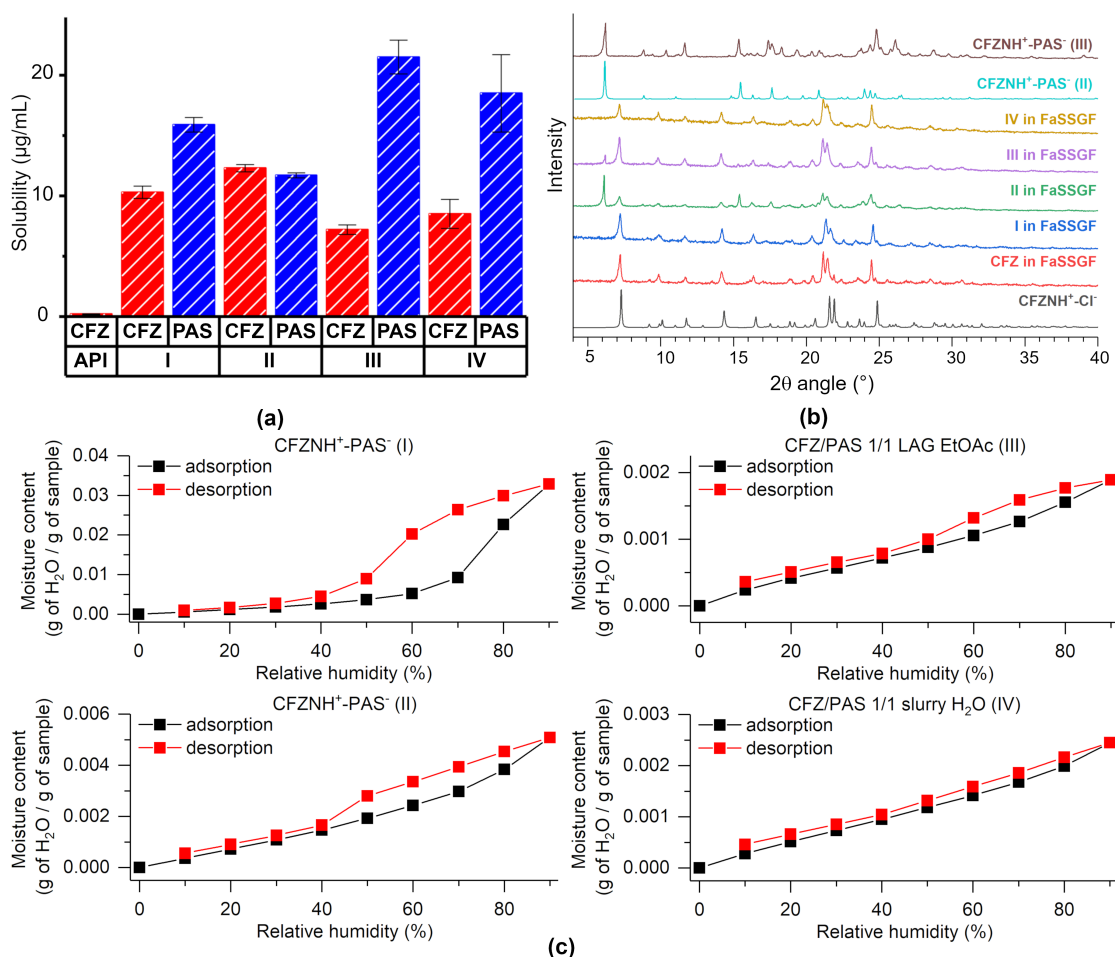
FIGURE 6.7: Solubility (a), stability in FaSSGF medium (b) and DVS analysis (c) of the four identified forms of $CFZNH^+$-PAS^- salt.

We were not able to grow single-crystals corresponding to forms II, III and IV. Forms II and III are obtained in EtOH and EtOAc, two solvents in which solvates of CFZ can also be formed (as previously demonstrated in Chapter 2). Under the crystallization conditions that we have used, it is these solvates that were preferentially formed. In this Chapter, we have shown the interest of powder diffraction in obtaining crystalline structures for those systems that prove difficult to crystallize. PXRD structure solution remains however complex. This is because a one-dimensional pattern is obtained by PXRD while SCXRD provides 3-dimensional data. Because of the one-dimensional nature of PXRD, some information is lost, which renders structure solution more difficult than from SCXRD data. Furthermore, the purity of the compound to be analyzed by PXRD, the sample preparation and the source and set-up of the diffraction apparatus have a very important effect on the quality of the collected data for structure resolution. Our laboratory PXRD data have allowed us to solve the structure of forms II and III. Structure II has been refined from these data, however data collected at the synchrotron would be useful to allow improvements in structure refinement of form II and are necessary for form III. Further study of the CFZ-PAS system could be considered. These perspectives and the difficulties that might be associated with them are discussed in the next section.

6.2 Perspectives

Solubility of salts is known to be dependent on solution pH. For a weakly basic drug like clofazimine, solubility is expected to increase at pH values below its pKa, because of protonation. As pH diminishes, solubility is expected to increase till a specific pH value, pH_{max}, at which the maximum solubility is reached. At pH values below pH_{max} the salt form of the basic drug is stable, and solubility is thus limited by the salt. When evaluating pH-solubility profile, solubility can decrease at very low pH because of common ion effect. Theoretical pH-solubility curve can be determined by the following equation: [11]

$$pH_{max} = pKa + log(\frac{S_{free\ base}}{S_{salt}}) \qquad (6.1)$$

The pH region above pH_{max} corresponds to the stability zone of the free base. In this pH range, salt disproportionation and precipitation of the free base occurs (Figure 6.8). pH-solubility curve determination is thus important to assess solid form stability, as the use of excipient with basic character can increase the pH of the formulation above pH_{max}, but also to understand/predict bioavailability of the drug. Determination of such a curve would thus be the next step in the characterization of CFZNH$^+$-PAS$^-$ salt. From solubility data, we can however expect a pH_{max} value around 4.5 - 5, the pH of the solution at the end of the solubility evaluation experiments. The amount of CFZ/CFZ-NH$^+$ and PAS/PAS$^-$ detected in solution does not match the expected 1/1 molar ratio. Indeed, HPLC data indicate that there is more PAS/PAS$^-$ in solution than CFZ/CFZ-NH$^+$, suggesting partial salt dissociation. PXRD analysis of the remaining solid phase does not indicate however clofazimine free base precipitation, which can be explained either by its amorphization or by the presence of a small amount of CFZ free base in comparison to the salt form. The

Theoretical pH-solubility curve for a basic compound
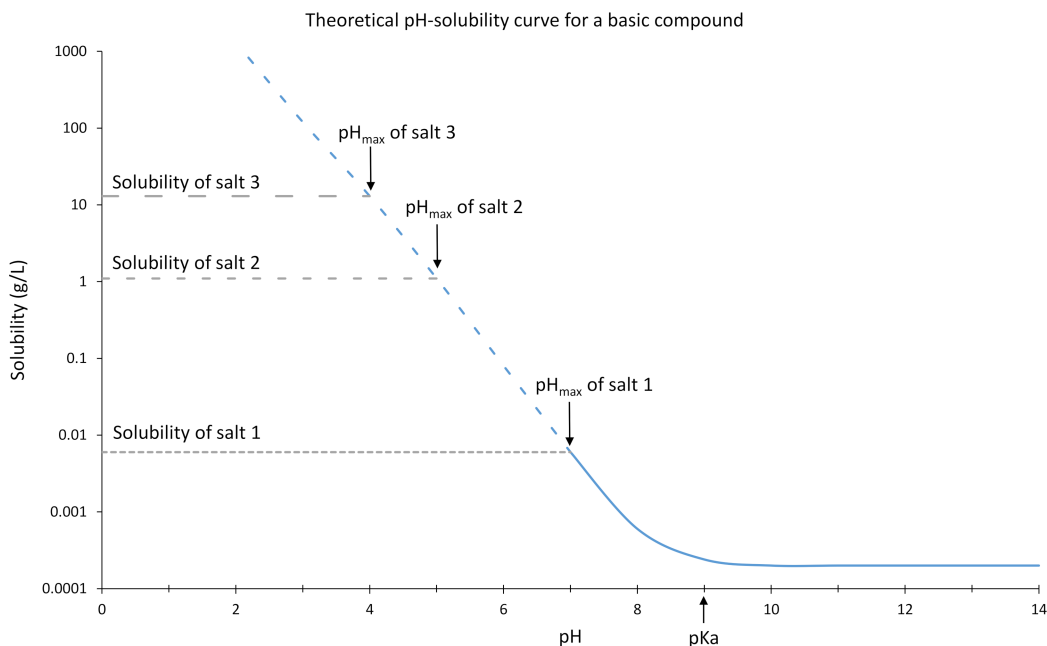
FIGURE 6.8: Theoretical pH-solubility curve for a basic compound (pKa of 9).

difficulty associated with salt preparation in order to improve solubility of a basic drug is that the more the salt (or the less the free base) is soluble and the lower is the pH_{max} (equation 6.1).

Immersion of $CFZNH^+$-PAS^- salt in simulated gastric fluid results in the precipitation of clofaziminium chloride, indicating anion exchange. Several studies have shown the possibility of maintaining supersaturation with polymers [12, 13, 14]. However, this type of approach has been investigated by Bannigan *et al.* and was not successful with clofaziminium salts [15]. Because of pH-solubility dependence and anion exchange, oral administration of clofaziminium salts to improve CFZ bioavailability may remain difficult.

Two alternative administration routes for clofaziminium salts are intravenous injection or inhalation. CFZ formulation, as nanosuspension or clofaziminium chloride microcrystals, have already been studied for intravenous injection. [16, 17] Murashov *et al.* have further shown that intravenous administration of clofaziminium chloride prevents skin pigmentation associated with oral administration of CFZ. [17] A difficulty is however anticipated as injection vehicles require isotonicity. This is often achieved by adding NaCl in the medium, which may cause again anion exchange and clofaziminium chloride precipitation. Another isotonic injection vehicle is a solution of glucose 5%. Solubility and stability evaluation of $CFZNH^+$-PAS^- salt in such medium would thus be interesting. Another important aspect to consider is the buffering capacity of blood which may cause CFZ precipitation at the injection site if the simultaneous process of dilution in the blood is not sufficient. In such a case, particular formulation may be prepared. For example, solithromycin precipitation at the injection site could be circumvented by improving the

buffering capacity of the injection vehicle. This was performed through the addition of aspartic and glutaric acids as well as histidine in the vehicle. The latter amino acid has the particularity of improving buffering capacity around pH 6. [18]

Several CFZ formulation for the inhalation routes have also been reported either as dry powder (with leucine and/or modified β-cyclodextrins as excipients or even without excipients) or as suspensions. [19, 20, 21, 22] Because of the above mentioned difficulties, the most appropriate formulation for CFZ salts inhalation would probably be as a dry powder. Such administration route would require particle size below 5 µm or even under 3 µm to reach the alveolar macrophages. [20] In this context, it would be particularly interesting to study the effect of ball milling on particle size distribution. Finally, other techniques for salt preparation could also be considered, such as spray drying, a technique allowing the control of particle size and shape.

Bibliography

[1] W. M. Haynes. *Handbook of Chemistry and Physics*. Boca Raton: CRC Press, Boca Raton: CRC Press, 95th edition, 2014.

[2] R. C. Rowe, P. J. Sheskey, and S. C. Owen. *Handbook of Pharmaceutical Excipients*. Pharmaceutical Press and American Pharmacists Association, London/Philadelphia /Washigton DC, 5th edition, 2006.

[3] R. K. Keswani, J. Baik, L. Yeomans, C. Hitzman, A. M. Johnson, A. S. Pawate, P. J. A. Kenis, N. Rodriguez-Hornedo, K. A. Stringer, and G. R. Rosania. Chemical Analysis of Drug Biocrystals: A Role for Counterion Transport Pathways in Intracellular Drug Disposition. *Molecular Pharmaceutics*, 12(7):2528–2536, 2015.

[4] S. L. Childs, G. P. Stahly, and A. Park. The salt- cocrystal continuum: the influence of crystal structure on ionization state. *Molecular pharmaceutics*, 4(3):323–338, 2007.

[5] J. A. Cordero, L. Alarcon, E. Escribano, R. Obach, and J. Domenech. A comparative study of the transdermal penetration of a series of nonsteroidal antiinflammatory drugs. *Journal of pharmaceutical sciences*, 86(4):503–508, 1997.

[6] C. C. P. da Silva, B. C. D. Owoyemi, B. R. Alvarenga-Jr, N. Alvarez, J. Ellena, and R. L. Carneiro. Synthesis and solid-state characterization of diclofenac imidazolium monohydrate: an imidazolium pharmaceutical ionic liquid. *CrystEngComm*, 22(32):5345–5354, 2020.

[7] S. H. Yalkowsky, Y. He, and P. Jain. *Handbook of aqueous solubility data*. CRC press, 2016.

[8] R. T. Forbes, P. York, and J. R. Davidson. Dissolution kinetics and solubilities of p-aminosalicylic acid and its salts. *International journal of pharmaceutics*, 126(1-2):199–208, 1995.

[9] W. Sun, L. Zuo, T. Zhao, Z. Zhu, and G. Shan. Five solvates of a multicomponent pharmaceutical salt formed by berberine and diclofenac. *Acta Crystallographica Section C: Structural Chemistry*, 75(12):1644–1651, 2019.

[10] M. Cheminformatics. Molinspiration [internet], accessed on 21-02-2020.

[11] P. H. Stahl, B. Sutter, A. Grandeury, and M. Mutz. Alternative solid forms: Salts. In *Polymorphism in the Pharmaceutical Industry: Solid Form and Drug Development*, pages 31–59. Wiley-VCH Verlag GmbH & Co. KGaA, 2019.

[12] S. L. Raghavan, A. Trividic, A. F. Davis, and J. Hadgraft. Crystallization of hydrocortisone acetate: influence of polymers. *International journal of pharmaceutics*, 212(2):213–221, 2001.

[13] D. B. Warren, H. Benameur, C. J. H. Porter, and C. W. Pouton. Using polymeric precipitation inhibitors to improve the absorption of poorly water-soluble drugs: A mechanistic basis for utility. *Journal of drug targeting*, 18(10):704–731, 2010.

[14] L. I. Mosquera-Giraldo, C. H. Borca, X. Meng, K. J. Edgar, L. V. Slipchenko, and L. S. Taylor. Mechanistic design of chemically diverse polymers with applications in oral drug delivery. *Biomacromolecules*, 17(11):3659–3671, 2016.

[15] P. Bannigan, V. Verma, and S. P. Hudson. Overcoming the common ion effect for weakly basic drugs: inhibiting the crystallization of clofazimine hydrochloride in simulated gastrointestinal media. *Crystal Growth & Design*, 19(3):1599–1609, 2019.

[16] K. Peters, S. Leitzke, J. Diederichs, K. Borner, H. Hahn, R. H. Müller, and S. Ehlers. Preparation of a clofazimine nanosuspension for intravenous use and evaluation of its therapeutic efficacy in murine mycobacterium avium infection. *Journal of Antimicrobial Chemotherapy*, 45(1):77–83, 2000.

[17] M. D. Murashov, J. Diaz-Espinosa, V. LaLone, J. W. Y. Tan, R. Laza, X. Wang, K. A. Stringer, and G. R. Rosania. Synthesis and characterization of a biomimetic formulation of clofazimine hydrochloride microcrystals for parenteral administration. *Pharmaceutics*, 10(4):238, 2018.

[18] D. Evans, S. Yalkowsky, S. Wu, D. Pereira, and P. Fernandes. Overcoming the challenges of low drug solubility in the intravenous formulation of solithromycin. *Journal of pharmaceutical sciences*, 107(1):412–418, 2018.

[19] R. K. Verma, W. A. Germishuizen, M. P. Motheo, A. K. Agrawal, A. K. Singh, M. Mohan, P. Gupta, U. D. Gupta, M. Cholo, R. Anderson, et al. Inhaled microparticles containing clofazimine are efficacious in treatment of experimental tuberculosis in mice. *Antimicrobial agents and chemotherapy*, 57(2):1050–1052, 2013.

[20] A. D. Brunaugh, S. U. Jan, S. Ferrati, and H. D. C. Smyth. Excipient-free pulmonary delivery and macrophage targeting of clofazimine via air jet micronization. *Molecular pharmaceutics*, 14(11):4019–4031, 2017.

[21] B. Banaschewski, D. Verma, L. J. Pennings, M. Zimmerman, Q. Ye, J. Gadawa, V. Dartois, D. Ordway, J. van Ingen, S. Ufer, et al. Clofazimine inhalation suspension for the aerosol treatment of pulmonary nontuberculous mycobacterial infections. *Journal of Cystic Fibrosis*, 18(5):714–720, 2019.

[22] H. Smyth and A. Brunaugh. Inhalable composition of clofazimine and methods of use thereof, September 24 2020. US Patent App. 16/652,904.

Appendices

List of publications

Marx, S., Bodart, L., Tumanov, N. & Wouters, J. (2019), 'Design and synthesis of a new soluble β-carboline derivative for preclinical study by intravenous injection', *International Journal of Molecular Sciences* **20**, 1491.

Bodart, L., Tumanov, N. & Wouters, J. (2019), 'Structural variety of clofaziminium salts: effect of the counter-ion on clofaziminium conformation and crystal packing', *Acta Crystallographica Section B: Structural Science, Crystal Engineering and Materials* **75**, 674-686.

Mambourg, K., Bodart, L., Tumanov, N., Lanners, S. & Wouters, J. (2020), 'Synthesis, crystal structure and conformational analysis of an unexpected [1,5]dithiocine product of aminopyridine and thiovanillin', *Acta Crystallographica Section C: Structural Chemistry* **76**, 205-211.

Bodart, L., Derlet, A., Buol, X., Leyssens, T., Tumanov, N. & Wouters, J. (2020), 'Combining Two Antitubercular Drugs, Clofazimine and 4-Aminosalicylic Acid, in Order to Improve Clofazimine Aqueous Solubility and 4-Aminosalicylic Acid Thermal Stability', *Journal of Pharmaceutical Sciences* **109**, 3645-3652.

Bodart, L. Prinzo, M., Derlet, A. Tumanov, N. & Wouters, J. (2021), 'Taking advantage of solvate formation to modulate drug-drug ratio in clofaziminium diclofenac salts', *CrystEngComm* **23**, 185-201.

Appendix A

To: Structural variety of clofaziminium salts: effect of the counter-ion on clofaziminium conformation and crystal packing†

Supporting information to chapter 3

TABLE A.1: Published and new structures implying clofazimine or clofaziminium.

Structure	Space group	a, b, c (Å); α, β, γ (°); V (Å^3)	Z	CSD refcode	Refs
CFZ (I)	$P\bar{1}$	10.507(4), 12.852(12), 9.601(2); 95.95(4), 97.22(1), 69.73(6); 1204.0(13)	2	DAKXUI01	[1]
CFZ (II)	$P2_1/a$	7.788(14), 22.960(13), 13.362(7); 90, 98.58(12), 90; 2363(5)	4	DAKXUI	[1]
CFZ (III)	$Pbca$	23.2417(15), 8.1118(5), 25.5891(16); 90, 90, 90;4824.4(5)	8	DAKXUI03	[1]
CFZ (IV)	$P2_1/c$	12.9083, 23.3031, 8.3092; 90, 95.1697, 90; 2489.27	4	DAKXUI02	[1]
CFZ-DMF	$P\bar{1}$	12.435(4), 12.807(5), 10.424(4); 111.74(3), 112.37(3), 90.90(3); 1402.0(10)	2	CEKTER	[2]
CFZ-(CH$_3$)$_2$CO (1:1)	$P\bar{1}$	10.0842(13), 12.0695(16), 12.6613(16); 75.278(2), 66.588(2), 69.051(2); 1309.3(3)	2	GESHIX	[3]
CFZ-NH$^+$-H$_2$PO$_4^-$-H$_2$O (1:1:0.25)	$P\bar{1}$	14.3064 (9), 15.1345 (9), 27.9096 (17); 96.495 (2), 92.025 (2), 110.640 (2); 5600.4(6)	8	/	[4]
CFZ-NH$^+$-HSO$_4^-$-MeOH (1:1:1)	$C2/c$	18.9579(11), 15.4754(9), 20.0404(12); 90, 100.360(2), 90; 5783.6(6)	8	/	[4]
CFZ-NH$^+$-MSA$^-$-H$_2$O (1:1:1)	$P\bar{1}$	9.5945(12), 11.0456(12), 14.4628(11); 110.173(9), 95.859(9), 94.929(9); 1419.1(3)	2	GESHET	[3]
CFZ-NH$^+$-2,4DHBA$^-$-MeOH (1:1:1)	$P\bar{1}$	9.4861(4), 12.5322(5), 15.3641(5); 98.415(3), 103.379(3), 110.450(4); 1612.40(11)	2	/	This work
CFZ-NH$^+$-SACC$^-$-MeCN (1:1:1.4)	$P\bar{1}$	7.9970(3), 13.5824(3), 16.6638(7); 80.214(3), 80.034(4), 83.036(3); 1748.87(11)	2	/	This work
CFZ-NH$^+$-TRPTA^{2-}-TRPTA-solvent (1:0.5:0.5:x)	$P\bar{1}$	11.7990(4), 12.0736(4), 14.6803(5); 72.472(3), 80.688(3), 72.030(3); 1891.44(12)	2	/	This work
CFZ-NH$^+$-Cl$^-$-H$_2$O (1:1:0.13)	$Pbca$	10.2664(4), 19.8275(7), 24.1558(9); 90, 90, 90; 4917.1(3)	8	RAFHUE	[5]
CFZ-NH$^+$-Cl$^-$ (1:1)	$Pbca$	10.74739(15), 19.1763(4), 24.2362(3); 90, 90, 90; 4994.96(14)	8	LABQUD	[6]
CFZ-NH$^+$-MSA$^-$ (1:1)	$P2_1/n$	10.0229 (18), 17.772 (3), 15.592 (3); 90, 103.028 (4), 90; 2705.9(8)	4	GESGAO	[3]
CFZ-NH$^+$-MLE$^-$ (1:1)	$P2_1/n$	11.2549(19), 20.816(3), 12.519(2); 90, 103.413(17), 90; 2853.0(8)	4	GESHAP	[3]
CFZ-NH$^+$-INA$^-$ (1:1)	$P\bar{1}$	9.8153(9), 12.1738(10), 15.2122(10); 72.455(7), 77.844(7), 66.479(8); 1580.7(2)	2	GESGES	[3]
CFZ-NH$^+$-NA$^-$ (1:1)	$P\bar{1}$	11.6032(13), 15.361(2), 18.733(3); 111.337(14), 91.280(11), 109.295(11); 2896.5(8)	4	GESGIW	[3]
CFZ-NH$^+$-MLN$^-$ (1:1)	$P\bar{1}$	9.8401(8), 12.4069(10), 13.0576(10); 74.129(1), 70.300(1), 67.520(1); 1367.50(19)	2	GESGOC	[3]
CFZ-NH$^+$-SCL$^-$ (1:1)	$P\bar{1}$	10.8702(6), 11.2066(6), 13.8272(8); 82.354(5), 88.960(5), 63.492(6); 1492.31(17)	2	GESGUI	[3]
CFZ-NH$^+$-CIT$^-$ (1:1)	$P\bar{1}$	14.7409(6), 15.8211(6), 16.2514(7); 71.928(1), 63.041(1), 70.747(2); 3130.6(2)	4	/	[4]
CFZ-NH$^+$-TRPTA^{2-}-TRPTA (1:0.5:0.5)	$P\bar{1}$	10.4028 (3), 10.8454 (3), 15.4229 (5); 71.183 (3), 73.984 (3), 76.148 (2); 1561.33 (9)	2	/	This work
CFZ-NH$^+$-SACC$^-$ (1:1)	$P\bar{1}$	8.2115 (7), 13.5327 (12), 14.325 (3); 89.04 (1), 88.864 (10), 83.781 (7); 2806.65(6)	2	/	This work
CFZ-NH$^+$-FA$^-$ (1:1)	$P2_1/c$	7.47882(9), 26.0041(3), 14.78241(16); 90, 102.5075(12), 90; 2806.65(6)	4	/	This work
CFZ-NH$^+$-SA$^-$ (1:1)	$P\bar{1}$	10.6455(6), 12.2850(5), 12.8049(8); 90.076 4), 113.218(6), 108.289(4); 1446.18(15)	2	/	This work

TABLE A.2: Selected hydrogen-bond parameters.

$D - H \cdots A$	$D - H$ (Å)	$H \cdots A$ (Å)	$D \cdots A$ (Å)	$D - H \cdots A$ (°)
CFZ-NH$^+$-FA$^-$ (1:1)				
$N3 - H3 \cdots O2$	0.83 (3)	2.48 (3)	3.003 (3)	122 (2)
$N3 - H3 \cdots O3^-$	0.83 (3)	2.26 (3)	3.040 (3)	156 (3)
$N4^+ - H4 \cdots O3^-$	0.84 (3)	2.17 (3)	2.972 (2)	160 (2)
$O1 - H1A \cdots O3^-$	0.94 (4)	1.62 (4)	2.550 (2)	176 (3)
CFZ-NH$^+$-SA$^-$ (1:1)				
$N4^+ - H4 \cdots O1^-$	0.85 (3)	1.98 (3)	2.824 (3)	170 (2)
$N3 - H3 \cdots O1^-$	0.83 (3)	2.11 (2)	2.871 (3)	152 (3)
$O4 - H4B \cdots O2^-$	0.94 (3)	1.56 (3)	2.497 (3)	177 (3)
$C15 - H15 \cdots O1^-$	0.93	2.31	3.233 (3)	174.6
$C29B - H29D \cdots Cl2$	0.97	2.80	3.416 (14)	122.2
CFZ-NH$^+$-SACC$^-$-MeCN (1:1:1.4)				
$N3 - H3 \cdots N5^-$	0.87(3)	2.03(3)	2.893(3)	170(3)
$N4^+ - H4N \cdots O3$	0.85(4)	2.45(4)	3.264(3)	160(3)
$C33 - H33 \cdots O3$	0.95	2.45	3.283(3)	146.0
$C24 - H24 \cdots O1$	0.95	2.42	3.314(3)	157.3
CFZ-NH$^+$-SACC$^-$ (1:1)				
$N4^+ - H4 \cdots N5^-$	0.79 (7)	2.22 (8)	2.99 (2)	163 (8)
$N4^+ - H4 \cdots N5A^-$	0.79 (7)	2.25 (8)	3.04 (2)	174 (8)
$N3 - H3 \cdots N5^-$	1.05 (7)	1.78 (7)	2.84 (2)	178 (5)
$N3 - H3 \cdots N5A^-$	1.05 (7)	1.88 (7)	2.92 (2)	165 (5)
$C24 - H24 \cdots O1$	0.93	2.48	3.40 (2)	167.9
$C26 - H26C \cdots O2$	0.96	2.55	3.49 (2)	166.1
$C26 - H26C \cdots O2A$	0.96	2.45	3.370 (18)	160.9
CFZ-NH$^+$-2,4DHBA$^-$-MeOH (1:1:1)				
$N4^+ - H4N \cdots O1A^-$	0.853 (19)	2.00 (2)	2.852 (10)	174.9 (17)
$N4^+ - H4N \cdots O1B^-$	0.853 (19)	2.00 (3)	2.854 (18)	176.2 (18)
$N3 - H3N \cdots O1A^-$	0.89 (2)	1.88 (3)	2.743 (13)	164 (2)
$N3 - H3N \cdots O1B^-$	0.89 (2)	1.86 (3)	2.73 (2)	169 (2)
$O3A - H3OA \cdots O2A^-$	1.02	1.66	2.556 (15)	144.5
$O4A - H4OA \cdots O5A$	0.82	2.02	2.786 (10)	155.2
$O5A - H5OA \cdots O3A$	0.82	2.39	3.192 (12)	166.6
$O3B - H3OB \cdots O2B^-$	1.02	1.42	2.33 (3)	146.4
$O4B - H4OB \cdots O5B$	0.82	2.10	2.86 (2)	154.5
$O5B - H5OB \cdots O4B$	0.82	2.17	2.64 (2)	116.1
$C14 - H14 \cdots O1A^-$	0.93	2.45	3.346 (11)	161.4
$C14 - H14 \cdots O1B^-$	0.93	2.57	3.467 (19)	162.1
$C23 - H23 \cdots O4A$	0.93	2.50	3.207 (8)	132.8
$C23 - H23 \cdots O4B$	0.93	2.41	3.204 (16)	143.3
CFZ-NH$^+$-TRPTA^{2-}-TRPTA-solvent (1:0.5:0.5:x)				
$N4^+ - H4 \cdots O1^-$	0.841 (16)	2.071 (16)	2.8985 (13)	167.7 (15)
$N3 - H3 \cdots O1^-$	0.866 (18)	1.947 (18)	2.7772 (14)	160.1 (16)
$O1A - H3B \cdots O1^-$	0.91 (2)	1.64 (2)	2.5442 (13)	171 (2)
$C15 - H15 \cdots O2^-$	0.95	2.44	3.3792 (17)	170.8
CFZ-NH$^+$-TRPTA^{2-}-TRPTA (1:0.5:0.5)				
$N4^+ - H4 \cdots O1^-$	0.86 (2)	1.98 (2)	2.8363 (19)	172.9 (18)
$N3 - H3 \cdots O2^-$	0.85 (2)	2.17 (2)	2.976 (2)	159 (2)
$N3 - H3 \cdots O1^-$	0.85 (2)	2.30 (2)	2.996 (2)	140 (2)
$O1B - H3B \cdots O2^-$	0.95 (3)	1.66 (3)	2.5936 (19)	170 (3)
$C14 - H14 \cdots O1^-$	0.93	2.40	3.276 (2)	156.7
$C20 - H20 \cdots O2^-$	0.93	2.54	3.307 (2)	139.7
$C26 - H26C \cdots O2B$	0.96	2.55	3.502 (3)	171.5

TABLE A.3: **T1**, **T2**, **T3**, **T4**, and **T5** torsions angles, C9-N4-C25 angle, and H-H distance between N3-H and N4-H in clofazimine/clofaziminium in published and new structures as well as in optimized structures. Data from structures presented in this work are written in italic. A, B, C and D annotations indicate different molecules in the asymmetric unit while 1 and 2 superscripts indicate the two positions observed in case of disorder. NA means that hydrogen is not present in cif file.

Structure	T1 (°) (C8-N3-C19-C20)	T2 (°) (C9-N4-C25-C27)	T3 (°) (C12-N1-C13-C18)	T4 (°) (H-N4-C9-C8)	T5 (°) (H-N3-C8-C9)	Angle C9-N4-C25 (°)	H-H distance between N3-H and N4-H (Å)
CFZ (I)	154.9(7)	-154.8(8)	92.1(8)	/	-9.9	119.2(5)	/
CFZ (II)	149.4(3)	-157.1(3)	82.1(3)	/	-13(2)	120.7(2)	/
CFZ (III)	-163.1(3)	-152.5(2)	87.8(3)	/	9.6(4)	120.4(2)	/
CFZ (IV)	-146.83	-99.94	110.71	/	0.72	120.71	/
CFZ-DMF	-149.90	-138.45	99.44	/	NA	118.18	/
CFZ-(CH$_3$)$_2$CO (1:1)	-146.4(2)	-159.5(2)	97.0(2)	/	5.1	119.2(2)	/
CFZ-NH$^+$-H$_2$PO$_4^-$-H$_2$O (1:1:0.25)	A: 133.8(5) B:-133.6(5) C: 135.2(6) D: 130.7(5)	A: -78.2(5) B: -156.3(4) C: -95.9(6) D: -76.3(7)	A: 63.6(5) B: 93.3(5) C: 82.9(7) D: 91.1(7)	A:-14.4 B: -2.1 C: 1.1 D:-11.3	A: 2.4 B: -1.9 C: -2.1 D: 3.9	A: 125.3(3) B: 124.1(4) C: 127.6(5) D: 125.8(4)	A: 1.8565 B: 1.7934 C: 1.7794 D: 1.8702
CFZ-NH$^+$-HSO$_4^-$-MeOH (1:1:1)	143.4(2)	-78.8(3)	81.1(3)	1.3	-14.2	124.7(2)	1.8226
CFZ-NH$^+$-MSA$^-$-H$_2$O (1:1:1)	174.9(2)	-154.3(3)	95.0(3)	-12(2)	-10.(2)	125.2(2)	1.83(4)
CFZ-NH$^+$-2,4DHBA$^-$-MeOH (1:1:1)	-142.18(15)	-169.69(14)	106.25(15)	-1(1)	13(2)	126.25(13)	1.83(3)
CFZ-NH$^+$-SACC$^-$-MeCN (1:1:1.4)	-135.7(2)	-144.6(7) [1] -69.3(14)) [2]	91(3) [1] 99(3) [2]	-0(3)	38(2)	122.8(7)[1] 129.1(8)[2]	2.01(4)
CFZ-NH$^+$-SACC$^-$ (1:1)	-137.0 (6)	-158.4 (6)	89.7 (7)	-12(7)	31 (4)	126.9 (6)	1.9 (1)
CFZ-NH$^+$-TRPTA^{2-}-TRPTA-solvent (1:0.5:0.5:x)	143.09(13)	-150.77(14)	83.78(14)	-3(1)	-28(1)	125.53(10)	1.91(3)
CFZ-NH$^+$-TRPTA^{2-}-TRPTA (1:0.5:0.5)	-148.7(2)	-166.14(17)	97.32(18)	7(2)	24(2)	124.72(14)	1.97(3)
CFZ-NH$^+$-Cl$^-$-H$_2$O (1:1:0.13)	-149.1(2)	-92.2(3) [1] -137(1) [2]	76.0(2)	13(2)	11(2)	125.7(2) [1] 118.2(5) [2]	2.04(3)
CFZ-NH$^+$-Cl$^-$ (1:1)	145.9(9)	-149(1)	97(1)	-13(5)	-10(10)	123(1)	1.7(2)
CFZ-NH$^+$-MSA$^-$ (1:1)	146.5(3)	-71.6(4)	85.4(4)	2(2)	-19(2)	125.9(3)	1.83(4)
CFZ-NH$^+$-MLE$^-$ (1:1)	-147.2(5)	-100.9(6)	92.8(5)	7(4)	25(3)	125.0(4)	1.98(6)
CFZ-NH$^+$-INA$^-$ (1:1)	-138.5(4)	-168.5(3)	101.2(4)	-6(2)	21(2)	125.6(3)	1.72(4)
CFZ-NH$^+$-NA$^-$ (1:1)	A: 142.3(4) B: 150.3(4)	A: -75.8(5) B: -71.0(5)	A: 77.1(4) B: 81.4(4)	A:-10.8 B: -6.2	A: -5.5 B: -5	A: 110.5(3) B: 124.3(3)	A: 1.7938 B: 1.7956
CFZ-NH$^+$-MLN$^-$ (1:1)	-145.9(3)	-158.0(3)	102.1(3)	1(2)	32.86	125.0(2)	1.99(4)
CFZ-NH$^+$-SCL$^-$ (1:1)	175.5(2)	-153.5(3)	97.9(2)	-8(2)	-3(2)	125.1(2)	1.92(4)
CFZ-NH$^+$-CIT$^-$ (1:1)	A: 145.9(3) B: -133.7(3)	A: -80.1(3) B:-160.6(3)	A: 89.6(3) B:108.1(3)	A: 5.0 B: 7.6	A:-10.0 B: 0.3	A: 125.6(2) B: 110.8(2)	A: 1.8315 B: 1.8583
CFZ-NH$^+$-FA$^-$ (1:1)	-124.4(2)	-146.0(3)	76.1(2)	-8(2)	34(2)	126.02(18)	1.96(4)
CFZ-NH$^+$-SA$^-$ (1:1)	153.0(2)	-83.6(3)	86.3(2)	0(2)	-16(2)	125.5(2)	1.88(4)
CFZ optimized	-151.32	-156.44	91.63	/	5.62	121.01	/
CFZ-NH$^+$ optimized	-122.86	-159.84	94.07	15.40	51.35	125.71	2.106
CFZ-NH$^+$-Cl$^-$ (1:1) optimized	147.26	-151.56	94.71	-3.41	-11.34	125.56	1.793

TABLE A.4: Atomic coordinates of optimized clofazimine (DAKXUI03).
E (RM06): -2180.82541943 Hartree

center number	atomic number	atomic type	X (Å)	Y (Å)	Z (Å)
1	17	0	8.542442	0.704357	0.209214
2	17	0	-6.9481	-2.29036	0.301462
3	7	0	-2.14619	1.164776	-0.00064
4	7	0	0.140856	2.748417	-0.17926
5	7	0	2.923027	-1.14088	-0.07092
6	1	0	2.783777	-2.15045	-0.13693
7	6	0	-2.28458	2.547588	-0.08207
8	7	0	0.835378	-2.65978	-0.00311
9	6	0	-1.1053	3.314653	-0.17091
10	6	0	-3.85825	0.03082	1.308589
11	1	0	-3.3956	0.426814	2.209955
12	6	0	1.547901	0.863029	-0.11714
13	1	0	2.373254	1.560195	-0.21463
14	6	0	-0.7402	-0.79419	0.042316
15	1	0	-1.60785	-1.44215	0.100702
16	6	0	0.561329	-1.40182	0.001783
17	6	0	-4.9809	-0.77869	1.383768
18	1	0	-5.42362	-1.03208	2.34267
19	6	0	0.249921	1.451792	-0.10542
20	6	0	-2.44695	5.326122	-0.25025
21	1	0	-2.51705	6.408721	-0.31543
22	6	0	-3.31285	0.341952	0.072493
23	6	0	-3.53125	3.17529	-0.08004
24	1	0	-4.44065	2.583892	-0.01418
25	6	0	1.735017	-0.48293	-0.05268
26	6	0	6.878357	0.175384	0.133305
27	6	0	4.226038	-0.65292	-0.00281
28	6	0	5.89341	0.914076	0.766634
29	1	0	6.161099	1.809141	1.321564
30	6	0	-1.21549	4.708614	-0.25385
31	1	0	-0.28766	5.271267	-0.32133
32	6	0	-0.90753	0.555862	-0.01269
33	6	0	-5.53832	-1.26958	0.212642
34	6	0	-3.87643	-0.15388	-1.09399
35	1	0	-3.42727	0.09907	-2.05206
36	6	0	-4.9974	-0.96589	-1.0281
37	1	0	-5.45329	-1.36314	-1.93033
38	6	0	-0.2188	-3.65343	0.025556
39	1	0	-1.04819	-3.32944	0.68098
40	6	0	5.238034	-1.38892	-0.62419
41	1	0	4.975503	-2.28888	-1.17732
42	6	0	-3.60499	4.553147	-0.1635
43	1	0	-4.58073	5.032876	-0.16135
44	6	0	4.573377	0.499034	0.704977
45	1	0	3.814891	1.056259	1.245423
46	6	0	6.557893	-0.98367	-0.55595
47	1	0	7.339542	-1.55883	-1.04455
48	6	0	-0.76555	-3.87152	-1.37932
49	1	0	-1.20876	-2.95781	-1.79154
50	1	0	0.045264	-4.18105	-2.04986
51	1	0	-1.531	-4.65621	-1.38624
52	6	0	0.348687	-4.94272	0.588143
53	1	0	1.160856	-5.30783	-0.05236
54	1	0	0.759522	-4.78602	1.590701
55	1	0	-0.4186	-5.7233	0.648061

197

Appendix A

center number	atomic number	atomic type	X (Å)	Y (Å)	Z (Å)
1	17	0	7.056535	-1.83325	-0.10889
2	17	0	-8.29076	0.831069	-0.25532
3	7	0	1.986052	1.21845	0.016537
4	7	0	-0.41207	2.611798	0.094537
5	7	0	-2.87044	-1.49724	0.280427
6	1	0	-2.8273	-2.2254	0.987232
7	7	0	-0.57662	-2.84764	-0.11481
8	1	0	-1.50507	-3.19261	-0.33617
9	6	0	3.202897	3.331344	0.012594
10	1	0	4.1611	2.821471	-0.00925
11	6	0	3.14538	4.704976	0.027658
12	1	0	4.072743	5.271274	0.015633
13	6	0	1.917066	5.389851	0.05962
14	1	0	1.906057	6.475633	0.069725
15	6	0	0.745516	4.685901	0.080842
16	1	0	-0.22634	5.17041	0.109056
17	6	0	0.759909	3.274028	0.06823
18	6	0	-0.40737	1.298616	0.083144
19	6	0	-1.64479	0.601186	0.163243
20	1	0	-2.54262	1.205452	0.256108
21	6	0	-1.69997	-0.75572	0.171512
22	6	0	-0.46629	-1.51892	0.014856
23	6	0	0.762381	-0.86201	0.002342
24	1	0	1.678887	-1.43236	-0.08841
25	6	0	0.813821	0.524543	0.038123
26	6	0	2.00929	2.598854	0.029963
27	6	0	3.230027	0.488114	-0.01457
28	6	0	3.827216	0.216216	-1.23502
29	1	0	3.366348	0.567761	-2.15574
30	6	0	5.012574	-0.50068	-1.26552
31	1	0	5.502925	-0.72341	-2.20855
32	6	0	5.576774	-0.935	-0.07274
33	6	0	4.976537	-0.65873	1.149448
34	1	0	5.440162	-1.00187	2.06956
35	6	0	3.792289	0.059804	1.17759
36	1	0	3.30424	0.290501	2.122241
37	6	0	-4.1561	-0.90832	0.167068
38	6	0	-4.5193	-0.24492	-1.0016
39	1	0	-3.8097	-0.16646	-1.82247
40	6	0	-5.78504	0.297301	-1.12814
41	1	0	-6.07633	0.81429	-2.03792
42	6	0	-6.69797	0.159085	-0.09073
43	6	0	-6.35278	-0.51263	1.070791
44	1	0	-7.07718	-0.61536	1.873451
45	6	0	-5.07632	-1.03648	1.200261
46	1	0	-4.79583	-1.54926	2.119174
47	6	0	0.536842	-3.78589	-0.29436
48	1	0	1.238437	-3.33726	-1.0157
49	6	0	-0.01156	-5.06698	-0.88611
50	1	0	-0.73028	-5.53593	-0.20219
51	1	0	0.794397	-5.78635	-1.05265
52	1	0	-0.50696	-4.89353	-1.84702
53	6	0	1.247951	-4.03899	1.023846
54	1	0	1.622656	-3.11914	1.485166
55	1	0	2.101326	-4.70757	0.872355
56	1	0	0.567728	-4.51828	1.736968

TABLE A.6: Atomic coordinates of optimized geometry of clofaziminium with Cl- counter-ion (LABQUD).

E(RM06): -2641.64794122 Hartree

center number	atomic number	atomic type	X (Å)	Y (Å)	Z (Å)
1	17	0	-3.27379	-3.89917	-0.38225
2	7	0	0.095202	2.936519	-0.43037
3	6	0	3.757824	3.303799	-0.11117
4	1	0	4.649915	2.701454	0.035816
5	17	0	-8.09389	1.673677	0.586502
6	7	0	2.334504	1.319351	-0.09732
7	6	0	2.713893	5.464003	-0.40772
8	1	0	2.810042	6.543039	-0.49229
9	7	0	-0.533	-2.49977	-0.3261
10	17	0	7.031537	-2.22103	0.588543
11	6	0	1.477936	4.87299	-0.48096
12	1	0	0.566891	5.448656	-0.62117
13	7	0	-2.78412	-0.84749	-0.14344
14	6	0	1.337	3.476707	-0.37178
15	1	0	-2.91335	-1.87072	-0.25096
16	6	0	2.50132	2.695225	-0.19041
17	6	0	1.100736	0.741508	-0.17869
18	6	0	-0.04056	1.634336	-0.32635
19	6	0	0.909135	-0.61941	-0.14209
20	1	0	1.767179	-1.27377	-0.05894
21	6	0	-1.32675	1.055277	-0.34656
22	1	0	-2.15329	1.749207	-0.44986
23	6	0	-1.55473	-0.29498	-0.23405
24	6	0	-0.37642	-1.19263	-0.23385
25	6	0	-4.01235	-0.18451	0.028548
26	6	0	-5.13582	-0.75764	-0.56983
27	1	0	-5.0168	-1.66719	-1.15531
28	6	0	-6.38655	-0.19398	-0.39573
29	1	0	-7.26117	-0.63977	-0.86074
30	6	0	-6.51852	0.947152	0.379402
31	6	0	-4.16833	0.944026	0.832816
32	1	0	-3.31778	1.365247	1.360611
33	6	0	3.48509	0.476738	0.06962
34	6	0	3.867293	0.090829	1.344782
35	1	0	3.300615	0.441189	2.204705
36	6	0	4.962601	-0.74222	1.508536
37	1	0	5.27952	-1.05787	2.498183
38	6	0	5.657784	-1.17419	0.387891
39	6	0	4.181193	0.042924	-1.04758
40	1	0	3.8581	0.357686	-2.03754
41	6	0	-5.41897	1.513459	1.002824
42	1	0	-5.54386	2.391144	1.630882
43	6	0	5.278596	-0.78842	-0.89006
44	1	0	5.839203	-1.14029	-1.75107
45	6	0	0.54871	-3.4903	-0.33039
46	1	0	1.412921	-3.04428	-0.84218
47	6	0	0.917983	-3.84915	1.099768
48	1	0	1.246471	-2.97446	1.673051
49	1	0	1.724537	-4.59028	1.114467
50	1	0	0.048181	-4.28132	1.608237
51	6	0	0.103184	-4.70726	-1.11753
52	1	0	-0.18416	-4.43898	-2.13881
53	1	0	-0.7644	-5.18499	-0.65038
54	1	0	0.921459	-5.43324	-1.16594
55	6	0	3.85547	4.674	-0.21969
56	1	0	4.834138	5.142751	-0.1577
57	1	0	-1.47856	-2.94228	-0.34855
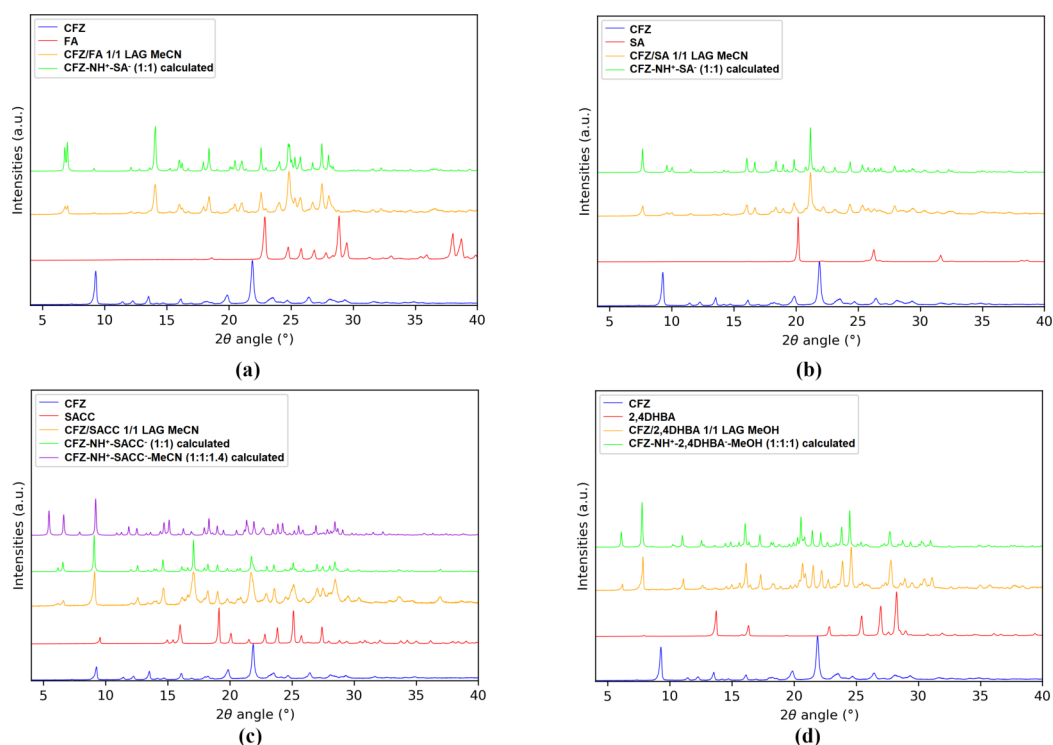
FIGURE A.1: Powder patterns of (a), from bottom to top, CFZ, FA, CFZ/FA LAG MeCN batch powder and **CFZ-NH$^+$-FA$^-$ (1:1)** calculated pattern from SCXRD data, (b) CFZ, SA, CFZ/SA LAG MeCN batch powder and **CFZ-NH$^+$-SA$^-$ (1:1)** calculated pattern from SCXRD data, (c) CFZ, SACC, CFZ/SACC LAG MeCN batch powder and **CFZ-NH$^+$-SACC$^-$ (1:1)** and **CFZ-NH$^+$-SACC$^-$-MeCN (1:1:1.4)** calculated patterns from SCXRD data, (d) CFZ, 2,4-DHBA, CFZ/2,4-DHBA LAG MeOH batch powder and **CFZ-NH$^+$-2,4DHBA$^-$-MeOH (1:1:1)** calculated pattern from SCXRD data.

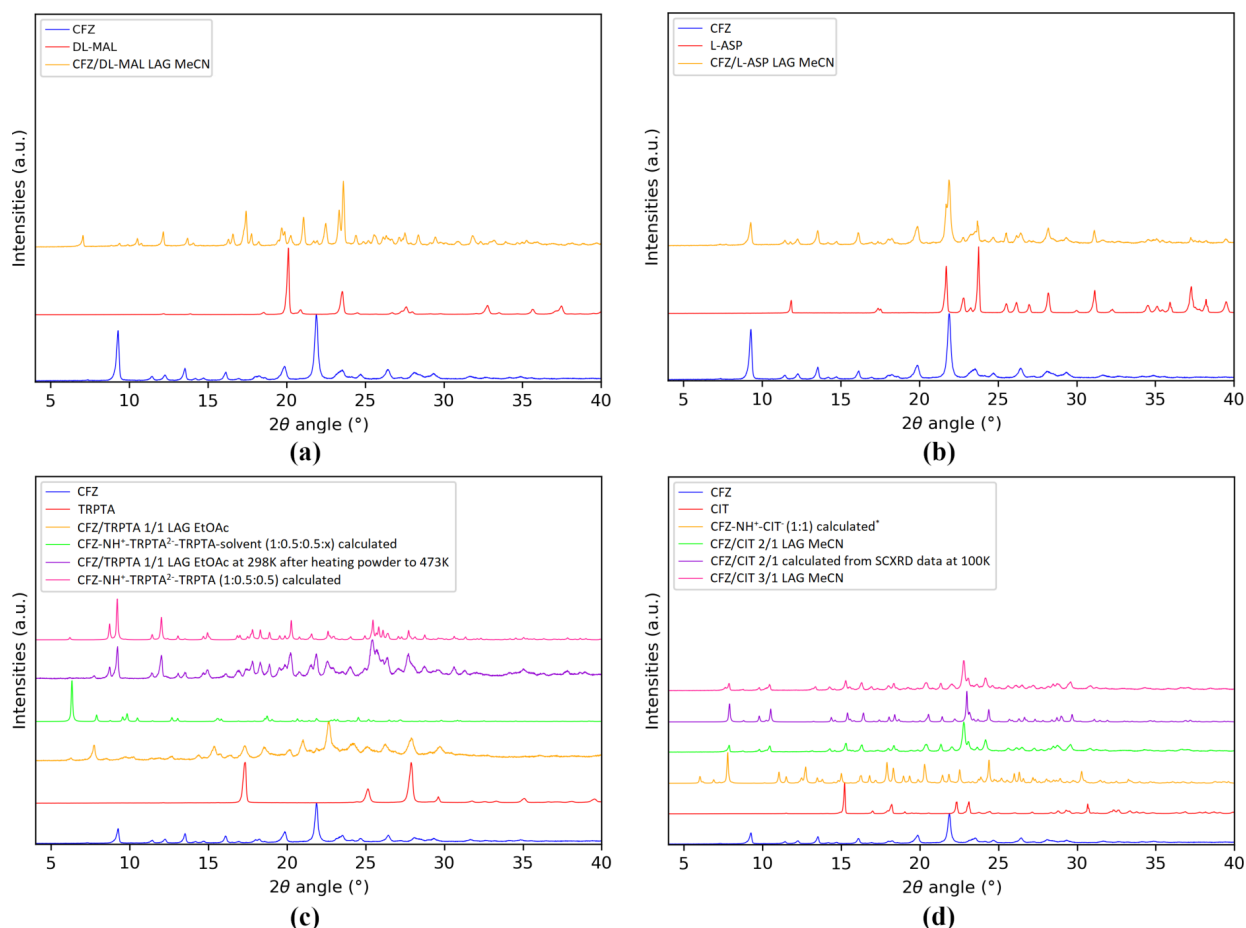FIGURE A.2: Powder patterns of (a), CFZ, acsDL-MAL and CFZ/DL-MAL LAG MeCN batch powder, (b) CFZ, L-ASP, CFZ/L-ASP LAG MeCN batch powder, (c) CFZ, TRPTA, CFZ/TRPTA LAG EtOAc, **CFZ-NH$^+$-TRPTA^{2-}-TRPTA-solvent (1:0.5:0.5:x)** calculated pattern from SCXRD data, CFZ/TRPTA LAG EtOAc batch powder at 25 °C after heating to 200 °C and **CFZ-NH$^+$-TRPTA^{2-}-TRPTA (1:0.5:0.5)** calculated from SCXRD data, (d) CFZ, CIT, **CFZ-NH$^+$-CIT$^-$ (1:1)** calculated from SCXRD data [4], CFZ/CIT 2/1 LAG MeOH/MeCN 50/50, CFZ-CIT 2/1 calculated from SCXRD data obtained at 100K (structure intrinsically disordered) and CFZ/CIT 3/1 LAG MeOH/MeCN 50/50.
* SCXRD data from cif file available in the publication of Bannigan *et al.* [4].
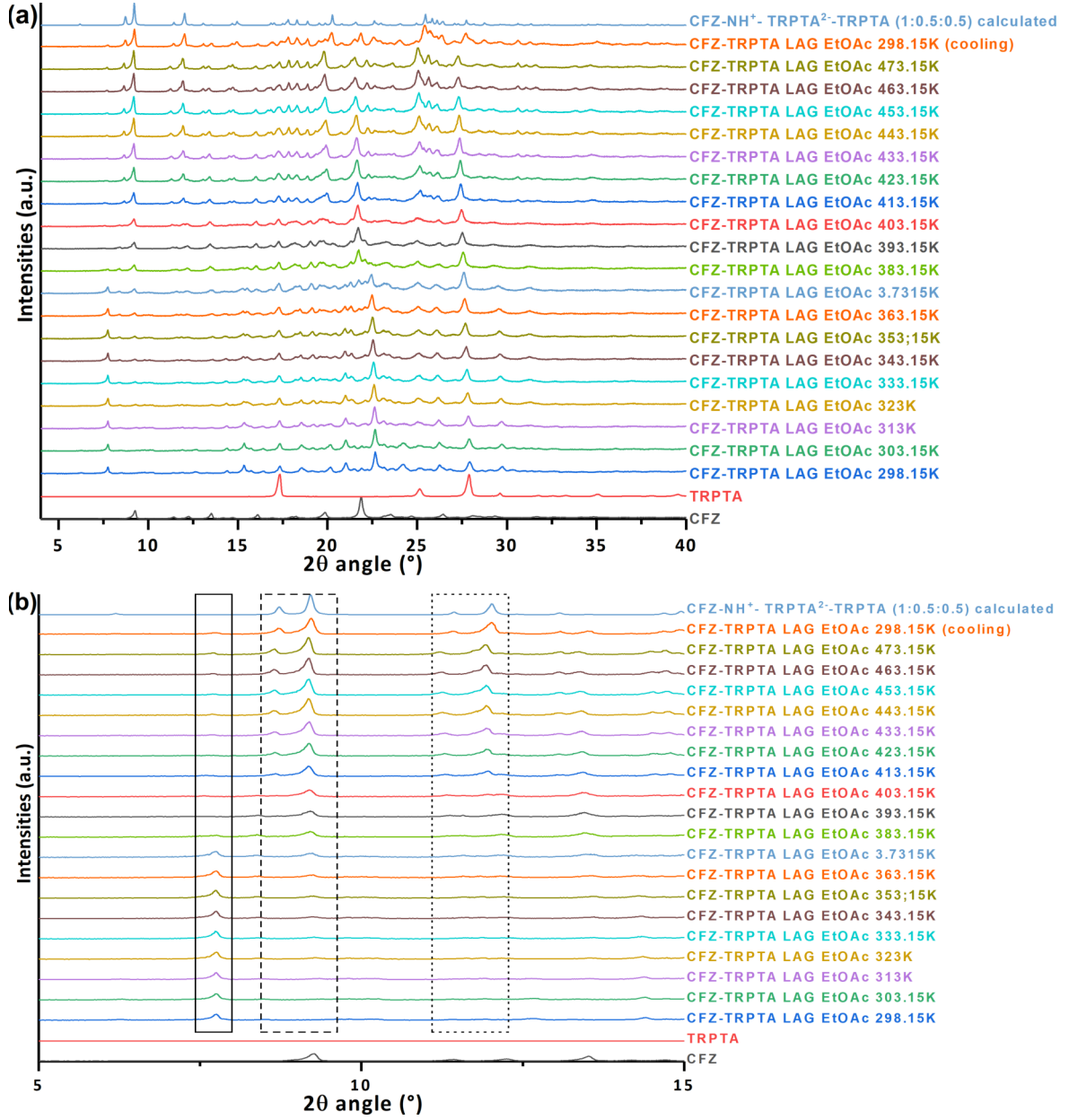
FIGURE A.3: (a) Variable temperature powder X-ray diffraction of CFZ/TRPTA LAG EtOAc batch powder and comparison with calculated pattern of **CFZ-NH$^+$-TRPTA^{2-}-TRPTA (1:0.5:0.5)**. Desolvation of a solvated crystalline powder occurred to give a non-solvated crystalline powder matching the calculated powder pattern of **CFZ-NH$^+$-TRPTA^{2-}-TRPTA (1:0.5:0.5)**. (b) Zoom on the 5-15° 2θ region, disappearing peak upon heating at 2θ value of 7.7° highlighted by plain line frame, appearing peaks upon heating at 2θ values of 8.8 and 9.2° (dashed frame) as well as 11.5 and 12.0° (dotted frame).

(a)

(b)

FIGURE A.4: Channel arrangement and solvent accessible voids in the structure of **CFZ-NH$^+$-TRPTA^{2-}-TRPTA-solvent (1:0.5:0.5:x)** (view along a-axis) (a) and in the one of **CFZ-NH$^+$-TRPTA^{2-}-TRPTA (1:0.5:0.5)** (view along a-axis) (b).
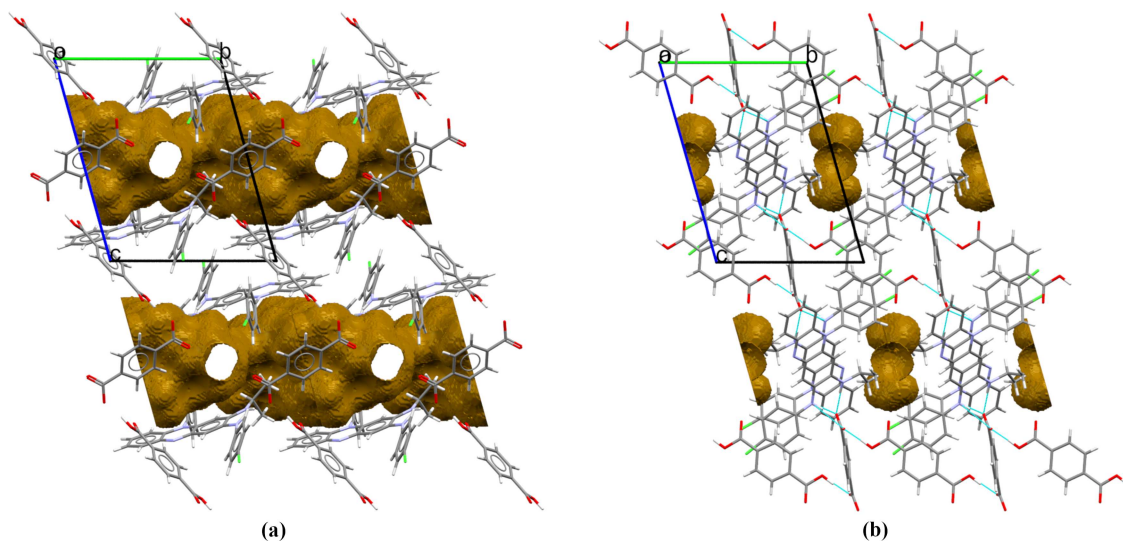

(a)

(b)

(c)

(d)
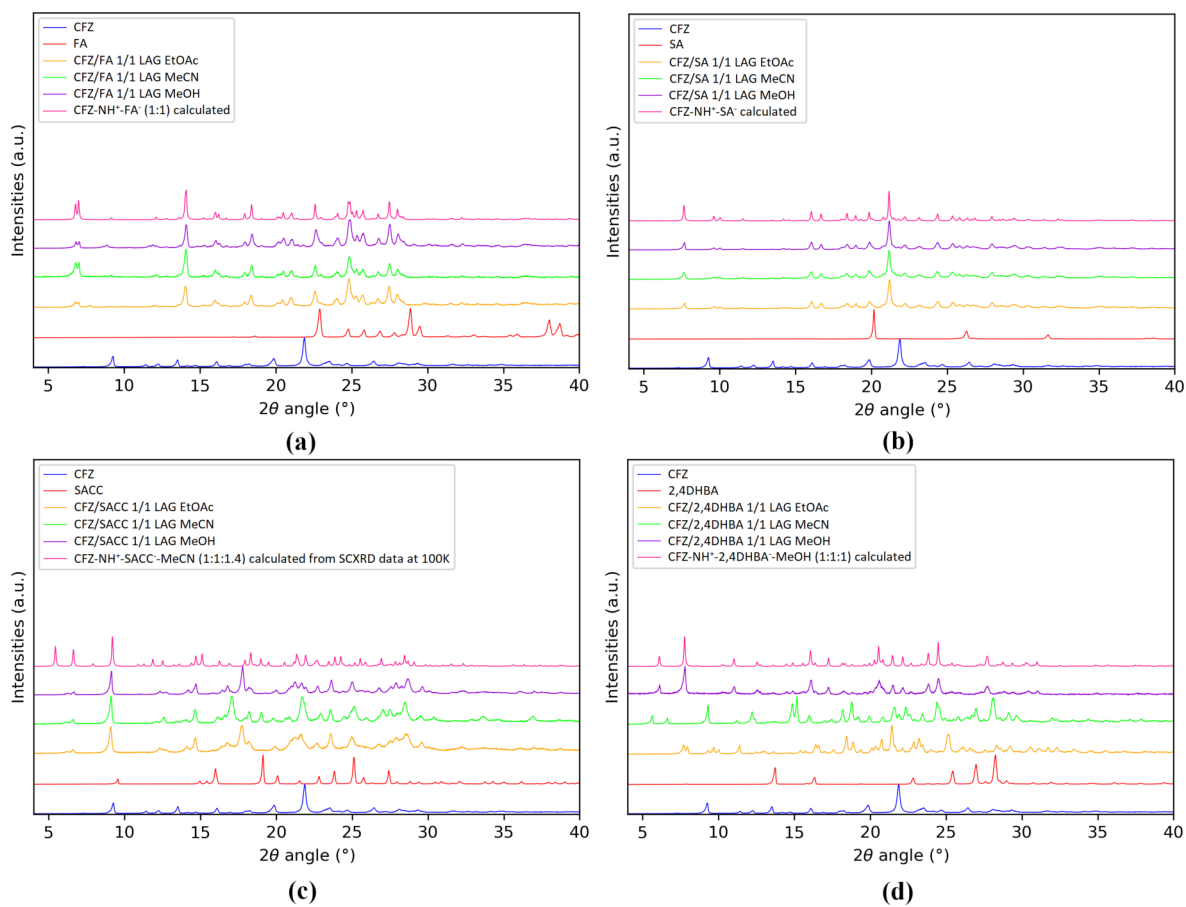
FIGURE A.5: Effect of different solvents while grinding (a) CFZ with FA, (b) CFZ with SA, (c) CFZ with SACC.
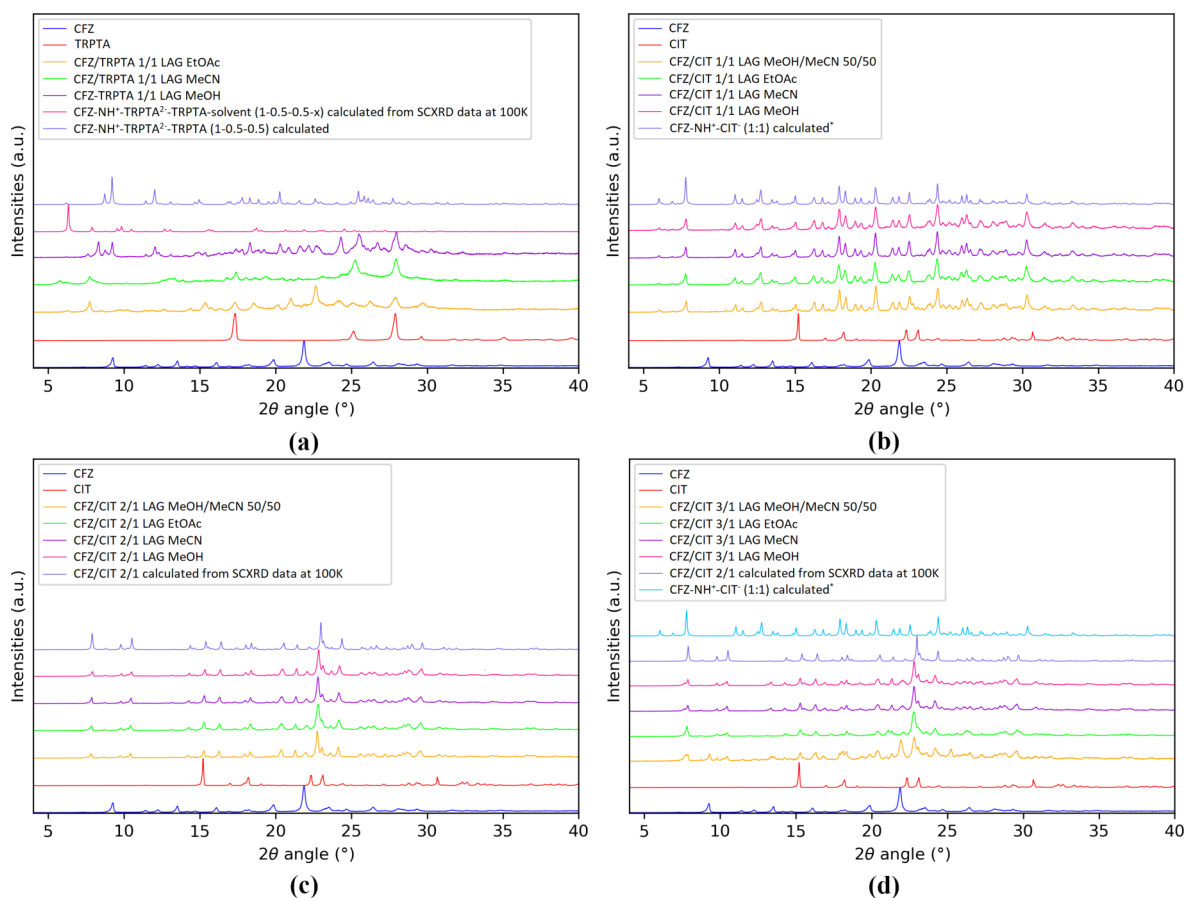
FIGURE A.6: Effect of different solvents while grinding (a) CFZ with TRPTA, (b) CFZ with CIT in 1/1 molar ratio, (c) CFZ with CIT in 2/1 molar ratio and (d) CFZ with CIT in 3/1 molar ratio.

Liquid-assisted grinding experiments were performed in three solvents (MeCN, MeOH and EtOAc) for all combinations described in this paper. For the unsolvated salts, changing the solvent during grinding experiment does not affect the outcome of the reaction. Instead, for solvated salts, indeed, the powder pattern change in function of the solvent used during liquid-assisted grinding.
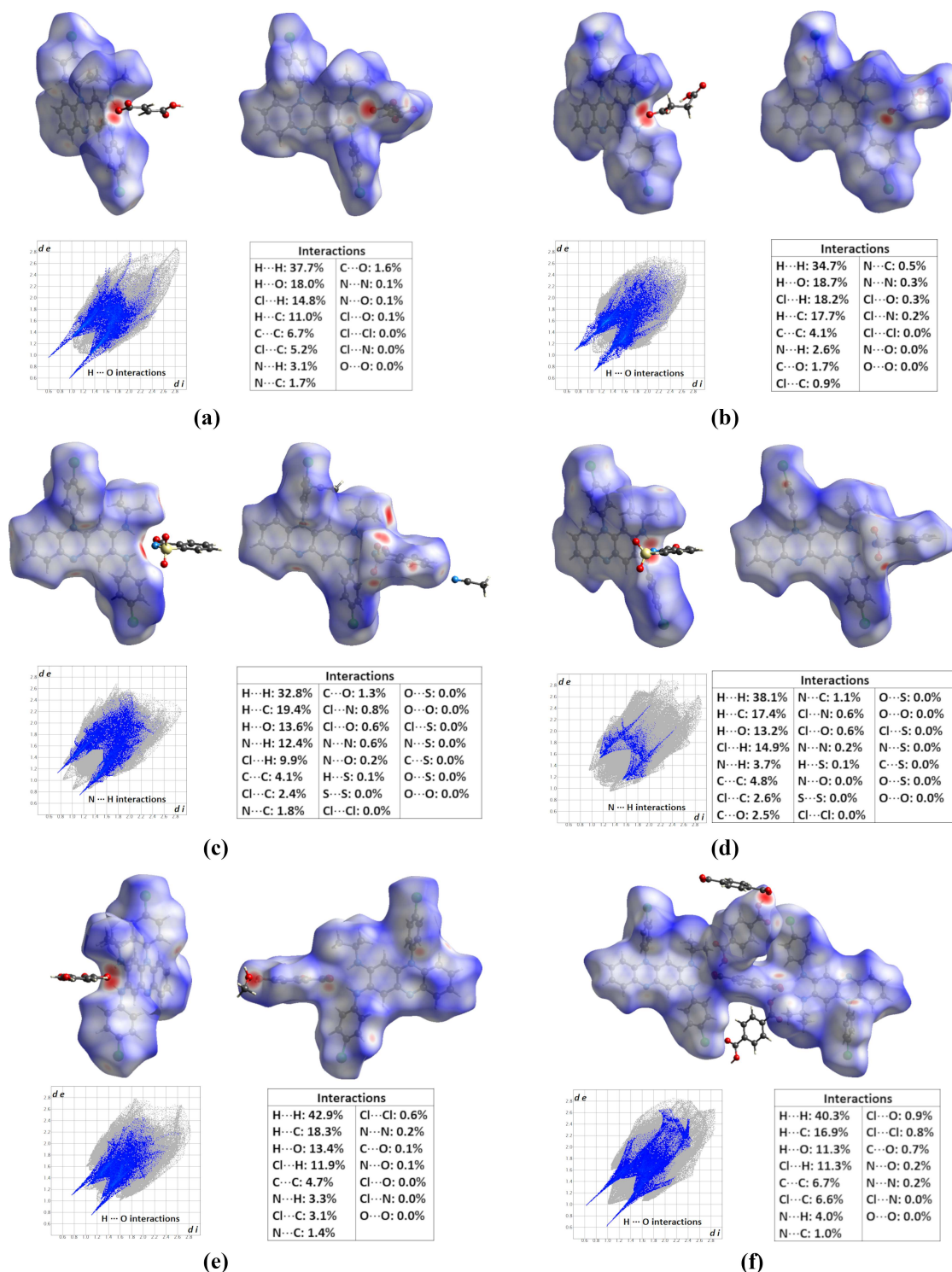
FIGURE A.7: Hirshfeld surface analysis (red regions highlighting close contacts), 2D-fingerprint plots (based on the surface generated on the molecules/ions present in the asymmetric unit) and percentage contribution to the Hirshfeld surface area for the different close contacts in the structures of (a) **CFZ-NH$^+$-FA$^-$ (1:1)** (b) **CFZ-NH$^+$-SA$^-$ (1:1)**, (c) **CFZ-NH$^+$-SACC$^-$-MeCN (1:1:1.4)**, (d)**CFZ-NH$^+$-SACC$^-$ (1:1)**, (e) **CFZ-NH$^+$-2,4DHBA$^-$-MeOH (1:1:1)** and (f) **CFZ-NH$^+$-TRPTA^{2-}-TRPTA (1:0.5:0.5)**.

Appendix A

Hirshfeld surfaces and fingerprint plots of de (distance from the surface to the nearest atoms outside the surface) vs. di (distance from the surface to the nearest atoms located inside the surface) were generated using CrystalExplorer (version 17.5) [7, 8, 9, 10]. Surfaces were generated using the normalized contact distance 'dnorm' descriptor [11]. White surfaces correspond to contacts with distance around the sum of van der Waals radii while red and blue surfaces highlight shorter and longer contacts respectively [11]. For the structure of **CFZ-NH$^+$-SA$^-$ (1:1)** disorder of SA$^-$ was removed (and occupancies of C29A, H29A, H29B, C30A, H30A and H30B were modified from 0.739 to 1) for surface and fingerprint plots generation. For the structure of **CFZ-NH$^+$-2,4DHBA$^-$-MeOH (1:1:1)** 2,4DHBA$^-$ and MeOH disorder was removed and corresponding occupancies were modified to 1. Concerning the structure of **CFZ-NH$^+$-SACC$^-$-MeCN (1:1:1.4)** MeCN is disordered over three position, with positions of C37-C38-N7 being very close to the ones of C37A-C38A-N7A. In consequence, one MeCN molecule (C37A-H37D-H37E-H37F-C38A-N7A) was removed and occupancies of C37-H37A-H37B-H37C-C38-N7 were modified accordingly (occupancies of 0.464 modified to 0.953 (which is the sum of the occupancies of C37A-H37D-H37E-H37F-C38A-N7A and C37-H37A-H37B-H37C-C38-N7). Disorder of isopropyl of CFZ was also removed and occupancies of C25B-H25B-C26B-H26D-H26E-H26F-C27B-H27D-H27E-H27F were modified to 1 before Hirshfeld surface and 2D fingerprint plots generation. In the structure of **CFZ-NH$^+$-SACC$^-$ (1:1)**, SACC$^-$ is disordered and second position of SACC was removed (and occupancies were modified to 1 for the remaining SACC position) prior Hirshfeld surface and 2D fingerprint plots generation. 2D-fingerprint plots shown on Fig. A.7 corresponds to the Hirshfeld surface generated by selecting all atoms from the unit cell (for **CFZ-NH$^+$-TRPTA^{2-}-TRPTA (1:0.5:0.5)**), Hirshfeld surface was generated on **CFZ-NH$^+$-TRPTA^{2-}-TRPTA-CFZ-NH$^+$ (1:1:1:1)** assembly which corresponds to a charge balanced assembly).

Related literature

For additional literature relating to the supporting information, see Eggleston *et al.* [2] , Hirshfeld [10], McKinnon *et al.* [11], Spackman & Jayatilaka [8], Spackman & McKinnon [9] and Turner *et al.* [7].

Bibliography

[1] P. Bannigan, J. Zeglinski, M. Lusi, J. O'Brien, and S. P. Hudson. Investigation into the Solid and Solution Properties of Known and Novel Polymorphs of the Antimicrobial Molecule Clofazimine. *Crystal Growth and Design*, 16(12):7240–7250, 2016.

[2] D. S. Eggleston, W. E. Marsh, and D. J. Hodgson. Structures of the Antileprosy Phenazine Derivatives Clofazimine-N,N- Dimethylformamide, C27H22C12N4.C3H7NO, and B 1912, C30H27ClN4. *Acta Crystallographica*, C40:288–292, 1984.

[3] G. Bolla and A. Nangia. Clofazimine mesylate: A high solubility stable salt. *Crystal Growth and Design*, 12(12):6250–6259, 2012.

[4] P. Bannigan, E. Durack, C. Madden, M. Lusi, and S. P. Hudson. Role of Biorelevant Dissolution Media in the Selection of Optimal Salt Forms of Oral Drugs: Maximizing the Gastrointestinal Solubility and in Vitro Activity of the Antimicrobial Molecule, Clofazimine. *ACS Omega*, 2(12):8969–8981, 2017.

[5] E. M. Horstman, R. K. Keswani, B. A. Frey, P. M. Rzeczycki, V. LaLone, J. A. Bertke, P. J. Kenis, and G. R. Rosania. Elasticity in Macrophage-Synthesized Biocrystals. *Angewandte Chemie - International Edition*, 56(7):1815–1819, 2017.

[6] R. K. Keswani, J. Baik, L. Yeomans, C. Hitzman, A. M. Johnson, A. S. Pawate, P. J. Kenis, N. Rodriguez-Hornedo, K. A. Stringer, and G. R. Rosania. Chemical Analysis of Drug Biocrystals: A Role for Counterion Transport Pathways in Intracellular Drug Disposition. *Molecular Pharmaceutics*, 12(7):2528–2536, 2015.

[7] M. J. Turner, J. J. McKinnon, S. K. Wolff, D. J. Grimwood, P. R. Spackman, D. Jayatilaka, and M. A. Spackman. CrystalExplorer17, 2017.

[8] M. A. Spackman and D. Jayatilaka. Hirshfeld surface analysis. *CrystEngComm*, 11:19–32, 2009.

[9] M. A. Spackman and J. J. Mckinnon. Fingerprinting intermolecular interactions in molecular crystals. *CrystEngComm*, 4(66):378–392, 2002.

[10] F. L. Hirshfeld. Bonded-Atom Fragments for Describing Molecular Charge Densities. *Theoretica Chimica Acta*, 44:129–138, 1977.

[11] J. J. Mckinnon, D. Jayatilaka, and M. A. Spackman. Towards quantitative analysis of intermolecular interactions with Hirshfeld surfaces. *Chemical Communications*, (37):3814–3816, 2007.

Appendix B

To: Taking advantage of solvate formation to modulate drug-drug ratio in clofaziminium diclofenac salts†

Supporting information to chapter 4

Table of experimental details

TABLE B.1: Experimental details.

	CFZNH$^+$-DCF$^-$-MeOH (1:1:0.74)	CFZNH$^+$-DCF$^-$-EtOH (1:1:1)	CFZNH$^+$-DCF$^-$-EtOH (1:1:1)	CFZNH$^+$-DCF$^-$-MeCN-H$_2$O (1:1:1:2)
Crystal data				
Chemical formula	$C_{27}H_{23}Cl_2N_4\cdot$ $C_{14}H_{10}Cl_2NO_2\cdot$ $0.741(CH_4O)$	$C_{27}H_{23}Cl_2N_4\cdot$ $C_{14}H_{10}Cl_2NO_2\cdot$ C_2H_6O	$C_{27}H_{23}Cl_2N_4\cdot$ $C_{14}H_{10}Cl_2NO_2\cdot$ C_2H_6O	$C_{27}H_{23}Cl_2N_4\cdot$ $C_{14}H_{10}Cl_2NO_2\cdot$ $C_2H_3N\cdot 2(H_2O)$
Mr	793.42	815.59	815.59	846.61
Crystal system, space group	Monoclinic, $C2/c$	Triclinic, $P\bar{1}$	Triclinic, $P\bar{1}$	Triclinic, $P\bar{1}$
Temperature (K)	295(2)	295(2)	100(2)	100(2)
a, b, c (Å)	16.7209(3), 17.2504(5), 27.8319(7)	12.5818(4), 13.4486(3), 13.5318(3)	12.5325(5), 13.1139(3), 13.1773(4)	11.6515(3), 11.7149(3), 16.0793(4)
α, β, γ (°)	90, 93.438(2), 90	80.291(2), 71.638(2), 71.710(2)	82.032(2), 71.833(3), 74.538(3)	103.558(2), 90.461(2), 105.250(2)
V (Å^3)	8013.4(3)	2057.12(10)	1979.61(12)	2052.78(9)
Z	8	2	2	2
μ (mm^{-1})	3.04	2.98	3.09	3.03
Crystal size (mm)	0.21 × 0.13 × 0.07	0.76 × 0.24 × 0.09	0.52 × 0.25 × 0.17	0.65 × 0.34 × 0.20
Data collection				
T_{min}, T_{max}	0.678, 0.827	0.601, 0.894	0.395, 0.706	0.360, 0.628
No. of measured, independent and observed [$I > 2\sigma(I)$] reflections	23679, 7080, 4722	27818, 7236, 6397	21176, 6977, 6386	18621, 7196, 6969
R_{int}	0.040	0.024	0.046	0.019
$(\sin\theta/\lambda)_{max}$ (Å^{-1})	0.597	0.597	0.598	0.597
Refinement				
$R[F^2 > 2\sigma(F^2)]$, $wR(F^2)$, S	0.059, 0.193, 1.02	0.050, 0.146, 1.06	0.057, 0.166, 1.07	0.031, 0.080, 1.03
No. of reflections	7080	7236	6977	7196
No. of parameters	519	536	511	538
No. of restraints	21	82	0	0
$\Delta\rho_{max}$, $\Delta\rho_{min}$(e Å^{-3})	0.42, -0.37	0.64, -0.56	0.91,-0.47	0.52, -0.41
	CFZNH$^+$-DCF$^-$-SAL-H$_2$O (4:4:9:1)	CFZNH$^+$-DCF$^-$-PPP (2:2:5)	CFZNH$^+$-DCF$^-$-PPP (2:2:5)	CFZNH$^+$-DCF$^-$ (1:1)
Crystal data				
Chemical formula	$4(C_{27}H_{23}Cl_2N_4)\cdot$ $4(C_{14}H_{10}Cl_2NO_2)\cdot$ $9(C_7H_6O_2)\cdot H_2O$	$2(C_{27}H_{23}Cl_2N_4)\cdot$ $2(C_{14}H_{10}Cl_2NO_2)\cdot$ $5(C_9H_{10}O)$	$2(C_{27}H_{23}Cl_2N_4)\cdot$ $2(C_{14}H_{10}Cl_2NO_2)\cdot$ $5(C_9H_{10}O)$	$(C_{27}H_{23}Cl_2N_4)\cdot$ $(C_{14}H_{10}Cl_2NO_2)$
Mr	4195.16	2209.89	2209.89	769.52
Crystal system, space group	Triclinic, $P\bar{1}$	Triclinic, $P\bar{1}$	Triclinic, $P\bar{1}$	Triclinic, $P\bar{1}$
Temperature (K)	100(2)	295(2)	100(2)	295(2)
a, b, c (Å)	10.4132(5), 21.2266(7), 25.0657(7)	10.7319(4), 13.6005(6), 21.5496(9)	10.5086(4), 13.4783(5), 21.4224(8)	12.4461(6), 13.2751(5), 13.3667(6)
α, β, γ (°)	66.238(3), 89.969(3), 86.658(3)	73.502(4), 77.404(4), 73.540(4)	73.629(3), 76.913(3), 73.271(3)	84.423(3), 67.963(4), 66.662(4)
V (Å^3)	5060.5(3)	2859.7(2)	2752.92(19)	1876.21(16)
Z	1	1	1	2
μ (mm^{-1})	2.61	2.30	2.39	3.21
Crystal size (mm)	0.42 × 0.14 × 0.04	0.20 × 0.12 × 0.07	0.25 × 0.11 × 0.06	0.36 × 0.07 × 0.05
Data collection				
T_{min}, T_{max}	0.413, 0.910	0.859, 0.935	0.711, 0.875	0.699, 0.936

	CFZNH$^+$-DCF$^-$-SAL-H$_2$O (4:4:9:1)	CFZNH$^+$-DCF$^-$-PPP (2:2:5)	CFZNH$^+$-DCF$^-$-PPP (2:2:5)	CFZNH$^+$-DCF$^-$(1:1)
No. of measured, independent and observed [$I > 2\sigma(I)$] reflections	53166, 17765, 13730	28672, 10049, 6767	28107, 9723, 7857	17078, 6630, 5192
R_{int}	0.069	0.051	0.038	0.037
$(\sin\theta/\lambda)_{max}$ (Å^{-1})	0.598	0.595	0.598	0.598
Refinement				
$R[F^2 > 2\sigma(F^2)]$, $wR(F^2)$, S	0.060, 0.171, 1.03	0.052, 0.160, 1.02	0.035, 0.090, 1.03	0.048, 0.141, 1.03
No. of reflections	17765	10049	9723	6630
No. of parameters	1552	937	753	480
No. of restraints	717	445	0	0
$\Delta\rho_{max}$, $\Delta\rho_{min}$(e Å^{-3})	0.48, -0.50	0.32, -0.29	0.26, -0.24	0.53, -0.37

	CFZNH$^+$-DCF$^-$-DCF (1:1:1) (I)	CFZNH$^+$-DCF$^-$-DCF-MeCN (1:1:1:2)	CFZNH$^+$-DCF$^-$-DCF-EtOAc (1:1:1:1)	CFZNH$^+$-DCF$^-$-DCF (1:1:1) (II)
Crystal data				
Chemical formula	$C_{27}H_{23}Cl_2N_4 \cdot$ $C_{14}H_{10}Cl_2NO_2 \cdot$ $C_{14}H_{11}Cl_2NO_2$	$C_{27}H_{23}Cl_2N_4 \cdot$ $C_{14}H_{10}Cl_2NO_2 \cdot$ $C_{14}H_{11}Cl_2NO_2 \cdot$ $2(C_2H_3N)$	$C_{27}H_{23}Cl_2N_4 \cdot$ $C_{14}H_{10}Cl_2NO_2 \cdot$ $C_{14}H_{11}Cl_2NO_2 \cdot$ $C_4H_8O_2$	$C_{27}H_{23}Cl_2N_4 \cdot$ $C_{14}H_{10}Cl_2NO_2 \cdot$ $C_{14}H_{11}Cl_2NO_2$
Mr	1065.66	1147.77	1153.76	1065.66
Crystal system, space group	Triclinic, $P\bar{1}$	Triclinic, $P\bar{1}$	Triclinic, $P\bar{1}$	Triclinic, $P\bar{1}$
Temperature (K)	295(2)	295(2)	295(2)	295(2)
a, b, c (Å)	10.8837(2), 14.4737(3), 17.7519(4)	15.0694(11), 15.2735(10), 15.5991(13)	15.0569(4), 15.3773(4), 15.4247(4)	11.9326(3), 15.2549(4), 16.0042(4)
α, β, γ (°)	101.568(2), 105.173(2), 94.286(2)	74.882(7), 61.685(8), 64.227(7)	76.043(2), 61.975(3), 63.541(3)	89.161(2), 70.570(2), 69.693(2)
V (Å^3)	2620.06(10)	2839.6(4)	2820.07(16)	2559.79(12)
Z	2	2	2	2
μ (mm^{-1})	3.41	3.20	3.24	3.49
Crystal size (mm)	0.54 × 0.34 × 0.06	0.31 × 0.24 × 0.14	0.62 × 0.30 × 0.15	0.30 × 0.20 × 0.06
Data collection				
T_{min}, T_{max}	0.358, 0.831	0.711, 0.849	0.356, 0.719	0.503, 0.815
No. of measured, independent and observed [$I > 2\sigma(I)$] reflections	26706, 9218, 8043	27894, 10010, 7543	27162, 9942, 8898	25042, 9036, 7679
R_{int}	0.022	0.032	0.022	0.025
$(\sin\theta/\lambda)_{max}$ (Å^{-1})	0.597	0.598	0.598	0.598
Refinement				
$R[F^2 > 2\sigma(F^2)]$, $wR(F^2)$, S	0.050, 0.141, 1.05	0.050, 0.159, 1.08	0.042, 0.122, 1.05	0.045, 0.129, 1.04
No. of reflections	9218	10010	9942	9036
No. of parameters	657	744	714	657
No. of restraints	0	34	24	1
$\Delta\rho_{max}$, $\Delta\rho_{min}$(e Å^{-3})	0.49, -0.50	0.44, -0.36	0.38, -0.40	0.62, -0.50

Hydrogen-bonds parameters

TABLE B.2: Selected hydrogen-bond parameters.

D−H···A	D−H (Å)	H···A (Å)	D···A (Å)	D−H···A (°)
CFZNH$^+$-DCF$^-$-MeOH (1:1:0.74)				
N3−H3···O1	0.83(4)	1.98(4)	2.792(3)	168(4)
N4−H4···O1	0.90(4)	2.00(4)	2.899(3)	171(4)
N4−H4···O2	0.90(4)	2.58(4)	3.262(4)	133(3)
N5−H5···O1	0.79(4)	2.13(4)	2.805(3)	145(4)
O3A−H3OA···O2^i	0.82	2.07	2.710(6)	134.7
C24−H24···O2^{ii}	0.93	2.56	3.356(5)	143.3
CFZNH$^+$-DCF$^-$-EtOH (1:1:1) 295 K				
N3−H3···O1	0.82(3)	2.10(3)	2.907(3)	170(2)
N3−H3···O2	0.82(3)	2.53(3)	3.104(2)	128(2)
N4−H4···O1	0.89(3)	2.57(2)	3.196(2)	127.6(19)
N4−H4···O2	0.89(3)	1.98(3)	2.845(2)	165(2)
N5−H5···O2	0.84(3)	2.09(3)	2.803(2)	143(3)
O3A−H3A1···O1	0.82	2.15	2.817(14)	139.1
O3B−H3B···O1	0.82	1.85	2.672(3)	176.7
C23−H23···O2^{iii}	0.93	2.58	3.463(3)	158.6
CFZNH$^+$-DCF$^-$-EtOH (1:1:1) 100 K				
N3−H3···O1	0.81(3)	2.03(3)	2.834(2)	174(3)
N3−H3···O2	0.81(3)	2.59(3)	3.125(2)	125(2)
N4−H4···O1	0.88(3)	2.55(3)	3.135(2)	124(2)
N4−H4···O2	0.88(3)	1.96(3)	2.809(2)	162(2)
N5−H5···O2	0.82(3)	2.09(3)	2.804(2)	145(3)
O3−H3OB···O1^{ii}	0.88(4)	1.85(4)	2.719(2)	171(4)
C23−H23···O2^{iii}	0.95	2.49	3.390(2)	158.2
CFZNH$^+$-DCF$^-$-MeCN-H$_2$O (1:1:1:2)				
N3−H3···O1	0.848(18)	1.909(19)	2.7532(15)	173.1(16)
N4−H4···O1	0.832(19)	1.993(19)	2.8068(15)	165.5(16)
N5−H5···O1	0.83(2)	2.05(2)	2.7940(16)	148.7(17)
O4−H4OA···N2^{iv}	0.85(3)	2.08(3)	2.9157(16)	168(2)
O4−H4OB···O3	0.92(3)	1.79(3)	2.7060(18)	169(2)
O3−H3OB···O4^v	0.85(3)	2.00(3)	2.8192(18)	163(2)
O3−H3OA···O2	0.88(3)	1.86(3)	2.7353(17)	177(2)
CFZNH$^+$-DCF$^-$-SAL-H$_2$O (4:4:9:1)				
N3−H3···O1^{ii}	0.92(4)	1.92(4)	2.819(3)	166(3)
N4−H4···O1^{ii}	0.84(4)	2.10(4)	2.904(3)	162(3)
N8−H8···O3	0.924(18)	1.94(2)	2.834(3)	163(3)
N9−H9···O3	0.81(4)	2.25(4)	3.028(3)	163(3)
N10−H10···O3	0.83(4)	2.14(4)	2.896(3)	151(3)
N5−H5···O1	0.96(4)	1.97(4)	2.846(3)	151(3)
O5S−H5OS···O2^{ii}	0.99(5)	1.57(5)	2.564(3)	177(4)
O7T−H7OT···O4^{vi}	1.00(5)	1.52(5)	2.514(3)	176(4)
O9U−H9OU···O10U	0.84	1.94	2.607(8)	135.2
O9V−H9OV···O10V	0.84	1.93	2.659(13)	144.9
O11W−H11W···O12W	0.84	1.90	2.569(9)	135.2
O11X−H11X···O12X	0.84	1.70	2.43(2)	142.8
O13Y−H13Y···O14Y	0.84	1.65	2.419(16)	151.4
O15−H15O···O13Y	0.84(2)	1.90(2)	2.683(14)	154(6)
O15−H15P···O13Y^{ii}	0.85(2)	2.54(7)	3.210(18)	137(9)
O15−H15P···O15^{ii}	0.85(2)	1.93(7)	2.700(19)	150(11)
C38−H38···O2^{vi}	0.95	2.49	3.391(4)	159.5
C79−H79···O4^{vi}	0.95	2.43	3.262(4)	146.1
C1−H1···O12W^{vii}	0.95	2.37	3.051(6)	128.6
C29−H29B···O13Y	0.99	2.52	3.468(11)	160.0
C18−H18···O6S^{vii}	0.95	2.34	3.247(4)	159.6
C55−H55···O8T^{viii}	0.95	2.37	3.221(3)	149.2
C61−H61A···O7T^{iv}	0.95	2.58	3.370(4)	141.3
C28W−H28W···O5S	0.95	2.53	3.295(12)	137.4
C14−H14···N2^{ix}	0.95	2.54	3.416(4)	153.3
C25−H25···Cl6^x	1.00	2.67	3.601(3)	154.4

TABLE B.2: Selected hydrogen-bond parameters.

D−H···A	D−H (Å)	H···A (Å)	D···A (Å)	D−H···A (°)
C59−H59···N7^{viii}	0.95	2.57	3.441(4)	153.1
C66−H66···Cl2	1.00	2.77	3.651(3)	147.8
CFZNH$^+$-DCF$^-$-PPP (2:2:5) 295 K				
N3−H3···O1	0.89(3)	1.89(3)	2.760(3)	165(3)
N4−H4···O1	0.86(3)	1.94(3)	2.802(3)	175(3)
N5−H5···O2	0.95(3)	1.91(4)	2.787(3)	153(3)
C15−H15···O3	0.93	2.53	3.230(12)	132.3
C18−H18···O4	0.93	2.49	3.238(6)	137.7
CFZNH$^+$-DCF$^-$-PPP (2:2:5) 100 K				
N3−H3···O1	0.87(2)	1.89(2)	2.756(2)	169.5(18)
N4−H4···O1	0.86(2)	1.95(2)	2.798(2)	173.2(19)
N5−H5···O2	0.91(2)	1.95(2)	2.766(2)	148.8(19)
C15−H15···O3^{ii}	0.95	2.49	3.174(2)	128.9
C18−H18···O4^{ii}	0.95	2.48	3.217(2)	134.0
CFZNH$^+$-DCF$^-$(1:1)				
N3−H3···O1	0.77(3)	2.21(3)	2.966(3)	167(3)
N3−H3···O2	0.77(3)	2.42(3)	3.025(3)	136(3)
N4−H4···O1	0.89(3)	1.82(3)	2.697(3)	167(3)
N5−H5···O2	0.84(3)	1.99(3)	2.765(3)	154(3)
CFZNH$^+$-DCF$^-$-DCF (1:1:1) (polymorph I)				
N3−H3···O2	0.87(3)	2.01(3)	2.860(3)	168(2)
N4−H4···O1	0.87(3)	2.18(3)	3.028(2)	163(2)
N5−H5···O1	0.86(3)	2.30(3)	3.007(3)	139(3)
N6−H6···O4	0.85(3)	2.18(3)	2.953(3)	151(3)
O3−H3O···O2	0.91(4)	1.59(4)	2.496(2)	168(3)
C3−H3A···O3^{xi}	0.93	2.49	3.376(3)	159.0
C31−H31···O3^{ii}	0.93	2.57	3.232(3)	128.0
CFZNH$^+$-DCF$^-$-DCF-MeCN (1:1:1:2)				
N3−H3···O1^{iii}	0.80(3)	2.04(3)	2.837(3)	178(3)
N4−H4···O1^{iii}	0.86(3)	1.97(3)	2.803(3)	164(3)
N5−H5···O2	0.82(3)	2.09(3)	2.848(3)	154(3)
O3−H3B···O2^{iii}	0.93(4)	1.64(4)	2.557(3)	171(4)
N6−H6···O4	0.89(3)	2.09(3)	2.904(3)	151(3)
C38−H38···O4^{xii}	0.93	2.28	3.170(3)	160.6
C43−H43A···O3^{viii}	0.97	2.59	3.553(3)	171.1
CFZNH$^+$-DCF$^-$-DCF-EtOAc (1:1:1:1)				
N3−H3···O1^{iv}	0.82(2)	2.00(2)	2.815(2)	173(2)
N4−H4···O1^{iv}	0.78(2)	2.03(2)	2.794(2)	165(2)
N5−H5···O2	0.84(2)	2.07(2)	2.846(2)	152(2)
O3−H3O···O2^{iii}	0.84(3)	1.73(3)	2.562(2)	171(3)
N6−H6···O4	0.83(2)	2.14(2)	2.898(2)	152(2)
C38−H38···O4	0.93	2.26	3.168(3)	164.8
CFZNH$^+$-DCF$^-$-DCF (1:1:1) (polymorph II)				
N3−H3···O1	0.87(3)	1.96(3)	2.817(2)	168(2)
N4−H4···O1	0.86(3)	1.91(3)	2.769(2)	176(2)
N5−H5···O2	0.86(3)	2.04(3)	2.835(2)	153(2)
N6−H6···O4	0.84(3)	2.14(3)	2.932(3)	156(3)
O3−H3O···O2	0.97(4)	1.62(4)	2.568(3)	167(4)
C4−H4A···O3^{xiii}	0.93	2.48	3.347(3)	155.9
C38−H38···O4^{xiv}	0.93	2.38	3.303(3)	169.0

Symmetry codes: (i) x-1/2, y+1/2, z; (ii) -x+1, -y+1, -z+1; (iii) -x, -y+1, -z+1; (iv) x+1, y, z; (v) -x+2, -y+2, -z+2; (vi) x-1, y, z; (vii) -x+1, -y, -z+1; (viii) -x+1, -y+1, -z; (ix) -x+2, -y, -z+1; (x) x, y-1, z+1; (xi) -x+2, -y+2, -z+1; (xii) x, y, z+1; (xiii) -x+2, -y+1, -z+1; (xiv) -x, -y+2, -z+1.

Ellipsoid plots of the different structures described in this work

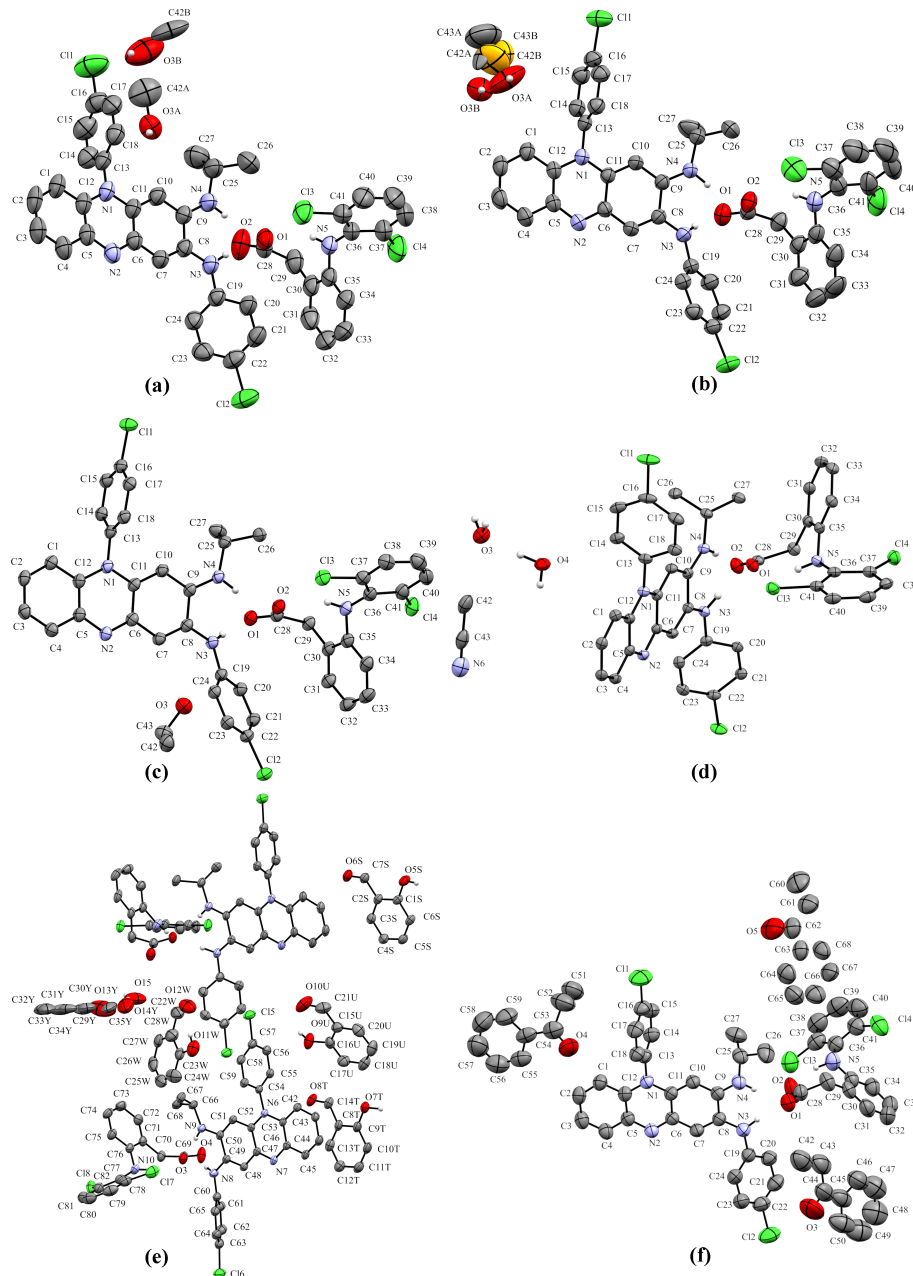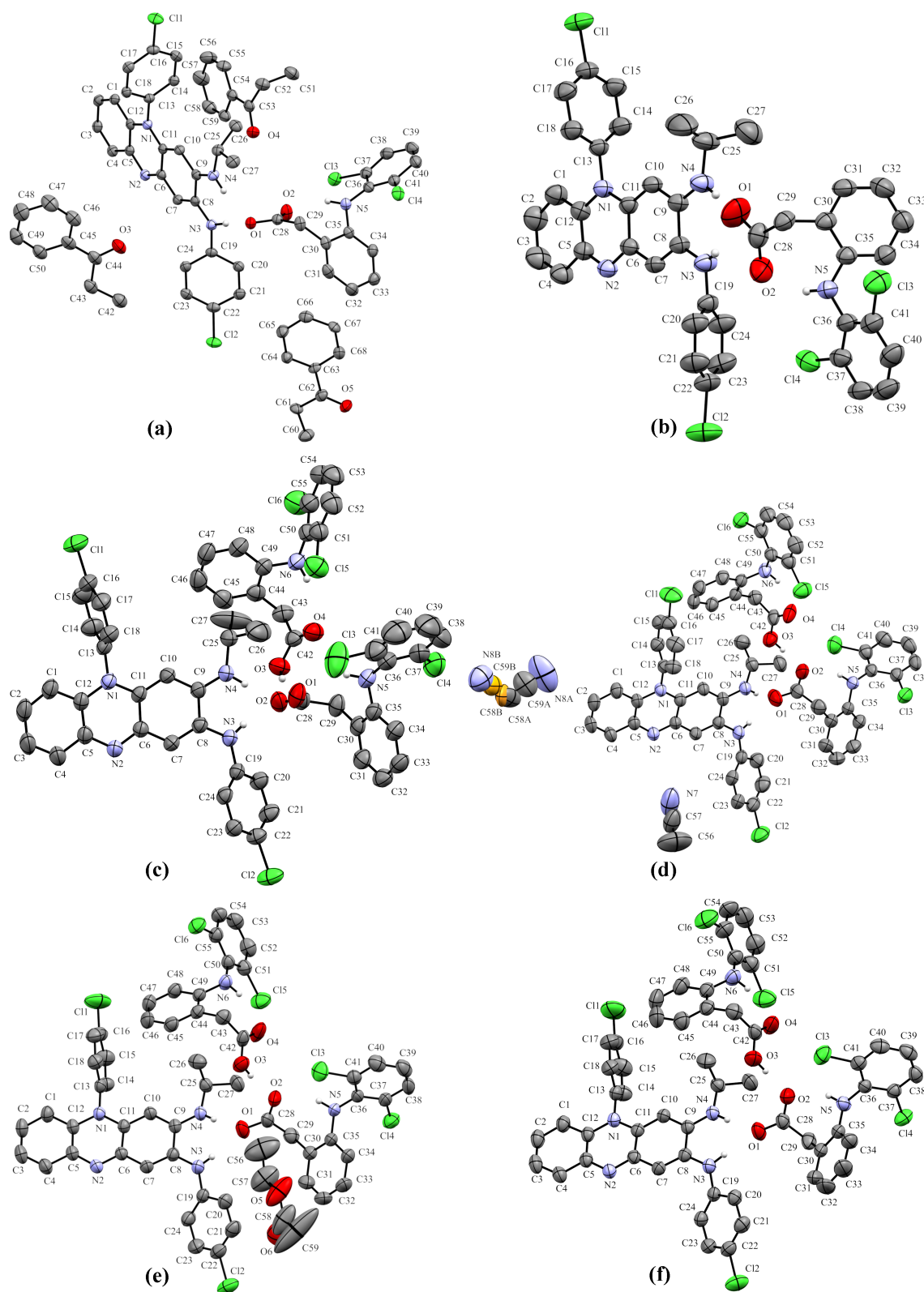FIGURE B.1: Ellipsoids plots (50% probability level) and labeling of (a) **CFZNH⁺-DCF⁻-MeOH (1:1:0.74)**, (b) **CFZNH⁺-DCF⁻-EtOH (1:1:1)** (295 K, orange carbons highlighting EtOH disorder), (c) **CFZNH⁺-DCF⁻-EtOH (1:1:1)** (100 K), (d) **CFZNH⁺-DCF⁻-MeCN-H₂O (1:1:2:1)**, (e) **CFZNH⁺-DCF⁻-SAL-H₂O (4:4:9:1)** (disorder and labeling of first CFZNH⁺ and DCF⁻ not shown) and (f) **CFZNH⁺-DCF⁻-PPP (2:2:5)** (295 K, disorder not shown).

FIGURE B.2: Ellipsoids plots (50% probability level) and labeling of (a) **CFZNH⁺-DCF⁻-PPP (2:2:5)** (100 K), (b) **CFZNH⁺-DCF⁻ (1:1)** (295 K), (c) **CFZNH⁺-DCF⁻-DCF (1:1:1)** (polymorph I), (d) **CFZNH⁺-DCF⁻-DCF-MeCN (1:1:1:2)** (MeCN disorder highlighted by orange carbon atoms), (e) **CFZNH⁺-DCF⁻-DCF-EtOAc (1:1:1:1)** and (f) **CFZNH⁺-DCF⁻-DCF (1:1:1)** (polymorph II).
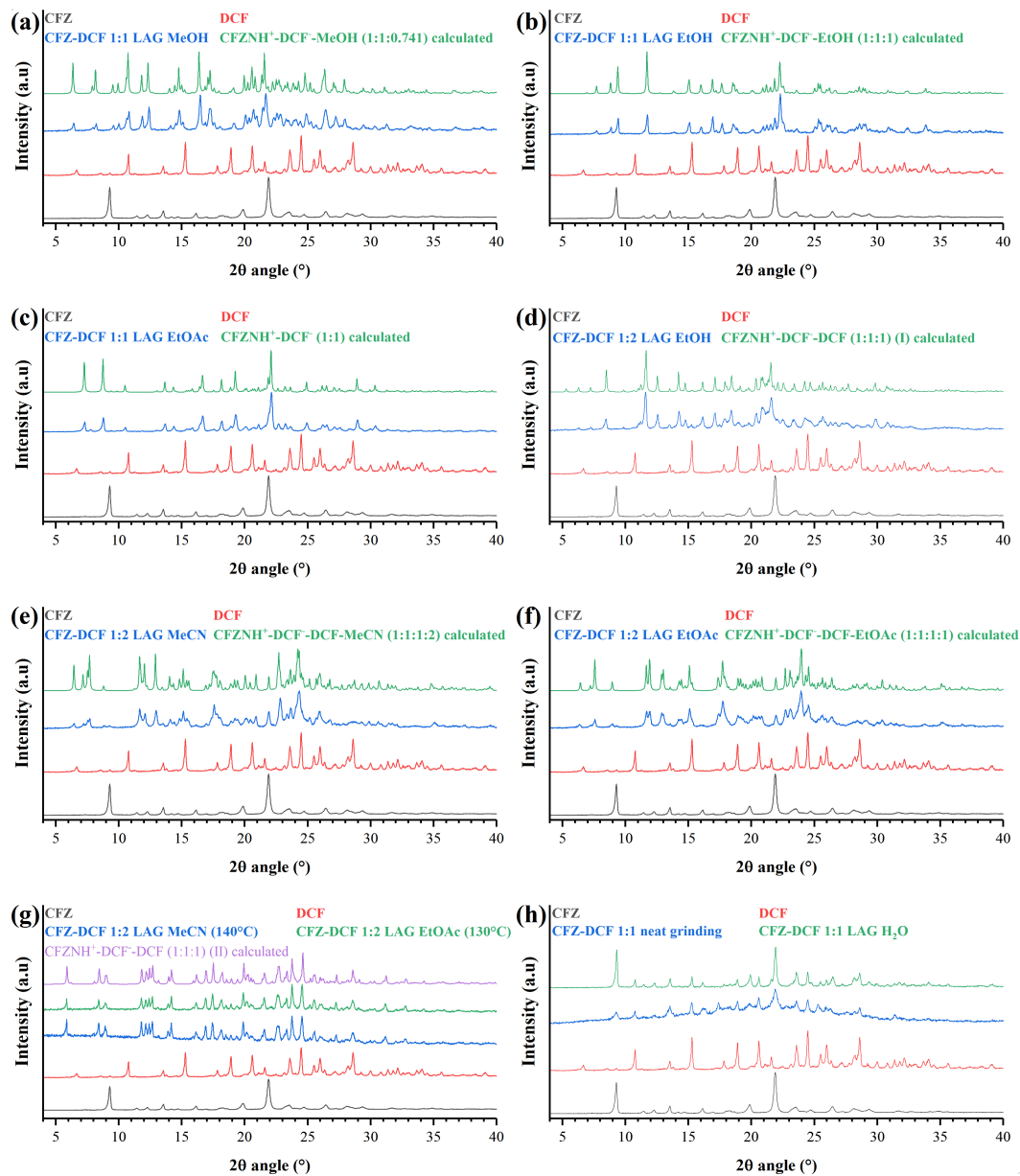
PXRD analysis

FIGURE B.3: PXRD patterns of, from bottom to top CFZ, DCF and (a) CFZ-DCF 1:1 LAG MeOH and **CFZNH$^+$-DCF$^-$-MeOH (1:1:0.74)** calculated, (b) CFZ-DCF 1:1 LAG EtOH and **CFZNH$^+$-DCF$^-$-EtOH (1:1:1)** calculated, (c) CFZ-DCF 1:1 LAG EtOAc and **CFZNH$^+$-DCF$^-$ (1:1)** calculated, (d) CFZ-DCF 1:2 LAG EtOH and **CFZNH$^+$-DCF$^-$-DCF (1:1:1)** (polymorph I) calculated (e) CFZ-DCF 1:2 LAG MeCN and **CFZNH$^+$-DCF$^-$-DCF-MeCN (1:1:1:2)** calculated, (f) CFZ-DCF 1:2 LAG EtOAc and **CFZNH$^+$-DCF$^-$-DCF-EtOAc (1:1:1:1)** calculated, (g) CFZ-DCF 1:2 LAG MeCN after heating to 140 °C, CFZ-DCF 1:2 LAG EtOAc after heating to 130 °C and **CFZNH$^+$-DCF$^-$-DCF (1:1:1)** (polymorph II) calculated, and (h) CFZ-DCF 1:1 neat grinding and CFZ-DCF 1:1 LAG H$_2$O.

Several (solvated/hydrated cocrystal of) salts were prepared by liquid-assisted grinding. PXRD patterns of the obtained powders are compared with the one of the starting materials (CFZ and DCF) and with the calculated pattern of the corresponding (solvated/hydrated cocrystal of) salt. Grinding CFZ with DCF in 1:1 molar ratio in presence of MeOH, EtOH, EtOAc led respectively to the formation of the following crystalline phases: **CFZNH$^+$-DCF$^-$-MeOH (1:1:0.74)**, **CFZNH$^+$-DCF$^-$-EtOH (1:1:1)** and **CFZNH$^+$-DCF$^-$ (1:1)** while **CFZNH$^+$-DCF$^-$-DCF (1:1:1)** (I), **CFZNH$^+$-DCF$^-$-DCF-MeCN (1:1:1:2)** and **CFZNH$^+$-DCF$^-$-DCF-EtOAc (1:1:1:1)** are prepared by ball-milling experiments of CFZ with DCF in 1:2 molar ratio in presence of few drops of EtOH, MeCN and EtOAc respectively. Powder corresponding to **CFZNH$^+$-DCF$^-$-DCF (1:1:1)** (II) is obtained by desolvation of **CFZNH$^+$-DCF$^-$-DCF-MeCN (1:1:1:2)** or **CFZNH$^+$-DCF$^-$-DCF-EtOAc (1:1:1:1)** upon heating. Finally, powders prepared by neat grinding and water-assisted grinding of clofazimine and diclofenac correspond to physical mixture of CFZ with DCF.

TG/DSC analysis

Powders of **CFZNH$^+$-DCF$^-$-MeOH (1:1:0.74)**, **CFZNH$^+$-DCF$^-$-EtOH (1:1:1)**, **CFZNH$^+$-DCF$^-$ (1:1)**, **CFZNH$^+$-DCF$^-$-DCF (1:1:1)** (polymorph I), **CFZNH$^+$-DCF$^-$-DCF-MeCN (1:1:1:2)** and **CFZNH$^+$-DCF$^-$-DCF-EtOAc (1:1:1:1)** were analysed by TG/DSC.
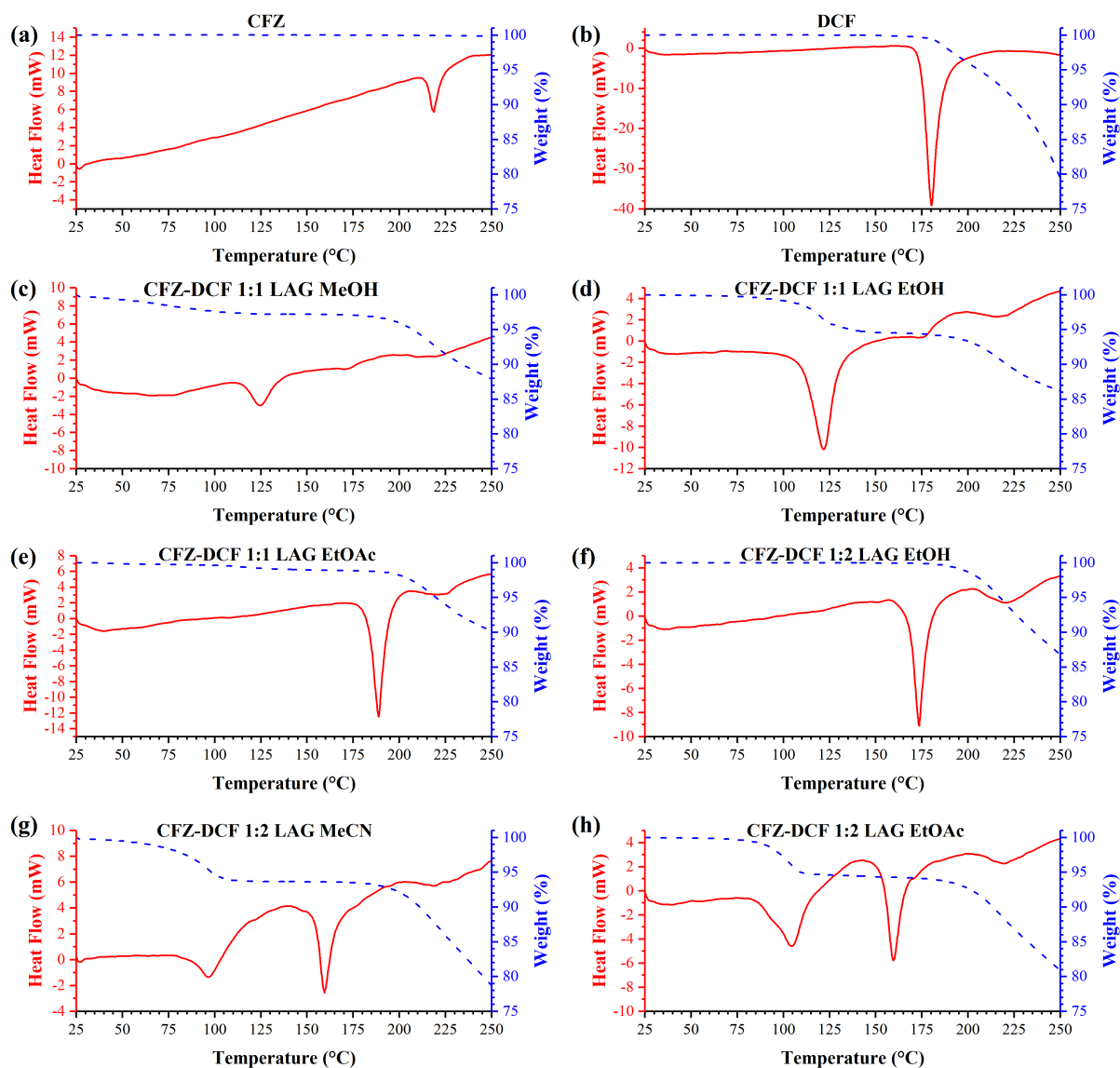

FIGURE B.4: TG/DSC analysis of (a) CFZ, (b) DCF, (c) CFZ-DCF 1:1 LAG MeOH, (d) CFZ-DCF 1:1 LAG EtOH, (e) CFZ-DCF 1:1 LAG EtOAc, (f) CFZ-DCF 1:2 LAG EtOH, (g) CFZ-DCF 1:2 LAG MeCN and (h) CFZ-DCF 1:2 LAG EtOAc. TG and DSC curves are illustrated by blue dashed lines and plain red lines respectively.

A total weight loss of 2.6% is observed between 30 and 150 °C for **CFZNH⁺-DCF⁻-MeOH (1:1:0.74)** (calculated MeOH content: 2.99%). The powder of **CFZNH⁺-DCF⁻-MeOH (1:1:0.74)** melts at 118 °C (as confirmed by an analysis performed on a a Koffler apparatus).

A weight loss of 5.6% is determined for **CFZNH⁺-DCF⁻-EtOH (1:1:1)** which is consistent with the calculated EtOH content (5.6%). Interestingly, the endothermic event at 113 °C corresponds to desolvation and melting, which suggests that EtOH is strongly bound in the structure of this solvated salt.

The unsolvated salt, **CFZNH⁺-DCF⁻ (1:1)** melts at 186 °C.

The unsolvated cocrystal of salt **CFZNH⁺-DCF⁻-DCF (1:1:1)** (polymorph I) melts at 171 °C.

Concerning **CFZNH⁺-DCF⁻-DCF-MeCN (1:1:1:2)**, a 6.2% weight loss is observed between 30 and 180 °C, which is consistent with the calculated MeCN content (7.2%). After desolvation the unsolvated cocrystal of salt **CFZNH⁺-DCF⁻-DCF (1:1:1)** (polymorph II) is obtained (Figure B.6). This unsolvated cocrystal of salt has a lower melting point (157 °C) than **CFZNH⁺-DCF⁻-DCF (1:1:1)** (polymorph I) (171 °C) and than the unsolvated salt **CFZNH⁺-DCF⁻ (1:1)** (186 °C).

Finally, a 5.6% weight loss between 50 and 180 °C is determined for **CFZNH⁺-DCF⁻-DCF-EtOAc (1:1:1:1)**, which is 2% lower than the calculated solvent content from SCXRD data (7.6%). This desolvation leads to the formation of the **CFZNH⁺-DCF⁻-DCF (1:1:1)** (polymorph II) unsolvated cocrystal of salt, which melts at 157 °C.

Investigation of CFZNH$^+$-DCF$^-$-MeOH (1:1:0.74) desolvation upon heating

The powder of **CFZNH$^+$-DCF$^-$-MeOH (1:1:0.74)** has been heated till 100 °C for five minutes. Subsequent PXRD analysis reveals the presence of a mixture of **CFZNH$^+$-DCF$^-$-MeOH (1:1:0.74)** with another crystalline phase (which could not be identified) after heating to 100 °C. The powder was further heated to 110 °C and the obtained crystalline phase corresponds neither to the **CFZNH$^+$-DCF$^-$ (1:1)** unsolvated salt nor to any of the **CFZNH$^+$-DCF$^-$-DCF (1:1:1)** cocrystals of salt (polymorphs I and II).
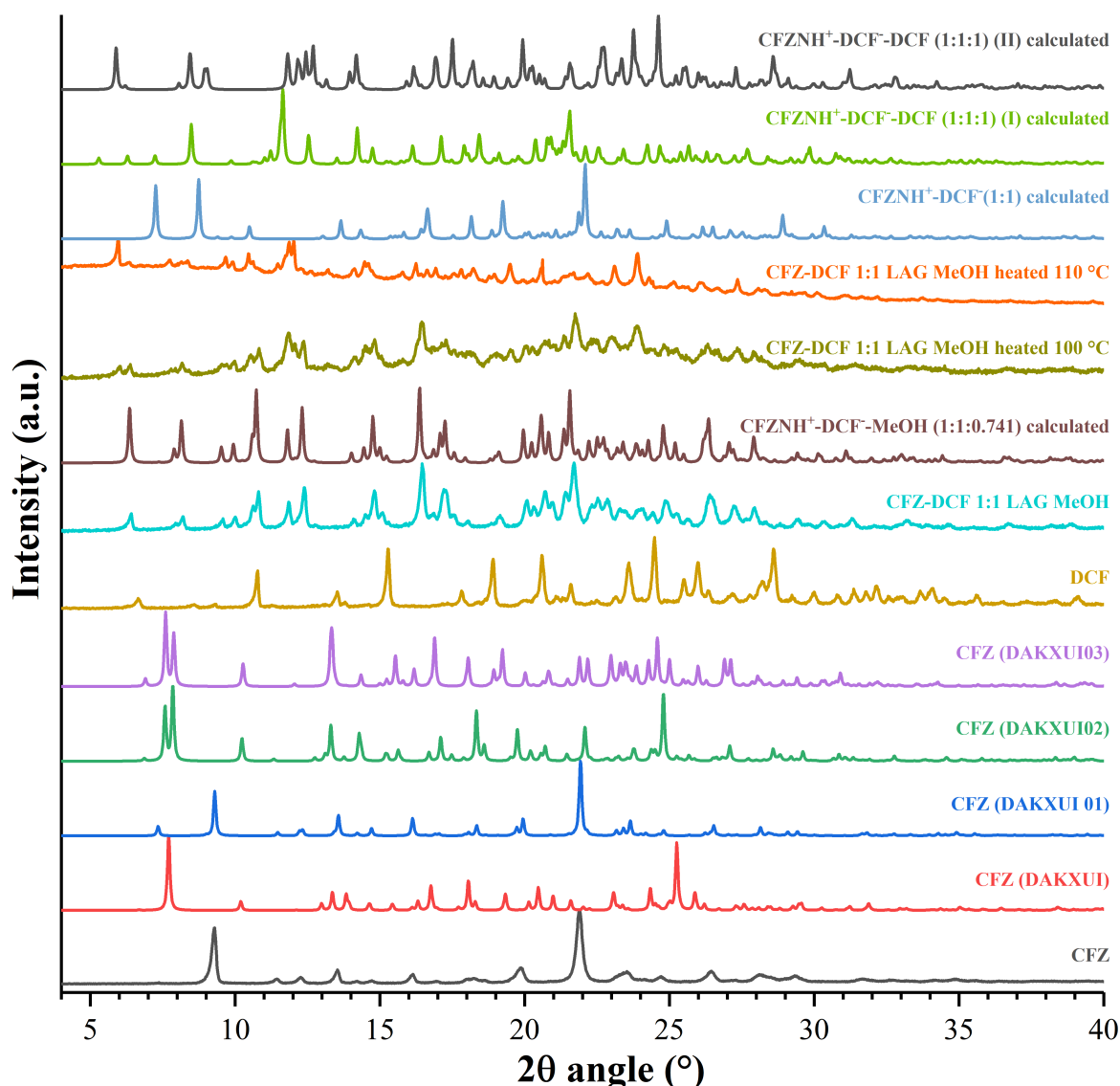

FIGURE B.5: PXRD patterns of CFZ-DCF 1:1 LAG MeOH before and after heating (to 100 and 110 °C) compared with the ones of CFZ polymorphs and CFZ-DCF unsolvated (cocrystal of) salts.

Variable-temperature powder X-ray diffraction performed on CFZ-NH⁺-DCF⁻-DCF-MeCN (1:1:1:2)

VT-PXRD analysis of CFZ-DCF 1:2 LAG MeCN indicates that solvent evaporation leads to a new crystalline phase, which does not correspond to **CFZNH⁺-DCF⁻-DCF (1:1:1)** (polymorph I) unsolvated cocrystal of salt.
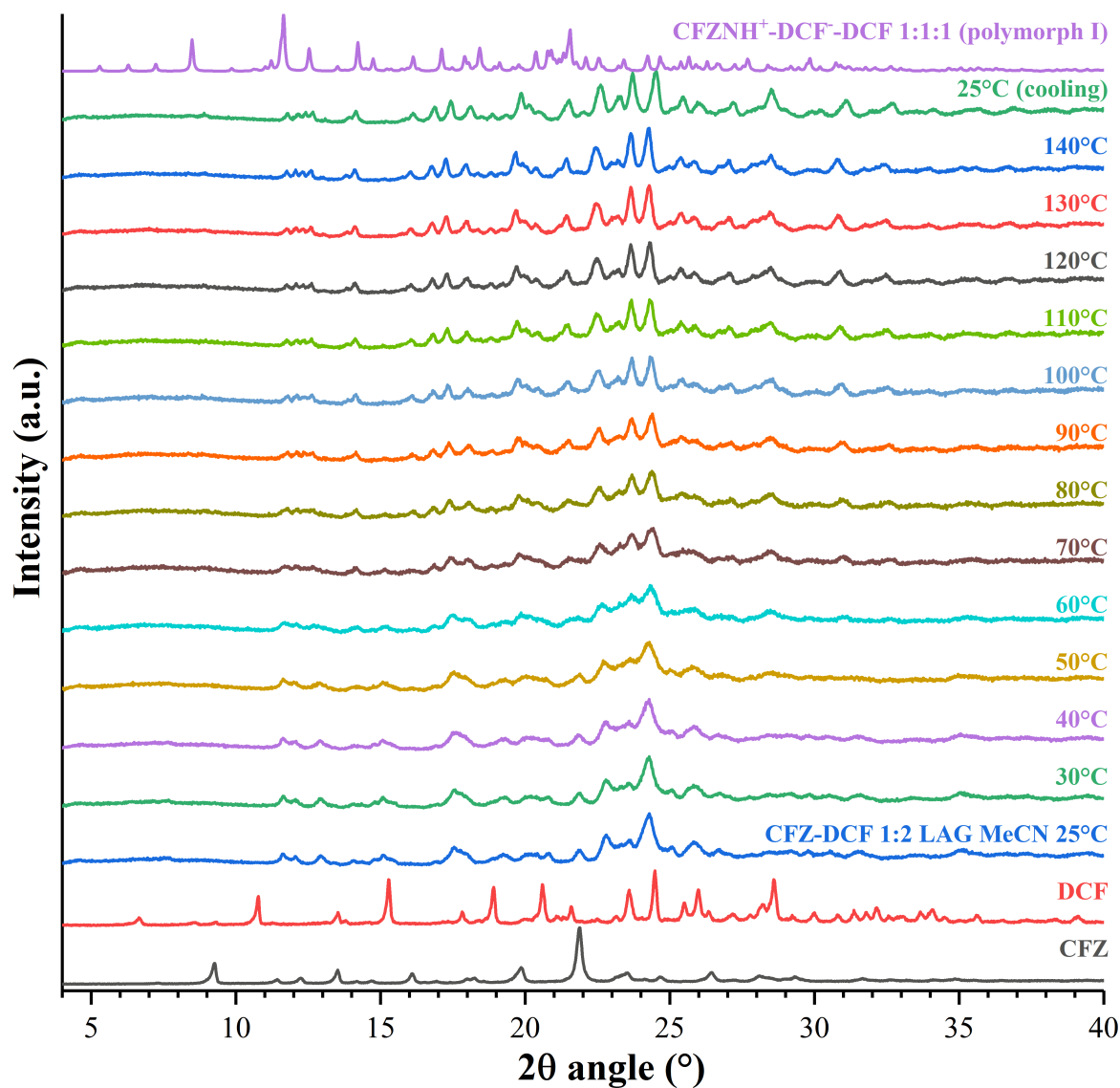

FIGURE B.6: VT-PXRD analysis of CFZ-DCF 1:2 LAG MeCN.

Appendix C

To: Identification of a multicomponent crystalline complex of clofazimine and 4-aminosalicylic improving clofazimine solubility and 4-aminosalicylic acid thermal stability†

Appendix C

Supporting information to chapter 5

Comment on the choice of solvent for liquid-assisted grinding

Several solvates of clofazimine and clofaziminium salts are reported in the literature. More particularly, two clofazimine solvates (with dimethylformamide, CSD refcode: CEK-TER [1]) and with acetone [2]), two hydrated salts (clofaziminium methanesulfonate monohydrate, CSD refcode: GESHET [2] and clofaziminium chloride hydrate, CSD refcode: RAFHUE [3]) and three solvated salts (clofaziminium saccharinate acetonitrile solvated salt, CSD refcode; YORHUL [4]; clofaziminium 2,4-dihydroxybenzoate methanol solvate, CSD refcode: YORJEXL [4] and bis(clofaziminium) terephthalate terephthalic acid unknown solvate,CSD refcode: YORJIBL [4]). The main goal of this work is to identify new non-solvated salts combining clofazimine with 4-aminosalicylic acid. The latter possesses several H-bond acceptors and in consequence, most protic solvents were avoided in order to prevent the formation of toxic solvates. Indeed, evidences of solvate formation with methanol were obtained by characterizing a powder prepared by liquid assisted grinding of clofazimine with 4-aminosalicylic acid in presence of MeOH. More particularly, TG/DSC analysis performed on this powder revealed weight loss between 25 and 110 °C. This weight loss is associated to a wide endotherm on the corresponding DSC curve. Between 130 and 165 °C, two exotherms are observed on the DSC curve. A variable temperature PXRD performed on CFZ-PAS 1/1 LAG MeOH revealed the formation of CFZ-PAS form II upon heating. This crystalline phase was not further investigated because of the difficulty to grow single crystal for structure determination and because of the evidences indicating toxic solvate formation (MeOH) by this route of preparation. Two other protic solvent were selected: ethanol (because of its low toxicity) and 2-propanol (to see if solvate formation could be avoided with solvent of higher molecular volume than methanol). Both solvent lead to the obtention of clofaziminium-4-aminosalicylate form II. First aprotic solvent selected was acetonitrile because a non-solvated salt (clofaziminium saccharinate, CSD refcode: YORJATL [4]) was recently reported and this crystalline phase was obtained by desolvation of clofaziminium saccharinate acetonitrile solvate (CSD refcode: YORHULL [4]). These data suggest acetonitrile as a suitable solvent for non-solvated salt preparation. A second aprotic, solvent ethyl acetate was also selected because of its higher molecular volume in comparison to acetonitrile. This higher molecular volume should render solvent insertion in the structure more difficult than with acetonitrile.

Table of experimental details

TABLE C.1: Table of experimental details

	Polymorph I		MeCN solvate		Polymorph II
Chemical formula	$C_{27}H_{23}Cl_2N_4^+ \cdot$ $C_7H_6NO_3^-$	$C_{27}H_{23}Cl_2N_4^+ \cdot$ $C_7H_6NO_3^-$	$C_{27}H_{23}Cl_2N_4^+ \cdot$ $C_7H_6NO_3^- \cdot$ C_2H_3N	Chemical formula	$C_{27}H_{23}Cl_2N_4^+ \cdot$ $C_7H_6NO_3^-$
Formula weight (g/mol)	626.52	626.52	667.57	Formula wieght (g/mol)	626.52
Crystal system, space group	Triclinic, P$\bar{1}$	Triclinic, P$\bar{1}$	Triclinic, P$\bar{1}$	Crystal system, space group	Triclinic, P$\bar{1}$
Temperature (K)	295	101	100	Temperature (K)	295
a, b, c (Å)	8.3540(3), 13.0939(3), 14.6199(4)	8.1963(4), 13.0827(5), 14.5830(7)	8.1061(2), 13.5422(4), 15.7785(6)	a, b, c (angstrom)	10.8826(13), 11.308(2), 14.3558(13)
α, β, γ (°)	88.464(2), 87.916(2), 81.056(2)	88.252(4), 88.528(4), 80.923(4)	82.832(3), 80.338(3), 81.587(2)	α, β, γ (°)	91.672(13), 91.993(11), 117.767(10)
Volume (Å^3)	1578.37(8)	1543.09(12)	1680.19(9)	Volume (Å^3)	1560.2(4)
Z	2	2	2	Z	2
Radiation type	Cu Kα	Cu Kα	Cu Kα	Radiation type	Cu Kα_1
μ (mm^{-1})	2.20	2.25	2.11	Specimen shape	Cylinder
Crystal size (mm)	0.67×0.24×0.05	0.63×0.24×0.05	0.85×0.26×0.03	Specimen size (mm)	4×0.7
Absorption correction	Analytical	Analytical	Analytical	Specimen mounting	Thin-wall 0.7 mm capillary
T_{min}, T_{max}	0.428, 0.892	0.432, 0.894	0.508, 0.946	Data collection mode	Trhansmission
Measured, independent and observed [$I > 2\sigma(I)$] reflections	14073, 5555, 3666	13917, 5445, 3579	15758, 5919, 5360	Scan method	Step
R_{int}	0.029	0.055	0.027	$2\theta_{min}$, $2\theta_{max}$ (°)	3.995, 41.060
$(\sin\theta/\lambda)_{max}$ (Å^{-1})	0.597	0.597	0.597	$2\theta_{step}$ (°)	0.015
$R[F^2 > 2\sigma(F^2)]$, $wR(F^2)$, S	0.058, 0.195, 1.05	0.051, 0.151, 1.03	0.038, 0.104, 1.02	R$_p$	8.79
No. of reflections	5555	5445	5919	R$_{wp}$	11.34
No. of parameters	600	609	501	R$_{exp}$	0.368
No. of restraints	355	997	16	R$_{Bragg}$	7.29
H atom treatment	constrained	mixed	mixed		
Largest diff. peak and hole (e.Å^{-3})	0.39, -0.39	0.57, -0.51	0.33, -0.39	χ^2	949.390
CCDC deposition number	2010381	2010382	2025549	CCDC deposition number	2010383

Hydrogen-bonds parameters

TABLE C.2: Selected hydrogen-bond parameters

Symmetry codes: (i) -x+1, -y+1, -z+2; (ii) x-1, y, z; (iii) -x+1, -y+1, -z; (iv) x+1, y, z; (v) -x+2, -y+1, -z+1; (vi) -x+2; -y+1, -z+2; (vii) -x, -y+2, -z; (viii) -x, -y+1, -z.

D−H···A	D−H (Å)	H···A (Å)	D···A (Å)	D−H···A (°)
CFZNH$^+$-PAS$^-$ Polymorph I (295 K)				
N3−H3···O1A	0.86	2.54	3.236(18)	138.4
N3−H3···O2A	0.86	1.97	2.784(13)	158.5
N3−H3···O1B	0.86	2.53	3.32(3)	154.0
N3−H3···O2B	0.86	2.32	3.06(3)	144.8
N3−H3···O1C	0.86	1.79	2.633(17)	165.5
N4−H4···O1A	0.86	2.07	2.763(15)	137.6
N4−H4···O2A	0.86	2.37	3.205(17)	162.6
N4−H4···O2B	0.86	2.07	2.85(3)	150.1
N4−H4···O1C	0.86	1.85	2.704(15)	176.1
C27−H27B···O3A^i	0.96	2.53	3.488(10)	173.0
O3A−H3AA···O1A	0.82	1.76	2.491(16)	147.5
O3B−H3AB···O1B	0.82	1.91	2.64(3)	147.3
N5A−H5A···Cl1^i	0.86	2.55	3.181(11)	131.4
N5B−H5C···O1B^{ii}	0.86	1.93	2.71(3)	149.3
N5B−H5D···Cl1^i	0.86	2.69	3.491(18)	155.2
N5C−H5F···O2C^{ii}	0.86	1.49	2.07(3)	121.6
O3C−H3AC···O1C	0.82	2.10	2.65(3)	124.0
CFZNH$^+$-PAS$^-$ Polymorph I (100K)				
N3−H3···O1A	0.84(4)	2.57(4)	3.151(15)	128(3)
N3−H3···O2A	0.84(4)	2.02(4)	2.816(18)	158(4)
N3−H3···O1B	0.84(4)	1.86(4)	2.643(14)	155(4)
N3−H3···O1C	0.84(4)	2.50(5)	3.12(3)	132(3)
N3−H3···O2C	0.84(4)	2.32(5)	3.12(3)	159(4)
N4−H4···O1A	0.83(4)	1.96(4)	2.742(18)	158(4)
N4−H4···O2A	0.83(4)	2.60(4)	3.31(2)	145(3)
N4−H4···O1B	0.83(4)	1.95(4)	2.749(15)	161(4)
N4−H4···O1C	0.83(4)	1.92(5)	2.72(3)	162(4)
C27−H27C···O3A^{iii}	0.98	2.46	3.436(5)	174.4
O3A−H3AA···O1A	0.84	1.74	2.491(17)	148.2
O3B−H3B···O1B	0.84	1.83	2.57(3)	146.0
N5B−H5BB···O1B^{iv}	0.88	2.58	3.46(3)	175.1
N5B−H5BB···O2B^{iv}	0.88	1.23	1.85(3)	121.9
N5C−H5CA···Cl1^{iii}	0.88	2.65	3.474(12)	156.8
N5C−H5CB···O2C^{iv}	0.88	2.01	2.81(3)	150.1
O3C−H3C···O2C	1.16(15)	1.60(14)	2.67(3)	150 (10)
CFZNH$^+$-PAS$^-$-MeCN (1:1:1) solvate				
N3−H3···O1^i	0.89(2)	1.86(2)	2.7359(16)	170.8(17)
N4−H4···O21^i	0.83(2)	2.28(2)	3.0669(19)	157(2)
C15−H15···N6A^{iv}	0.95	2.45	3.27 (3)	143.5
C15−H15···N6B^{iv}	0.95	2.52	3.30 (2)	139.5
C18−H18···N2^v	0.95	2.54	3.427(2)	155.5
C24−H24···O3^{vi}	0.95	2.57	3.3537(19)	139.6
C27B−H27F···O2^i	0.98	2.51	3.243(7)	131.6
N5−H5A···O2^{iv}	0.93(3)	2.08(3)	2.982(2)	164(3)
O3−H3B···O1	0.92(3)	1.63(3)	2.5027(15)	157(2)
CFZNH$^+$-PAS$^-$ Polymorph II (295 K, from powder data)				
N3−H3N···O1	0.87(4)	1.97 (14)	2.83 (14)	171 (6)
N4−H4N···O1	0.86(6)	2.03 (15)	2.88 (15)	170 (5)
C3−H3···Cl1^{vii}	0.93(6)	2.65 (7)	3.40 (7)	138 (3)
C14−H14···O2^{ii}	0.93(6)	2.26(16)	2.76(16)	114(7)
C14−H14···N2^{viii}	0.93(6)	2.47 (4)	3.36 (4)	162 (6)
C15−H15···O2^{ii}	0.93(11)	1.99(15)	2.62(15)	123(7)
C23−H23···N4^{iii}	0.93(4)	2.45(4)	3.24(4)	142(4)
C24−H24···N3^{iii}	0.93(4)	1.86(4)	2.77(3)	163 (3)

Observed, calculated and difference pattern from structure solution of CFZNH$^+$-PAS$^-$
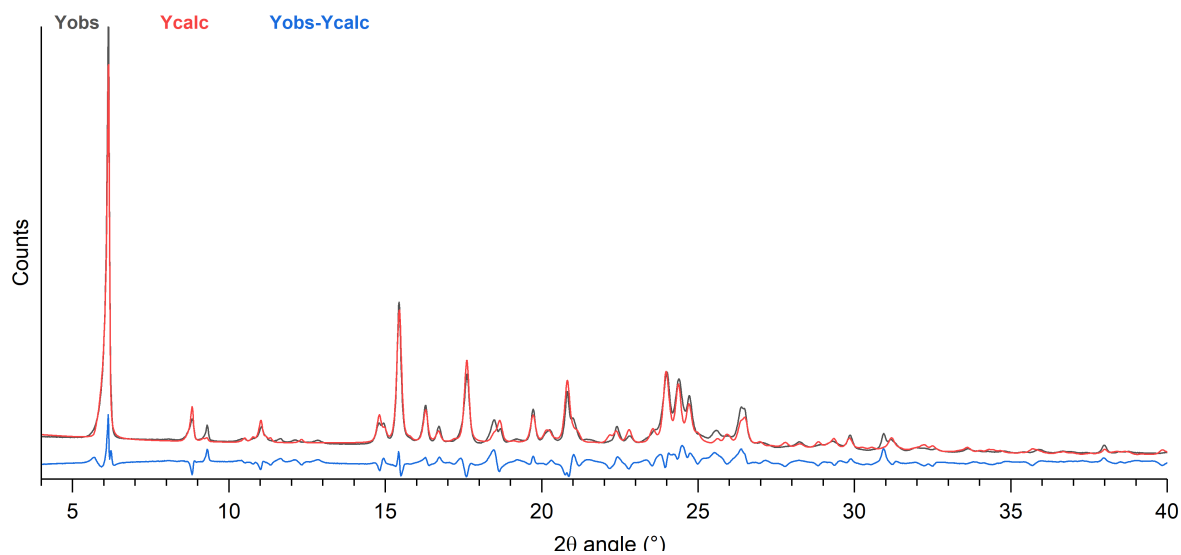

FIGURE C.1: Observed, calculated and difference pattern from structure solution of CFZNH$^+$-PAS$^-$ polymorph II from CFZ/PAS 1/1 LAG EtOH powder.

Short description of CFZNH$^+$-PAS$^-$-MeCN (1:1:1) solvate structure

In CFZNH$^+$-PAS$^-$-MeCN (1:1:1) solvate structure, MeCN and the isopropyl group of clofaziminium are disordered. Clofaziminium cation and 4-aminosalicylate anion interact through strong charge-assisted H-bonds (N4$^+$-H$\cdots$O2$^-$ and N3-H$\cdots$O1$^-$, Table C.2). Other H-bond interactions are presented in Table C.2. Furthermore, clofaziminium cations are stacked in a head to tail fashion (centroid-centroid distance: 3.5610(8) Å, orthogonal projection distance: 3.4247(5) Å and horizontal displacement of 0.975 Å). This stacking is further stabilized by C18-H18$\cdots$N2 H-bond.
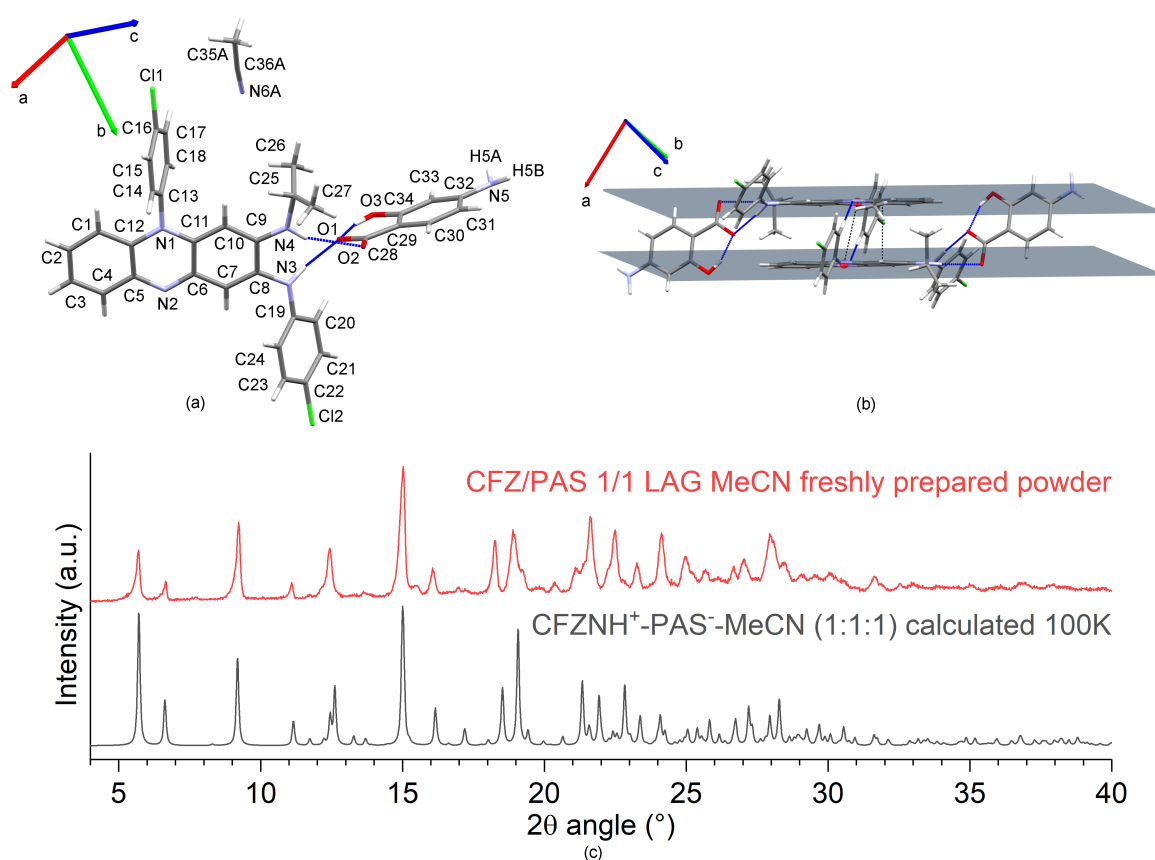

FIGURE C.2: CFZNH$^+$-PAS$^-$-MeCN (1:1:1) solvate (a) asymmetric unit and labeling (disorder not shown), (b) π-π stacking between CFZNH$^+$ cations (centroids (red) and planes (grey) calculated with C5, C6, N1, N2, C11 and C12 atoms) and (c) powder pattern of CFZNH$^+$-PAS$^-$-MeCN (1:1:1) calculated from SCXRD data collected at 100 K compared with the powder pattern of CFZ/PAS 1/1 LAG MeCN (freshly prepared powder).

Variable-temperature powder X-ray diffraction of CFZ/ PAS 1/1 LAG MeCN

Powder of CFZ/PAS 1/1 LAG MeCN freshly ground corresponds to a solvate (presence, among others, of peaks at 2θ values of 5.6, 6.0 and 12.4°). Upon heating, the anhydrous $CFZNH^+$-PAS^- salt (polymorph I) starts to appear. Indeed, peaks at 2θ values of 5.6, 6.0 shift to 6.0 and 6.8°, the peak at 12.4° disappears and several peaks appear at 2θ values of 17.3, 18.8 and 28.3°. At 110 °C, $CFZNH^+$-PAS^- polymorph I is obtained. Between 130 °C and 150 °C, a phase transformation occurs and a new crystalline phase seems to be present. At 175 °C, a crystalline phase similar to polymorph II is obtained. However, polymorph II is not recovered after cooling.
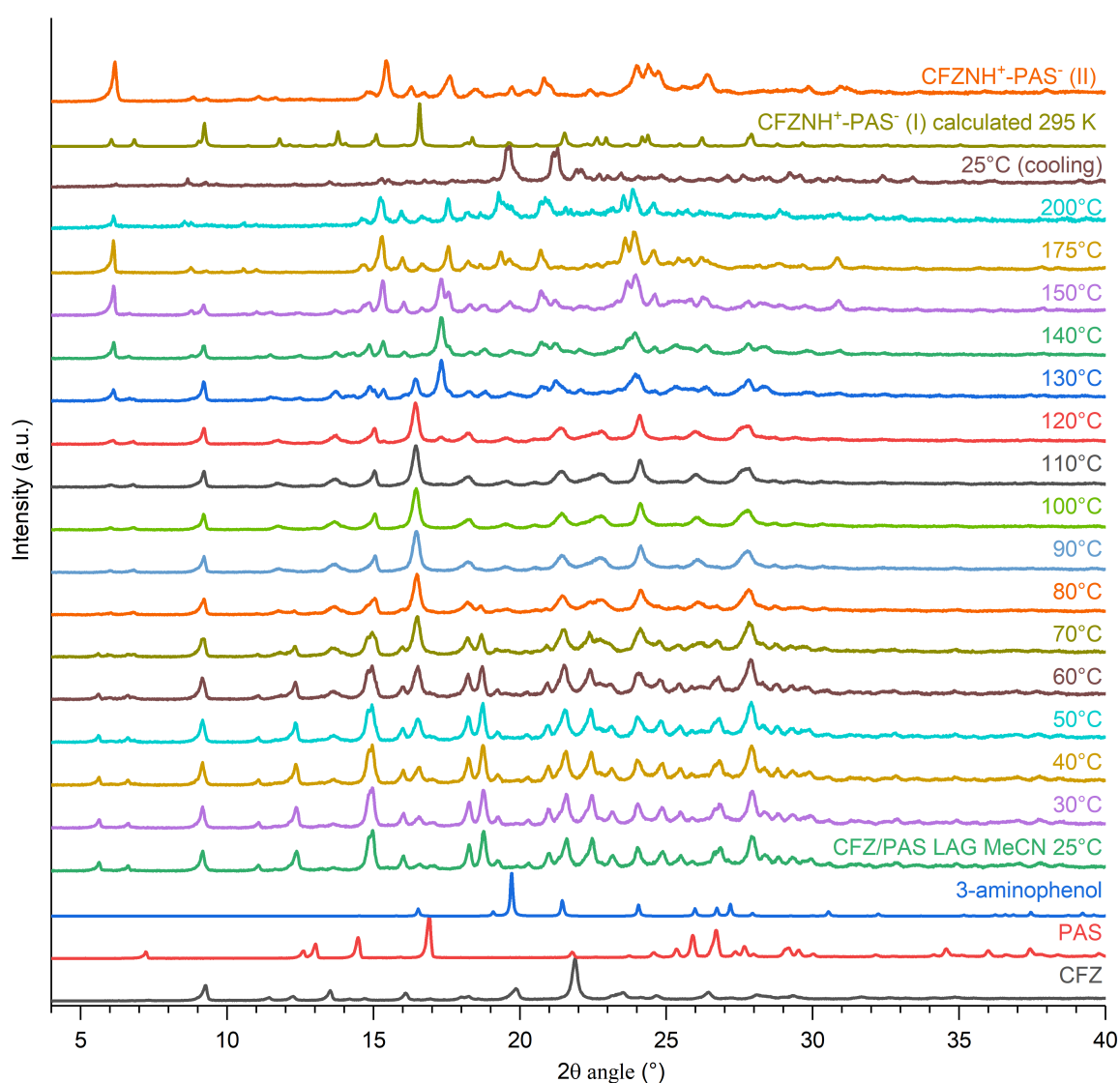

FIGURE C.3: VT-PXRD patterns of CFZ/PAS 1/1 LAG MeCN.

Appendix C

PXRD pattern of the crystalline phase recovered after TG/DSC analysis performed till 160 and 180°C

Upon heating, we observe partial/complete conversion of polymorph I to polymorph II. We suspect that it is a kinetically controlled process and we were not able to determine exact conversion conditions. Indeed, PXRD pattern recorded at 175°C during VT-PXRD data collection matches quite well with PXRD pattern of polymorph II. However, PXRD patterns of powder recovered after TG/DSC analysis performed till 160 and 180°C seems to be a mixture of polymorph II with another phase.
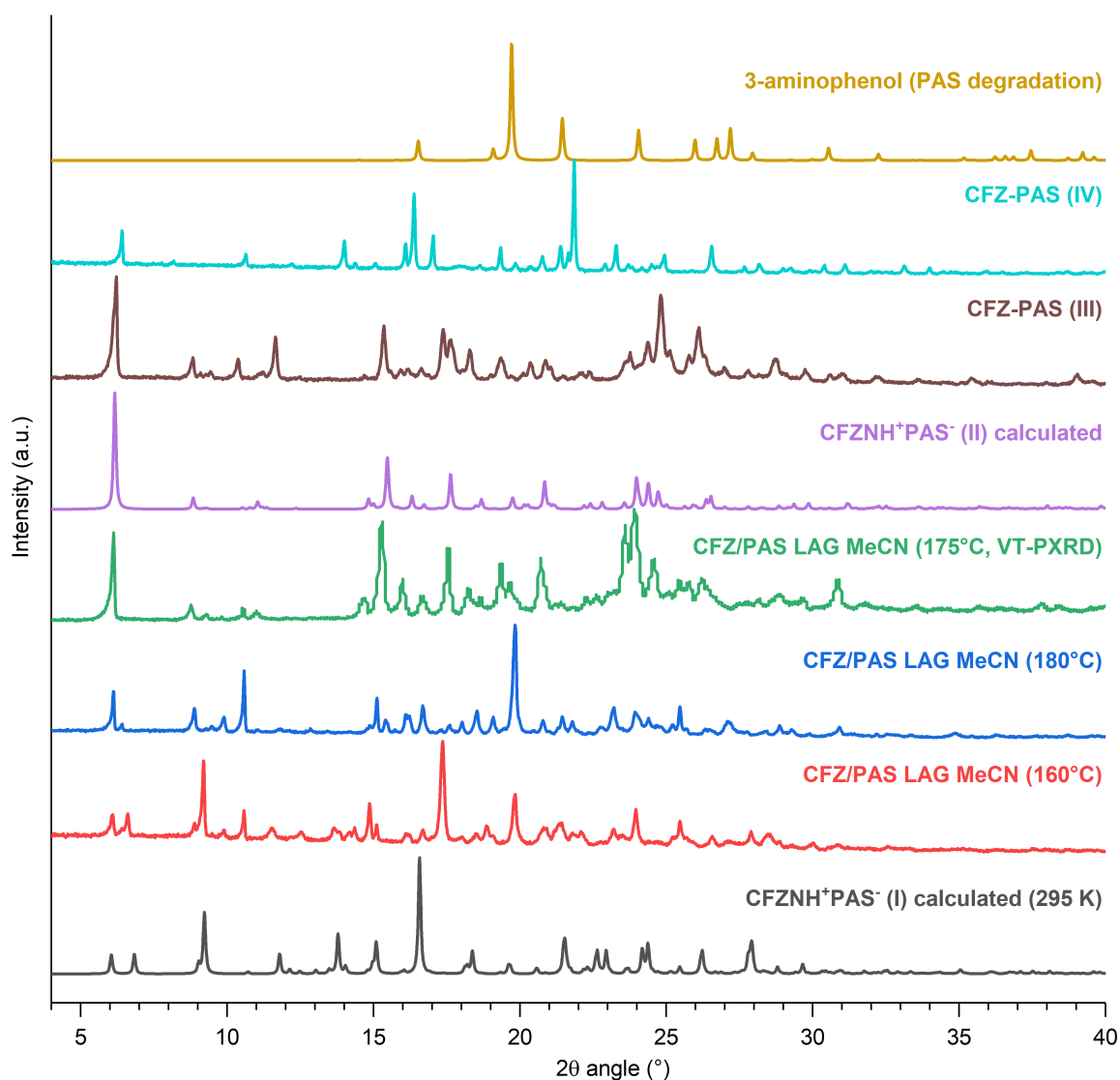

FIGURE C.4: PXRD patterns of CFZ/PAS 1/1 LAG MeCN after TG/DSC analysis till 160 and 180°C compared with pattern obtained at 175°C during VT-PXRD experiment, with CFZNH$^+$-PAS$^-$ forms I, II III and IV as well as with 3-aminophenol (PAS degradation product).

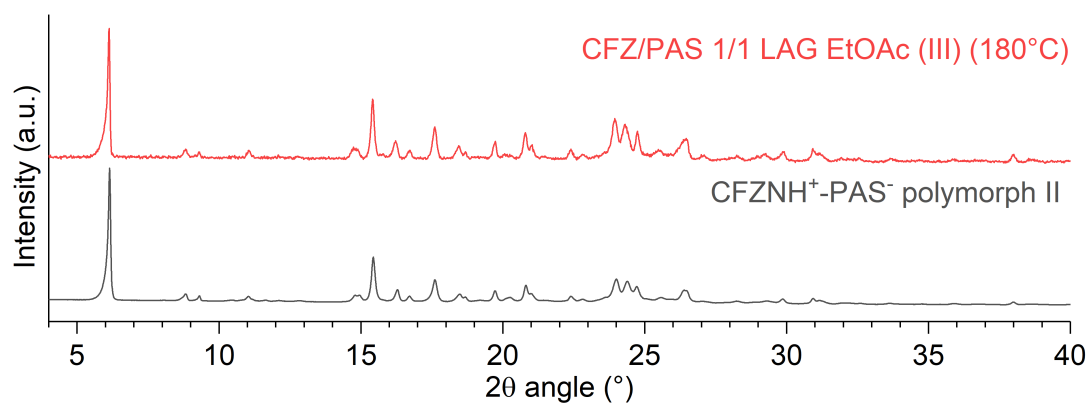# CFZ/PAS 1/1 LAG EtOAc (form III) converts to CFZNH$^+$-PAS$^-$ form II upon heating

FIGURE C.5: PXRD pattern of CFZNH$^+$-PAS$^-$ form II compared to the one obtained after heating form III up to 180 °C and cooling at room temperature.
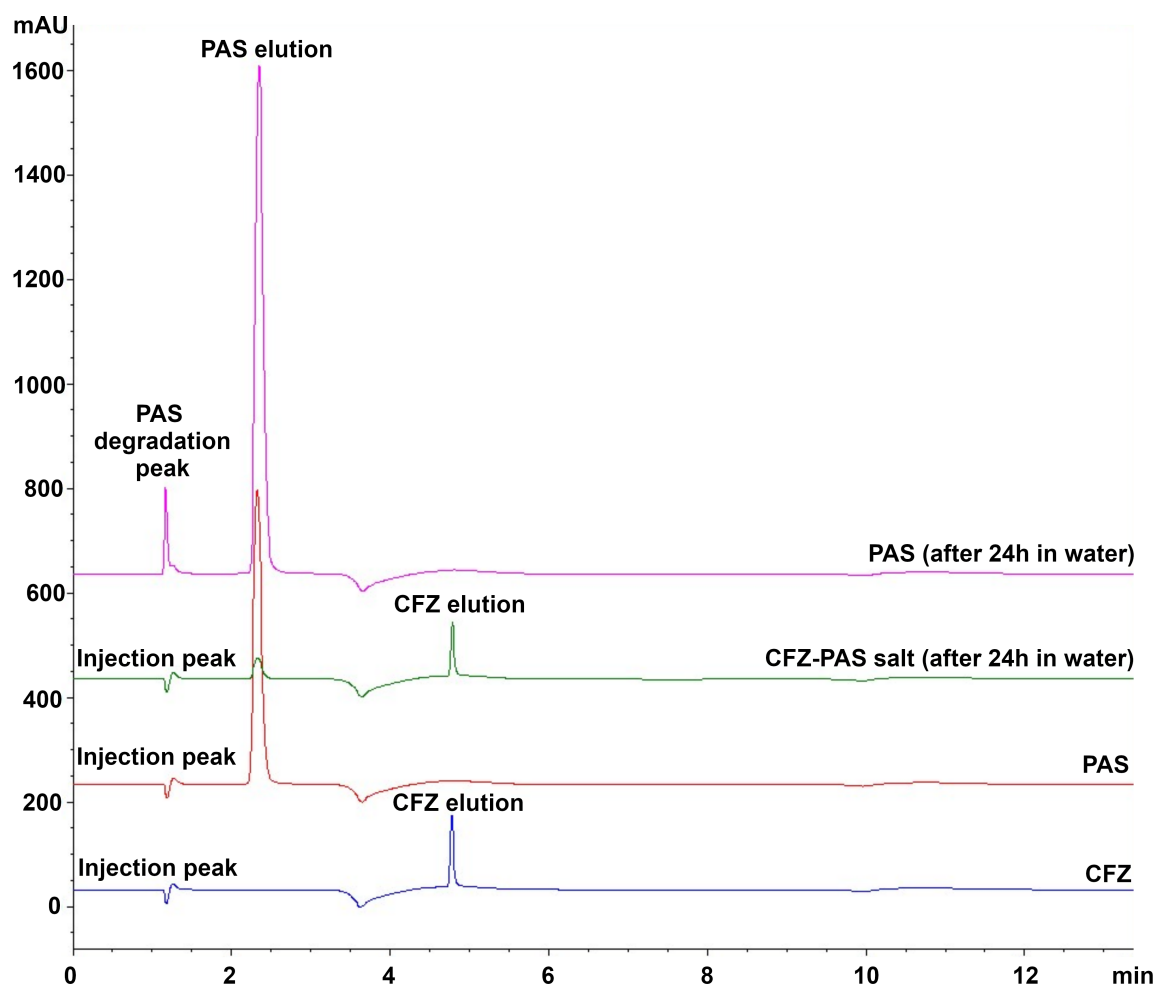
Typical HPLC chromatograms

FIGURE C.6: Typical chromatograms of pure CFZ (from calibration curve, prepared in MeCN/H$_2$O 50/50 volume/volume), pure PAS (from calibration curve, no degradation of PAS in MeCN/H$_2$O 50/50 volume/volume), CFZNH$^+$-PAS$^-$ salt after 24h of immersion in water, and PAS after 24h of immersion in water (the degradation product of PAS is not retained on the column).

Bibliography

[1] D. S. Eggleston, W. E. Marsh, and D. J. Hodgson. Structures of the antileprosy phenazine derivatives clofazimine–N, N-dimethylformamide, C27H22Cl2N4. C3H7NO, and B1912, C30H27ClN4. *Acta Crystallographica Section C: Crystal Structure Communications*, 40(2):288–292, 1984.

[2] G. Bolla and A. Nangia. Clofazimine mesylate: A high solubility stable salt. *Crystal Growth and Design*, 12(12):6250–6259, 2012.

[3] E. M. Horstman, R. K. Keswani, B. A. Frey, P. M. Rzeczycki, V. LaLone, J. A. Bertke, P. J. Kenis, and G. R. Rosania. Elasticity in macrophage-synthesized biocrystals. *Angewandte Chemie*, 129(7):1841–1845, 2017.

[4] L. Bodart, N. Tumanov, and J. Wouters. Structural variety of clofaziminium salts: effect of the counter-ion on clofaziminium conformation and crystal packing. *Acta Crystallographica Section B: Structural Science, Crystal Engineering and Materials*, 75(4), 2019.